On the analysis and design of in-wheel motor for vehicle application

Dissertation

zur Erlangung des akademischen Grades

Doktoringenieur
(Dr.-Ing.)

von M.Sc. Sergey Perekopskiy
geb. am 16.01.1988 in Makeevka, Donezka obl., Ukraine
genehmigt durch die Fakultät Maschinenbau
der Otto-von-Guericke Universität Magdeburg

Gutachter:
Prof. Dr.-Ing. Roland Kasper
Prof. Igor Gorobets

Promotionskolloquium am 18.09.2020

For my family

Abstract

The revolutionary changes in automotive industry which are based on the following trends in environmental protection, lead to the new requirements that must be met in modern vehicles. Thus, for the automotive industry, electric powered vehicles are becoming an increasingly relevant factor in the competition against climate change. The expert community is united in the opinion that e-mobility is becoming the dominant factor in improving the operating efficiency of vehicles. At the same time, the key aspects of changes in the context of the development of vehicles represent directions that bring serious changes to the traditional automotive industry, especially in its design and technological basis. One special example of a possible way of change represents an in-wheel motor which provides a powerful and compact drive solution for electric vehicles.

The in-wheel motor as a modular element of an electric drive has long been known. In-wheel motors for a vehicle have remarkable advantages as compactness and present a wide field of research for possible integration in vehicle structures. Currently, the development of motor-in-wheeled electric transport drives is continuously increasing. However, such a constructive solution for the vehicles could not be implemented until recently for a variety of reasons. First of all, due to the impossibility of development of a compact, highly efficient drive that meets its power and torque requirements. Therefore, the main disadvantage of the in-wheel motor is an unsprung weight. This is why a usage of modern lightweight technologies in in-wheel motors is significant.

The purpose of this thesis is to present for the first time the findings and conclusions about the potential of the novel in-wheel motor design with significant specific power and torque density for a vehicle with regard to manufacturability and functionality. For this purpose, the design methodology of the in-wheel motor was presented, which has an ambivalent manner. On the one hand the ascertainment of increased potentials for modern lightweight technologies and materials according to their application on the in-wheel motor is applied to minimize the total weight of the motor. On the other hand, an increase of the power and torque characteristics is realized by the usage of new concept of the motor active parts – novel winding technique and arrangement of the magnets. In addition, features such as functionality, stiffness and robustness have been considered due to the innovative approach of specific load compensation in the in-wheel motor. Relevant research has demonstrated that integration of the in-wheel motor in common vehicles together with a unique coupling element is soluble. The potentials of the developed methodology were demonstrated by component and system testing of the completed prototypes.

Kurzfassung

Die revolutionären Änderungen in der Automobilbranche, die auf den Tendenzen des Umweltschutzes beruhen, führen zu den neuen Anforderungen, die in modernen Fahrzeugen erfüllt werden müssen. Für die Automobilindustrie werden somit die elektrisch angetriebenen Fahrzeuge zu einem immer wichtigeren Faktor im Wettbewerb gegen den Klimawandel. Die Experten sind sich in der Meinung einig, dass die Elektromobilität zu einem dominierenden Faktor wird, da die Steigerung der Fahrzeugeffizienz somit gewährleistet ist. Gleichzeitig stellen die Schwerpunkte der Veränderungen im Zusammenhang mit der Entwicklung von Fahrzeugen die neuen Entwicklungsrichtungen dar, die gravierende Veränderungen für die traditionelle Automobilindustrie mit sich bringen, insbesondere in Bezug auf Design und technologische Basis. Ein spezielles Beispiel der möglichen Art und Weise von Veränderungen stellt ein Radnabenmotor dar, der eine leistungsstarke und kompakte Antriebslösung für Elektrofahrzeuge bietet.

Der Radnabenmotor als modulares Element des Elektroantriebs ist schon lange bekannt. Radnabenmotoren für die Fahrzeuge haben erhebliche Vorteile wie die Kompaktheit und stellen ein weites Forschungsfeld für eine mögliche Integration in die Fahrzeugstruktur dar. Zurzeit nimmt die Entwicklung von elektrischen Radnabenantrieben kontinuierlich zu. Allerdings war es bis vor kurzem aus einer Vielzahl von Gründen nicht möglich, eine solche konstruktive Lösung für die Fahrzeuge einzusetzen. Zunächst einmal aufgrund der Unmöglichkeit, einen kompakten, hocheffizienten Antrieb zu entwickeln, der den Leistungs- und Drehmomentanforderungen genügt. Folglich ist der Hauptnachteil des Radnabenmotors eine ungefederte Masse. Aus diesem Grund ist der Einsatz moderner Leichtbautechnologien im Radnabenmotor von Bedeutung.

Ziel dieser Arbeit ist es, erstmals die Erkenntnisse und Schlussfolgerungen über das Potential der neuartigen Radmotorkonstruktion mit signifikanter spezifischer Leistungs- und Drehmomentdichte für ein Fahrzeug im Hinblick auf Herstellbarkeit und Funktionalität darzustellen. Zu diesem Zweck wurde die Entwurfsmethodik des Radnabenmotors in zwiespältiger Weise vorgestellt. Zum einen wird die Ermittlung erhöhter Potentiale für moderne Leichtbautechnologien und -werkstoffe entsprechend ihrer Anwendung auf den Radnabenmotor angewendet, um das Gesamtgewicht des Motors zu minimieren. Zum anderen wird eine Erhöhung der Leistungs- und Drehmomentcharakteristika durch den Einsatz eines neuen Konzeptes der motoraktiven Teile - neuartige Wicklungstechnik und Anordnung der Magnete, realisiert. Zusätzlich wurden solche Eigenschaften wie Funktionalität, Steifigkeit und Robustheit durch die Verwendung eines innovativen Ansatzes der spezifischen Lastkompensation im Radnabenmotor berücksichtigt. Aktuelle Untersuchungen haben gezeigt, dass die Integration des Radnabenmotors in ein konventionelles Fahrzeug in Verbindung mit einem speziellen Kupplungselement lösbar ist. Die Potentiale der entwickelten Methodik wurden durch Komponenten- und Systemtests an den fertigen Prototypen demonstriert.

Acknowledgements

The present dissertation and the research were conducted from February 2016 until March 2020 at the chair of the Mechatronics at the Institute of Mobile Systems of the Otto von Guericke University Magdeburg.

First, I would like to thank Prof. Dr.-Ing. Roland Kasper for the opportunity to carry out research in such exiting scientific area and for the supervision and extensive support during my research work. I would also like to thank Prof. Igor Gorobets for the submission of the second examination report and his intense interest to the topic of dissertation. I would also like to thank the head of my examination committee Prof. Dr.-Ing. habil. Manja Krüger.

I do appreciate the excellent and outstanding co-operation with all partners from LeiRaMo project and especially to Mr. Falk Höhne from Elektromotoren und Gerätebau Barleben GmbH for hours of discussion and finding of solutions.

I am also very grateful to all my colleagues from the university and especially from the chair of Mechatronics for their cooperation during my research. I would like to express my special thanks to M.Sc. Martin Schmidt for assistance by prototype testing and discussions in the theoretical side, Dipl.-Ing. Ralf Hinzelmann and Dipl.-Ing. Andreas Zörnig for their helpful discussions and suggestions by the development of the motor, Dr. Jörg Sauerhering for his constant readiness to explain and discuss thermodynamical aspects, M.Sc. Markus Höfer for his support in manufacturing and assembling of the prototypes, interesting discussions and suggestions, and encouragement during research.

I would like to thank my numerous bachelor and master students for their work on a number of different topics, which help to succeed scientific targets. I would also like to mention the various support provided by the University's workshops as well as the secretariats and administration. My special thank goes to all colleagues of mechanical workshop at the Institute for Mobile Systems for their fast and accurate manufacturing of parts for prototypes, especially to Mr. Sven Förster and to Mr. Uwe Kuske. I also would like to express my gratitude to all my small "army" of student assistants, who furiously “fought” side by side on the "battlefield" of prototype manufacturing. Without all these people, it would be impossible to carry out meaningful research work.

At last but not least, I would like to express my gratitude to my friends. Above all, I would like to thank my friends John, Michael, Chad, Anthony and James Newell Osterberg for their endless support and captivating by the idea of getting things done. I would like also to take this opportunity to express my deep sense of gratitude towards my family who supported me throughout during research and writing this dissertation. Finally, my heartfelt appreciation goes to my wife Alina, without her help this work would have been written three to four months earlier.

Magdeburg, 15.04.2020

Sergey Perekopskiy

A deal of poverty grows out of the carriage of excess weight.

Henry Ford

Contents

List of Figures

List of Tables

Notations

Roman Symbols

Symbol	Unit	Meaning
A	mm	Wheel diameter
A_{con}	mm^2	Cross-sectional area of the conductor
A_f	m^2	Frontal area of the vehicle's body
B	mm	Rim width
B_H	T	Magnetic flux density
B_{Hm}	T	Mean magnetic flux density
$(BH)_{max}$	kJ/m^3	Value of the energy product
C	-	Humps for additional internal fixation of tubeless tyre beads
C_{dw}	N	Dynamic load rating
C_0	N	Basic static load rating
C_t	Nm/°	Angular stiffness of wheel hub bearing
c_w	-	Aerodynamic drag resistance coefficient
D	-	Drop center is a bead perch of tyres
D_{ir}	mm	Rotor inner diameter
d_M	mm	Minimum distance between the magnets
E	-	Wheel mounting surface
F	mm	Offset of a wheel
F_A	kN	Axial load
F_{ad}	N	Aerodynamic drag
F_{cm}	N	Value of each peak-to-peak amplitude
F_{cm_1}	N	Mean value of the cogging force
F_{grad}	N	Grading resistance
F_L	N	Lorentz force
F_t	N	Traction effort
F_T	N	Torque force
F_{tr}	N	Traction resistance
F_R	kN	Radial load
F_{rd}	N	Rolling resistance
f_{rr}	-	Rolling resistance coefficient
F_x	kN	Longitudinal force
F_y	kN	Lateral force
F_z	kN	Vertical force
G	mm	Hub hole diameter
g	m/s^2	Gravitational acceleration

H	mm	Pitch center diameter
h_{ag}	mm	Air gap height
h_c	mm	Height of the climbed curb
h_f	mm	Height of the foil
h_H	mm	Thickness of the rotor housing
h_{iag}	mm	Wire insulation height
h_{in}	mm	Height of the slot opening
h_{inl}	mm	Height of the inlay
h_{is}	mm	Height of the insulation
h_M	mm	Height of the rotor housing
h_{meag}	mm	Height of the magnetic effective air gap
h_{st}	mm	Height of the winding strand
h_{sl}	mm	Height of the slot
h_{wag}	mm	Height of the copper wire
h_{ws}	mm	Height of the wire for the slot winding
k_M	-	Motor constant
I	A	Current
I_{max}	A	Maximum current value
L_{10}	h	Required service life
l_a	mm	Length of the lever arm
L_{agw}	mm	Length of the air gap winding
L_{agwh}	mm	Length of the winding heads of the air gap winding
l_{cc}	mm	Length interspersed by the magnetic field
L_{con}	mm	Total conductor length
l_M	mm	Length of the magnet
L_s	km	Mileage
L_{sw}	mm	Length of the slot winding
L_{swh}	mm	Length of the winding heads of the slot winding
M	Nm	Driving torque
M_{el}	Nm	Generated motor torque
m_M	kg	Weight of the magnets
m_v	kg	Maximum authorized weight of the vehicle
M_L	Nm	Torque load
M_{max}	Nm	Maximum torque
M_{mech}	Nm	Drive torque
M_n	Nm	Nominal torque
M_x	Nm	Heeling moment
M_y	Nm	Twist moment
M_z	Nm	Aligning moment
n	min^{-1}	Rotational speed
n_M	-	Number of magnets

n_{max}	min^{-1}	Maximum rotational speed
n_{Mph}	mm	Width of one magnet with radial or axial magnetization
n_{no}	-	Number of strips per slot
n_{ph}	-	Number of phases
n_{ptp}	-	Number of peak-to-peak amplitudes per measurement
n_{st}	-	Number of slots in stator
n_w	-	Number of wires
p	-	Life-equation exponent
P_{el}	kW	Electrical power
P_n	kW	Nominal power
P_m	N	Load rating of the bearing
P_{max}	kW	Maximum power
P_{mech}	kW	Mechanical power
P_{ohmic}	kW	Ohmic losses
p_p	-	Number of pole pairs
P_{r_max}	mm	Force acting at the maximum possible eccentricity
r_{ag}	mm	Air gap radius
R_{con}	Ω	Winding resistance
r_{dyn}	mm	Wheel dynamic rolling radius
r_o	mm	Radius of the wheel without load
R_{rad}	mm	Radius of groove in rotor back iron
r_{st}	mm	Radius of the stator
r_{stat}	mm	Radius of the loaded wheel
r_t	mm	Radius of the tyre
S_0	-	Static load safety factor
T_{cog}	Nm	Cogging torque
T_{cog_pp}	Nm	Cogging torque on the pole pair
t_{req}	s	Required time for acceleration from stillstand to 100 km/h
T_{w_max}	°C	Maximum winding temperature
T_{w_min}	°C	Minimum winding temperature
V	km/h	Speed of the vehicle
V_{as}	mm^3	Available assembly space
V_{grad}	km/h	Vehicle climbing maximal speed
V_{max}	km/h	Maximum vehicle speed
U_M	V	Induced counter-voltage
W	J	Internal magnetic energy
w_{iag}	mm	Wire insulation width
w_{is}	mm	Width of the insulation
w_M	mm	Magnet width
w_{no}	mm	Thickness of NO20 electrical steel
w_{nom}	mm	Thickness of NOMEX insulation paper

w_{open}	mm	Opening width
w_{sl}	mm	Width of the slot
w_{st}	mm	Width of the winding strand
W_v	inch	Wheel size
w_{wag}	mm	Width of the copper wire
w_{ws}	mm	Width of the wire for the slot winding

Greek Symbols

Symbol	Unit	Meaning
α	°	Road angle
α_{Al}	1/K	Expansion coefficients of aluminum
α_{NO20}	1/K	Expansion coefficients of NO20 steel
Δ_{bi}	mm	Expansion of the back iron
Δ_{st}	mm	Constriction of stator main body
η_{motor}	-	Efficiency of the motor
μ	-	Magnetic permeability
μ_f	-	Friction coefficient steel-steel
μ_r	-	Relative magnetic permeability
ρ_{air}	kg/m^3	Air density
ρ_w	Ωm	Conductor resistivity
θ	°	Rotor position angle
θ_{pp}	°	Angle for one pol pair
ω_{max}	rad/s	Maximum angular velocity of the in-wheel motor
ω_M	rad/s	Angular frequency of the motor
ω_r	rad/s	Desired wheel speed

Abbreviations

Abbreviation	Description
2D	Two-dimensional
3D	Three-dimensional
ABS	Anti-lock braking system
AC	Alternating current
ACIM	Alternating current induction motor
AG	Aktiengesellschaft (joint-stock company)
Al	Aluminium
Al-Mg	Aluminium-Magnesium
AlNiCo	Aluminium-nickel-cobalt
BLDC	Brushless direct current motor
CAD	Computer-aided design
CAN	Controller area network
CFRP	Carbon fiber reinforced polymer

DC	Direct current
DLR	German Aerospace Center (Deutsche Zentrum für Luft- und Raumfahrt e. V.)
EMF	Electromotive force
EMC	Electromagnetic compatibility
EPDM	Ethylene propylene diene monomer
ESP	Electronic stability program
FEM	Finite element method
IP	Ingress protection
IFAM	Institute for manufacturing technology and advanced materials
IGBT	Insulated gate bipolar transistor
LBF	Institute for structural durability and system reliability
MOSFET	Metal-oxide-semiconductor field effect transistor
NdFeB	Neodymium-iron-boron
Ni-Cu-Ni	Nickel-copper-nickel
OE	Original equipment
OEM	Original equipment manufacturer
PC	Personal computer
PMBLDC	Permanent magnet brushless direct current motor
PMDC	Permanent magnet direct current
PMSM	Permanent magnet synchronous motor
PWM	Pulse-width modulation
RMS	Root mean square
SAS	Sandwich structure
SKF	Svenska Kullagerfabriken
SLS	Selective laser sintering
SmCo	Samarium-cobalt
SRM	Switched reluctance motor
SUV	Sport utility vehicle
UK	United Kingdom
UN	United Nations
USA	United states of America
US	United states
UV	Ultraviolet
WFT	Wheel force transducer

1. Introduction

One of the biggest problems of the modern world is the urgency of an immediate solution to improve the Earth's atmosphere, which is polluted by huge masses of harmful products – waste from various industrial enterprises and vehicles. Efforts to mitigate ongoing climate change led, with the Kyoto Protocol, for the first time to statutory emission development targets for members of the United Nations. By ratifying the Protocol of 191 countries, this third UN climate conference in 1997 is regarded as a milestone in international climate policy. The 191 countries committed to the achievement of individual targets in terms of their greenhouse gas emissions. In the first commitment period, greenhouse gas emissions should be reduced by five percent compared to 1990 levels. With the second commitment period, which begins in 2013 and ends in 2020, the target must be raised to an overall reduction of 20% compared to 1990 emissions. The next target for the following years is confirmed in the Paris Agreement and estimates the reduction of greenhouse gas emissions for the period 2021 to 2030. The commitment declares a level of reduction of greenhouse gas emissions at the rate of 40% compared to 1990. The Paris Agreement in 2015 contributed to a change in public sentiment. It was acknowledged that it is impossible to solve the problem of climate change and slow down the global warming of the planet only by the individual efforts of several countries. Society recognized and accepted the idea that everyone should make a contribution to mitigate the climate change.

The European Union has more ambitious plans in climate politic. The climate protection plan of the EU sets a target in 2050 as a reference year. Until then, the transport sector should be free of greenhouse gas emissions. As it is shown in Figure 1.1, (a) and (b), this is due to the fact that the transport sector and especially road transport plays a major role in the European energy consumption.

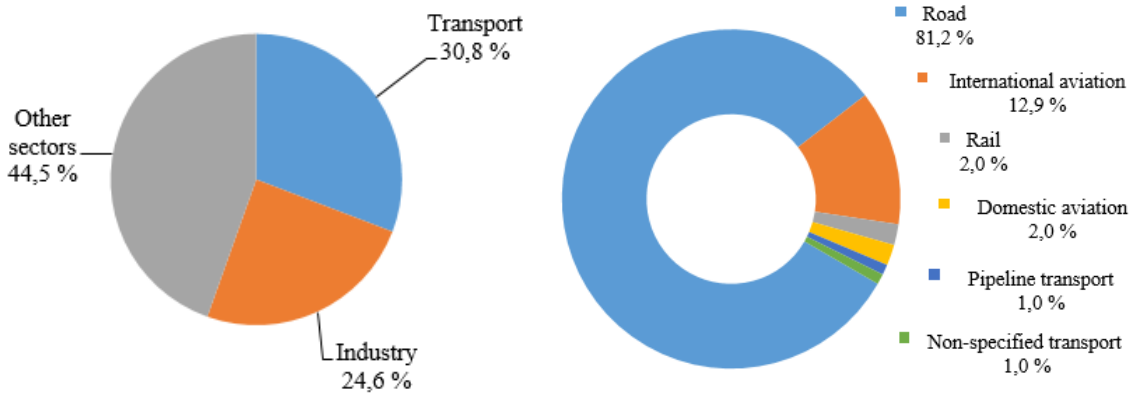

a b

Figure 1.1 – Final energy consumption by sector in the EU in 2017 [48] (a) and transport energy consumption by source mode in the EU in 2017 (b) [170]

Vehicles with internal combustion engines are more likely to belong in air-polluting devices in so far as their hazardous waste is thrown directly at ground level, or rather wherever there are people. The dangers of exhaust gases from vehicle engines were discussed for the first time in the 1960s, when the number of respiratory diseases caused by the "smog" sharply increased [67]. "Smog" began to appear frequently in the cities of the State of California as a result of the running of vehicles with internal combustion engine [100]. Years of research were needed in order to identify the main hazardous air pollutants, such as Sulphur dioxide (SO_2), Ammonia (NH_3), volatile organic compounds (NMVOC), Nitrogen oxides (NO_x) and fine particulate matters. This issue has been taken seriously since then, which has led to environmental issues of the vehicle being given a high priority in consumer characteristics and safety at the vehicle design stage. A systematic study of hazardous emissions has led to legal documents (standards) limiting the concentration of hazardous substances

in the exhaust gases. The strictest in this respect until today are the "Euro" standards in the EU and the US state of California laws.

Regulations ECE-R83-02 UN, known as "Euro 1", came into effect in 1993. Since their introduction, automotive companies in Europe have only produced vehicles that meet these requirements. As can be seen in Figure 1.2, there have been many changes in Euro standards since 1993, and today the world leaders in the automotive industry are already orienting their products to the ambitious requirements of the Euro standard of the sixth version. During the operative period of Euro standards since 1993, the amount of hazardous substances in exhaust gases has decreased by more than the factor of two. During the period since 1975, the content of toxic components in greenhouse gas per vehicle decreased by 70%.

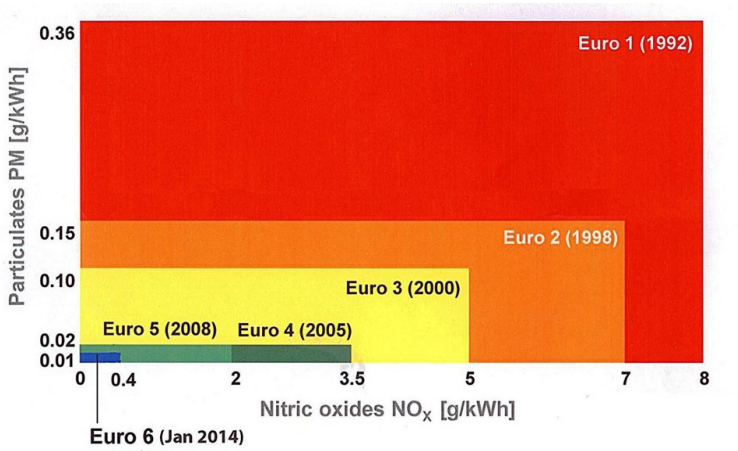

Figure 1.2 – EU Emissions Standards, Exhaust emissions Euro 1-6 [120]

In addition, due to the high volume of traffic in cities, there are more and more additional regulations for the maintenance of air quality and noise pollution. In order to protect human health from hazardous emissions, many European cities introduced regulations for environmental zones that allow to move there only for vehicles that meet certain emission standards.

The global vehicle fleet is growing rapidly and the 1 billion-unit mark was reached for the first time ever in 2010 [180]. The number of vehicles on 1st of January 2019 has already reached around 1.3 billion [109] and the global auto industry expects to sell more than 77 million vehicles by the end of 2019. According to growth of the global vehicle fleet, the fuel consumption of vehicles is also increasing every year.

There are some possible approaches for reducing of exhaust emissions by the vehicle operation like a minimization of the mechanical energy demand of vehicle, optimization of the internal combustion engine drive system, optimization of vehicle operation and traffic flow [120]. But the main and general disadvantage of modern vehicles is the usage of internal combustion engines. Internal combustion engines are very inefficient by converting the chemical energy in terms of fuel to the mechanical energy. However, more than 60% of energy losses are attributed directly to internal combustion engines. The other losses in the form of transmission losses are about 6%, losses in idle mode are about 16% and about 3% may be losses spent on the consumption of different accessories. This means that the final energy output is below 15%. Also, internal combustion engines have almost completely exhausted their ability to increase efficiency and have the obvious issues with high oil prices. In addition, global oil reserves will not be available indefinitely.

In order to fulfil mobility needs in the future, new drive technologies are required. In view of the foregoing, it becomes clear that the direction associated with the so-called "green technologies" in the automotive industry is the most promising way for the development of road transport. The electrification of the drive represents a possible leap in technology.

Therefore, there is currently a worldwide trend towards active development of the electric vehicle segment. According to Morgan Stanley's report, electric vehicles will be sold more than gas-powered vehicles by 2040. Global demand shifts towards to the simple, efficient, compact, cost-effective and fully integrated smart solutions. This is why vehicle manufacturers need to integrate electric drives into their vehicle fleets and increase the sales of electric vehicles. As can be deduced from Figure 1.3, electromobility has developed into

a key technology for achieving the climate protection targets, which is why the number of electric vehicles worldwide increased by 660 % between 2014 and 2018.

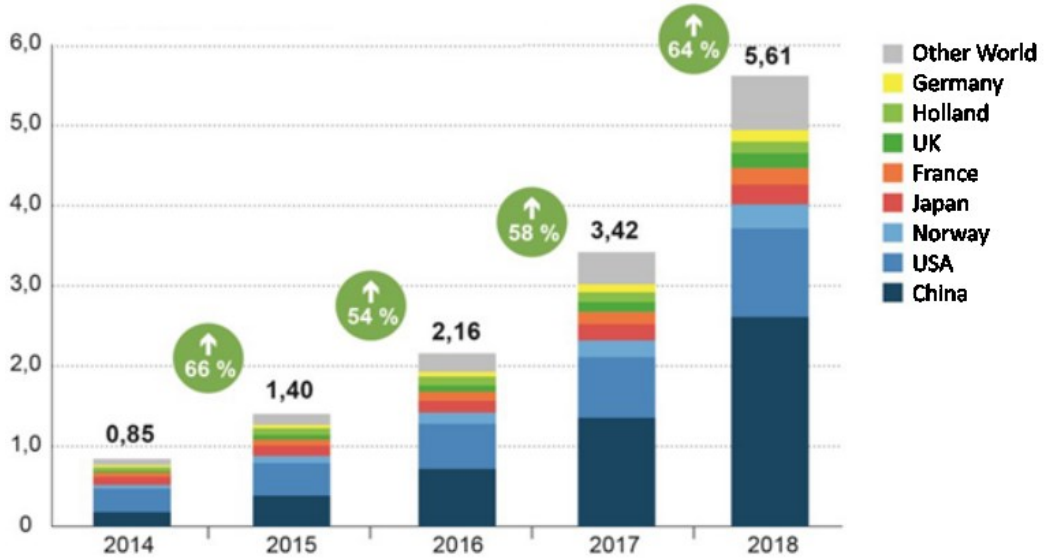

Figure 1.3 – Inventory development of electric vehicles worldwide until 2018 [132], [194]

Not many people know that electric vehicles were developed by the automotive industry at the beginning of the 20th century. However, already in 1881 French electrical engineer Trouvé developed the first electrically powered vehicle in the form of a three-wheeled bicycle (Figure 1.4, (a)) based on the first lead-acid batteries [63]. And Ferdinand Porsche built the first Lohner-Wagen in 1899 (Figure 1.4, (b)). In the course of the Universelle Exposition in Paris in 1900, Porsche exhibited the Lohner-Porsche electric vehicle equipped with electric motors on the front wheel hub. Later on, down the line, based on the Lohner-Porsche-Elektromobil, also the first model of a vehicle with a combined power plant was created – Mixt Wagen. In this vehicle a gasoline engine was used as an actuating source for the generator, from which electricity was removed by the battery supplying the vehicle's electric drive.

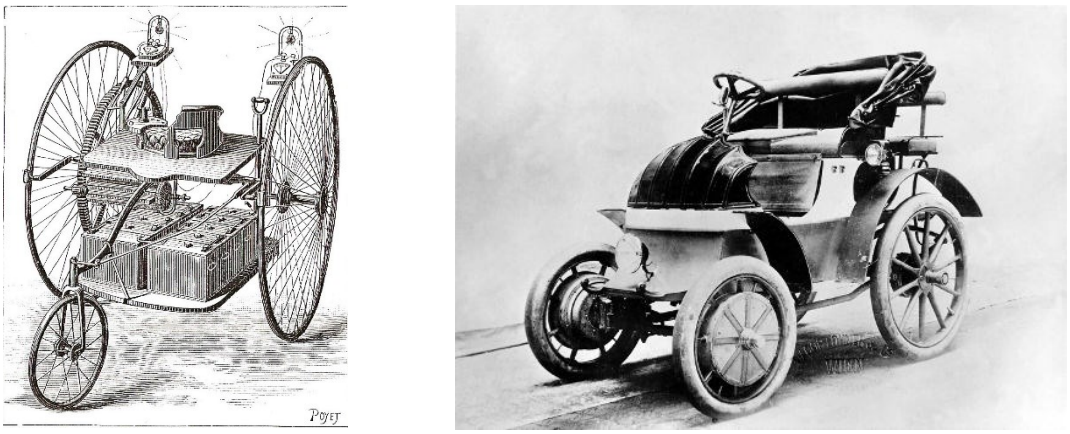

a b

Figure 1.4 – The first vehicles: a - Electric vehicle of Trouvé [38], b - Lohner-Porsche-Elektromobil [97]

The first generation of electric vehicles have sometimes even shown to be more powerful and reliable than passenger vehicles equipped with an internal combustion engine. However, internal combustion engines have been continuously developed and improved and have become a mainstream powertrain solution for a means of transport. In the end they were able to prevail against the electric drive because they had a much greater range. In addition, vehicles with internal combustion engines were quickly refueled, while the charging of electric vehicles was longtime. Before World War I, about 30 thousand electric vehicles were used in the USA and

Great Britain [118]. In 1913 Ford introduced the assembly line for vehicles for the first time, namely for vehicles with combustion engines. For this reason, also the production of electric vehicles almost came to an end by the begin of the 1920s. Further technical advances like the invention of mufflers and the electric starter improved disadvantages of vehicles with internal combustion engine. Therefore, electric vehicles were practically no longer built since 1920. However, there were exceptions: After the Second World War, a small percentage of electric vehicles were in use in Japan, and in the United Kingdom, a certain number of electric vehicles in the 1950s-60s provided a solution to the transport problems of urban services such as delivery and postal services. By the beginning of the 70s, there were about a million electric vehicles in the world, and basically, they were used in the field of public services of big cities, postal departments, railway stations and airports, hospital complexes – these are micro-electric buses, vans, pickups and other special vehicles. These electric vehicles had a low maximum speed (30-35 km/h) and a limited range (60-65 km) [165].

Currently, there are appearing designs and technological projects that provide sufficient efficiency for electric vehicles. At the same time, competition between traditional brands of vehicles with internal combustion engines, electric vehicles and cars with combined power plants is increasing more and more.

In the case of electric drives, they are an important element required to enable sustainable mobility concepts. Furthermore, the integration of the electric machine in the powertrain of electric vehicles opens up various powertrain topologies. The researchers of recent years are increasingly concerned with a variety of electric motors for application in vehicles. Electric motor offers great advantages and potential in the passenger car and commercial vehicle sector. However, these are contrasted with the great constructive and monetary effort associated with the integration of electric drives in existing vehicle concepts.

One possible solution to this problem is the in-wheel drive, in which the electric motor together with power electronics is integrated into the rim of a vehicle. By comparison of a traditional electric drive system with a system where the main elements are in-wheel motors, the last has unquestionable advantages. Especially the transfer of the drive unit from the vehicle interior into the wheels offers a great advantage in the vehicle package and the weight distribution of the vehicles. In addition to the advantage of weight reduction, there is another great advantage – a freedom in vehicle design and construction. Vehicles can be shorter and the passenger area can be more generous. The elimination of the drive train allows completely new vehicle concepts. This is why in-wheel motors open up a design that can be specially adapted to a wide range of functionalities.

An in-wheel motor, as a modular element of an electric drive, has been known for a long time. However, the use of such constructive solution for vehicles until recently was impossible for several reasons. First of all, because of the impossibility in developing a compact, highly economical drive that conforms the necessary requirements of having high continuous torque and be light-weight at the same time. The requirement for low weight is associated with an unintended increase in the additional unsprung mass, which leads to a higher dynamic load on the wheels and requires a high torque for various operating conditions. Thus, the motor wheel should be powerful, high-torque and dynamic on the one hand, and reliable, safe and fault-tolerant on the other. In order to synthesize the optimal ratio of these parameters in a particular motor, it is necessary to solve many interdisciplinary problems.

2. State of the Art

The state of the art of the present work describes the general drive techniques of the electric vehicle achieved at the present moment with a special interest on the in-wheel motor. The first section provides a brief overview about the different types of electrical machines and discusses possibilities of their integration into vehicles. Furthermore, the second section provides an overview of existing electrical power train concepts and takes notice of classification of the in-wheel motor solutions. The principal characteristics of the in-wheel motor are presented in the third section. In this context, the boundary conditions of the application are also discussed and the relevant requirements are derived. Various approaches of the previously presented in-wheel motors are investigated in the fourth section. In this chapter, the investigated in-wheel motor concepts are presented. Subsequently, these in-wheel motors are compared with regard to their characteristics, gravimetric power and torque densities and their presentation date is evaluated. Based on the outlined state of the art, the chapter closes with a problem statement and objective of this work.

2.1. Taxonomy of Electrical Machines

Electrical machines are used to transform electrical energy. The mainly two operating scenarios of electrical machines can be divided into two modes: motor or generator. If electrical energy is transformed into mechanical energy, then it is called a motor operation mode. The transformation of mechanical energy into electrical energy takes place by generator operation mode [156].

The electric motors can be divided into two groups: commutator and commutatorless motors. The first group indicates that the machine has a mechanical commutator, while the second group does not have a commutator and commutates electrically. Both variants consist of a stationary part – the stator, and a rotating part – the rotor. Furthermore, there is a difference between the active part, which is relevant for energy transformation, and the inactive part, which includes, for example, the housing of the electrical machine [156]. The active part includes stator and rotor windings (or in the case of permanently excited machines – permanent magnets), as well as all components that hold windings and magnets [108]. Basically, there is a possibility of using all known types of electric motors in electric vehicles. The decision for a specific vehicle depends on the expected driving conditions. More criteria such as cost, motor performance, maintainability, recyclability, service life, power density, efficiency, material selection, frequent starts and stops etc. must be taken into account by selecting the motor type [88]. Figure 2.1 demonstrates a taxonomy of main principles of electric machines with six sub grouped common types of the electric motors for the application in electric vehicles [30].

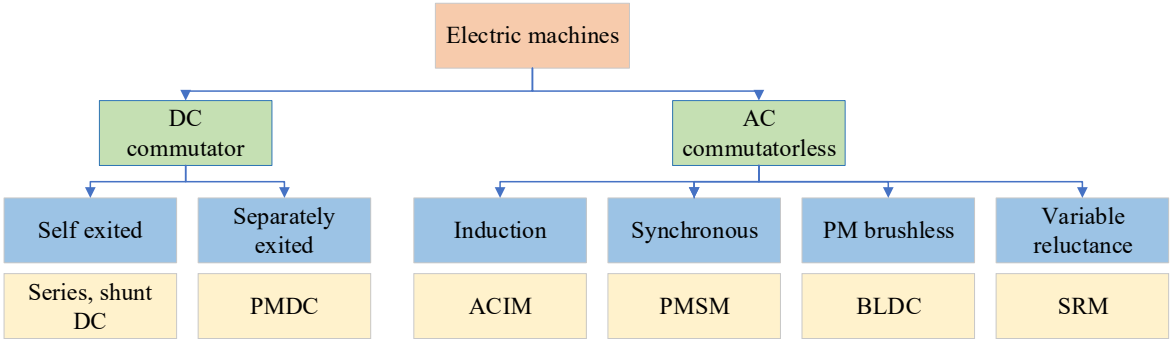

Figure 2.1 – Taxonomy of electrical machines

To get a closer view, electric motors presented in Figure 2.1 are compared in the following. Commutator motors are presented by traditional DC machines. In addition, DC machines are distinguished between self and separate excitation. The operation of DC machines requires commutation to generate a rotating field. The magnetic field in the DC motor is created through the contact between the brushes and the commutator by

applying the voltage to the rotor windings. Simultaneously, a magnetic field is created in the stator by permanent magnets or field winding. Hence, the rotation of the rotor is caused by the interaction of these two fields. Nowadays, the mechanically commutated DC motors are irrelevant for the use as the motor in passenger vehicles because of a significant loss generated by the commutator and by low copper utilization. This type of electric machine can still be found in low-power machines due to its low costs and simple controllability [88].

Nowadays, the commutatorless electric motors become more attractive for an application in electric vehicles, because of their high efficiency, high power density and low operating cost. In commutatorless or AC motors, the magnetic field is generated by applying voltage to the stator. This changes the orientation of the field according to the current flowing through the stator, creating a rotating magnetic field. The interaction of the stator with the rotor magnetic field causes the stator to rotate around its axis. The type of the AC motor determines how the magnetic field in the rotor is created. The deeper classification of the AC motors suggests the four main motor types: switch reluctance, permanent magnet brushless, induction and permanent magnet synchronous motor. The differences between these motor types are caused in the way of energizing their windings. Thus, the first two types use rectangular voltage of power supply, while the second two types have to be supplied with the sinusoidal voltage.

Induction motors are the most advanced technology among commutatorless motors. The characteristic property of the operation principle of the induction motor is the so-called slip, which is needed for torque generation. The slip is the difference between the speed of the rotor and the speed of the rotating magnetic field of the stator. That is why these motors are often called asynchronous. Compared with DC motor drives, the AC induction motors are more attractive for applications in electric vehicles due to their advantages of lightweight design, high efficiency, compact volume and low cost [30].

The variable reluctance motors consist of the stator and the rotor consists of salient poles or teeth. This kind of motor uses the magnetic reluctance to produce torque. This is achieved by the energizing of pair of opposing stator coils and the magnetic flux path is generated in the rotor. In this case, the rotor will start to rotate to minimize the reluctance of the magnetic path [81], [61]. On the one hand, the biggest advantage of a switch reluctance motor for electrical vehicle applications is a simple construction, low manufacturing cost, and outstanding torque-speed characteristics. On the other hand, big disadvantages include its sensitive air gap height, relatively high noise impact and a non-uniformity of operation due to torque ripples [49].

A synchronous motor with permanent magnets is a motor with a rotor consisting of permanent magnets and a stator consisting of windings. The rotor of synchronous motor has its own magnetic field, which is generated by permanent magnets. By this kind of motor, the rotor operates at the same speed as the rotating magnetic field of the stator. This type of electric machine is required with an increasing tendency in automotive area due to its large range of high efficiency and high-power density, silent running, compact form, reliability and minimum maintenance [30]. Nevertheless, the complexity of the control system required for speed control and the high costs limit the spread of this type of motor. But with the development of power semi-conductors and microprocessors, this cost factor measures up economically the selection of PMSM machines.

PM brushless DC motor presents the virtually inverted PMDC motor with commutator. The main advantage of this motor type is the ability to produce a large torque because of the rectangular interaction between current and flux. The difference to the PMSM motor builds the way of voltage supply, which is rectangular for PMBLDC and sinusoidal for PMSM [60].

From today's point of view, the top position for the application in the automotive propulsion is held by permanent magnet synchronous motors, which provide extraordinarily high efficiency [31]. This property of PMSM motor guaranties the lower energy consumption in a vehicle. In addition, this type of motor has undeniable advantages, making it the most promising technology for automotive traction applications:

- high torque and high power output per volume in combination with high efficiency,
- excellent dynamic performance,
- minimizing of cooling requirements,
- simplification of construction and maintenance low cost assembling,
- high integration level.

One of the new kinds of PMSM motors represents the motor with the application of special winding. This winding is a combined winding consisting of the air gap and slot windings [20] [91]. The fundamental

difference to the previous described PMSM motors is the flat copper wire winding, which is applied in a meandering shape on and in a very thin and therefore light slotted back iron of the stator. Thus, the lightweight design is combined with an optimized magnetic circuit and an efficient combination winding. The design generates a very high torque with small size and low ohmic and magnetic losses. This ensures a high energy density, making the concept perfectly suited for the use as an electric in-wheel motor.

2.2. Electric Drive Concepts and Types of In-wheel Motors

Historically, in terms of the realization of electric drive, the design of electric vehicles has changed significantly. The traditional topology of the powertrain clearly defines the boundary conditions in terms of space, aerodynamics and passenger and pedestrian safety, which requires additional compromises in vehicle design. However, the new electric cars have the greatest possible flexibility and design freedom, as they allow for the integration of the main parts of the transmission in a wide variety of designs. It has been suggested [30] that there are six variants of electric powertrain architecture. Depending on the number, position and power distribution of the electric motors, it is distinguished between central drives, near to the wheel drives (near-wheel drives) and in-wheel drives. The use or non-use of reduction gear doubles the variants and divides the classification into two groups: direct and indirect drive. In the following, the possible variants will be discussed in more detail. Figure 2.2 details the schematic representation of the main six possible configurations of the architecture for the electric vehicle, where the “M” is the motor and the “G” is the gear respectively.

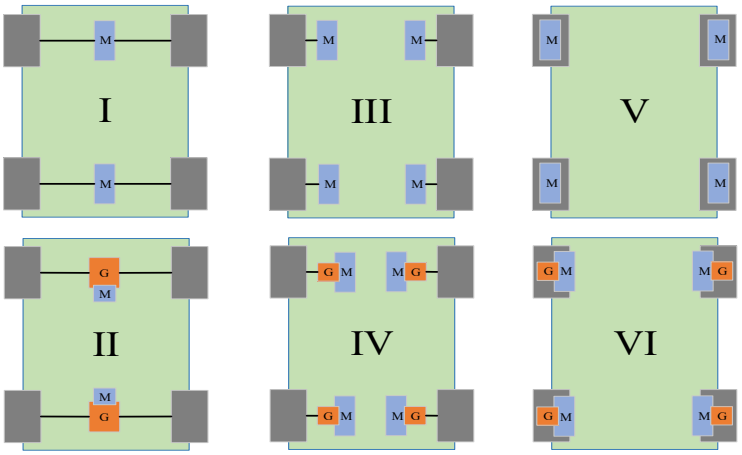

Figure 2.2 – Configurations of the architecture for the electric vehicle [71]

Variants I and II from Figure 2.2 correspond to the central drive version, when the vehicle has a combustion engine and the combustion engine is simply replaced by an electric motor. The first electric vehicles were realized in this way, because the costs of modification in this case are low. The difference between the variants I and II from Figure 2.2 is the absence of gear between the electric motor and drive axle.

In the topologies using near-wheel variant (see Figure 2.2, II and III) of an electric vehicle, the drivetrain is further simplified. Here, one electric motor per wheel is used because it eliminates the necessity of the connection of both axles (cardan shaft) and both axles can be driven independently. Besides the mechanical means, the differential action of an electric vehicle by cornering can be electronically provided by electric motors operating at different speeds [29].

The last possible variant is the so-called in-wheel solution presented in Figure 2.2, variant V and VI. This variant consists of wheel-individual electric motors, which are integrated into the rim. This enables it to influence the driving dynamics since all degrees of freedom on the powertrain side for this are given. Because of the fact that all wheels can be controlled independently, this concept is called single wheel drive [71]. Thus, speed control of the electric motor is equivalent to the control of the wheel speed and hence the vehicle speed. With the individually controllable electric motors, torque vectoring could be implemented very effectively, which greatly improves driving performance in curves. As by other arrangements, a distinction is made between gearless direct drives and high-speed drives with gears. By fully abandoning any mechanical gearing

between the motor and wheel, the motor is directly mounted into the wheel rim, so the direct torque transfer occurs without any mechanical loss or additional parts. It is also possible to use two or four motors, two or four driven wheels per vehicle. In this way, identical motors can be used for different vehicle classes. The highlights of the in-wheel motor solutions are going to be explained in more detail in the following sections.

Regarding the in-wheel motors, there are two types of them, with an internal rotor and with an external rotor, shown in Figure 2.3. In the case of the internal rotor, the motor shaft, which is attached to the wheel hub, rotates. In the external rotor variant, the motor housing, which is attached to the rim, rotates. In addition, there are two further possibilities for the external rotor:

- partially integrated in-wheel motor with external rotor, where the rotor is connected to the rim,
- fully integrated wheel hub motor with external rotor, where the motor housing is a part of the rim.

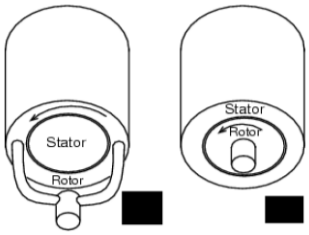

Figure 2.3 – Motor with internal (right) or external rotor (left) [173]

The outer rotor solution is well adapted to in-wheel motors since the rotor can be directly fixed to the wheel. Outer rotor solutions have a higher diameter of air gap and consequently higher specific torque, which makes them a better choice for vehicle propulsion application [11]. From another point of view, it is also easier to manufacture the stator windings because the stator surface point outwards. Moreover, outer rotor designs are around 15% lighter than an inner rotor machine with the same torque [181]. However, external rotor machines can be more difficult to cool in some applications because the windings that normally generate the highest losses are located in the inner part of the machine [65].

The further classification of the in-wheel solution can be divided in the structural difference by the arrangement of the motor active parts in relation to the wheel axle (see Figure 2.4). The classification whether axial or radial morphology is determined by the force application of rotor and stator active parts. An axial morphology of rotor active parts is often called bell-shaped rotor and a radial morphology is called disc rotor [102]. The axial morphology found its application in high power and high torque applications due to the large ratio of diameter to length. One of the specific advantages is the possibility of field weakening, which could be realized by changing the air gap thickness [126]. The disadvantage of axial morphology suffers from the problem of large axial force exerted on the stator by the rotor and limited to disc shape. In [103] it has now been suggested the to compare axial and radial arrangements using the PMSM electric machine. The analysis shows that a higher torque and thus a better power-to-weight ratio is achieved by radial motor design and from a larger effective radius. Regarding the electronic function, there is no difference between radial and axial arrangement of the magnets [103]. Additionally, [181] mentioned few further advantages of the radial arrangement as well as higher field intensity, easier manufacturing of magnets, and equalized magnetic forces between stator and rotor.

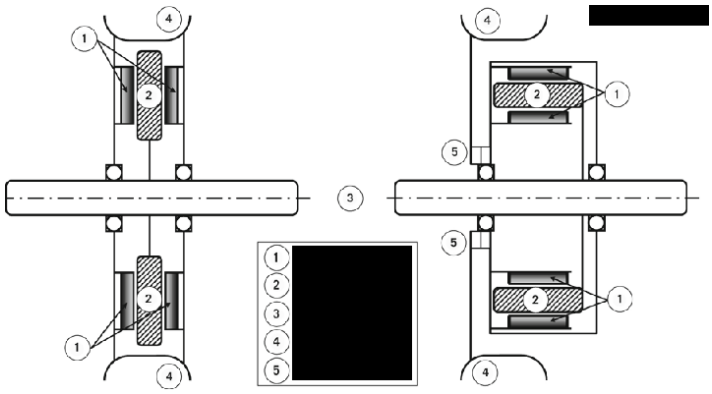

Figure 2.4 – Structural arrangements of the motor active parts: axial (right) and radial (left) [103]

2.3. Advantages & Disadvantages of In-wheel Motors

The application of wheel-hub motors brings fundamental advantages for electrical vehicles. Vehicles with electric in-wheel motors have a number of significant advantages over traditional concepts of electric vehicles, which are described in the following.

Efficiency: The most important advantage of the in-wheel motor is the comparably better efficiency, because of the deficiency of many complex and heavy transfer mechanisms between the motor and the wheel, like clutch system, transmission, drive shafts and differentials. This advantage includes the minimization of energy losses in the transmission of driving power through direct connection of motor and wheels. Therefore, the lower mass of the in-wheel unit enables a lower total weight as by common vehicle, thus the higher efficiency and increased range due to a better energy economy can be achieved [69].

Simplicity: Furthermore, the absence of interposed elements between the motor and the wheel ensures that the design of the in-wheel motor is extremely simple. Particularly noteworthy is the fact that when using in-wheel motors for changing the direction of rotation, no additional gear is required as with conventional gears, as it can be easily changed by the controller. Technological simplicity and lowering the number of parts in the vehicle also ensures low cost and reliable operation of in-wheel motor systems [101].

Integrability: In addition, the drive system allows further functions to be integrated into an in-wheel system. For example, the integration of the power electronics in the installation space of the motor and integrated cooling minimizes the number of connections for supply lines [59]. The integrated electronics also ensures short cable paths and high EMC safety. Furthermore, it is possible to combine braking, damping, suspension and steering in one component [106].

Design freedom: The elimination of traditional parts and units also means that there is more space for other components which could be a battery pack, fuel cell, generator or just cargo room. Thus, the vehicle architects change the way vehicles look and perform and enables completely new vehicle concepts, such as the so-called skateboard design, where all necessary powertrain components are placed in the underbody [107].

Response behavior: Generally speaking, in-wheel motors offer the possibility of achieving high driving dynamics by very quickly adapting an individual strong drive torque to each wheel due to the lower propulsion response time and a much more direct response behavior. This could be realized even at the lowest motor speed directly on the wheel. In comparison to conventional motors, where the driving torque first must be transmitted to the wheel through a large number of mechanical components [52].

Maneuverability: The controlled in-wheel motor makes the vehicle extremely maneuverable because all wheels can be rotated at different speeds and even into different directions. The vehicle is able to turn and park in the most difficult conditions as well as to instantly adapt to the quality of the road pavement. In particular, this statement corresponds to the corner modules, which can rotate around the axis of the suspension [146].

Individual wheel steering: The individual wheel control makes it easier to implement additional driving dynamic functions. Such functions include the simple implementation of all-wheel drive functions as well as new potentials in terms of driver assistance systems and safety systems [132]. All advanced electromechanical algorithms, such as ABS, ESP, traction control, brake assist, or even torque vectoring is easy to program into the control software, and they offer the top benefit by acting separately on each individual wheel. The individual wheel control allows not only a positive influence on handling and traction, but also offers significant advantages with regard to the longitudinal and lateral dynamics, because an individual force distribution is possible [69]. Additionally, the elimination of a heavy motor in the front or rear area changes the position of the vehicle's center of gravity. In case of usage of four in-wheel motors, the center of gravity is located in the geometric center of the vehicle, which optimizes the driving characteristics [178].

Recuperation: Energy recuperation in electric vehicles can be performed more easily than in conventional vehicles. The electricity, which can be stored and reused, can be generated by regenerative braking without losses through additional components such as gearbox, differential, etc. At in-wheel-motors, recuperation can be done directly by the motor itself, if the motor is used as generator. This enables to brake with the vehicle, whereby the conventional mechanical brake has to be used only for emergency situations [13].

Despite the fact that an in-wheel solution offers a number of crucial advantages over other technologies for electric vehicles, there are disadvantages and several technical barriers.

Unsprung weights: Anderson and Harty [5] reported that the obvious impact of implementation of the in-wheel motors in the vehicle consist in the increase of its unsprung weight. The unsprung weight thus leads to reduction in the road grip properties of the vehicle [122]. Less obvious effects are presented by increase of the yaw inertia and improvement in torque response rate. In addition, by increasing the unspring weight, the unsprung resonance frequency decreases and the sprung acceleration in the low frequency range increases. Humans are most sensitive to the vertical vibration of 4-8 Hz. Therefore, an increase of the sprung acceleration in this range due to increase of unsprung weight significantly reduces the comfort level [112]. In addition, a groundbreaking article on the unsprung mass shows that while perceptible differences occur with increasing unsprung mass, these differences are generally small and probably undetectable to the average driver [5].

Cooling: The available drive torque depends on the power capacity of the motor and, in addition to the efficiency, on the cooling [52]. However, even by a high efficiency of the in-wheel motor, there are significant losses and heat impacts at the windings of the motor are occurring [145]. This heat can be dissipated by an active (liquid) or passive (air) optimally designed cooling system.

Limited power output: The weight and dimensions of electrical machines are scaled with the required torque. In such a way, the weight of the wheel increases with rising power [21]. As a result, by using gearless direct motors, the available power is limited.

Sealing and ingress protection: Motor sealing systems that protect the in-wheel motor against environmental influences cause a disadvantage, which is that the motor operation must be guaranteed at various environmental conditions that are typical for the automotive industry sector (e.g. IP-6K9K protection). Friction losses as well as possible high circumferential speeds of the seals must be taken into account. The selection of a material combination is not a trivial task in this case [59].

Safety aspect: Another disadvantage relates to the functional safety of the in-wheel motor. An illustrative example of this problem is selective torque control on the wheels, because incorrect adjustment of the torque on the wheels causes undesirable jerking along the vertical axis of the vehicle [59].

Misuse: The requirements on mechanical components inside the in-wheel motor are particularly high. It is necessary to ensure that the complete system continues to be functional even in case of misuse or threat of operation. It is also necessary to anticipate any unexpected (vandalism) and predictable (curb, potholes on the road) situations during motor usage. For example, one of the most important parameters of the electric motor of the in-wheel-motor is the air gap between the stator and the rotor. The air gap must not average below the minimum value under all driving situations and loads. Avoiding these external loads and at the same time transmitting the drive torque to the wheel is not a trivial task that could therefore only be solved by developing special devices. However, the functionality of the motor must be provided under all driving situations and loads, otherwise there is a risk of malfunction, which would lead to the defect of the whole vehicle and building of a dangerous situation on the road [134].

Costs: Another disadvantage is the costs associated with the high cost of some motor components as well as development costs. In comparison to other drive concepts, in-wheel motors are 1.5 times more expensive than, for example, a central drive motor [151]. In addition, nowadays, such technology is not a mass-produced product, which significantly increases its cost.

Considering all relations between advantages and disadvantages, it becomes clear that the in-wheel motor, as a key component of drive technology, has a realistic prospect. However, commercialization of the in-wheel motors has yet to be achieved because of the difficulty of miniaturizing the motor [36]. Numerous successes in research and development are only a small step towards to the market introduction of the technology into the broad masses [102]. All technical obstacles should therefore be overcome in the coming years.

2.4. Situation on the Market

The above-mentioned advantages and disadvantages lead to a rising interest for in-wheel motors. An idea of an electric vehicle as well as the idea to place an electric motor inside the wheel are not new. The in-wheel motor first appeared in 1884 by the patent of the Wellington Adams, who patented an electric wheel motor equipped with a complex gear [3]. As it was mentioned in the introduction, the so-called Lohner-Porsche was built with four wheeled electric motors, but due to the use of lead batteries, which itself weighted 1800 kg, it

was too heavy. An in-wheel motor or also called wheel hub motor, is an electric motor which is placed inside the wheel. The technology of in-wheel motor is going through a renaissance nowadays. Recently, there have been increasing reports that a number of OEMs developing electric vehicles with motors inside the wheels and each organization is quick to extol the virtues of in-wheel motors, especially versus internal combustion engines [135], [152],[169]. In the following, the most important developments of the last 20 years are discussed.

2004: Michelin, in cooperation with Peugeot, developed the Michelin Active Wheel, in-wheel motor which is installed as a rear-wheel drive in the Peugeot BB1 car and was first demonstrated in October 2008 at the Paris Motor Show. For this system, a traction motor without collector and with a vibration damping system is used. However, due to the high cost of such an electric motor with excitation by permanent magnets, its application as a drive system is rather preferable by integrating an in-wheel motor without vibration control system. Mainly because of increase in dimensions required for the design. Presented in-wheel motor has a total rated power of 30 kW and only 58 Nm torque and each wheel module has a total weight of 43 kg [33].

2005: The collaborative project by 35 participating companies and under managing by Keio University called Eliica, developed an electric vehicle that uses in-wheel motors as the main drive with the target to achieve a maximum instantaneous speed of 370 km/h as well as a 0-160 km/h-acceleration time of 7 seconds, representing a motor performance that exceeds all types of existing sport cars [184].

2006: Bridgestone's Dynamic-Damping In-wheel Motor Drive System uses an inner rotor type. The system overcomes the disadvantage of unsprung weight by using the motors themselves to function as vibration dampers. The special feature of the motor is the spring system and two tubular dampers that insulate the motor from the unsprung mass. In-wheel motor of Bridgestone claims improved performance for advanced electric vehicles with their dynamic-damping system [27].

2012: The Fraunhofer Institute for Manufacturing Technology and Applied Materials Research (IFAM) presented its first wheel hub motor LARA in 2015. This in-wheel motor was specially designed for high torque density. The Fraunhofer in-wheeler is based on a permanently excited synchronous machine with an external rotor. The power electronics is located in the stator and is also liquid-cooled as the stator windings. The motor thus has its continuous power of 55 kW (72 kW peak power) and continuous torque of 700 Nm (900 Nm peak torque). According to [45] and [89], the motor can be integrated into a 15" rim and weighs 42 kg.

2013: The Australian startup Evans Electric has developed a drive system for electric vehicles comprising four motors. They are integrated directly into the four 19-inch wheels of the Mitsubishi Lancer Evo3. The disc-shaped motors are three-phase machines with a continuous power output of 75 kW and torque of 625 Nm [42].

2014: The ECOmove company with their in-wheel motor Qwheel present a powerful and compact electric solution for the powertrain. Based on a compact PMAC traction motor, the full power-train is located within the wheel. The developer gives an option to choose what should include the system: traction, braking (disc caliper, hand-brake and regenerative braking) and steering. In such way, a variety of requirements for torque, acceleration, speed and wheelbase are covered. The low-version of the system consisting the traction motor with gear has a total weight of 21 kg and delivers up to 44 kW power (24.5 kW continuous) and up to 490 Nm torque (384 Nm continuous) in each wheel [44].

2016: In 2016, the automotive supplier Schaeffler presented the current development status of its "E-Wheel-Drive" project with highly integrated in-wheel motor Gamma which is the third generation of Schaeffler developments. A single unit delivers up to 42.5 kW (continuous output 26 kW) and generates a torque of 810 Nm (continuous operation: 500 Nm). With a total weight of 53 kg, the wheel hub drive weighs 31 kg compared to a conventional wheel with wheel bearing and brake [37].

2019: At the Electric and Hybrid Vehicle Technology Expo in Stuttgart, Elaphe Propulsion Technologies presented their in-wheel motor L1500 for low-volume series manufacturing. The highlights of L1500 are their extremely high torque (up to 1500 Nm and 650 Nm continuous torque), high power output (up to 110 kW and 75 kW continuous power), low weight (34.8 kg) and unique, compact packaging. The special feature of the Elaphe is that the torque can be achieved without using any gears and the motors fit inside a 19-inch or larger wheel rim. The main idea of Elaphe is to integrate a developed motor in vehicles ranging from small cars to SUVs and light commercial vehicles with little or no compromise or re-engineering of the existing wheel hub and mechanicals, that is why the motor is compatible with rear, front and four-wheel vehicles [46].

2020: One of the most successful design solutions is the in-wheel motor of Protean Electric, one of the flagship companies in the in-wheel motor industry. Their current model, the PD18 has an integrated inverter, integrated control electronics and software controller. This integrated system of electric motor and control is called a system with distributed architecture. Here, the individual components are interconnected by a common information network to improve the reliability and safety of vehicle operation. In case of failure or incorrect operation of the system components, the motor reduces its performance, which does not lead to complete failure of the complete device. The motion controller of each motor is integrated by the corresponding control system in the vehicle, thus, it is possible to organize the process of control of the whole vehicle taking into account the variety of operating modes. As a result, a complex integrated component with obvious advantages over analogues with up to 80 kW power output (continuous power 60 kW) and up to 1250 Nm torque (continuous torque 600 Nm) with a motor weight of 36 kg is achievable [137].

a b

Figure 2.5 – Compact wheel module from: a - Schaeffler [147] and b - Protean Electric [136]

Since 2018, there has been a rapid further development and mutation of in-wheel motor sense and nowadays it is presented by corner modules (see e.g. Figure 2.5, (a) and (b)). It is caused by a specific need for mobility, making special vehicle concepts with corner modules necessary. Stakhanovites like Schaeffler and Protean have developed an innovative wheel module for this task, including the in-wheel motor and wheel suspension, along with the vehicle suspension system and the actuator of the electromechanical steering [147].

Common to all the concepts presented is that complicated manufacturing technologies are used, especially for the electromagnetically effective components. For traditional vehicles, excess weight in the structural design of the transmission is no critical point. But for the wheels, there is a completely different principle. That is why the total weight refers to the quantitative criteria as a criterion for the wide application and market expansion of the in-wheel motor. The next comparison criteria defined for the examination of the existing in-wheel motors are continuous torque and continuous power. The values of named criteria were presented in the literature mentioned above. To evaluate the criteria and distinguish between torque and power the weight of presented in-wheel motors was used. The trends of the relations of the torque/weight and power/weight relations over the last two decades are accordingly presented in Figure 2.6.

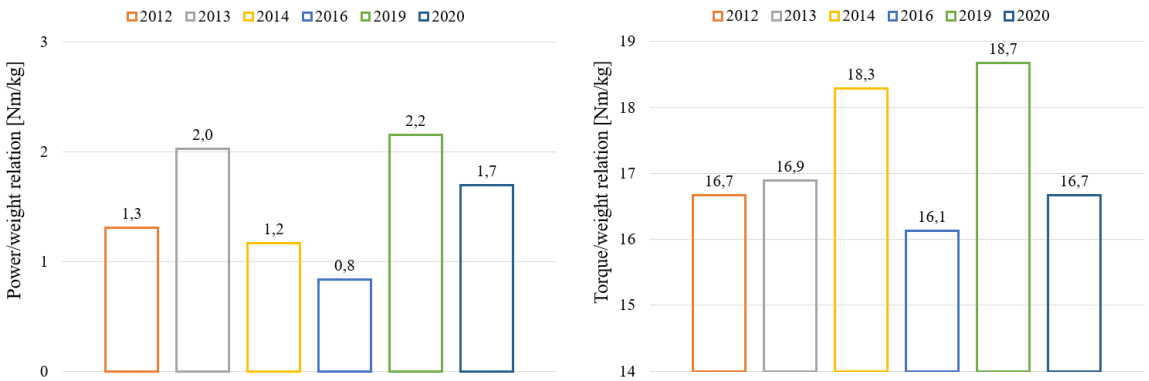

a b

Figure 2.6 – Trends of the power/weight (a) and torque/weight (b) relations

From the trends presented in Figure 2.6, (a) and (b), it becomes clear that in-wheel motor technology is gradually improving its quality performance of the considered criteria. The "strongest" representative on the market of in-wheel motors nowadays is a motor L1500 from Elaphe Propulsion Technologies with 2.2 kW/kg and 18.7 Nm/kg. The results for the year 2020 look stagnant, which is due to the fact that at the time of analysis only data for a quarter are available.

2.5. Existing in-wheel motors with air gap winding technology

As it was mentioned in 2.3 the main disadvantage of in-wheel motors is the additional weight which increases the amount of the unsprung weight in the vehicle. Therefore, by the development of the in-wheel motor a special attention on the lightweight design should be paid.

Since 2011, the Department of Mechatronics of Institute of Mobile Systems at the Otto-von-Gericke University Magdeburg developed, built and tested under the leadership of Prof. Dr.-Ing. Roland Kasper in-wheel motors with special winding – air gap winding (Figure 2.7). This special winding represents an ironless winding. An ironless winding is a winding that has no iron material between the conductors. The advantages of motors based on ironless winding technology are the following: lower losses compared to conventional motors, which enables to reach high efficiency in combination with a high power density. Relatively simple motor design is characterized by the fact that the motor requires only a low amount of conductor material and back iron, so by using of the innovative air gap winding in the permanent excited electric machine can be realized the material savings while keeping the equal magnetic flux density [20]. As a result, the motor with air gap winding has a compact lightweight design and therefore is especially attractive in the application area of electromobility. The first systematic study based on the air gap winding was performed by Borchardt in [17] and [19], where parametric model of a novel electrical machine that allows fast and precise magnetic circuit calculations was presented. And also, the ironless air gap winding technology was patented in 2013 under patent number WO2013/029579 A2 [92].

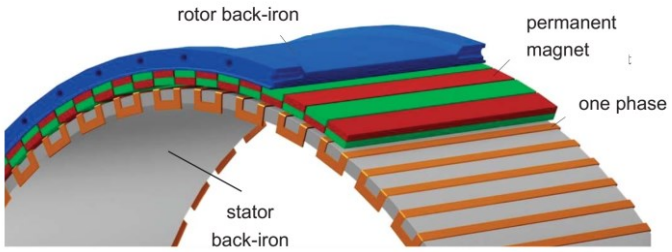

Figure 2.7 – Principle of the air gap winding [20]

The first prototype of an electric machine with the air gap winding, also known as Elisa I in-wheel motor, represents the lightweight construction concept for the application in automotive, shown in Figure 2.8, (a). The in-wheel motor Elisa I arose from the third-party funds research project sponsored by the state of Saxony-Anhalt in Germany in cooperation with the local state companies [54]. The Elisa I motor was planned as a pure motor for test bench measurements with the idea to use methods for the further serial production. Special feature of the motor is the near-series design, characterized by the integration of power electronics, universal connection to suspension system of the vehicle and the application of modern calculation methods for the simulation of mechanical, electrical and thermal properties of the motor. Therefore, it was particularly improved the magnetic components in terms of materials and geometry, as well as to reduce friction losses of the bearings by adding ball bearings in order to influence the efficiency and power density of the motor. The result of this project is the prototype of the in-wheel motor with such highlights as nominal torque of 300 Nm and nominal power of 40 kW provided by the casted stator with app. 300 mm outer diameter and the 100 mm magnet length [96]. The prototype with a weight of only 20 kg delivers a power-weight ratio of 2 kW/kg [97].

Nevertheless, project Elisa I met some problems in manufacturing method, whereupon was developed project Elisa II, see Figure 2.8, (b). In Elisa II design, the functional components were placed differently and calculated more specifically in order to meet the requirements for suspension space and weight. The in-wheel motor is calculated for the integration into a 15” rim. By using of a brake concept with internal brake caliper, the motor

can be combined with a wide range of common chassis systems. A further feature of the developed motor is the use of a lightweight sandwich structure consisting of balsa wood in the area of the side covers of the rotor to keep the unsprung weight of the motor as low as possible. Elisa II motor has more reliable construction and is made with higher accuracy. Power of the motor is declared by 40 kW by rated torque of 300 Nm. The motor is operated with maximal current of 100 A and voltage of 400 V. The motor weight is only 20 kg without breaks and 25 kg with breaks [188].

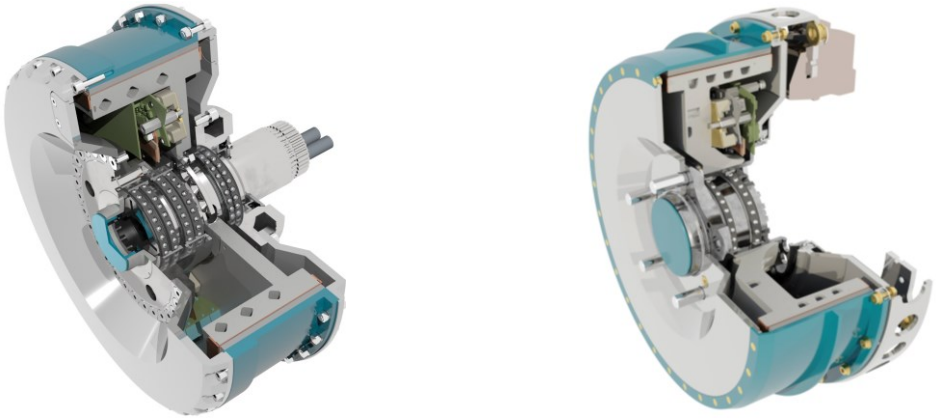

a b

Figure 2.8 – a - In-wheel motor Elisa I [188], b - In-wheel motor Elisa II [188]

As the next step of development based on the in-wheel hub motor Elisa II an in-wheel motor called Editha was developed, which can be mounted on the non-modified rigid axle of the Smart Fortwo. The service and parking brake system, the wheel carrier, the electrical connections and the cooling supply lines were designed to suit them in the given installation space of the vehicle. Another specific modification is running on the secondary bearing position that is designed as a thin-section four-point contact bearing with a flange ring to absorb tilting moments during braking [100].

In parallel with research activities aimed at improving the innovative winding technology, several projects have been initiated to implement this technology in other applications. The most technologically advanced follow-up project was 4.5 kW in-wheel motor for lightweight electric scooter with a speed range of up to 45 km/h, as it shown in Figure 2.9, (a). Flexibility and scalability of the motor design and its highlight - air gap winding, made it possible to develop a perfect design by unique integration of the motor into the rim at the total weight of the motor by 2.7 kg. This allowed to keep the total weight of the scooter by 32 kg. The structural feature of this motor was the flat stator design, which allowed the motor to have air-cooled cooling system [96].

Another example of air gap winding application is the project dedicated to a generator integrated into trailer wheels. This generator is used to recuperate braking energy, which can be used for the operation of various additional units such as a refrigeration system. The designed generator can generate up to 30 kW of power at speeds of up to 350 rpm. This air-cooled generator, integrated in the trailer wheels, has a great advantage of operating as an additional equipment without significant changes in the design of the trailer axles [96].

The extremely low power consumption of flyboats was used in the next project to overcome the range limitations of battery-operated boats. Two slim cylindrical motors based on the air gap winding technology (see Figure 2.9, (b)) were integrated into the flyboat, providing 11 kW of power to drive the boat. Due to the optimization of the cooling system it allows the speed range of 600-2600 rpm for this power value. This significant advantage helps to use low energy in the flight mode for the maximum speed, what allows to save the energy and reduces the size of the batteries [96].

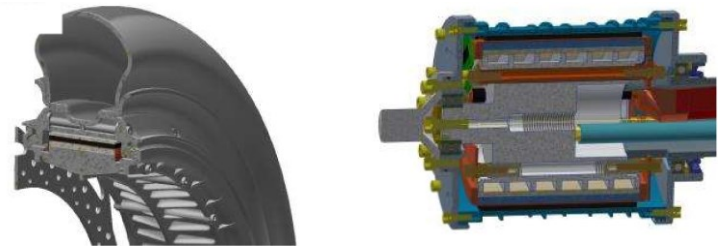

a c

Figure 2.9 – a - In-wheel for electric scooter [163], b – Motor for flyboat [163]

Further examples of the air gap winding technology application in mobility are electric longboard and high torque motor for the trial motorcycle and in the area of the green energy are small wind and water mills generators.

As the next step in the development of winding technology, the new design concept combining air gap and slot winding with the same magnetic structure was presented by Kasper and Borchardt [91] and patented in WO2017125416A1. For this purpose, the current Elisa I motor with only the air gap winding was modified by the additional winding integrated in the stator back iron as a slot winding. The schematic representation of combined winding is presented in Figure 2.10. Besides the back iron of the stator, which was modified in the height, the active parts of the motor remained unchanged. Using this modification, the torque of the existing Elisa I motor was increased to 480 Nm and power to 62 kW. At the same time the weight of the new design of the motor has only 1 kg more compared to the original design.

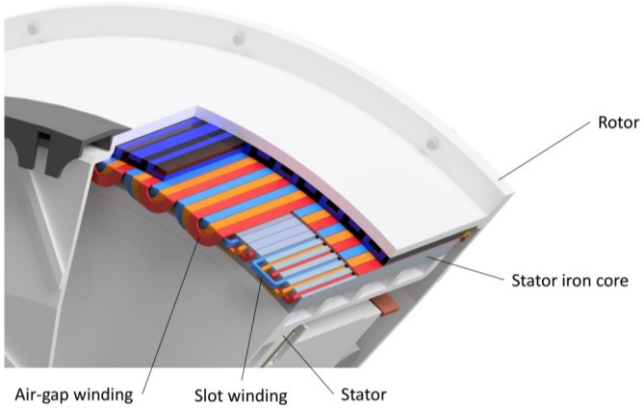

Figure 2.10 – Scheme of the combined winding

In addition to the above-mentioned investigations directly into innovative winding technology, by the realization of projects and scientific activities, many issues related to different motor systems were identified and investigated, such as:

- Borchardt and co-workers presented in [17] and [19] design and model of the in-wheel motor with air gap winding, in [20] described the modelling and calculation of the motor with air gap winding, provided design optimization of electrical machines with air gap winding [16] and [21], introduced the winding machine for the automated production of the air gap winding,
- Kasper and Borchardt provided in [91] the study dedicated to the combination of slot and air gap winding types, Kasper et.al. presented FEM modelling and measuring process of the water generator in [95] and described a new mathematical approach for eddy current loss in the motor with air gap winding [94],
- Zörnig et al. [189] analyzed the different bearing systems of the different in-wheel motors, the frictional torques of the components and presented design aspects of the first generations of the in-wheel motors with air gap winding in [188],
- Golovakha and co-workers presented in [57] the control solution for the developed in-wheel motors,

- Vittayaphadung et al. [174] analyzed the deformation of the wheel hub bearing in the in-wheel motor by using of FEM simulations,

- Sauerhering and colleagues proposed in [145] an approach to investigate the influence of cooling channel geometry and thermal interface materials on the thermal load of an electric motor with air gap winding,

- Hinzelmann et al. in [74] investigated and described the winding process application of the combined winding in the hydroelectric generator,

- Schmidt and co-workers in [150] defined and implemented measuring methods of an electric machine with air gap winding based on a mathematical model and in [149] provided a deep analysis of the losses in the motor with air gap winding,

- Stamann et al. investigated in [162] and [163] the joining technology for the air gap winding by usage of double-sided adhesive electrical insulation films with thermally conductive adhesive layers.

2.6. Problem Statement and Objective

Considering the increasingly important role of the electric motor in transport systems, manufacturers of future in-wheel motors for the application in electric vehicles must take into account a variety of requirements for the motor design. According to the previous presented data recently developed in-wheel motors are available with a power/weight ratio of 2.2 kW/kg and torque/weight ratio of 18.7 Nm/kg. However, some of these concepts have a practical realization also in existent vehicles and even low-volume series manufacturing.

The use of the in-wheel motor variant in the electric drivetrain of the vehicle is significantly complicated, because with the reduction of the power of the motor the use of its active volume decreases and the energy characteristics of the electric vehicle become more limited. Thus, perspective directions of development of processes of designing and manufacture of the in-wheel motors are on the one hand development of an energy-efficient design of the electric motor with high power and torque and on the other hand a satisfaction of strict layout and weight-and-dimensional characteristics. However, in achieving both primary objectives, it is also necessary to take into account the requirements of modern designs of the in-wheel motor to ensure the functionality, strength design and manufacturability of the relevant motor components. The implementation of these requirements requires a new unconventional motor design with increased utilization of its active volume. The PMSM electric machine with special winding meets this range of requirements to the fullest degree. To close a scientific gap and to investigate a new type of the in-wheel motor, the present dissertation is dedicated.

The following is a brief outline of this dissertation:

Chapter 3 explains the parameters needed for development processes of the in-wheel motor. Theoretical basis for the description of the requirements for in-wheel motor are known partly from Chapter 2 and it can be extended with a market research as well as an analysis of the product environment and supplemented by individual requests of potential users. The requirements on the part of electric motor could be explained mainly on the requirements of the vehicle and they are considered accordingly to the specified parameters on the vehicle. Some requirements should be determined because of the novelty of the concept of the in-wheel motor. At the next level for the requirements, the characteristics are to be identified on the basis of market demand. This way a coverage of all requirements from the both sides can be realized. Collected requirements will result in a concept design which is specified in a draft version. However, the focal points are the mechanical and electrical components of the in-wheel motor.

In order to comply with the requirements from Chapter 3, in Chapter 4 the model of the motor and its parts are developed to clarify the structure of the motor study and to identify important cause-effect relations. The development strategy is segmented between main parts of the in-wheel motor: the electrical and mechanical parts and cooling system. To simplify the development of the motor, its parts will be divided into different subsystems. The developed subsystems have to comply with the theoretically optimal model, but at the same time manufacturing errors, a variation of the characteristics and a further simplification are allowed. The subsystems of the motor and the applications of individual materials are to be understood as typical and they may vary in certain applications due to different boundary conditions.

The production of the electric motor is characterized in Chapter 5 using an application of wide variety of manufacturing technologies. Apart from the conventional manufacturing methods for the production of motor

components, there are also technologies and processes available that can always provide specific know-how in the field of electric motor production. This chapter focuses on the special factors of manufacturing and determination of the manufacturing of the full-scale motor in order to further validate the findings of this research. Based on the simulation results, topology-optimized design and material data, the technological methods for manufacturing the developed motor of analyzed materials is established. In the following, an implementation of the specific design for the developed solutions of the electric motor according to the Chapter 4 is carried out.

Chapter 6 concentrates on a validation of the developed in-wheel motor as well as on the impact of boundary conditions and assumptions determined in this study. For this reason, the prototypes are metrologically evaluated and the measured properties are analyzed. The prototypes are measured in special test stands regarding their electrical, magnetic and mechanical properties.

Finally, Chapter 7 as the conclusion of this dissertation, summarizes presented research and concentrates on the main results of the chapters.

3. Study of Requirements for Development

The previous chapter showed that in-wheel motor is an innovative and perspective technology for automotive industry. Nevertheless, a development without exact knowledge of the input parameters is difficult, because the extreme input values can lead to oversizing the motor. This chapter explains the parameters needed for development processes of the in-wheel motor. Theoretical basis for the description of the requirements for in-wheel motor are partly known from the previous chapter and it could be extended with a market research as well as an analysis of the product environment and be supplemented by individual requests of potential users. In-wheel motors are an excellent example of a product that requires interdisciplinary thinking to meet the requirement before prototyping can begin. The requirements on the part of the electric motor mainly depends on the requirements of the vehicle and they will be considered accordingly to the specified parameters on the vehicle. Some requirements must be determined because of the novelty of the concept of the in-wheel motor. On one hand, there is no specification on the customer's part and there are a lot of degrees of freedom by development processes and, on other hand, it brings the risk that the customer needs will be not detected or over detected. For this reason, as many motor parameters as possible should be wrapped. The next level for the determination of demand is the characteristics based on market demand. In this way it is possible to cover all requirements from both sides. The collected requirements can lead to a concept design, which is specified in a draft. However, the focal points are the mechanical and electrical components of the in-wheel motor.

3.1. Requirements for the Vehicle

In-wheel motor is a complex mechatronic system where the electric motor is integrated into a vehicle wheel. It is the main part of the electric vehicle, but there are further important components. In practice, electric vehicle and its subsystems have a significant influence on the motor. Therefore, a cooperation of different vehicle subsystems is necessary to ensure the execution of basic motor in-wheel functions. In this section, the requirements for electric vehicles are discussed, which are necessary to further develop the in-wheel motor. In this section, some of these aspects are analyzed, some solutions are presented and some assumptions are made.

Besides the big number of generally accepted requirements for passenger vehicles like safety, economy and others, for the subsequent development of the in-wheel motor it is necessary to highlight parameters that have a direct impact on the development. The requirements for the in-wheel motor are discussed partly from the point of view of the objectives and partly from the point of view of the state of the art. The most important or general requirements for the in-wheel motor which are to be developed can be divided into the groups. The assumed requirements can be observed in Table 3.1 and correspond to representative vehicles available in the market nowadays.

Requirement	Vehicle	In-wheel motor
Geometry	●	●
Weight	●	●
Kinematics		●
Velocity	●	●
Energy		●
Aerodynamics	●	
Loads	●	●
Drive layout		●

Table 3.1 – General requirements of the vehicle and the in-wheel motor

Weight: To analyze the effect of various vehicle characteristics on the dimension of an in-wheel motor, various classes of vehicles are considered. There is a big variety of passenger vehicles on the market which is classified

in segments. The requirements for each segment vary significantly to each other. It is therefore first necessary to select the vehicle segment and a specific modification of the vehicle in order to determine the requirements of the vehicle in such a way that the integration capability is covered as far as possible, as well as the possible demand, especially for urban transport.

This work does not aim to compare general characteristic of the American, European and Asian markets, it will focus on the analysis of popular vehicles in Germany and which vehicles are most rationally compatible for application of in-wheel motor technology. The German vehicle market, showed on Figure 3.1, is strongly influenced by the following segments: compact cars, superminis and mid-size vehicle segments which together represent almost two thirds of the vehicle stock in 2018.

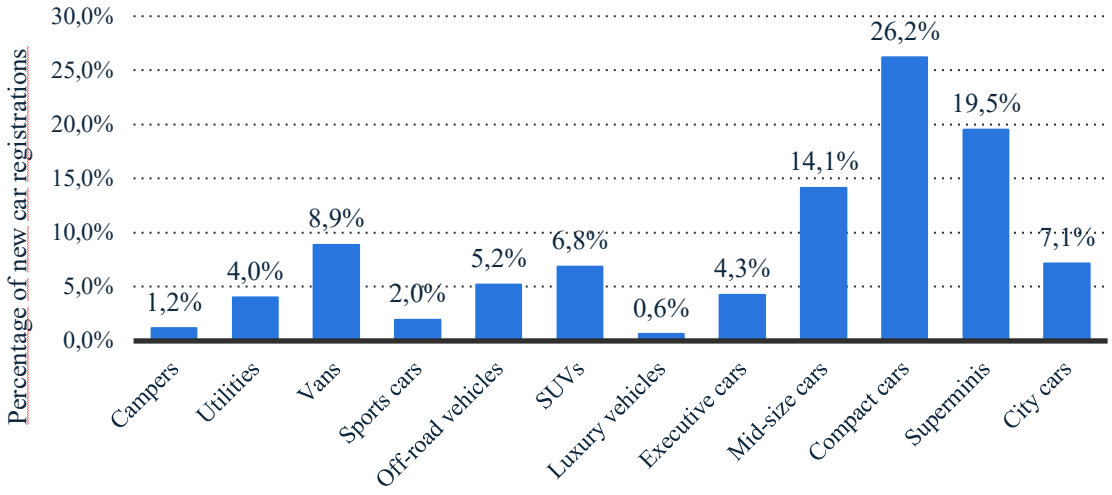

Figure 3.1 – Passenger car stock in Germany on January 1, 2019 by segments [109]

However, the segment profile of the passenger car stock in Germany is changing. It has been reported [56] that the car stocks of the mid-size and executive vehicle classes have decreased by around 15% since 2009 and the number of segments in some cases has gained in importance. These include above all the SUVs with a rise up to 180.4% and an increase in their percentage from 3.2% to 6.8%. This trend is due to the fact that SUVs can carry more people and cargo, are more comfortable, more fuel efficient and safer than other categories of passenger vehicles [139].

For any new application of technology in the automotive field, the demand for requirements of minimum weight is indispensable because weight influences the loads acting in the vehicle system. And loads and forces that arise from the vehicle drive are acting directly on the in-wheel motor. The value of the loads and forces is strongly influenced by the empty and total weight of the vehicle. According to [96] the average empty weight of the passenger vehicle in Germany in 2018 was 1515.5 kg. For the further development of the motor, mass-produced passenger vehicles widely known to the consumer – Audi A4 Limousine and Mercedes-Benz A-Class A220 – were used as the target passenger cars in terms of weight characteristics. Both automotive brands are a whole family of middle-class models with an average empty weight of 1450 kg and a total weight of 2000 kg by Audi A4 Limousine and empty weight of 1485 kg and total weight of 2010 kg by Mercedes-Benz A-Class A220. Thus, the maximum authorized weight m_v is 2010 kg and this weight will be used in further calculations.

Geometry: Based on the target vehicles, it is also possible to determine the size of the wheel's rim, which limits the assembly space for the integration of the motor. For the complete integrability of the developed motor, it is necessary to take into account the possibility of installing the motor into a wheel of a smaller diameter, so in the future the usage of an ultra-compact motor covers a larger range of wheel sizes. From this perspective, it also covers a larger segment of the customers' requirements.

A wheel by itself has to sustain a lot of load-scenarios: It carries the load of the vehicle, withstands lateral, drive and braking forces, and also absorbs friction and heat from braking. The wheel structure should follow a specific design so that the wheel can easily meet all these requirements. There are a lot of diverse wheel designs

but they should always primarily ensure the safety of the vehicle. A vehicle wheel presents a complex rotationally symmetric design consisting of rim (for mounting of a tire) and wheel disc (for attaching to a hub), moreover, the stiffness of the wheel in the plane of its rotation is significantly higher than its bending stiffness. The general construction of the wheel is shown in Figure 3.2, in which the letters indicate the following elements: A – wheel diameter, B – rim width, C – humps for additional internal fixation of tubeless tire beads, D – drop center is a bead perch of tires, E – wheel mounting surface, F – offset of a wheel, is a distance from the wheel mounting surface to the center line of the wheel, G – hub hole diameter, H – pitch center diameter. The significant dimensions for the wheel are a mounting diameter (A) and a width of the rim profile (B). Wheel dimensions are usual indicated in inches.

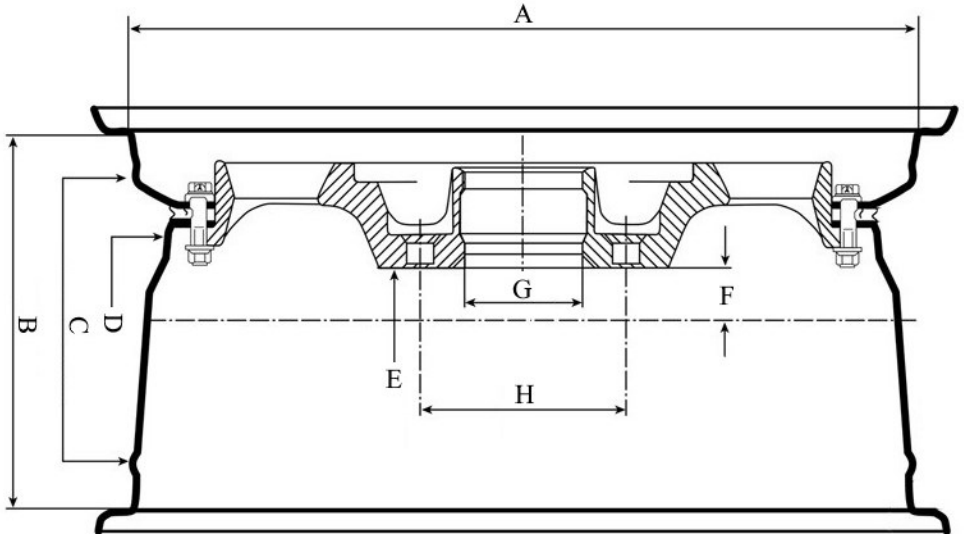

Figure 3.2 – General dimensions of the wheel [64]

A limiting factor for further integration of the in-wheel motor parts and assembly units are the already accepted target vehicles and suitable wheels for them. Accepted target vehicles are equipped with 16” wheels as a one of several possible sizes for wheels.

A value of the drop center in radial direction and the wheel offset in axial direction serves as a geometric limit for the further integration of the in-wheel motor. The rim base is the area between the rim flanges. Types of the wheels according to the variants of the rim base are shown in Figure 3.3. The most advantageous option of the variant relating to the integration criteria in the wheel is the variant of the flat base rim. However, the installation of modern tires without any drop center is inconceivable, so a compromise had to be found between the value of the drop center and the maximum offset to get the largest space for integration.

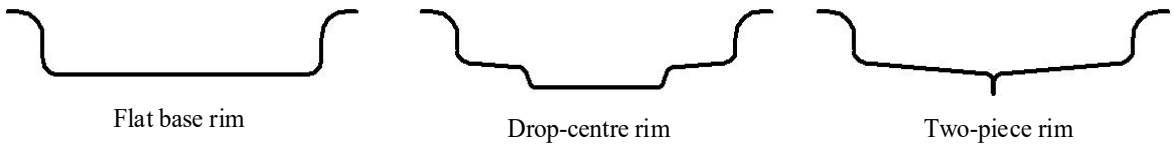

Figure 3.3 – Types of rims by the rim base

Another criterion for the wheel selection is the structural design. The distinction between structural designs of the wheels is shown in Figure 3.4. Wheels can be represented in integral and differential structural design. Multi-part wheels have the advantage that in case of damage only damaged parts must be replaced. In addition, the rim width and offset can be changed relatively easy and each section of the wheel can be made with the most suitable material, e.g. tough aluminum alloy can be used for the rim and lightweight magnesium alloy for the wheel disc. Another advantage for the integration of the in-wheel motor is the availability of an additional interface connection possibility by the usage of bolts that screw the parts of the rim together.

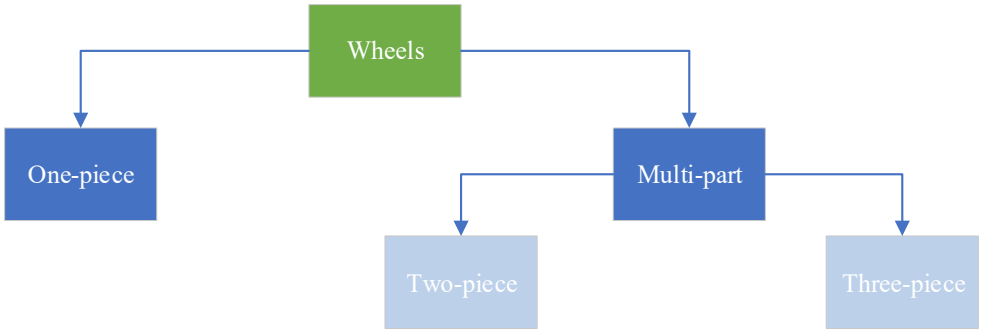

Figure 3.4 – Structural designs of wheels

According to the described facts, for further development, the 3-piece wheel ML of Schmidt with a size W_v of 16'' is selected, which allows to achieve a working space in form of a cylinder with an outer diameter of 356 mm and an axial width of 165 mm. The grey area shown in Figure 3.5 below indicates the potential volume of space for the in-wheel motor. More technical data for the selected wheel contains the Appendix A.

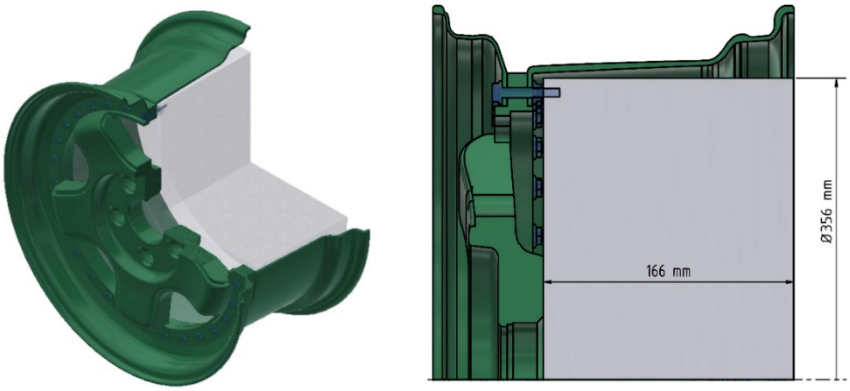

Figure 3.5 – Working space for in-wheel motor

Maximum speed: Recommended speed for vehicles on the German freeway amounts to 130 km/h, although this speed is maximum allowed vehicle speed throughout Europe. From this point of view, the requirement on the maximum speed of the vehicle should be increased by 10-15% to realize an overtaking of other vehicles on the freeway. Thus, the maximum vehicle speed V_{max} was taken to be 150 km/h. The maximum vehicle speed has a direct influence on the desired wheel speed ω_r and a proper influence on the maximum angular velocity of the in-wheel motor ω_{max}. It can easily be calculated from the vehicle's speed using the wheel dynamic rolling radius r_{dyn} as:

$$\omega_{max} = \frac{V_{max}}{r_{dyn}} \tag{3.1}$$

Wheel dynamic rolling radius r_{dyn} depends on the tire of the vehicle. The tire is an important link in between the road and the vehicle. This connection between the road and the vehicle transmits all forces and moments from the driving operation, and its transmission behavior plays an important role in the safety, handling and comfort of the entire vehicle. Considering that the developed in-wheel motor should cover the widest possible range of use, it was decided to use the Goodyear Vector 4 Seasons 205/60 R16 RF tire for calculations. The technical data and characteristics of the tires are available in Appendix B. Definite tire is an all-season tire that could be mounted on a selected wheel. All-season tires, also known as universal or multi-season tires, combine the requirements for summer and winter weather conditions. All-season tires are developed by world tire manufacturers as a compromise between summer and winter tires. They are easy to drive thanks to stable cornering and strong traction in both wet and dry conditions. The main task that should fulfill an all-season tire is a sufficient level of safety on the winter road and the convenience of driving on the summer road.

Jazar [87] defines that the value of the dynamic rolling radius can be calculated from the radius of the wheel without load r_o and the radius of the loaded wheel r_{stat} as:

$$r_{dyn} = \frac{2}{3} r_o + \frac{1}{3} r_{stat} \tag{3.2}$$

The calculation of the dynamic rolling radius according to Equation (1.2) results in 632.8 mm for the vehicle parameters and according to Equation (1.1), the identified maximum angular velocity of the in-wheel motor n_{max} amounts 1258.2 min^{-1} or ω_{max} amounts 131.8 rad/s.

Aerodynamics: Abhishek et al. [1] defines that a drag reduction on vehicles can significantly reduce the rate of energy consumption of vehicles. The flow resistance of a vehicle depends on its shape, the medium through which it moves and its size. In the case of a vehicle, the medium is air, which can be considered incompressible in the usual speed range, that is why a drag resistance coefficient c_w of the vehicle is created by the relative movement between the vehicle surface and air [25]. Another important parameter is a frontal area of the vehicle A_f, which is the area of the parallel projection of a vehicle to the plane that is perpendicular to the vehicle's longitudinal axis [10]. Values of c_w and A_f for the already accepted target vehicles Mercedes-Benz A-Class A220 and Audi A4 Limousine are similar and presented in Table 3.2.

Loades: Axle load distribution provides a portion of the data necessary for the kinematic layout of a suspension system [70], but is also very important to consider the load distribution on the axles of the vehicle, because the distribution of loads on the axles has a direct effect on the components and parts of the in-wheel motor. In addition, in-wheel motors are planned which drive only one axle or, in other words, only 2 wheels. Due to this type of motor design, there is more space for the placement of the other vehicle components and it is easier to create an optimal load distribution of 50% on the front axle and 50% on the rear axle (Figure 3.6). This is also based on the statement, that by the development and further calculation of the parts and components of the motor, the load conditions will be identical for each axle. This means that the in-wheel motor has a higher integration level and can be used in the future for any of the axles of the vehicle or together on both axes of the vehicle to get a four-wheel drive vehicle.

Figure 3.6 – Axle load distribution

Drive layout: Depending on the selected drive concept, there are certain advantages and disadvantages. However, an integration of the motor into the front wheel of the vehicle causes serious technical and physical problems. Due to the negative effect on the driving dynamics [123], a drive layout with integrated motor in the rear wheel is decided. This results in a more dynamic distribution of the wheel load and, in addition, an integration in the rear wheel provides more flexibility regarding to the design of the in-wheel motor. In addition, significantly shorter supply lines of energy source or required water cooling can be achieved.

The assumed characteristics and requirements on the in-wheel motor can be observed in Table 3.2.

Parameter	Symbol	Unit	Value
Vehicle weight	m_v	kg	2010
Drag coefficient	c_w		0.27
Frontal area	A_f	m^2	2.2
Wheel size	W_v	in	16
Dynamic radius	r_{dyn}	mm	316.8
Maximum speed	V_{max}	km/h	150
Loads distribution		%	50/50

Table 3.2 – Assumed requirements of the vehicle

3.2. Topology of the In-wheel Motor

In this section, a structural synthesis is carried out according to the functional basics of the in-wheel motor. As a result, the possible topologies and requirements of the topology of housing elements are presented. Thereafter, an integrability of the wheel hub bearing, as the main support element in in-wheel motor assembly, is analyzed to satisfy the requirements of low volume and high stiffness.

3.2.1. Functional Basics of the In-wheel Motor

In this section, the in-wheel motor is described in more detail concerning its structure, and an overview of its modules (components) and a brief explanation of their function is given. These components can be derived from their functional principles.

As it is stated in section 3.1, the in-wheel motor is integrated into the 16″rim and it must be noted at this point that the motor has an outrunner rotor type design as the most attractive and common option for the application in vehicles [112].

Figure 3.7 exemplary shows an outrunner rotor design of a motor with components and a centrally positioned wheel hub bearing as a draft design. As a traditional in-wheel motor topology, the motor stator is rigidly fixed to the chassis and the rotor is rigidly fixed to the wheel hub bearing. The motor consists of a wheel hub bearing unit, a fixed stator with the power electronics, an outrunning rotor running relative to the stator, and further components and subsystems, which are described in more detail below.

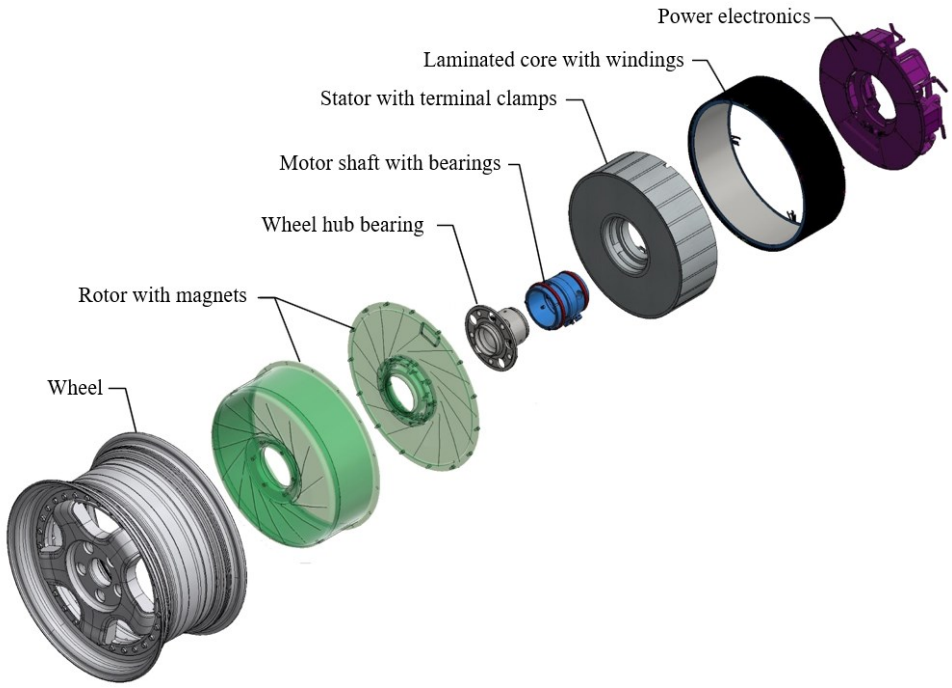

Figure 3.7 – Overview of in-wheel motor components (outrunner rotor type)

Motor shaft: Firstly, the motor shaft is firmly connected to the suspension, which is a part of the chassis and therefore of the vehicle. A rotor is placed above the bearings on the motor shaft and the rotor rotates with the motor speed. One of the additional requirements of the motor shaft is to provide communication and supply lines.

Stator: The stator is a central part of the electric motor, to which a back iron, windings with terminal clamps and electronic components are attached. The cooling of the electric motor runs through the stator and dissipates the resulting heat of the motor.

Laminated core or back iron: The back iron or laminated core consists of a magnetically conductive material which has the function of conducting the magnetic flux bundled while keeping power losses as low as possible.

Winding: The winding lies on the stator of the motor and generates the rotating stator's magnetic field. The conductors of the winding are parallel to the axis of the wheel in order to generate a torque in the required direction.

Terminal clamp: The terminal clamps represent a connection element. With the help of the terminal clamps, the individual wire-strands of the windings are interconnected to form a complete phase of winding. This component reduces the number of electrical leads routed to the motor.

Power electronics: The power electronics are also integrated into the electric motor unit package. The power electronics consists of the power section and control electronics. The function of this combination is to commutate the individual strings according to the desired form of commutation. The electronics directly integrated in the stator has an advantage in terms of electromagnetic compatibility, as there is no need to lay pulse cables within the suspension.

Wheel hub bearing: The hub is mainly used to attach a bearing which allows the wheel to rotate around an axle [54]. Wheel hub bearing is an important unit in the wheel, which influences driving safety and driving comfort of the vehicle. A dimensioned wheel hub bearing transfers the wheel loads directly to the wheel carrier or to the shaft of the motor.

Bearing or supplementary bearing: Bearings are the mechanical connecting element between the fixed and rotating parts. The rotor is pivoted on the wheel hub bearing unit. Since the stator and rotor are moving relative to each other, the bearings have the function of a low-friction running over a long period of time.

Rotor (Housing): The "outer shell" of the motor represents the housing. The housing is to protect the internal components from external influences. At the same time housing can mean rotor, when the rotor is directly integrated into the housing. The rotor represents the rotating part of the electric machine. This component is to generate an equal radial magnetic flux with low losses and stability of the motor running.

Permanent magnets: Permanent magnets generate the magnetic field. The magnetic field lines from the magnets extend across the air gap perpendicular to the axis in the stator. The magnets have a direct influence on the torque and thus on the operating behavior of the motor.

Position detection: The rotor angle position detection is required for the motors in order to commutate the winding phases at the right time or to be able to regulate the currents according to the rotor position.

A further possible unit of the vehicle wheel, that can be integrated into the in-wheel solution, is a braking assembly or an adopted brake system, which is not included in the objective of this thesis.

3.2.2. Structural Synthesis of the In-wheel Motor

An aspect concerning the topology has an indirect influence on the motor performance and requires a detailed analysis and extensive validation of the motor structure. A wide area of study on in-wheel motors is dedicated primarily to the calculations of electromagnetically active parts of the motor, such as rotor and stator and their interaction with each other. This is due to the fact that their parameters directly affect the performance of the motor relatively to its generation of the most important motor characteristics – power and torque. However, other parts of the motor, that are often called passive parts [54], also influence the motor performance resulting in its characteristics.

One of the most important criteria for the functional purpose of the in-wheel motor is the transmission of torque to the vehicle wheel. The central tendency for current coupling technologies in in-wheel motors is to transfer the torque to the wheel using the wheel bolts or direct connection of the motor shaft and wheel. According to this tendency and the variant of the motor with an outrunner rotor type, there are a lot of possibilities to organize a structure or topology of the in-wheel motor. The outrunner rotor type is well adapted to the in-wheel motors since the rotor is connected directly to the wheel mounting surface of the wheel [188].

Typical variant of the torque transfer is the in-wheel motor from Protean Electric, Inc., illustrated in Figure 3.8, (a), where the standard pitch center diameter of the wheel and the standard wheel bolts are used for the transfer of the driving torque [73]. By this configuration, the standard wheel hub bearing is directly connected to the motor parts and causes the influence of the loads on the air gap and its constant variability from driving operation.

The application of a carbon fiber-reinforced polymer wheel to an integrated electric motor is the special decoupled system shown in Figure 3.8, (b), which is the result of the development by Fraunhofer LBF during the collaborative research project "Fraunhofer Systemforschung für Elektromobilität" in the field of electromobility [152]. Due to this design, the motor rotor part is connected to the inner area of the wheel, not directly to the rim base. This prevents that any radial or lateral acting force will be transmitted directly to the electric motor. The outer part of the motor is connected to the inner area of the wheel hub. The special radii and tapered junctions based on the material properties realized in the wheel are provided for the suitable and consistent fiber lead and for the prevention of stress peaks determined by the sharp corners or stiffness inhomogeneity [78].

Additionally, some patented concepts of coupling could be termed, as in [15] considered, coupling solutions for the damping of the torsional vibration for the rotor about a rotation axis of an in-wheel motor by shifting the center of mass in tangential direction by the bearing of the wheel. Another concept of Yasuhiro et al. describes a developed system having a structure capable of efficiently transferring the driving torque of a motor to a wheel, equipped with a coupling [183].

a b

Figure 3.8 – Solutions for torque transferring: a - In-wheel motor from Protean Electric, Inc. [73], b - Demonstrator of Fraunhofer LBF [152]

The most common version of common in-wheel motor topology is presented in detail in Figure 3.9. The loads coming directly from the contact between the road and the tire are transferred to the tire through the wheel and to the wheel hub bearing onto the suspension. The important advantage of this topology is that the in-wheel motor can be easily installed as a one-piece unit. However, there is a disadvantage, namely that the wheel hub bearing has multifunctional tasks – firstly, to accommodate the loads coming from the wheel, and secondly, to ensure together with the rotor that the air gap between stator and rotor always remains approximately the same.

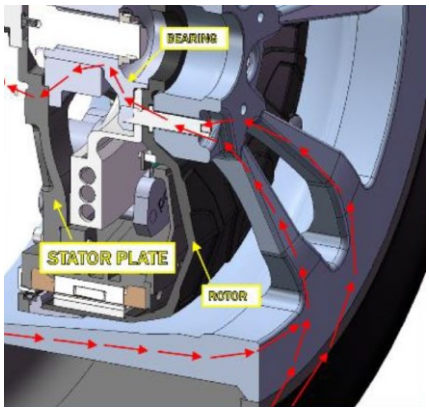

Figure 3.9 – Common topology and typical load transfer from the road via in-wheel motor [54]

The typical topology for the modern in-wheel motor shows the Figure 3.10, (a). The housing or rotor part, by this topology, is clamped between wheel disc and a wheel hub bearing and, in this way, the rigid coupling is realized. Increased safety requirements are imposed on both standard parts in this chain – wheel and wheel hub bearing, that are standard, original, calculated and certified parts, because original parts are produced according

to the automotive standards. According to the coming loads and conditioned by these topology deformations, the rotor will also get a part of the loads and induced displacements caused by force flow. Any load case of the rotor in fact has an effect on the parameters of the motor performance. Therefore, the statement that the air gap between the winding of the stator and the magnets of the rotor may not be smaller on average than the minimum value of all driving situations and loads contradicts this solution. To avoid external loads and simultaneously transfer the driving torque to the wheel is a complex task, that could be solved by using a stable rotor or by inserting an elastic coupling element between the wheel and rotor of the in-wheel motor. A stable rotor solution means that the rotor assembly has an oversized and heavy weight construction, where the side covers of the rotor are calculated for the bearable load. A promising alternative is the integration of the flexible coupling element between rotor and wheel, as it is shown in the Figure 3.10, (b). The rotor part of this solution is pivoted on both of the covers and the transformation of the torque arises through a flexibly mounted coupling element. On the one hand, the coupling element provides a torque transmission. And on the other hand, an elastic coupling element minimizes the influence of the external loads to assure consistent electromagnetic behavioral stability of the in-wheel motor. Design of the rotor part of this solution must satisfy the functional requirements mentioned in 2.2.1 and opens up the opportunity of lightweight construction.

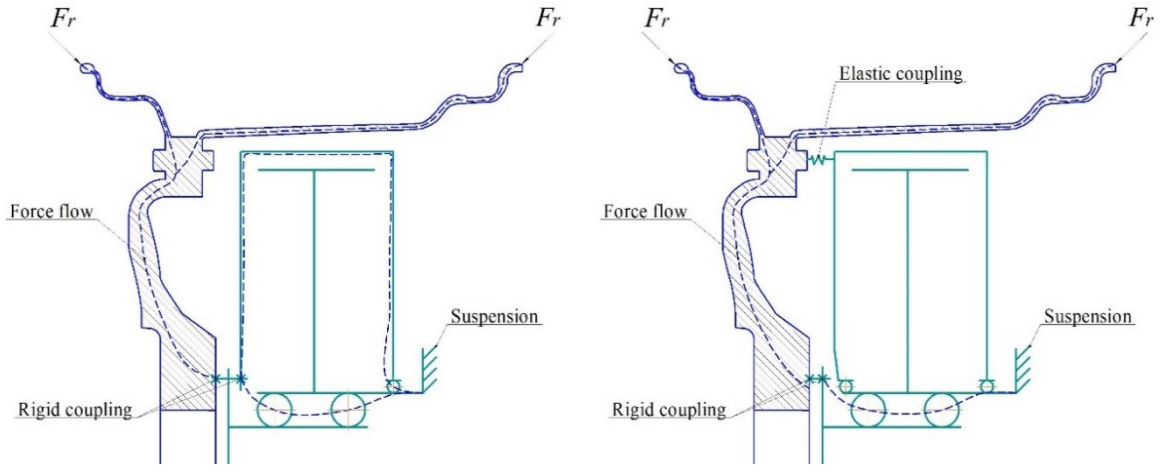

a b

Figure 3.10 – Variants of load transfer: a - Rotor coupled solution, b - Rotor decoupled solution

After comparing the topology options, the option shown in Figure 3.10, (b) was selected for further motor development as an option in which the coupling element can be mounted on the rotor of the in-wheel motor and the force flow is forwarded through the rigid wheel hub bearing. In addition, in order to research the combined action from the wheel hub bearing and the coupling element and its influence on the air gap as well as to provide the basis for the analysis of acting loads on the coupling element, a study of current researches that focused on the loads and conditions acting on the wheel of the vehicle should be undertaken.

3.2.3. Wheel Hub Bearing

The next step of the structural synthesis of the in-wheel motor is to analyze a wheel hub bearing. Wheel hub bearings are a very important part in terms of vehicle dynamics, sustainable performance and safety maintenance [12]. Biček et al. [11] pointing out that one of the major drawbacks to exploiting the motors is associated with the overloading of bearings. The function of the wheel hub bearing in the developed motor, as the main bearing, is the same as by standard automotive wide use application and consists of supporting and carrying the static and dynamic loads that occur on the wheel to the suspension of the vehicle. On the basis of the specific boundary conditions such as installation space, operating conditions, high rigidity, reliability and robustness, the wheel hub bearing requires to be modified to the concept of the in-wheel motor. As a result, the rigidity must be much higher than those of a conventional bearing unit when the load is increased. Further difficulty is provided by extremely limited installation space due to the high-power density of the motor. All mentioned factors are leading to the obligated precise integrability of the bearing unit. Another factor that

should be taken into account by concept is the light-weight design of the total concept. Selecting the type of bearing that is most suitable for the vehicle ensures safety and is very important in order to achieve the required performance. For the selection of the best bearing, one needs to consider and evaluate bearings from a variety of solutions [125].

Therefore, three generations of wheel hub bearings differ. The first, second and third generation of hub bearing vary depending on the integration of bearings and their peripheral components. But in general, wheel hub bearings are comprised of similar parts with similar properties and functionality, namely bearing outer ring, inner ring, cage, rolling elements (balls or tapered rollers) and seals.

Wheel hub bearings of the 1st generation (Figure 3.11, (a)) are compact units, which are equipped with defined and preset bearing clearance, for-life maintenance-free grease lubrication and usually also with a seal. The rolling elements, in this case – balls or tapered rollers, are arranged in two rows. The initial axial clearance is properly adjusted so that the preload falls into the specified range after installation.

Wheel hub bearings of the 2nd generation (Figure 3.11, (b)) combine the economic efficiency of 1st generation wheel hub bearings with the advantage of integrating a flange e.g. for the mounting on a brake disc or wheel mounting surface.

Wheel hub bearings of the 3rd generation (Figure 3.11, (c)) are highly integrated units with highest running accuracy. They have two mounting flanges – one for the brake or wheel, and the other for mounting on the suspension.

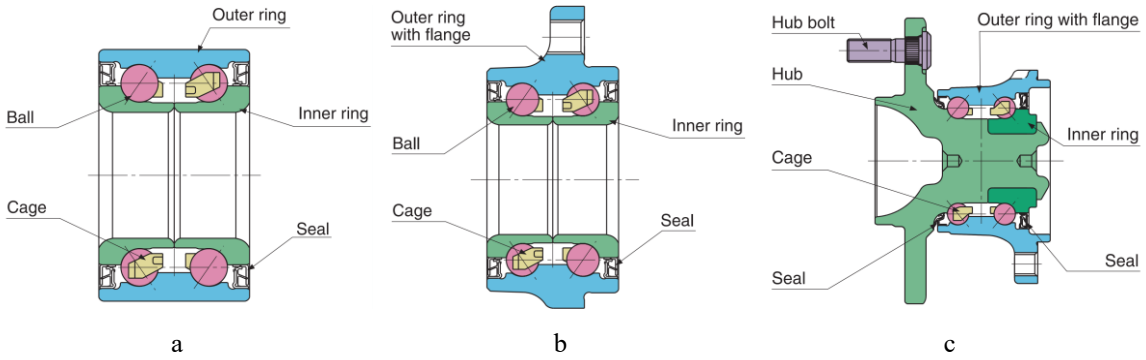

Figure 3.11 – Generations of the wheel hub bearings according to [125]: a - First generation, b - Second generation, c - Third generation

In order to fulfill requests for target vehicle models, an appropriate wheel hub bearing BAR 0230 from SKF product line was selected. Selected wheel hub bearing of the 3rd generation is a highly integrated unit with maximum running accuracy. The dynamic load carrying of BAR-0230 is maximized by a separate inner ring for the inside rolling element row. The wheel hub bearing is equipped with double row angular contact bearings. According to manufacturer's confirmation [159], the used greases are intensely tested under the high loads specific for wheels, thus the bearing is greased-for-life. Original hub bearing has two flanges to bolt the unit to the static part of the suspension with outer ring flange and to bolt the rotating inner ring with its threaded holes in the flange to the wheel. Characteristic benefit of the selected wheel hub bearing BAR-0230 compared to the other variants presented in the literature [189], demonstrates precise preloading. Preload of wheel hub bearing is achieved through specific tolerance modification, general process upgrade and innovative closed-loop control [174].

Thereafter, analyzing the integrability of the wheel hub bearing into the in-wheel motor assembly is needed to conduct a study on reduction of the volume of assembly space. Integration of a non-modified hub bearing unit decreases the available assembly space V_{as} for the motor package by 334810.285 mm^3. By inserting the original hub bearing, using the additional part in the motor assembly also required that a rigid connection to the suspension had to be functionally organized, which also means that the additional weight of this part increases the total weight of the motor assembly in the wheel. An additional part decreases also V_{as} by 1035833.7 mm^3 (Figure 3.12, (a)). Another integration approach, shown in Figure 3.12, (b), shows the outer ring of the wheel hub bearing optimized to the cylindrical shape. Cylindrical modification provides the advantage of, first off, simplicity by mounting the motor shaft, and second off, is a reduction of the assembly space V_{as} for the in-

wheel motor by 345671.9 mm^3 less than the variant shown in Figure 3.12, (a). Gained volume could effectively be used for the energy, cooling and communication supplies.

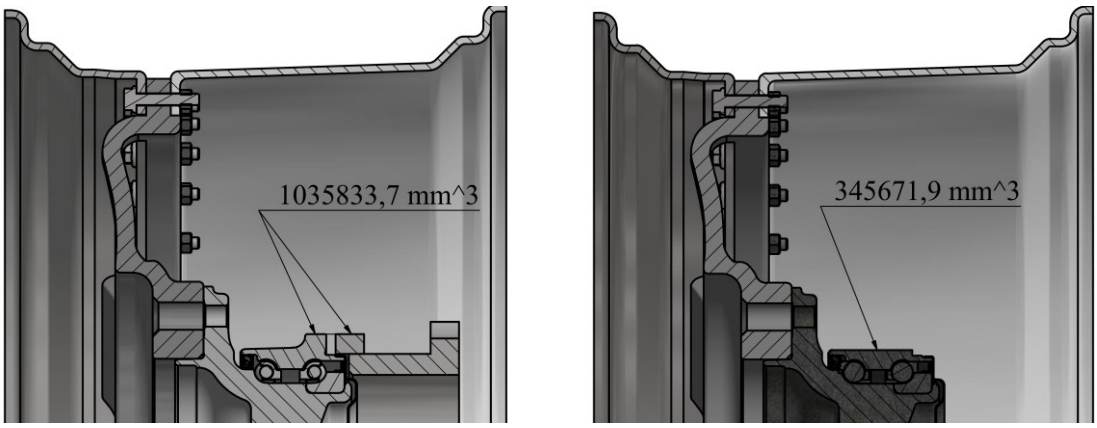

a b

Figure 3.12 – Variants of the integration for the wheel hub bearing: a - Non-modified wheel hub bearing unit, b - Modified wheel hub bearing unit

3.3. Requirements on the Elastic Coupling

In the previous section it has become clear that a topology of an in-wheel motor presents a great design challenge because the loads are transferred from the driving to the wheel and directly to the motor. Particularly critical driving situations in which thresholds or holes are run over or in which lateral contact of the tire, e.g. with a curb happens. Using the example of an in-wheel motor, the air gap between the winding of the stator and the magnets of the rotor is one of the most important parameters of the electric machine, which must not fall below a minimum value under all driving situations and loads. To minimize the influence of external loads on these critical motor parameters, the drive side of the motor is decoupled from the wheel or vehicle by means of an elastic structure described above.

The elastic coupling is to limit the transmission of deformations and forces due to driving maneuvers to the electric motor integrated into the wheel and thereby to minimize the influence on important parts and parameters of the motor such as an air gap or a supplementary bearing. Previous selected outrunner designs of the in-wheel motor presents a transmission of the forces of driving maneuvers through the wheel hub bearing. These forces have to minimally influence the relative position between rotating and non-rotating parts of the motor. However, a total weight of the wheel and an integrated in-wheel motor must be minimized caused by unsprung weight. Equally important is to use low-cost supplement bearings. To realize this variety of functional area, a coupling elastic element can be used. This element is intended to nullify the deformation to the parts of the motor and to lead them on a separate power transmission path directly to the suspension of the vehicle. A particular advantage of this transmission structure is that the external forces are not transmitted to the parts of the in-wheel motor, but at the same time the driving torque is forwarded from the motor to the wheel.

In this section, the variants of realization of the elastic element are described combined with the loads, which need to be transferred through the wheel hub bearing. Typical loads acting on the wheel during the driving maneuvers are determined by the standard and real tests for the conventional wheel, as one of the most loaded and rigid parts in the chain between road surface and suspension.

3.3.1. Loads on the In-wheel Motor

As suggested by Frajnkovič et al. [54] loads acting on the in-wheel motor could be discerned based on their origin of the internal and external loads. External loads are loads from the environment and connections of the motor. And internal loads are loads that the motor creates during its operation. The most important sources of internal and external loads are represented by Figure 3.13.

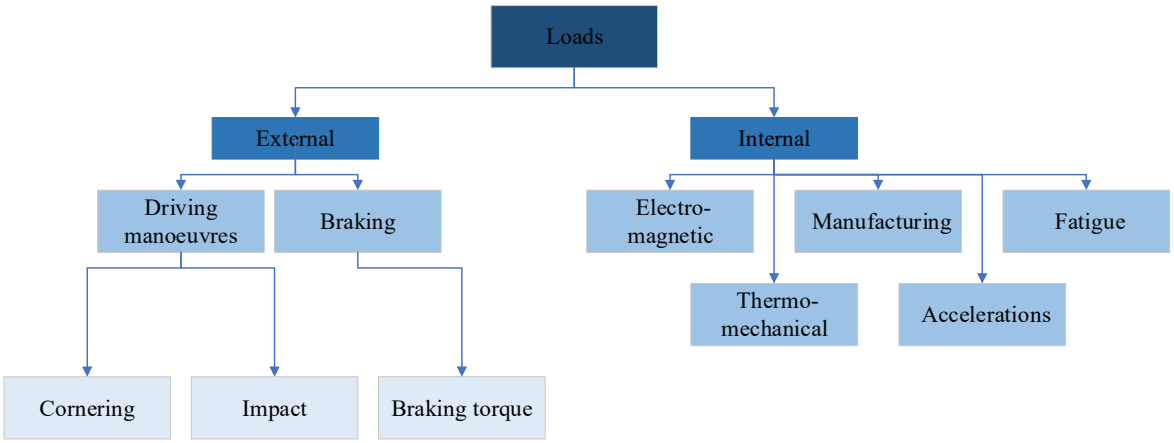

Figure 3.13 – Loads acting on the in-wheel motor

According to the requirement of the in-wheel motor stability formulated in the objective of this thesis, the highly sought loads introduce loads with driving maneuver background. The forces and moments acting on the wheels and originating from the driving maneuvers firstly are the vertical, transverse and longitudinal dynamic loads.

Vertical dynamic loads include components of the centrifugal force during cornering, load on the rear axle during acceleration, load on the front axle during braking, road unevenness, disruptive factors, e.g. bumps, potholes and thresholds as an impact load [25].

Vertical dynamic loads are caused by the vehicle motion. The centrifugal force acting on the center of gravity of the vehicle causes additional load on the outer wheels and the inner wheels are partially relieved. In addition to the effect of the centrifugal force, the outer front wheel is loaded by cornering. The cause of this is the inertial force, which counteracts the directional change (Figure 3.14).

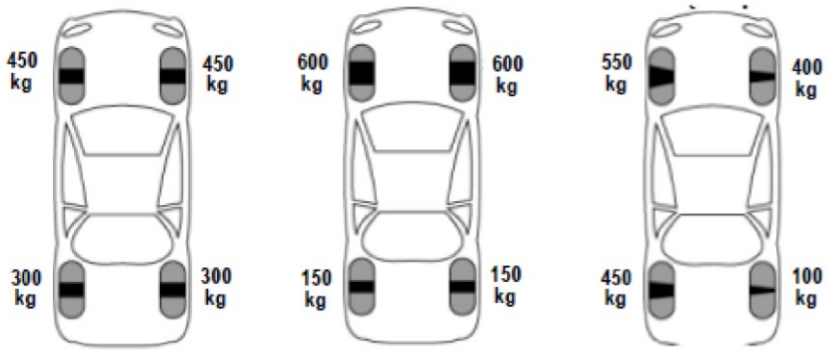

Figure 3.14 – Wheel loads during static load, braking and cornering [82]

The load on the axles also varies during braking and acceleration. During braking, the front axle is additionally loaded, while the rear axle is more relieved (wheel load transfer to the front axle). Therefore, the rear brakes are not as effective as the front brakes: less friction forces are generated on the rear tires because the friction force is proportional to the wheel load (Figure 3.14).

A pitching moment is generated during acceleration, which is compensated by wheel load transfers. Therefore, the front axle is relieved and the rear axle additionally loaded. Figure 3.15 shows an extreme case of acceleration: the front axle of the vehicle is loaded so high that no load on the rear axle occurs.

a b

Figure 3.15 – Pitching moment while: a - Braking, b - Accelerating [118]

During driving unpredictable shock factors can occur. This can be caused by bumps, thresholds or potholes. In addition, the road surface leads to vertical movements due to unevenness. Heißing and Ersoy [70] has already noted that a frequency range up to approx. 30 Hz is expected, which makes it a relatively large excitation source for the vehicle.

The horizontal loads are part of transversal dynamics and occur by cornering. The horizontal dynamics of the wheel as well as the tire skew is very significant for the tires and thus also for the driving behavior and safety.

The last kind of loads are loads from longitudinal dynamics: drive and braking torque. The driving torque is generated by the motor and redirected to the wheel. Braking torques come from disc or drum brakes, thereby the friction force, which acts through the brake pad on the disc or drum is multiplied by the force arm. The moments are limited by the road grip of the tires. If a torque value becomes too big, the tire slips on the roadway.

Each revolution for the wheel is a cyclic load. Heim and co-workers [68] reports, that during the operating distance of 300 000 km approx. 1.5 x 10^8 oscillation cycles are generated. As a result, wheel tests must be taken into account not only for strength under static loads but also fatigue loads.

In order to estimate the influence of the loads transferring through the wheel hub bearing and functionality of the elastic element by decoupling of the rotor part, a simplification of load scenario needs to be realized and critical load case scenarios need to be determined.

3.3.2. Critical Load Scenarios and Generation of the Loads on the In-wheel Motor

The previous section demonstrates how the vehicle and driving manoeuvres of the in-wheel motor interact with different loads from the main vehicle function - driving. The complexity of loads and their combined acting during driving can be simplified by the model of wheel deformation. The analytical model of the deformation in a present case is a complex problem due to the following reasons:

- rotation of the rotor causes continuous change of the load's application with the connection of the wheel to the in-wheel motor,
- the magnitude and direction of the load is not constant,
- dynamic loads, assembly and manufacturing errors, the connection's deflections and environmental influence also cause difficulties of mathematical modeling.

To obtain a determination of generated end loads acting on the wheel, there are the forces and moments acting on the wheel simply explained. These loads are three-axis forces, which is longitudinal force F_x, lateral force F_y, vertical force F_z, and three-axis moments – heeling moment M_x, twist moment M_y, and aligning moment M_z (see Figure 3.16).

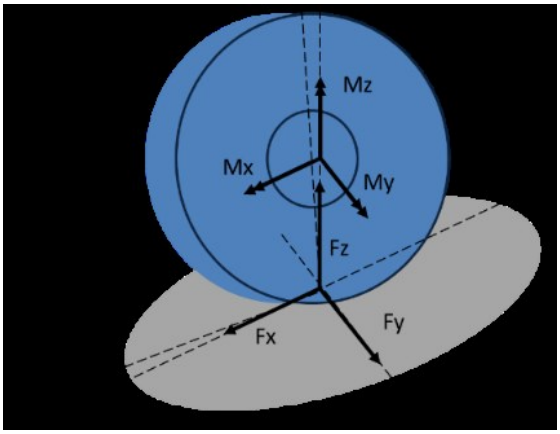

Figure 3.16 – Forces and moments acting on the wheel

For further contemplation, all loads are split into three directions: radial loads resulting from the wheel loads in the direction of the wheel center line, axial loads resulting from the lateral forces and driving or braking torque.

The vertical force F_z acting in the vertical direction is composed of a static and dynamic component. The static component results from the vehicle weight and the axle load distribution. The axle load distribution depends on the center of gravity and the dynamic component depends on the driving condition. To estimate the real wheel loads, the driving tests are required. For example, a determination of the dynamic part of the loads is possible by crossing of predefined thresholds, whereby the wheel is accelerated in vertical direction. Since the wheel is slow and damped, the wheel load F_z acts in the opposite direction. Irmscher et al. [86] described the measuring wheel WFT-Cx that can estimate the real wheel load F_z, which has a linear relation to the speed of the vehicle and increases with the speed of the vehicle.

According to [25] a linear relationship between vertical force and velocity of the vehicle that can be described by Equation (3.3):

$$F_z = 0{,}036 \cdot V_v + 3{,}8115 \tag{3.3}$$

For further modeling, a vehicle speed of 50 km/h was assumed, as permitted maximum speed in built-up areas. This results in wheel load F_z of 10.3565 kN.

The axial load on the wheel results from the lateral forces. The lateral forces on the tire arise when the wheel is turning at a slip angle α in distinction from the vehicle direction. Typical value for slip angle reaches at the maximum 12°. Relationship between the slip angle and the lateral force is up or down to ±3° linearly dependent on dry road conditions. To determine the height of lateral forces F_y, a driving test should be administered. It has been suggested [71], that by the fluctuating of the lateral force F_z by ±10 kN, a maximum wheel load of F_y of 10kN is expected.

The torque load results from the driving torque and the braking torque. Additionally, the emergency braking torque should be considered as a critical load case. Figure 3.17 describes braking torques for different vehicle segments. The braking torques at 1g complying with compact or medium and upper or luxury class vehicles works out at M_y = 2000 Nm.

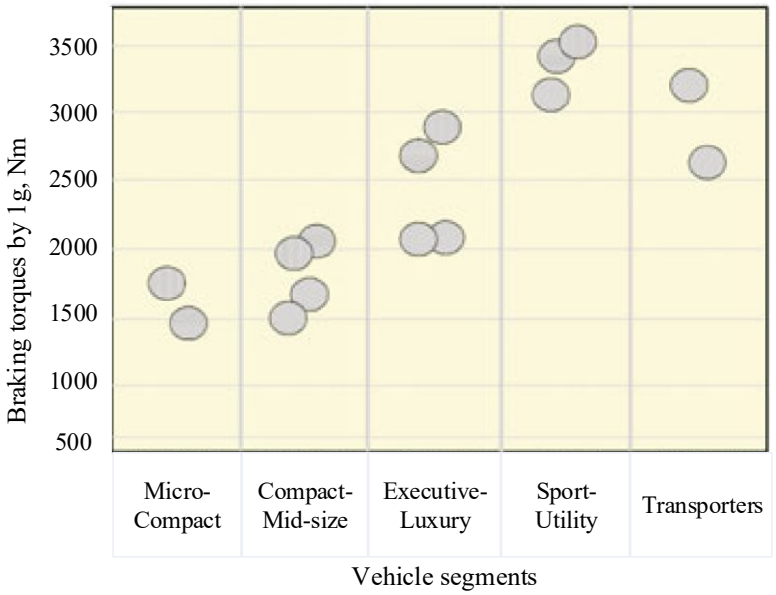

Figure 3.17 – Braking torques for different vehicle segments [71]

Consequently, there are three critical load cases for the further modeling identified further as radial load F_R of 10.4 kN, axial load of F_A = 10 kN and torque load of M_L = 2000 Nm. In addition to the loads from electric traction, these loads must be taken into account for the sizing of the in-wheel motor and for determining of the elastic coupling element parameters.

3.3.3. Transfer of Torque by Elastic Element

The possible use of an elastic element as a coupling to reduce the loads and thus the deformations transferring on the rotor can fulfill requirements of integration into the in-wheel motor. However, the determination of arrangement, type and position of the elastic element becomes a major factor, because this part of design depends on a great variety of factors.

Elastic element in the sense of the machine part represents a coupling. Couplings are machine elements which main function it is to transmit torque and rotation by frictional or positive connection from one rotating part to another. As an additional task, couplings can compensate axial, radial and/or angular misalignment. A flexible but torsionally rigid compensating coupling (see Figure 3.10, (b), 3.2.2) is required between rotor housing and wheel. It is also possible to compensate torsional shocks and vibrations with coupling. If the connection between two elements is to be disconnected during operation, switchable couplings are used. Non-switchable couplings are used if it is not necessary or possible to make the coupling releasable/switchable. The next classification criterium is flexibility of couplings, while the flexible couplings are distinguished between torsionally stiff and torsionally elastic ones. Flexible couplings or compensating couplings are designed to be moveable and torsionally flexible in order to compensate misalignments, vibrations and torque shocks. In order to ensure that the selected coupling fulfils all the functions required, coupling must be selected according to various criteria in addition to some basic factors such as mounting, manufacturing, wear, service life and susceptibility to failure.

In order to use a coupling in an in-wheel motor, it must fulfil more requirements in addition to the main requirements mentioned above. For example, the installation space is very important, because the space between the rotor and the wheel is very limited. Another important requirement of the application on vehicles is driving comfort, which has its origin in unsprung weights. Therefore, it must be ensured, that the unsprung weight, which includes the weight of the coupling, is reduced to its minimum value. In principle, there are several standard variants of such couplings, which can find an application on developing the in-wheel motor. Standard solution in the area of flexible couplings can be represented for example by metal bellow couplings or lashing couplings.

Figure 3.18, (a) defines a typical metal bellow coupling. An approach of metal bellow coupling enables to compensate horizontal and angular movements [155]. However, in-wheel motors are also loaded with vertical forces by the transmission of torque and by deformations of the wheel. The metal bellow coupling could break by the application of loads of this kind, what results in the complete functional failure. This fact makes the use of the metal bellow couplings impossible and they are not further considered for the in-wheel application.

As a transmission element by lashing coupling, shown in Figure 3.18, (b), configure integrated lashes, what allows to transmit a force from one coupling part to another. In the core of the lashes there is an elastic package, which function it is to compensate for radial, axial and angular misalignments. An advantage of this coupling type is the option to vary the flexibility of the lashes to become a different characteristic of compensation. At first glance, it might seem logical that the lashing coupling as a coupling system for the application in in-wheel motor requires an additional space in axial direction, but that does not meet the requirements of minimal installation space. A further difficulty relates to the adaptability of the in-wheel motor through the use of such a coupling, requiring the integration of lashing accessories for the connection to the rotor and wheel.

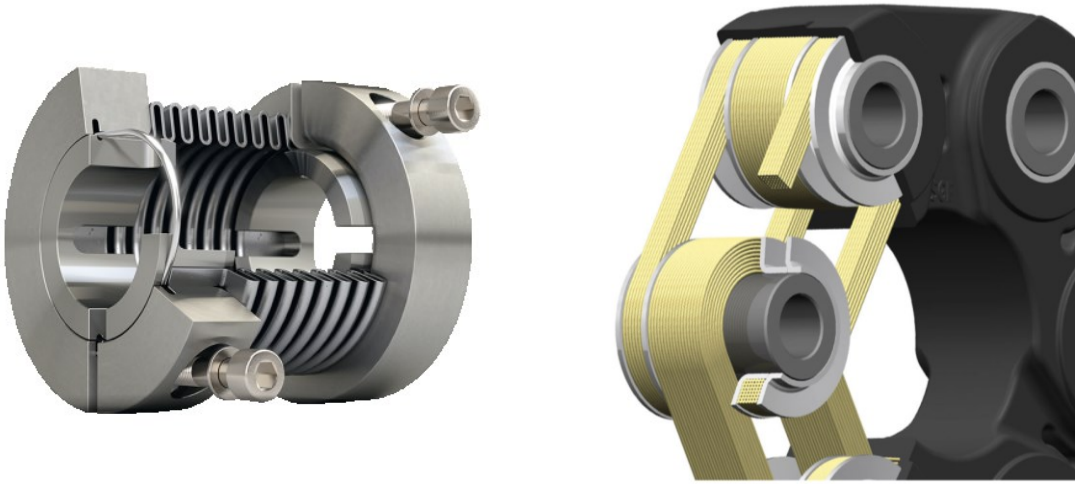

a b

Figure 3.18 – Standard variants of couplings: a - Metal bellow coupling [115], b - Lashing coupling [166]

The standard methods of torque transmission and decoupling of load influence are implemented in many units of the modern vehicle. Further development is focused on the solution of the principal problem with the help of the integration of the elastic element directly into the rotor housing and using available interfaces of the multiple wheel. That allows to solve the problem at a significant level and at the same time to satisfy the main requirements of compensation of loads and side requirements of weight, certain flexibility by material selection and mountability in in-wheel motor.

The task above can be solved by special designed tooth coupling. The main requirement on the tooth is to demonstrate an elasticity, preferably bending elasticity, with value which prevents tilting and thus an unwanted transmission of force without reducing the torsional stiffness for transmission of the driving torque. And the tooth must also be connected to each other in such a way that a form-fit connection is created that blocks one degree of freedom, while the other degrees of freedom are not restricted in their movement and a movable, detachable connection is created. Developed solutions in the area of transmission elements and their contact areas with separate additional part for the rotor (a) and for the wheel (b) are presented in Figure 3.19.

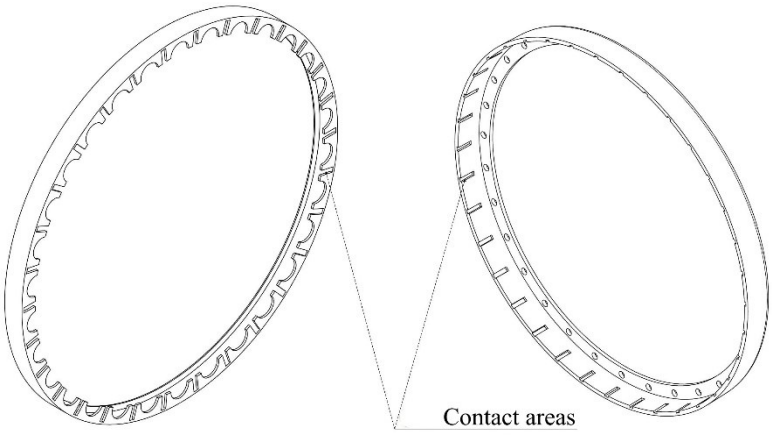

Figure 3.19 – Variants of contact areas for developed coupling structure: a - With separate additional part for the rotor, b - With separate additional part for the wheel

The approach with a separate additional part for the wheel (Figure 3.19, (b)) allows to compensate the rotor body for loads coming from the wheel by the degrees of freedom in the directions shown in Figure 3.20, with F_A as an axial and F_R as a radial load represented. An additional part of this solution is mounted directly to the three-piece wheel with screws that realize the assembly of the wheel. A disadvantage of this solution is obtained by the connection of the second part of the structure on the rotor, which brings an additional junction to the whole system.

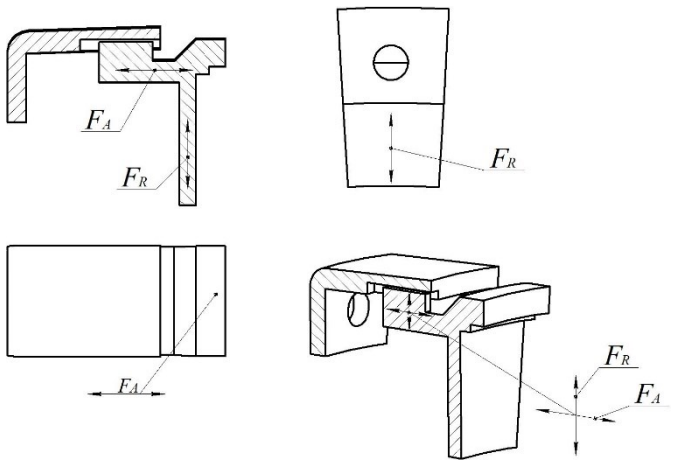

Figure 3.20 – Loads compensation by the elastic element with separate additional part for the wheel [91]

The compensation possibilities of the second variant of solution with a separate additional part for the rotor is shown in Figure 3.21. The elastic coupling element presents a ring with cut-outs, further called slots, and the second part of the transferring structure are the screws of the three-piece wheel with turned ends. The cylindrical screw ends engage in these slots and have the function to connect outer and inner ring. These screws are movable in radial and axial direction in the slots, thus no deformations from the wheel are transmitted to the rotor of the in-wheel motor. Additionally, the screws have a connection on the side surface of the slots in the tangential direction and are able to forward the torque to the wheel. The main requirement for this solution is expected from the material of coupling element, which relates to a high torsional strength caused by the functional use of the in-wheel motor.

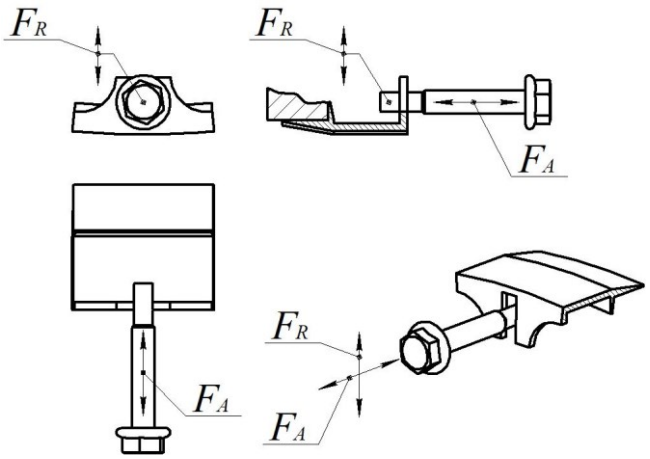

Figure 3.21 – Load compensation by the elastic element with separate additional part for the rotor [91]

Both solutions, with a separate additional part for the wheel or for the rotor, comply with the main requirements for the elastic coupling element. As the next step of the analysis it was decided to implement an additional requirement as manufacturing complexity in order to develop more of the variants. At first sight, both solutions are thin-walled rings with big diameter/length relation and additional slots in longitudinal direction by the first variant and keys in transversal direction by the second. In the first production step, both coupling elements can be produced by turning. The solution with a separate additional part for the wheel has rectangular slots with sharp edges. The required slots have an important design feature - two flat surfaces are perpendicular to each other. The use of conventional production methods in this case involves rounding off the shape of the teeth and the slots. However, the necessary slot geometry can be achieved with a special tool such as the angle milling head. An angle milling head allows to produce a slot that cannot be reached with standard axis kinematics and tools. In addition, the rotor must be equipped with teeth that can be engaged as an elastic coupling element. The elastic element with a separate additional part for the rotor is in technological advantage by the usage of a standard end milling process. The favorite design also requires an application of standard parts – screws of the three-part wheel, which must be adapted by conventional turning.

As an additional requirement, a contact between two parts of the coupling can be analyzed. As already mentioned in 3.3.1, a flexible coupling element is also cyclically loaded by the drive. Due to the specific design of the flexible coupling element, a contact surface is more advantageous for possible wear and occurring contact stress, since a contact in this case is two lines (contact between a cylindrical body lying on the plane surface).

Based on the additional requirements for the elastic coupling element, the solution with an additional part for the rotor has the highest value and is therefore selected as the preferred solution for further detailed design and simulation.

3.4. Motor Requirements

This section contains an analysis of the requirements for the electric motor for the in-wheel system. For this purpose, first of all, the traction force for the target vehicle and basic requirements for the electric motor of the in-wheel system are defined. Regarding the electric motor system, the synchronous motor with permanent magnets, as an electric motor type with the highest potential of application in the automotive industry [141], is described and analyzed. Furthermore, the motor requirements of parameters primarily related to output power and torque are determined. This approach is applicable as checking procedure for the determination of motor parameters. The analysis of limiting load characteristics of the motor is carried out by the condition of providing the constant torque mode and constant power mode in the range of driving scenarios and operating characteristics. Subsequently, the significance of using a cooling system was determined on the basis of the determined motor parameters.

3.4.1. Energy Demands of the Vehicle

The extension of the in-wheel system to passenger vehicles faces significant difficulties, as the use of the active volume of the motor decreases with the reduction of the unit power of the electric motor. Conversely, restrictions imposed on the unsprung mass of a passenger vehicle require a significant reduction in the size of the motor, which in turn is accompanied by a decrease in its specific energy characteristics and is in contradiction with the availability of a limited power supply on board of an electric vehicle. The requirement for high energy performance is valid for all parts of the electric power transmission and, above all, for integrated electric motors. The movement of an electric vehicle in an urban environment is characterized by frequent stops and subsequent acceleration to a specified speed. Analytical study of this movement is usually carried out by using the experimental speed graphs. The characteristics of the movement of an electric vehicle in a city depend on its structural design and the functional purpose of the vehicle (transportation of mail, public services, etc.) and have to be developed for each city separately with regard to its characteristics. The most responsible mode of car traffic is acceleration from parking to maximum speed and gradeability on a slope. Therefore, to determine a driving performance using in-wheel motors certain requirements have to be fixed:

- Maximum speed of 150 km/h (see 3.1),
- Driving a slope of 30%,
- Acceleration from stillstand to 100 km/h in at least 20 s,
- Grade on a street curb.

The general vehicle movement can be mathematically described with the general principles of mechanics. Traction effort F_t is transferred to wheels and is acting in the direction of movement of the vehicle. By the movement of the vehicle also traction resistances F_{tr} occur as tire rolling resistance, aerodynamic drag and grading resistance. When the F_t value exceeds the F_{tr} value, the vehicle starts moving in the direction of F_t and it can be expressed by the Newton's Second Law of Motion as:

$$\frac{dV}{dt} = \frac{\sum F_t - \sum F_{tr}}{m_v} \tag{3.4}$$

According to Equation (3.4), traction effort F_t must be provided by the in-wheel motor system. In order to derive the requirements for the in-wheel system, it is necessary to define various requirements for the integrated electric motor.

For determination of the main requirements for the integrated motor, the forces acting on the driving vehicle and having the greatest impact on these requirements must be identified. The forces of traction resistance include aerodynamic drag F_{ad}, rolling resistance F_{rd} and grading resistance F_{grad} as it is shown in Figure 3.22.

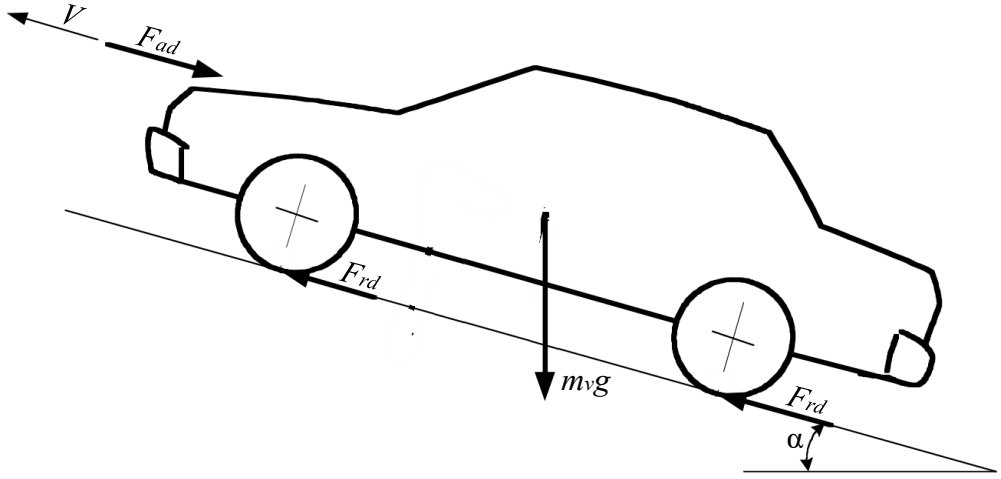

Figure 3.22 – Forces acting on a vehicle

An aerodynamic drag F_{ad} is the resistance to the air flow and depends on the air density ρ_{air}, the aerodynamic drag coefficient of the body of the vehicle c_w, the frontal area of the vehicle's body A_f, and the speed of the vehicle V in accordance with the Equation (3.5):

$$F_{ad} = \frac{1}{2} \cdot \rho_{air} \cdot c_w \cdot A_f \cdot V^2 \tag{3.5}$$

The rolling resistance F_{rd} of the vehicle wheels in contact with the road surface mostly depends on the rolling resistance coefficient f_{rr}, which furthermore depends on the rolling resistance as a function of the driving speed and according to recommendations in literature [50] have a value of 0.017 at 150 km/h. Taking into account the dynamic radius r_{dyn}, an expression for the force of rolling resistance could be expressed as:

$$F_{rd} = \frac{f_{rr}}{r_{dyn}} \cdot m_v \cdot g \tag{3.6}$$

To assess the traction effort F_t and power required to drive at maximum speed, the road is considered to be strictly horizontal. Then an expected resistance force F_{tr} at maximum speed requires a power P_{mech}, that can be calculated by multiplying by the maximum speed V_{max}:

$$P_{mech} = F_{tr} \cdot V_{max} \tag{3.7}$$

V_{max} is determined above in section 3.1 in compliance with the requirement of the target vehicle. According to Equation (3.7) and predefined and precalculated data, the required power to achieve the maximum speed of the vehicle has to be 69.9 kW. For simplification of the future calculations, the required power of 70 kW was accepted.

Maximum traction effort is also determined by the slope of the road, which needs to be crossed either in short-time mode or permanently. Normally the maximum slope for passenger vehicles is to be found on multilevel parking and mountain roads. For parking areas in Germany, the road angle α is brought up to 30% or 17° [50]. Accordingly, an analysis of grading resistance F_{grad} should take into account both, the force of rolling resistance and the projection of the force of gravity:

$$F_{grad} = m_v \cdot g \cdot \left(\sin\alpha + \frac{f_{rr}}{r_{dyn}} \cdot \cos\alpha \right) \tag{3.8}$$

In order to be able to make an explicit statement about the suitability of the developed in-wheel motor, the required drive torque M_{mech} related to one wheel can be illustratively calculated based on the value of F_{grad}.

$$M_{mech} = \frac{1}{2} \cdot F_{grad} \cdot r_{dyn} \tag{3.9}$$

At this point, a decision about the motorization of the vehicle axis can be made by the distribution of required torque on one or two axes. Required drive torque value is 1080.5 Nm and can be provided from the one axis of the vehicle. However, motor torque M_{mech} for each in-wheel motor is expected by 540.25 Nm which is suitable for traction as well as for braking.

For the further determination of parameters of the motor, the following assumption is made: vehicle climbing grade with a maximal speed V_{grad} of 75 km/h, whose value is half of the value for V_{max}. Accordingly, a power demand for a situation, where a 30% slope is climbed by the vehicle, has a value of 71.1 kW per in-wheel motor. Comparing the required power values for two critical applications of a motorized vehicle, it can be concluded that the electric motor of the in-wheel motor must be calculated in accordance to satisfy the power demand.

The power needed for acceleration from stillstand to 100 km/h in required time t_{req} (20 s) is calculated as:

$$P_{mech} = \frac{{V_{max}}^2 \cdot m_v}{t_{req}} \tag{3.10}$$

The height of curb that must be climbed by the vehicle has an important role during parking maneuvers. An electric vehicle has to be able to overcome the same obstacles as vehicles with internal combustion engine have. According to [14] the curbstone height in Germany ranges from 10 cm to 12 cm. The length of the lever arm depends on the climbed curb height and radius of the tire and can be calculated as:

$$l_a = \sqrt{2 \cdot h_c \cdot r_t - h_c^2} \tag{3.11}$$

The amount of driving torque M_{mech} that the electric motor has to deliver to overcome the curbstone can be calculated by:

$$M_{mech} = l_a \cdot \frac{m_v}{2} \cdot g \tag{3.12}$$

The results of calculated torque and power values as requirements of the in-wheel motor presents Table 3.3:

Requirements	Torque M_{mech}, Nm	Power P_{mech}, kW
Maximum speed by 150 km/h	265.7	70
Driving a slope of 30%	540.3	71.1
Acceleration from stillstand to 100 km/h in 20 s	-	87.25
Grade on a street curb	1133.3	-

Table 3.3 – Torque and power needed for the fulfillment of requirements of the driving performance of the in-wheel motor

Also, it should be paid attention to the operating mode of the developed in-wheel motor. As an example, Tesla Motors' vehicles can be introduced, which have a high-power density of 4.5 kW/kg [2]. However, this parameter is given for short-term operation and tests show, that the Tesla Model S is losing its dynamics after a short time due to motor protection from overheating. In addition, under normal conditions, the specified 515 kW power is not needed so often that the motor has time to warm up significantly, so that the normal driver does not have to struggle with the power limitation mode during normal daytime operation. In this regard, the overload conditions for the developed electrical motor are required to be determined as 70 kW power and 565 Nm torque value.

3.4.2. Parameters of the Motor

Common strengths of motors for electric vehicles are high efficiency, optimal controllability and a very small environmental impact [90]. Further important aspects of electric machines for an immediate in-wheel application are as follows:

- the maximum efficiency level for continuous operation,
- high efficiency ratio over the entire speed range,
- a limited value of unsprung masses,
- a torque overload ability in accordance with the power supply capacity (current, voltage and power limitations) and significant torque reserve for improved driveability and gradeability,
- low noise level (including magnetic origin),
- absence of contacts, simplicity of maintenance.

Graphic representation of the load characteristics of an electric motor for achievable driving performance can be displayed in a torque-speed diagram as in Figure 3.23. This diagram provides information that the motor is able to be operated backwards and forwards, as well as that the motor can be driven and braked (see e.g. [40] and [76]), which is a significant aspect for an application in an electric vehicle. The main focus of this diagram is the area in which the vehicle moves forward, as this is the main function of the vehicle. The forward braking area corresponds to the operation of the motor as generator to recuperate the kinetic energy of the vehicle.

Furthermore, there are two ranges that are distinguished: the constant torque range (basic speed range) and the field weakening range. In the first range, the continuous torque (nominal torque) or the peak torque for a short time (e.g. acceleration or climbing a curb) can be specified and is already available for starting. In case that speed is increased at nominal torque, the mechanical power also increases until the nominal power is reached.

That is why for the possibility of rotational speeds by nominal power the torque must be reduced with increasing speed. By these conditions a range of constant power is realized. Therefore, the electric motor has to be able to demand higher power to deliver the discussed range of specified motor performance scenarios.

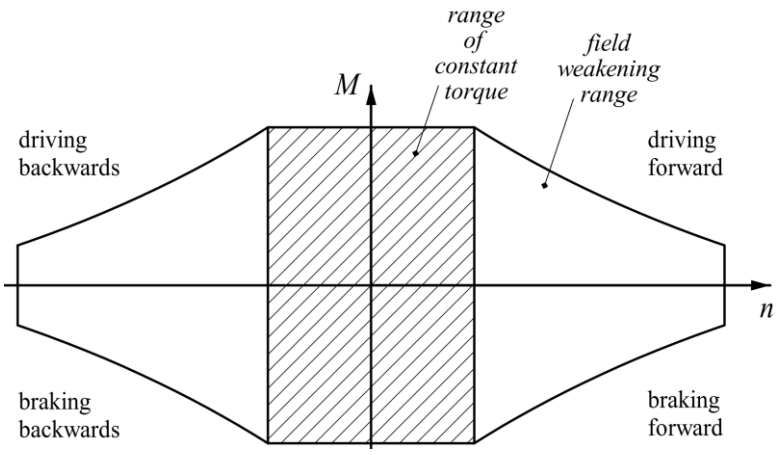

Figure 3.23 – Torque-speed diagram for permanent magnet synchronous motor

From the diagram it is possible to calculate the current, voltage and electrical power limits of the motor. A torque-speed diagram can be influenced by relatively simple parameter variations, for example by varying the number of pole pairs, what allows to define any operating point of the motor in a relatively simple way. It is also necessary to consider the fact, that an in-wheel motor is a system that is operated under conditions of limited power supply. These are limitations e.g. of maximum current of supply cables, battery current and voltage, etc. This circumstance inevitably develops an electric motor to ensure the operation of the motor in two control ranges: left and right from of the nominal speed. It should be noted that the control downwards of nominal speed can be provided by the torque constancy mode and control upwards can be provided by the power constancy mode.

The fulfillment of in-wheel motor requirements leads to the implementation of new non-traditional motor designs with increased active volume level. The last mentioned is possible due to the application of the synchronous motor with permanent magnets or so-called PMSM by using a special combined winding.

The torque generating in a PMSM motor takes place in the magnetically active air gap between stator and rotor. To generate a sufficiently high torque in the installation space limited by the wheel, the motor must have a specific force density related to the air gap to be as high as possible. The actual torque generation is based on the main effect of the force effect in the magnetic field. One part of the meandering copper winding is the air gap winding and another part is the slot winding. The air gap winding is glued onto a thin foil directly onto the stator back iron and the slot winding is inserted into the slots of the back iron. The cross-section view of the winding phases is shown schematically in Figure 3.24. The meander-shaped structure and changing orientation of the permanent magnets corresponds to the alternating current flows in the respective phases. Since all three phases together are as wide as a permanent magnet, each magnetic pole can be used at the same time for torque generation by using the Lorentz force. This results in an evenly variation of torque over the total circumference of the in-wheel motor.

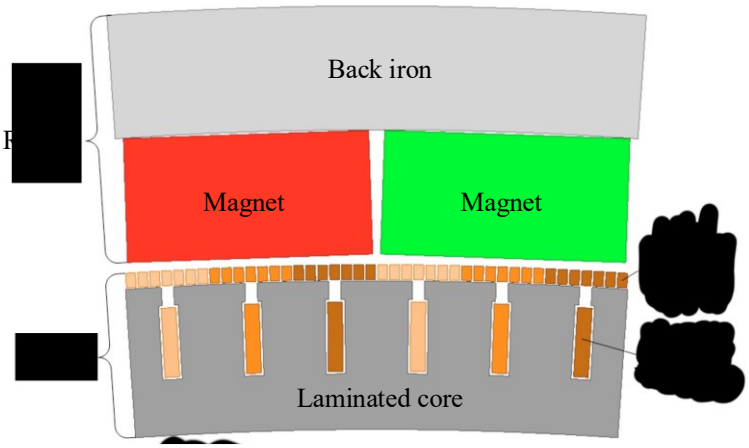

Figure 3.24 – Schematic diagram of combined winding [17]

Interactions that are responsible for energy conversion can be explained on the basis of the physical appearance of the Lorentz force. The Lorentz force is a force which acts on a current carrying conductor (combined windings) in a magnetic field. The general Equation for the Lorentz force according to [20] is:

$$F_L = l_{cc} \cdot I \cdot B_H \tag{3.13}$$

with the current I, the length l_{cc} interspersed by the magnetic field, the magnetic field B_H. For a common torque, it must be ensured that each individually formed force acts in the same direction. For this purpose, the current flow directions must be the same. The generated motor torque for combined winding can be approximately calculated as a torque that is proportional to the number of pole pairs, the magnetic flux of the permanent magnets and the air gap radius, as Equation (3.14) describes:

$$M_{el} = 2 \cdot p_p \cdot r_{ag} \cdot F_L = p_p \cdot r_{ag} \cdot l_{cc} \cdot I \cdot B_H \tag{3.14}$$

Thus, the motor torque is at first depending on the variable string current, the final proportional relation between torque and current is expressed by the motor constant k_M:

$$M_{el} = k_M \cdot I \cdot B_H \tag{3.15}$$

k_M can be expressed as:

$$k_M = 2 \cdot p_p \cdot r_{ag} \cdot l_{cc} \cdot B_H \tag{3.16}$$

The same motor constant k_M can be used for the proportional relationship between induced counter-voltage U_M and angular frequency of the motor ω_M:

$$U_M = \omega_M \cdot k_M \tag{3.17}$$

An electric quantity flowing through the cross-section of a circuit is an amount of current in the circuit. Consequently, the electrical power is directly proportional to the potential difference and the current in the circuit (see Equation (3.18)):

$$P_{el} = U_M \cdot I \tag{3.18}$$

Thus, from the calculation of the required torque of the electric motor for an in-wheel motor, it can be seen that the motor constant k_M and the value of the magnetic field B_H have a leading influence. It is worth mentioning that k_M depends on the motor parameters, which are essentially geometric. And the influence on the value of the magnetic field can be achieved only by two options: Either the selection of the magnetic assembly or application of different materials. Furthermore, advanced parameters of the motor with air gap and slot winding can be determined according to the approaches highlighted in [90][19] [20][91].

3.4.3. Losses and Cooling of the Motor

High output of mechanical power in the in-wheel motor results in a big amount of generated heat. Losses are occurring in the form of heat, that must be dissipated via cooling, which is explained in this section. Due to this, a considerable attention must be paid on various loss effects for the electric motor. Losses occur during the converting of electrical energy into mechanical energy. Generally, these losses are expressed by the efficiency, which describes the relation between input power and output power. Efficiency provides information about the supplied and removed power and the proportion of losses regarding a motor [26].

$$\eta_{motor} = \frac{P_{mech}}{P_{el}} \tag{3.19}$$

First, mechanical losses occur in the form of friction at the motor bearing and sealing or due to the air drag resistance. Copper losses are the biggest source of inefficiency in motors. These losses describe losses of energy as heat losses due to the electrical resistance of the wire used for winding [51]. The current I by the copper losses is quadratic and this means that with increasing load, the copper losses increase exponentially. Additional losses in form of iron losses, including eddy current losses and hysteresis losses, losses in the core are arising. Iron losses depend on motor speed and are minimized by the use of a core material with low remanence and high electrical resistance, which is often achieved through special lamination. In addition, because the magnetic field in the motor windings changes over time, these changings cause eddy currents in electrically inactive parts [117]. The eddy current loss occurs in the form of heat and heat accumulates in the iron parts of the motor. Further sources of losses in motor are insignificant and include magnetostriction, electromagnetic radiation and dielectric losses in materials used for core isolation and windings.

According to the second law of thermodynamics, a process in which energy conversions occur, results in heat dissipation. This heat must be dissipated from the process, with its system boundary, for example an electric motor, otherwise the temperature of the system would continue to rise and components of the motor could fail. Considering the cooling methods for the in-wheel motor, a comparison between the cooling methods and the cooling medium can be made. Surface cooling, internal cooling and closed-circuit cooling are the three main cooling methods [40]. The mentioned cooling methods are designable as direct or indirect cooling. In case of indirect cooling, there is a spatial separation between the heat source and the heat sink, e.g. by heat-conducting walls. In case of direct cooling, the cooling medium (heat sink) is in direct contact with the heat source.

Closed-circuit cooling is an indirect form of cooling in which the primary cooling medium is conveyed in a closed circuit and the heat is supplied to a secondary cooling medium. This concept enables intensive cooling of closed cooling structures using fluids (water, water glycol mixture, etc.) instead of air as a coolant. In the literature, there are several applications of the closed-circuit cooling to electric vehicles using a water jacket in the machine housing [124] [186].

From 3.4.1 it is known that the electric motor is able to provide twice as much of the nominal torque for a short time, with an intensive heat emission being expected. A necessary requirement for the operation of the motor is the ability to dissipate resulting heat loss for every required application. For these purposes, active circuit cooling of the windings as the part of the motor, which is most exposed to heat, is required. Therefore, an active liquid cooling for the windings limits the winding temperature T_{w_max} to 125°C according to the automotive thermal requirements [8]. Furthermore, as the target in compliance with the automotive thermal requirements according to [8], a Grade 1 with the temperature range from -40°C for winter conditions to T_{w_max} for the maximum motor coil temperature was accepted, thus a high thermal stress on the in-wheel motor system is expected.

The highest temperature differences occurring between the windings and the cooling channel essentially depend on the thermal resistances [145]. From the technological and manufacturing point of view, thermal resistances of windings are the electrical insulation of the wires, any production-related air gaps between parts and the distance to the cooling channels and their internal resistance. An effective cooling has to be able to keep the temperature difference between the copper winding and the cooling fluid as small as possible. In addition, a low flow resistance in the cooling channels, a small temperature difference between the inflowing and outflowing cooling medium and a maximum difference of 10°C is also required. From this perspective, a sufficient thermal conductivity and a thin layer of insulation and adhesive bonds between the motor

components are required. These requirements prevent possible mechanical stress by excessive temperature differences. The findings of the cooling requirements can be considered in more detail within the development process of the in-wheel motor.

3.5. Motor Weight Requirements

In addition to the requirements analyzed in the previous section for the driving performance, the driving behavior is an important parameter in terms of human perception [24]. In this section, the requirement for the lowest weight for the developed in-wheel motor system and possible solutions of this problem are presented.

3.5.1. Unsprung Weights Consideration

Unsprung weight or non-suspended weight is an important parameter, because it is a key part of the total evaluation, engineering and development of a vehicle. Traditional development of chassis always has the goal to keep the unsprung weights as low as possible in order to guarantee a high level of driving behavior, which depends on the compromise between agility, driving safety and driving comfort. For example, human perception of a vibration in vertical direction between 4 and 8 Hz and a vibration between 1 and 2 Hz in the transversal direction are considered to be annoying and uncomfortable [58]. The vehicle's suspension, as a part of the chassis, has the main function to isolate and to absorb vibrations caused by road disturbances [157]. Nishioka in [122] estimated, the larger the so-called unsprung mass is (i.e. the mass of unsprung parts such as wheels, pivots and suspension levers), the worse the vehicle's road holding performance will be due to variations of the road engaging the force of the tire when the vehicle is running on an unstable road. The integration of an electric motor in the wheel serves additional requirements with regard to the vehicle dynamics, because the weights of the motor and necessary components add up to the unsprung weights, therefore a more precise analysis of these effects is necessary. Some preliminary work focused on the effect of unsprung weights has been carried out by [5] and [6], however there are still some critical issues like high vibration frequency up to 80 Hertz that can act on the embedded electronics [151]. There was a study done by Watts et al. [177] and a very rigorous analysis conducted on a very difficult situation with a relatively small and lightweight vehicle (Ford Focus). By the evaluation of both variants (without and with additional unsprung weights on the wheel) in terms of objective, numerical as well as subjective measures were found, so that there is a difference in how the vehicle behaves, but that difference could be recovered with traditional riding and handling techniques. Several further studies addressing to unsprung weights, for example [121] and [176], have been carried out. They conclude, that increase in unsprung weights causes negative influence on vertical and pitch acceleration of the vehicle, that can lead to degradation of the vehicle driving behavior. Otherwise, integration of the in-wheel motor is possible by the rebalancing the vehicle parameters to achieve the best driving performance. In [167] the authors also show that the added wheel mass has no effect on the stability of the vehicle and that the frequency response is within the accepted comfort range. More recent evidence proposes that the suspension system of a standard vehicle can be used for an in-wheel application without loss of comfort or safety [172].

To overcome the disadvantage of unsprung weights an active suspension system has been developed, e.g. Bridgestone has designed the Advanced Dynamic Damper Motor – a technology to control the unsprung weight of the vehicle [114]. It involves the usage of the vibration absorption system, where the motors provide the function of vibration dampers. This means that the vibration of the electric motors is compensated by their own vibration from the road and tires, which improves the stability and comfort of driving. The Bridgestone proves to be a success of this approach, as unsprung weight management provides reliability and durability of the in-wheel motor. A further example of a solution to the problem of unsprung weight is Michelin's experience with Active Wheel technology [110]. By Active Wheel an integrated in-wheel motor control system compares and optimizes the weight balance of the wheels. With a significant mass of unsprung vehicle components such as an in-wheel motor (up to 40 kg), the importance of this control system increases.

The arguments provided above prove that chassis components can and must be adapted to the higher unsprung weights in order to reduce the negative effects of unspung weights. Nevertheless, based on the assumption that the effect of the increased unsprung weight on the driving behavior is acceptable, minimizing unsprung weights

by minimizing the total weight of the in-wheel motor has an attractive potential for additional improvements. An approach of the weight limitation through the lightweight design of the in-wheel motor has been taken into account in this work to minimize the influence of unsprung weights on dynamic loads and to optimize the vehicle's performance.

Lightweight design criteria have to meet two areas conflicting with each other. At first sight, the total weight of the motor must be kept as low as possible to reduce the impact of non-suspended weight on the vehicle performance. And, at the same time the low weight decreases the stiffness of the motor parts, which can affect a value of the air gap and, accordingly, the main function of the electric motor.

3.5.2. Material Analysis

The easiest method for a lightweight construction is to use materials with a low density. Currently in literature, only a few application examples of lightweight technologies for in-wheel motors can be found. Recently within the MEHREN research project, the Schaeffler AG is working on the next generation of in-wheel motors, shown in Figure 3.25, (a), together with Ford and Continental as well as the RWTH Aachen University and the University of Applied Sciences in Regensburg. However, the main objective of this project is rather to find an area for a multi-engine electric vehicle with highly efficient use of space and energy and uncompromising driving safety [178].

There are other projects where the lightweight construction of the chassis is the main research trend. Another example is the research project FAIR in which BMW Group, Schaeffler AG and DLR develop a concept with an axle e-drive and a 2-step gear box [138].

The LEICHT project is also more oriented towards a significant weight reduction by integrating the motor in an intelligent way through the development of innovative lightweight chassis systems, taking into account the electrical drives [75].

Via the application of a carbon fiber reinforced polymer wheel with an integrated electric motor, shown in Figure 3.25, (b), and demonstrated by Fraunhofer LBF in the field of electromobility, the reduction of weight and noise emissions is being researched, with the application of high modulus fibers in fiber reinforced plastics, compared to the use of metal instead [55].

a b

Figure 3.25 – a - In-wheel motor from Schaeffler AG [178], b - Demonstrator of Fraunhofer LBF [153]

The overview of above introduced concepts shows that there are many possibilities of lightweight solutions for e-mobility, based on the application in in-wheel motors. But there is a lack of information about the precise use of sandwich structures of carbon fiber reinforced plastics and aluminum foams. Therefore, it seems to be necessary to introduce what potentials carbon fiber reinforced plastics and aluminum foam applications have for the lightweight concepts of in-wheel motors.

Material analysis is one of the important stages in motor design. Each material has its own unique properties, which determine the degree to which its tasks are fulfilled. From another point of view, material selection is aiming for the identification of future manufacturing processes [47].

For applications ranging from satellites, aircraft, ships, automotive, rail cars, wind energy systems and bridge construction, the use of sandwich structures increases rapidly. Sandwich constructions have many

advantages for the development of parts that have always been solid and can therefore be given a new design in lightweight structures. Sandwich solutions are being extensively and increasingly used in lightweight constructions because they are light in weight, energy efficient, aesthetically attractive and can easily be handled and built [168].

The sandwich structure, as it is shown in Figure 3.26, has always the same basic idea: two facings (skins) which are relatively thin and have high-strength characteristics, enclose a relatively thick and lightweight core with specified stiffness in a direction that is normal to the faces of the structure [136].

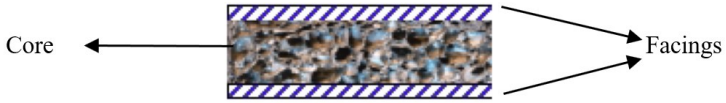

Figure 3.26 – Structure of a typical sandwich [136]

There are many alternative forms of sandwiches known by combining different facings and core materials. The facings can be steel, aluminum, wood, fiber reinforced plastics etc. The core part can, for example, be made of cork, rubber, plastics or synthetic or metal foam materials [35]. The possibility of combining materials to form sandwiches enables optimum designs to produce particular applications. In such a way, the positive properties of individual materials can be combined and the negative properties can be eliminated in sandwich structures [7].

Carbon and glass fiber reinforced plastics: The use of fiber reinforced composites in vehicles has grown significantly, but mostly through the application of glass fiber reinforced plastics in areas of vehicle body parts [113]. These composites have a high specific stiffness and strength and excel conventional steel and cast materials in terms of fatigue strength and thermal expansion. Fiber reinforced composites are created by combination of fibers in a matrix. Carbon fibers possess much higher strength than fibers of glass. This is why they rather fit into applications that require a high stiffness.

Carbon fiber reinforced plastics have densities of about 1.3 to 1.8 g/cm^3, glass fiber reinforced plastics are in a range of about 1.8 to 2.2 g/cm^3. However, a high level of engineering costs must be taken into account by replacing conventional materials through fiber reinforced plastic composites. But for prototypes, the in-wheel motor can be used to show what kind of potential exists in terms of weight savings [136].

Metal foams: Metal foams are a new class of materials with low densities and novel physical, mechanic, thermal, electric and acoustic properties [7].

The biggest advantage of metal foams is a low density in combination with a high stiffness. The cellular structure also allows a very good energy absorption and damping capacity. The first series of applications in mechanical engineering as a lightweight construction and damping element and in automotive engineering as crash absorbers have proved this statement to be true.

In the production of metal foams, a large number of variants of forms and parts could be realized. The variety of products based on metal foam sandwich technology shows Figure 3.27. A goal is to obtain varieties that have suitable forms and shapes for further implementations in lightweight designs for in-wheel motor parts.

Figure 3.27 – Variety of products based on metal foam sandwich technology [136]

3.6. Preliminary Results

In the presented chapter, the requirements for the in-wheel motors are determined. Firstly, to limit the possible area of application, assumptions and requirements according to the target vehicle based on the most widespread segments of the passenger vehicle stock in Germany were made. Furthermore, the topology based on the functional basics of the in-wheel motor was described and structural synthesis of the motor topology was performed. A wheel hub bearing was selected as a rigid element in the force flow. A wheel hub bearing is required to satisfy two conflicting properties: minimal weight and maximal stiffness. From this point of view, a wheel hub bearing of the 3rd generation was selected. According to the established topology, requirements on the elastic coupling element were developed. For this reason, loads acting on the wheel were classified and the most critical load scenarios were considered and subsequently, the generation of the critical loads for the in-wheel motor was carried out. As a possible solution in the area of torque transfer, the standard couplings were observed and a need of special coupling structure was detected. The presented two variants of elastic coupling are able to meet not only the requirement for torque transfer with different contact areas but also with different manufacturing demands. In addition, a technologically less difficult variant was preferred in order to avoid potential challenges in production during further development. The performance of the electric motor was investigated by the requirement on the energy demands of the target vehicle. For this reason, a general description of the vehicle movement was mathematically transcribed to determine the typical resistance and energy demands of the driving performance. Therefore, certain operating conditions like the maximum speed of 150 km/h, driving a slope of 30%, acceleration from stillstand to 100 km/h in at least 20 s and grade on a street curb were fixed. Depending on the operating condition, there were parameters primarily related to each other and output power as well as torque for these conditions were specified. The analysis of limiting load characteristics of the motor was carried out based on the condition of providing the maximum torque and maximum power in the range of operating scenarios. Hereupon, according to the determined motor parameters and thereby resulting losses, the importance of using an active cooling system was derived. The foregoing discussion was attempted on the most contradictory condition of the in-wheel motor – the demand for the low weight, caused by the requirement on the high driving performance by the high driving behavior. The main aspect here is that an unsprung weight attributable to the in-wheel motor was considered as a reason that this effect would not be prohibitive according to the known developments and research. However, to keep unsprung weight low is certainly a design requirement. The most common method for lightweight construction were analyzed materials with a low density and lightweight technologies according to their application on the in-wheel motor. Modern lightweight technologies – aluminium foams and carbon fiber reinforced polymers in designs for in-wheel motors were decided to reduce the weight of the motor.

A brief description of technical requirements for the in-wheel motor according to the analysis as well as summary data of parameters and characteristics are presented in Table 3.4.

Requirement	Symbol	Unit	Value
Requirements on the vehicle			
Vehicle weight	m_v	kg	2010
Wheel size	W_v	inch	16
Structural design of the wheel			multi-part wheel
Working space		mm	Ø356 x 156
Dynamic radius	r_{dyn}	mm	316.8
Maximum speed	V_{max}	km/h	150
Drag coefficient	c_w		0.27
Frontal area	A_f	m^2	2.2
Drive layout with load distribution			rear-wheel, 50%
Requirements on the topology			
Brake system			not included
Wheel hub bearing			BAR-0230, modified
Angular stiffness of wheel hub bearing	C_t	Nm/°	5500
Requirements on the elastic coupling			
Radial load	F_R	kN	10.4
Axial load	F_A	kN	10
Torque load	M_L	Nm	2000
Loads compensation	Technological easy elastic element, part of the rotor		
Requirements on the motor			
Electric motor type			PMSM, outrunner
Maximum angular velocity	n_{max}	min^{-1}	1258.2
Nominal power	P_n	kW	70
Maximum power	P_{max}	kW	87.25
Nominal torque	M_n	Nm	565
Maximum torque	M_{max}	Nm	1133.3
Temperature range	T_{w_min} ... T_{w_max}	°C	-40 … +125
Requirements on the weight			
Target weight	m_m	kg	Less 20
Desired materials			Standard materials, CFPR, Al-foams

Table 3.4 – General parameters for development of the in-wheel motor

4. Development of Concept-dependent Components

The previous chapter clarified that requirements for the development of the in-wheel motor are highly variable. Interrelation and interdependence of requirements have a significant influence on the performance of the electrical motor. In order to comply with the requirements that are critical for the motor, the model of the motor and its parts serve as a development instrument to make the structure of the motor study more comprehensible and to identify important cause-effect relations. The development strategy is segmented between main parts of the in-wheel motor: the electrical and mechanical parts and the cooling system. To simplify the development of the motor, its parts were divided into different subsystems. The developed subsystems have to comply with the theoretically optimal model, but at the same time manufacturing errors, a variation of the characteristics and a further simplification are allowed. Certain boundary conditions can be drawn from empirical engineering knowledge. The subsystems of the motor and the applications of individual materials are to be understood as typical and they may vary in certain applications due to different boundary conditions.

4.1. Electrical Part

The development of the electrical motor first begins with the rotor configuration, because the rotor has a geometrical limitation of the wheel. The stator with its components and other motor relevant parts are described below.

4.1.1. Rotor

Since the first bounding constraint is already accepted as the maximum diameter of the working space for the developed motor, the second restriction represents materials that can be applied for the parts of the rotor before final design and implementation could be started. Further rotor calculation depends directly on these two boundary conditions. As an additional restriction, a minimum distance between the rotor outer housing and the outer diameter of the considered working space of 3 mm is assumed.

4.1.1.1. Materials and Designs

For the development phase, firstly, standard materials are taken for all parts to define the main concept of the in-wheel motor and to have a reference for the next analysis.

Figure 4.1 demonstrates the biggest parts of the motor, which are the covers and the housing of the rotor. These parts are very suitable with more potential in the area of weight reduction. They present a thin-walled structure that ideally fits for an implementation of lightweight concepts like aluminum foams or carbon fiber reinforced plastics.

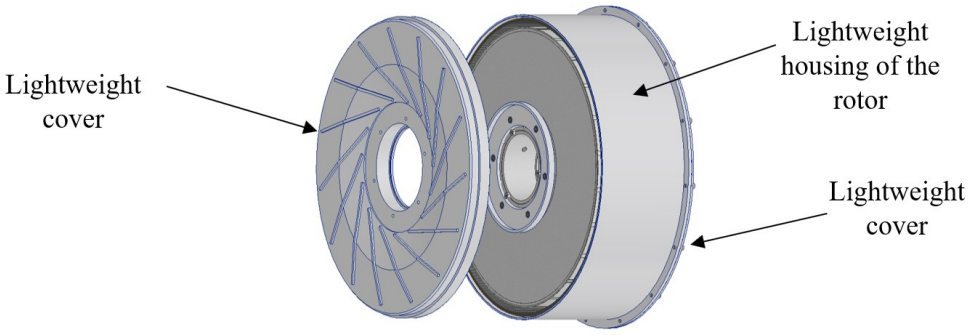

Figure 4.1 – Selected parts of the motor for implementation of lightweight concepts

In a first step, a new design of rotor housing and cover parts made of aluminum foams was developed according to the requirement profile. The concept presented in Figure 4.2, (a) includes two metal foam parts – right and left covers. For both covers SAS-structures were selected which consist of 3 layers: 0.5 mm thick facings in this case and 5 mm aluminum foam builds the core. The stability of the rotor housing made only from CFRP is not especially high and can cause vibrational loads. The use of the sandwich for the rotor housing consisting of aluminum foam core and CFRP facings increases the stability of the parts. Both designs also include parts for the bearing from one side and the threaded connection from another side (see Figure 4.2, (b)).

a b

Figure 4.2 – Concepts of rotor: a - Rotor housing of aluminum foam (sandwich), b - Development of a hybrid of aluminum foams and CFRP

Table 4.1 presents a comparison of the approximate weights of designs for the motor parts using lightweight technologies. Compared to standard materials, aluminum foams and CFPRs are lighter and have a potential for weight reduction, but technologically they are not characterized as the easiest way during the manufacturing process. This points out the fact that standard materials represent a more realistic approach for the manufacturing of the first prototypes of the developed in-wheel motor and the usage of the presented lightweight technologies, as it is explained in the following sections.

Component / Variant of version	Standard materials	CFPR	Aluminum foams	Combination, CFPR + Aluminum foam
	Weight, kg			
Rotor assembly	10.3	8.84	8.07	8.45

Table 4.1 – Calculated weights of rotor assembly

Details regarding the considered material for rotor back iron is presented in the literature (see e.g. [16] [17] [21]). The rotor back iron is made of a ferromagnetic material with nonlinear permeability, which provides a 1.97 T magnetic flux density and saturation at 50 kA/m. Variants of rotor back iron and its relevance are more detailly described in the following section.

As it was presented in 3.2.1 and 3.4.2, permanent magnets have a direct influence on the motor development and future driving performance. The best magnetic material in terms of remanence flux density and coercivity is NdFeB [34]. That is why sintered NdFeB magnets currently appear to be the most promising solution. The main advantage of these magnets is the obtained value of the energy product $(BH)_{max}$, which is the largest of all known materials with up to 5 T by ambient temperature and higher [28]. Secondly, NdFeB magnets are characterized by a high Curie temperature of about 160-170°C for types with an operating temperature of 80 ºC [43]. The remanence flux density depends on the magnet temperature and as the magnet heats up, it is reflected in an increase in current to produce an output torque [179]. For this reason, the main requirement for the operation of the motor is to create operating conditions under which the magnets never enter the irreversible demagnetization zone to avoid their demagnetization. However, NdFeB magnets are produced to cope with operating temperatures up to 200°C nowadays, which opens up a broad perspective for their application. One of the most important and essentially determining advantages of NdFeB magnets in terms of economics is their

relatively low price in comparison with other types of known magnetic materials. NdFeB also has better mechanical properties compared to e.g. SmCo-magnets, which is important for the production process [4]. As mentioned by Hackmann [61], other magnets like ferrites or AlNiCo-magnets provide a low energy product $(BH)_{max}$ and these magnets would require too much material to achieve the desired energy density in the air gap. In order to make a choice with regards to the requirement on maximum temperature (see 3.4.3) for prototyping purposes, the generic material N45SH as a material for permanent magnets was used. NdFeB materials are sensitive to corrosion and react with oxygen in an untreated state resulting in very fast oxidation. Therefore, NdFeB magnets need a corresponding surface protection. This is realized by using Ni-Cu-Ni coating. The parameter values of accepted material are presented in Appendix C.

4.1.1.2. Number of Magnets and Magnetization Type

The number of magnets n_M has a significant influence on the motor performance. According to Equation (3.14), the pole pairs number or doubled number of magnets is proportional to the torque M_{el} and can be recognized as a pure geometrical coefficient. On the one hand, a maximization of the number of magnets leads to increasing motor torque, but on the other hand there is a complex of restrictions caused by the geometrical limitations of the inner diameter and the length of the rotor part and manufacturing limits of the magnet width w_M. Considering the given rotor outer diameter in accordance with physically limited working space of the wheel, the first restriction on the rotor inner diameter D_{ir} has its maximum at 350 mm. Therefore, the distance of 3 mm is provided as a gap between wheel rim and rotor housing.

In case of a high number of magnets (n_M>100), the difference between the width of the magnet and the arc length required for its mounting consists of less than 0.001 mm. Assuming that the length of the arc is not relevant for the calculation of the number of magnets, this difference can therefore be neglected for further calculations.

The distance between the two magnets must consider the tolerances in magnet manufacturing. The tolerance range used for the manufacture of 10 mm wide magnets is ±0.1 mm. By reducing the tolerance range, the manufacturing of magnets becomes considerably more expensive [164]. According to the relevant tolerance range and to the dimension chain, the minimum distance d_M between the magnets requires at least a value of 0.2 mm. Under these circumstances, this parameter may have a higher value and may be adapted for the required even number of magnets. The potential number of magnets can be calculated as:

$$n_M = \frac{\pi \cdot D_{ir}}{d_M + w_M} \tag{4.1}$$

In this work, two magnetization types – a conventional radial magnetization and a Halbach array magnetization – are presented with the target to minimize the weight of the rotor part of the developed motor, while the magnetic flux density in the air gap between stator and rotor is maximized and maintained.

Conventional radial magnetization requires a back iron of the rotor. Therefore, the magnets are mounted on the back iron with alternating polarity as shown in Figure 4.3, (a). The function of the back iron is to provide the containing and conducting of the magnetic fields. To describe the behavior of the magnetic flux density in the air gap by the variation of magnets, the parametric model was built upon a numerical finite elements' method analysis (see [21] for a model description). According to this model, a height of 5 mm for the back iron allows the magnetic flux density to reach up to 1.10 T in the air gap.

As the next step of development, the inner diameter D_{ir} for the mounting of magnets has to be reduced by the height of the back iron and has a value of 340 mm. The rotor back iron as a fully cylindrical part is presented in Figure 4.4, (a). According to Equation (4.1), the developed motor by conventional radial magnetization can be implemented with the number of magnets n_M = 104.

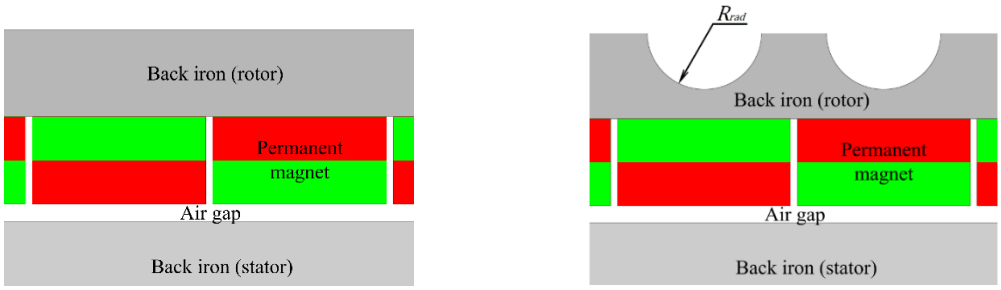

a b

Figure 4.3 – a - Magnetic circuit design for conventional radial magnetization [21], b - Shaping of the back iron of the rotor

A possible solution to minimize the weight of the back iron of the rotor is shaping, as it is showed in Figure 4.3, (b) and Figure 4.4, (b). From this point of view, it is possible to make radial grooves with R_{rad} of 4 mm into the rotor iron. The grooves must be positioned exactly radial to the magnet centers. A comparison of the weight calculation of the back iron in CAD shows that the mentioned solution allows to reduce a rotor back iron weight of about 2 kg, so the shaping can reduce the weight by 40%.

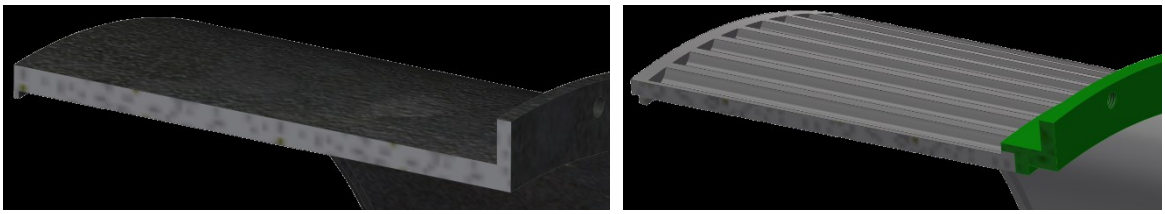

a b

Figure 4.4 – Variants of the rotor back iron: a - As fully cylindrical part, b - With radial shaping

Halbach array magnetization, first presented by Halbach has an arrangement of permanent magnets resulting in a non-symmetric magnetic field [62]. Halbach magnetization consists of alternating axial and radial magnets as it is shown in Figure 4.5. The key advantages of the Halbach array are that the field on the one side is approximately doubled by the confined flux and the opposite side has a minimal stray field, which helps with confinement and consequently reduces the chance of a flux leakage. These advantages have a significant impact on the motor design, because the use of magnetic materials other than permanent magnets is not necessary. Thus, there is no need to use back iron for retaining and the conducting of magnetic fields.

Further presented analyses are based on the assumption that for convenience of calculation and an aliquot number of magnets the inner diameter D_{ir} is 342.6 mm. Based on this limitation, the outer diameter of the rotor part as a support housing for magnets is considered to be 350.4 mm, which allows a 2.8 mm gap to the wheel rim and a thickness of the rotor housing of h_H = 3.9 mm. As it can be derived from Figure 4.5, the Halbach array is represented by a double number of physical magnets. To receive the magnetic field of a magnet, two halves of axially magnetized magnets and a fully radially magnetized magnet are required. Thus, the magnets with axial and radial magnetization become the half of the width compared to conventional radial magnetization. According to this, also a smaller tolerance range of ±0.05 mm can be used. According to Equation (4.1), the number of magnets n_M for Halbach array can be calculated by 112 pieces. In terms of the tolerance range, the width of one magnet with radial or axial magnetization n_{Mph} is 4.7±0.05 mm. It is important to highlight that the weight of the rotor housing for magnets is only 1.38 kg if it is made of conventional aluminum alloy.

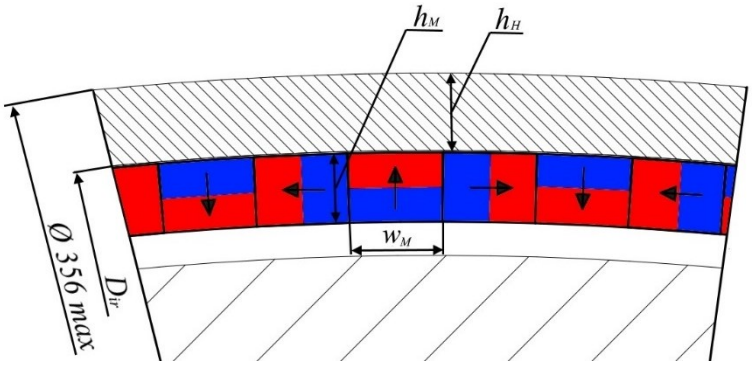

Figure 4.5 – Halbach array magnetization

Under the considered conditions, remarkable differences by the magnetization require additional weight and volume by conventional radial magnetization. Research by Borchardt et al. [16] suggests that the comparison of the weight of magnetization arrangements by conventional radial magnetization and Halbach array provides an option of a weight reduction of about 51% of the rotor unit weight.

A simple comparison can be organized using Maxwell to observe the difference in magnetic fields by using dipole and Halbach array arrangement. The following simulation shows two identical configurations according to material and geometry, whereby the plate of the back iron in dipole variant is made of steel (Figure 4.6, (a)) and for Halbach array made of aluminum as depicted in Figure 4.6, (b).

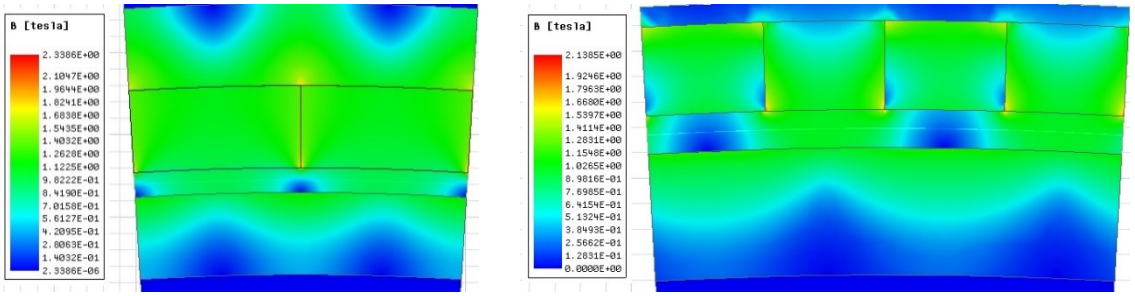

a b

Figure 4.6 – FEM-simulation of magnetic flux distribution for: a - Standard dipole, b - Halbach array

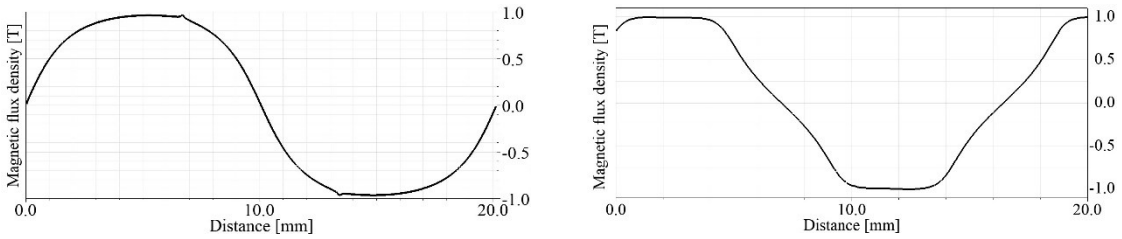

a b

Figure 4.7 – Results of simulation of magnetic flux density for: a - Standard dipole, b - Halbach array

The simulation results shown in Figure 4.7 provide that Halbach arrays have clear advantages over a standard dipole magnet configuration. The back iron of the rotor proves to be more effective in reducing leakage, although its influence on improving the magnetic field density in the air gap is not as significant. Based on the results of the simulation, a Halbach array is offered for further use in the developed motor, which can effectively reduce the weight.

4.1.1.3. Necessary Magnet Weight

In order to meet the required performance and lightweight requirements, great attention must be paid to the required volume and the respective weight of the magnets m_M during further development. This can be realized using the magnet's geometric parameter – height h_M and the length l_M.

A geometric parameter related to the driving performance of the developed motor is the length of the permanent magnets. According to Equation (3.14), the length of the magnets has a proportional impact on the motor torque. Based on the requirements for the working space of the motor and taking into account the additional geometric spaces in the axial direction for the position of the windings, the length of the permanent magnets l_M has been assumed to be 100 mm. In case of insufficient torque of the motor, this parameter can be used for a detailed calculation of the motor parameters.

For the variant with a height value of the magnet h_M of 5 mm, a translational model of the magnetic circuits for the Halbach array arrangement with similar geometry boundaries was presented by Borchardt in [21] in order to simulate the magnetic flux density in the air gap. The translational model in this case is preferable, while the differences to the rotational model are irrelevant. According to this approach, the mean magnetic flux density B_{Hm} for Halbach configuration with 1.5 mm air gap h_{ag} is to be expected at 1.1 T.

To analyze the influence of different heights of the magnets h_M on the magnetic flux density, six different heights were studied over the range of 2.5 mm to 5.0 mm (2.5, 3.0, 3.5, 4.0, 4.5, 5.0). In order to limit the leakage flux and to minimize reluctance in the magnetic flux path, the value of the air gap was fixed at 1.5 mm.

Figure 4.8 shows the results of the FEM-simulation of the magnetic flux density for different heights of the magnets h_M. The software program used to analyze the data was Ansys Maxwell.

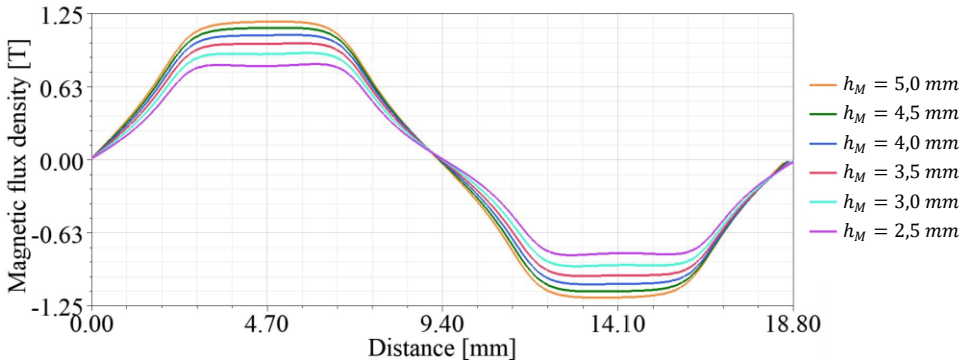

Figure 4.8 – Results of the simulation of the magnetic flux densities for different heights of magnets

The analysis identifies a significant difference between approachable magnetic flux densities for different magnet heights. The higher the value of h_M, the higher the magnetic flux density in the air gap. For the development process, the height of the magnet h_M of 3.5 mm was considered as the value that meets the production and machining limitations due to the high brittleness of thinner magnets and also due to the handling that causes swarf/sludge formation [129]. From this point of view, the total weight of the magnets m_M can be reduced by 31.5% to 1.35 kg in comparison to the height of 5 mm.

In addition, as shown in Figure 4.6, (a), no ferromagnetic impurities adhere to the outer surface of the rotor in the Halbach array, since the low magnetic flux is almost non-existent on the weak side - considering the thickness of the rotor housing.

All results were obtained without the winding in the air gap, because the windings in deenergized condition do not have a significant effect on the magnetic flux density [95]. Simulated results can then be used to determine the geometry of the windings in the air gap.

4.1.2. Stator

The key aspect in this section is the definition of the characteristics of the stator as one of the main electric components of an in-wheel motor. Therefore, the suitable materials for the main stator body are used as the basis for the analysis of the estimated weight for the stator unit. Furthermore, approaches are presented and

used to determine the winding and inlay characteristics for providing the necessary motor performance. The implementation of the improved winding and inlay concept is evaluated on the basis of the theoretical, technical and technological realization requirements and is integrated into the concept of the motor.

4.1.2.1. Materials

The materials of the stator as a second active part of the motor include not only the selection of materials for the main parts – stator body, back iron and windings – but also for supplementary components such as insulations, thermal couplings and magnetically conductive elements.

The design concept shown in Figure 4.9, (a) of the stator base body is developed in order to achieve the desired aims of a lightweight construction. The densities of the individual materials indicate which material proportions must be reduced in order to reduce the total weight of the stator. The first concept design consisted of an aluminum base body with a magnesium cover and sleeve to close the one-sided cooling channels in the base and surface area of the stator. The weight of this variant adds up to 3.83 kg, which compared to the full aluminum variant resulted in a weight reduction of only 6.6%. In order to reduce the weight, it was essential to significantly increase the content of magnesium in the stator body. Following this principle, the design concept of a further variant is developed as it is shown in Figure 4.9, (b). The developed variant is characterized by the circumstance that the stator base body also became an Al-Mg hybrid component. In the specific implementation, the higher-loaded stator base body ground remained as an aluminum component, while the cooling ring of the stator base body is replaced by magnesium. The one-sided cooling channels should be closed with an aluminum cover. A magnesium sleeve is still used to close the cooling channels on one side in the cover area of the stator base body. The Al-Mg variant has a weight of 3.45 kg and thus fulfilled the lightweight requirements. Compared to the full aluminum variant, the weight saving amounts to 15.9%. Nevertheless, due to the fundamental redesign of the Al-Mg lightweight stator, it is necessary to develop an assembly technology suitable for production for connecting the stator base body bottom segment made of aluminum with the stator base cooling segment made of magnesium. This resulted in the demand for a new Al-Mg composite technology through production.

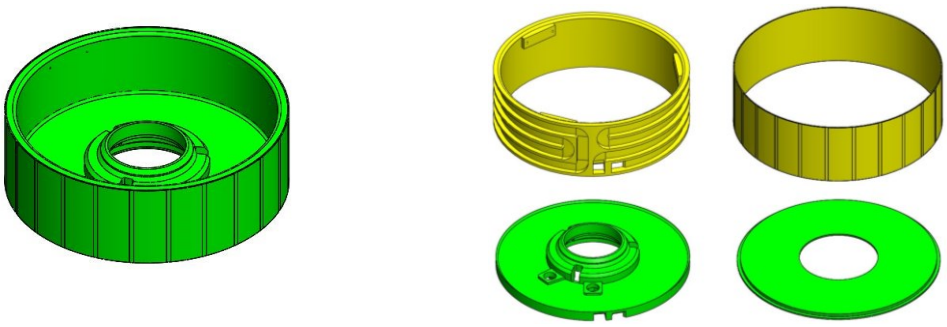

a b

Figure 4.9 – Stator body concepts: a - Full aluminum, b - Hybrid Al-Mg

To determine the materials used for the stator windings, it should first be clarified which structure a winding concept has. Figure 4.10 shows a cross-section of the adhesive structure of the air gap winding.

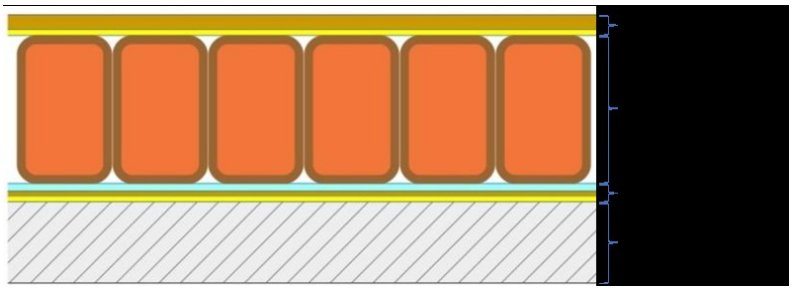

Figure 4.10 – Structure of the air gap winding [163]

In accordance to the manufacturing process of the stator motor active parts, the first layer presents a stator back iron. The stator back iron consists of electrical sheets, which allow to reduce eddy current losses induced by the fast-moving alternating magnetic field through the stator, whereby the very simple geometry of the flux-carrying parts of the back iron enables simple and cost-effective sheet metal design. The electrical sheet is one of the most important materials in electrical engineering [77]. Depending on the application, the electrical sheet has to meet various requirements, whereby the most important are the magnetic properties: a high permeability and a low loss, which have a particular significance for the realization of magnetic circuits. As it was figured out above, the losses generated in the stator back iron are divided into hysteresis and eddy current losses. A calculation method for determining the individual losses is given for example in [72] and [175]. Based on the results presented by Zhitkova et al. in [186], it can be concluded that the NO20 electrical steel is most suitable for the back iron development of the stator, as it is a typical economic material for high-performance electrical traction drives. The biggest advantage by using NO20 is that the eddy currents in the back iron can be neglected. A small sheet thickness of 0.2 mm has a significant impact on the motor performance, and an increase in efficiency and thermal load on the motor can be expected within the permissible limits. An application of the NO20 reduces iron losses to a minimum at high magnetization frequencies. Another advantage of using NO20 electrical steel is that it has a high permanence as well as a high flux density and therefore, a higher torque density is to be anticipated. More details on the NO20 electrical steel are given in the Appendix D.

The insulation of the stator is located between the stator back iron and the copper wires of windings with the function to protect the winding from damage. In order to achieve a high utilization of available space in the air gap and a high thermal conductivity (dissipation of the generated heat), the insulation should have a layer thickness which is as small as possible [72]. Research by Stamann et al. [163] pointed out that in addition to the mechanical properties of the adhesive bond, thermal resistance, electrical insulation and dielectric strength must also be taken into account when selecting an adhesive type to be used for fixing the air gap winding. It has been suggested in [162] that the optimal adhesive result is obtained by fixing the copper wire of the air gap winding with double-sided electrical adhesive foils on the stator. Double-sided adhesive foils are capable of providing the main function of the stator insulation to retain the winding on the surface of the stator back iron. Constant coating thickness of the foil by this technique plays a major role with regard to the very high demands on the manufacturing tolerances for the parts in the air gap. Furthermore, the process cleanliness as well as the so-called immediate adhesion are additional advantages of this adhesive technique. Based on these requirements and according to the analysis presented in [163], the foil 70984 was selected to fix and insulate the air gap winding. The detailed data sheet with more parameters of this foil can be found in Appendix E.

The next layer presents a copper wire as a part of the stator air gap winding. The stator winding is the main component of the electric motor because it conducts the current and thus the torque of the electric motor is generated. The most well-known parameter of the winding presents a fill factor, which can be explained as a proportion between the effective and the theoretically maximum cross-sectional area of the copper conductors. Apart from this statement, the insulation of the wire must be as thin as possible to provide the highest value of the copper content in the windings. As a result, a low phase resistance is to be expected, which leads to the low copper losses and enables a high motor efficiency. Additionally, as it is shown in Figure 4.10, a high power density due to the high fill factor is provided by the rectangular cross-section of the wire. The developed motor uses polyamide-imide enameled rectangular copper wire with the class N of insulation, which is capable of operating up to a temperature of 220°C [83]. The exact size and number of the used wires will be subsequently chosen in 4.1.2.2. An example of copper wire and insulation for air gap winding with its tolerances is presented in Appendix F.

The last layer of the air gap winding presents a bandage. The bandage is used in order to prevent the influence and possible contact with the rotating parts on the windings, which have to be fixed in radial direction. The winding packages are usually mechanically fixed by bandage tapes or rings. The most important mechanical properties in this case are the tensile strength and the adhesive strength of the bandaging material. For the developed motor, the 3M® insulating tape made of glass fiber fabric was used. This tape is a 0.17 mm thick woven insulating glass fiber fabric tape with thermoplastic, and pressure sensitive adhesive is used for electrical insulation and mechanical protection at temperatures up to 230°C. More properties of the selected bandaging tape are given in Appendix G.

The combined winding of the motor has a second winding – the slot winding. The slot winding, as it is presented in Figure 4.11, is composed of the enameled rectangular copper wire similar to the wire of the air gap winding. As it can be found in Appendix F, the polyamide-imide enameled wire has a thickness of 0.025 mm and tolerance range of ±0.015 mm, which provides a sufficient insulation for the non-slotted application. The rough and uneven structure of the stator back iron is able to radially damage the insulation of the copper wire by different loads, most significantly by various types of vibrations or displacements of NO20 sheets. To obtain the required dielectric strength and meet the requirements for creepage distances, additional insulation is required. As a separate insulation, a NOMEX® insulating paper for slot windings is used. Further information on the considered insulation paper can be found in Appendix H.

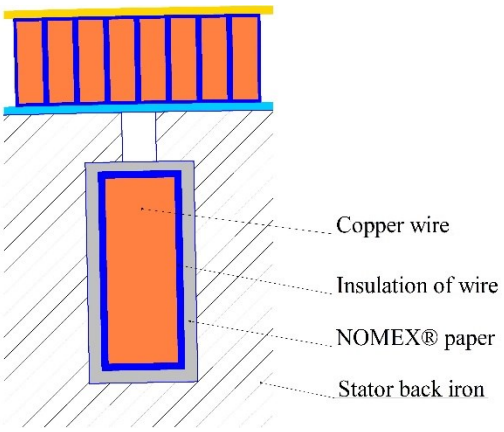

Figure 4.11 – Structure of the slot winding

The terminal clamps, as it was reported above (see 3.2.1), are also a part of the stator unit and shall fulfil conditions and meet requirements on the operational environment of the electric motor. Terminal clamps must mechanically connect the elements of the winding according to their function, but these elements are also under voltage. The core problem of the connection points of the windings constitutes additional thermal stress by sophisticated heat dissipation. Based on a given study of the factors affecting the terminal clamps, it is justified to use the SLS PA3200 material, which has excellent mechanical properties and, with its high accuracy, is suitable for this application. More detailed properties of this material can be found in Appendix I.

It should be noted, that the materials for the stator unit as well as the for the rotor unit were only chosen for initial dimensioning.

4.1.2.2. Winding Topology and Sizing

The stator winding is one of the most important part of any motor because it carries current and thus generates torque. Current carrying and cooling capacity of the windings has a crucial influence on the performance of an electric motor. The most important parameter of the winding is the fill factor, which is defined as the ratio of the effective cross-sectional area of the copper conductors to the theoretical maximum cross-sectional area of the available winding space. The fill factor has a direct influence on the copper amount and accordingly it leads to the influence on the phase resistance, thus ensuring an efficiency of the motor. For this reason, maximizing the amount of copper in the motor through the design of the windings takes a leading position. The secondary tasks by the design of the windings are dielectric strength and the number of individual conductors per strand, as well as the back iron of the stator and the insulation system. Therefore, the innovation of the new combined winding, consisting of air gap and slot winding, is applicable to obtain the high fill factor value.

The first layer of winding, the air gap winding, is characterized by the fact that the conductor is mounted directly on the outer surface of the stators' back iron, and is thus directly in the magnetic field of the air gap between the rotor and the stator. Applying the air gap winding, the soft magnetic material between the windings, the pole shoes, can be completely eliminated. Therefore, the weight of the assembly responsible for the force development can be reduced. Due to the layout of the windings in the air gap, the length of the copper wires is relatively short. Thus, a very small resistance of the air gap windings is noticeable, because the air gap winding has a relatively large cross-section and requires relatively small amounts of winding material [92]. In

addition, because of the position of the air gap winding, the inductance of the windings is also very low, resulting in especially short time constants of the electrical circuit. The respective winding strands of the phases are arranged opposite to the magnetic pole. Coupling is affected directly via the Lorentz force acting on a conductor in the magnetic field. Due to the magnetic field generation of permanent magnets and the resulting reduced weight of the rotor, a mechanically very dynamic behavior can be expected. Using this concept, high dynamic lightweight motors with a very high power density can be realized.

By Borchardt et al. [17] it was highlighted, that higher current densities are obtainable by the rectangular cross-section of the strands, thus material demand of copper and ohmic losses decreases. In case of a rectangular cross-section of the individual winding strands, the winding strands have a shorter side h_{st} as the height and a longer side w_{st} as the width of the strand [92]. Thus, impact of both parameters is very critical to the design of the air gap winding. Moreover, the impact of both parameters is very critical to the design. An increase in magnetic flux and, as a result, a relatively high magnetic force per wire can be achieved by increasing the w_{st}/h_{st} relation. Kasper and Borchardt especially preferred w_{st}/h_{st} ratios between 4 and 20 [92]. According to the function of the motor, the air gap winding moves through the alternating magnetic field, whereby the eddy currents occur. An elimination of eddy currents in the winding strands can be achieved by splitting the winding strands into separate wires. Therefore, according to [17], eddy currents can be varied very precisely in terms of wire widths or according to [17] can be totally neglected by the slotting of strands. The sizing of the width of the winding strand is already geometrically limited to the width of the magnet and can be calculated considering the value of the air gap.

To obtain a homogeneous field, the mechanical air gap, as it is shown in Figure 4.12, has to be kept as small as possible for the developed motor, because Lorentz forces here are considered as driving forces and have a direct influence. The mechanical air gap presents a shorter distance between the permanent magnet surface and the outer surface of the wire in the air gap. The winding positioned in the air gap with the shorter side parallel to the magnetic field lines ensures a relatively small air gap and thus a relatively high torque. A smaller air gap height increases not only the magnetic flux and motor torque but also the costs due to increased precision in manufacturing [22]. Moreover, one argument cannot be ignored in order to consider the air gap value - the small winding strand height increases the resistance. Thus, the ohmic losses increase too. According to the considered value of the air gap h_{ag} at 0.5 mm (see 4.1.1), it is necessary to determine the winding parameters. An expected value of the height of the winding strand for the air gap winding can be calculated as:

$$h_{st} = h_{wag} + 2\,h_{iag} \tag{4.2}$$

After setting the values for the elements of the air gap winding, the magnetic effective air gap h_{meag} can be calculated as follows:

$$h_{meag} = h_{ag} + h_{st} + h_f \tag{4.3}$$

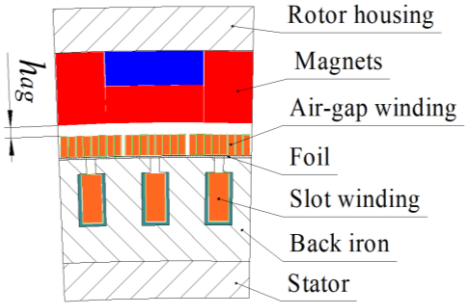

Figure 4.12 – Cross-section of the motor active parts of the developed electric motor

For the developed motor, an even number of wires n_w in the winding strand by eight was selected to provide symmetrical distribution over the wire length and resistance inside each phase. Taking into account the width of the copper wire w_{wag} and the required wire insulation width w_{iag}, the average tolerances for wire production were also considered. Thus, the width of one winding strand w_{st} can be calculated as:

$$w_{st} = n_w \cdot \left(w_{wag} + 2\, w_{iag}\right) \tag{4.4}$$

The width of one winding strand w_{st} has to be taken into consideration by the calculation of the free space between strands to receive a guaranteed manufacturability of the air gap windings. For the developed motor, the minimal distance between winding strands has a value of 0.15 mm in case of maximal size of width of wire w_{wag} and insulation w_{iag}. Minimum size of the widths according to manufacturing tolerances allows more freedom for the winding process, but simultaneously reduces the fill factor of the winding strands. Figure 4.13, (a) summarizes the geometric data on the air gap winding.

One of the ways for the improvement of the developed electric motor and to meet the requirements of the motor performance is the new principle of an electric machine with combined winding, which is the supplement of the idea of the meandering air gap winding by an additional slot winding [95]. According to the approach of combined winding, presented in [90] and [92], the use of an additional slot winding provides more torque and power per motor active mass/volume. In accordance with [90], the average torque for a similar geometry of the winding is expected in the range of more than 600 Nm by the maximum power of up to 80 kW. Adding the slot winding offers the possibility to build the electric machine more effectively, because the magnetic field is used for both windings at the same time and because this construction has a higher potential for lightweight construction. Compared to the only-air gap winding design, solely the additional weight of the slot winding should be added to the total weight of the developed in-wheel motor. Further advantages as described by Kasper and Borchardt in [93] are compactness, efficiency, high dynamic and high-torque characteristics with a slight increase of the manufacturing costs.

The idea of slot winding is technically realized by inserting conductors in the special slots of the stator back iron. In addition to different positioning, the combination of windings means the usage of different electromechanical conversion principles [90]. Compared to the air gap winding, the slot winding uses a principle of magnetic force between electromagnet generated in the stator and the permanent magnets of the rotor. Teeth of the back iron bind a part of the magnetic field lines due to the lower magnetic resistance, and generate the surface currents through further magnetization. In the non-current case together with the remaining field in the slots, the cross currents form two Lorentz forces per slot which have the same value due to the symmetry, but act in opposite directions and thus cancel each other out. Description given in [175] outlines an increase in the separate magnetic field formed around the conductors in the slot, if a current flow is applied to the conductor. The magnetic force and the magnetic field increase on the side of the slotted winding, i.e. congruent to the magnetic field, so that the torque occurs. Hence, an additional torque is generated while the same B-field for both windings is used.

The arrangement and energization of both windings are designed in such way that two windings influence each other as little as possible. Inserting the slot winding to the position of the air gap winding has an impact on the back EMF. As a result, the slot windings are placed symmetrically to the center of the appurtenant stands of the air gap winding. According to [95], to enable a high voltage level and higher values of inductance, the slot and air gap windings are connected in a simple series connection. Additionally, [154] reported that windings connected in series also ensure that the inductance of the stator is increased, thus the motor is operated in the field weakening range.

As it has been suggested in [90], the limitation of the width of the slot w_{sl} is a useful approach to prevent a possible saturation. From this limitation and depending on the cross-section of the air gap winding, the geometric parameters of the wires for the slot winding can be calculated. The value of the maximum current and electrical resistance of both windings have to be identical. For this reason, the value of the strand cross-section of the air gap winding can be used as a reference for the geometry of the slot winding.

An expected occurrence of the cogging torque causes a jogging and unsmooth motion of the developed motor [79]. Additional shoes integrated into the slots of the back iron, as can be seen in Figure 4.13, (b), decrease the cogging torque by carrying the magnetic flux. The geometry and the height of the slot opening h_{in} require an additional torque reduction study, which follows in the next sections.

The values of the insulation thickness w_{is} and h_{is} can be calculated in accordance with manufacturing tolerances and the thickness of NOMEX insulation paper has a standard value. Finally, the width w_{ws} and the height h_{ws} of the wire for the slot winding can be calculated as:

$$w_{ws} = w_{sl} - 2\,w_{nom} - 2\,w_{is} \tag{4.5}$$

$$h_{ws} = h_{sl} - 2\,w_{nom} - 2\,h_{is} \tag{4.6}$$

For illustration purposes, Figure 4.13 depicts all the geometric parameters listed above of the developed motor having the air gap and the slot windings.

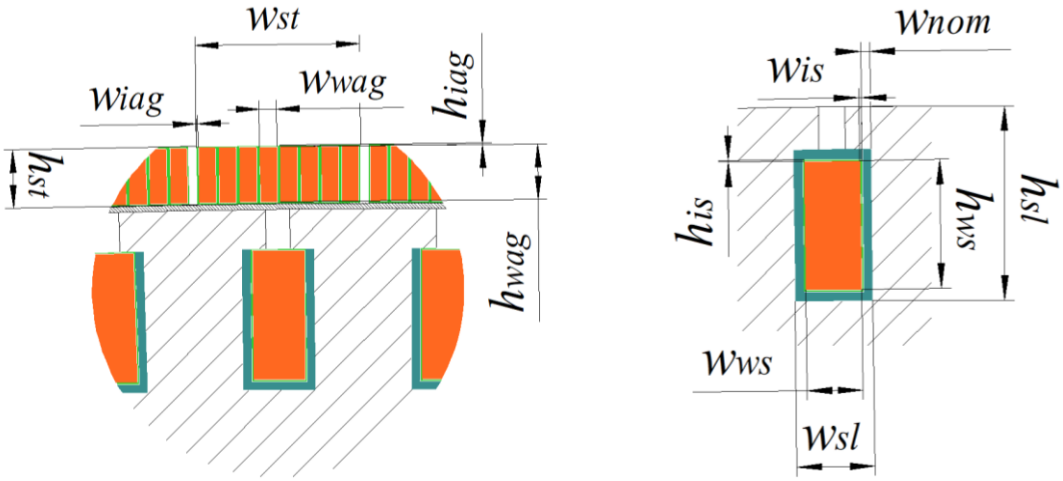

a b

Figure 4.13 – Geometric parameters of windings of the developed motor: a – Air gap winding parameters, b - Slot winding parameters

More details concerning parameterization and dimensioning of the electric motor as well as other aspects related with the detailed electric design can be found in [22].

4.1.2.3. Slot Inlays

The torque of a PMSM motor is not absolutely constant and is characterized by different fluctuations. These torque fluctuations are an undesirable component of the motor torque that are typical for most of the electrical machines with permanent magnets, because it results in unwanted effects such as vibrations, rising of the noise level and variations of the motor rotation frequency. In the field of electric PMSM machines, various definitions of the torque ripple can be found. The main components of the torque fluctuations by PMSMs are caused by electromagnetic torque and cogging torque. Willberger in [179] has reported that the electromagnetic part of torque fluctuations is associated with the discrepancy of the back EMF and the phase currents. The term “cogging torque” has come to be used to refer to the fluctuation of the tangential component of the interaction force in the PMSM motor [32]. The analysis given in [45] proposes that one of the most frequent requirements of manufacturers on the PMSM motor is that unwanted cogging torque should not be detectable during starting or the starting from standstill should be possible without jerking. Torque instability is undesirable in many applications, including drive systems in passenger vehicles in which it can cause additional vibrations. Especially when the motor is used to achieve a good dynamic response to other systems of the vehicle, such as the chassis, the cogging torque is undesirable, which can lead to malfunction of the motor drive. Additionally, as a further disadvantage is reported by Perez [135] that the control of the motor that has a high value of the cogging torque can be difficult, because it creates challenges for the control systems by the determination of speed and the position of the motor. In accordance with above described facts, further studies need to be carried out that take cogging torque into account and actions for its significant reduction.

The cogging torque can be caused by the different origins. The main source of the cogging torque is the interaction of the magnets with the slots of the stator. It can be explained as the dependency of higher and lower energy states of the magnetic energy in the air gap according to the rotor position. Basically, the variation of the air gap width around its circumference of the stator provides the difference between the magnetic reluctance for the flux circuit at the permanent magnet of the rotor and at the slotted structure of the back iron on the stator

as the rotor turns. This variation results in torque ripple. In addition, if no current is applied to the stator, the rotor also orients itself in certain positions relative to the stator. When the rotor is moved out of this position, an additional torque is generated, which is also known as cogging torque by absence of currents.

Meier [116] use further origins of torque ripple are:

- non-ideal sinusoidal temporal progressions of the currents and voltages produce the fluctuations of the applied power and result in the torque ripple,
- defects such as rotor eccentricity, geometric faults or unequal magnet magnetization,
- impact of the spatial harmonics in the magnetic field of the magnets and the windings.

A recent review of the literature on the reducing cogging torque and the torque ripple found that there are many methods with electromagnetic background. For example, based on the energy method and Fourier expansion, Chen et al. [32] proposes an analytical method to make the optimal design to reduce the torque ripple of the in-wheel motor. Various approaches have been proposed to solve the issue of cogging torque:

- skewing the stator and smoothing down the transition of the magnetic flux from one stator slot to another, which, in practice, leads to high manufacturing costs [104];
- control based techniques whereby the shape of the current produces an additional torque to compensate the torque ripple [142];
- obtaining a more sinusoidal flux density in the air gap by the optimization of the shape and the arrangement of the permanent magnets [144];
- combining the poles and slots to receive a large number of them [135].

To receive a controllable solution for the developed electric motor, it is necessary to reduce the cogging torque as much as possible at the design stage. In addition to the general requirement, which states that the correctly designed PMSM is generally characterized by cogging torque values smaller than 1.5-2.5% of the nominal torque [66], the main requirements to limit the cogging torque originates from the automotive industry by OEMs and requires the maximum of cogging torque value to be 1% of the nominal torque during controlled operation for the applications in electric vehicles [143].

To analyze geometries and their influence on the cogging torque, a finite element method is used and the model of the relevant motor part has been created with Ansys Maxwell. Ansys Maxwell is a powerful design tool which enables to create the shapes of an electrical motor with a full scale of properties such as slot shape or magnet shape. As a reference of the value of the cogging torque, the opened slot was firstly simulated. The characteristic of the cogging torque can be explained by the interaction of a single pole pair with opened stator slots.

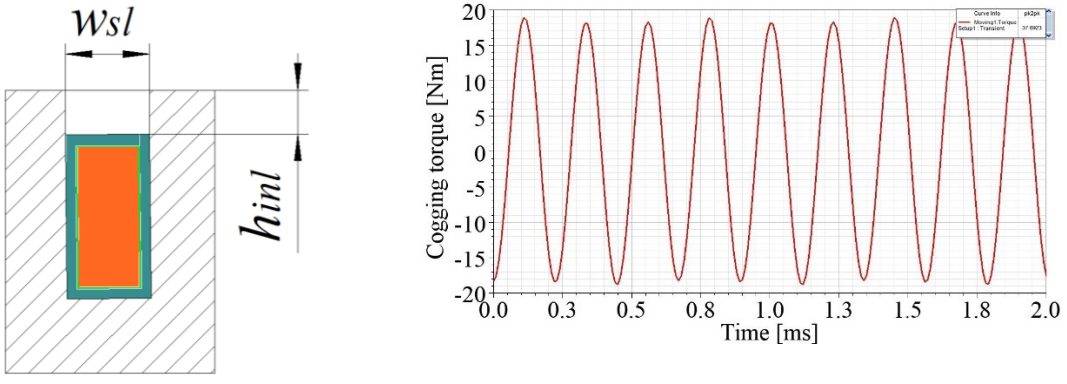

a b

Figure 4.14 – Open slot variant: a - FEM model of geometry, b - Cogging torque value of opened slot

Figure 4.14 shows the characteristics of the cogging torque over a slot in which only one pole pair is mounted onto the rotor. The curve shown in Figure 4.14, (b) is normalized to the peak value of the cogging torque and amounts to 37.69 Nm. Using the Figure 4.14, (b), it is easily shown that the cogging torque on a stator tooth is periodic with a period depending on the pole number and slots in the back iron. In accordance with [66], the

net cogging torque can be calculated as the algebraic sum over all poles or, by the assumption of constant value of the cogging torque on each pole pair, as the product of the cogging torque on one pole pair and the pole pair number:

$$T_{cog} = \sum_{i=1}^{p_p} T_{cog\_i} = T_{cog\_pp} \cdot p_p \tag{4.7}$$

Similar to the advantage of the winding principle presented by Borchardt et al. [19], the development of the cogging torque means that each magnetic pole is used simultaneously to generate a cogging force.

Several studies, have been carried out to provide an analytical calculation on cogging torque [187]. Based on the energy method, the cogging torque can be determined by the analytical model as a negative derivative of the internal magnetic energy W of the machine with respect to the motor's rotor position angle θ can be calculated according to [81] as:

$$T_{cog}(\theta) = -\frac{\partial W(\theta)}{\partial \theta} \tag{4.8}$$

Where the magnetic energy of the machine W can be calculated as:

$$W(\theta) = \frac{1}{2\mu_r} \int_V {B_H}^2 \, \partial V \tag{4.9}$$

where B_H is the flux density at various parts of the machine, i.e., air gaps, permanent magnets and irons, and μ_r is the corresponding to permeability.

In accordance with Equation (4.9), the value of magnetic permeability μ can be used as a variable of properties in the slot and must provide the minimizing of the cogging torque, but at the same time the weakening of electromechanical coupling is not allowed.

In addition, an investigation of the geometric parameters can be carried out to determine the influence of the inlay shape on the reduction of the cogging torque and the back EMF value. Due to technological constraints, the width of the slot is constant along the full height of the slot. This is caused by the inserting of the copper wire in the slot before the slot inlay in the slot will be installed. This means that a larger volume of copper can be used for the slot winding and at the same time the separation of the back iron structure through the realization of the pole shoe is a challenge.

According to Figure 4.13, the height of the wire of the slot winding leads to the changing of the inlay height. This has an impact on the slot winding factor. In this regard, while designing the motor, it is necessary to choose the relation of h_{inl} and h_{ws}, which provides a compromise between the tendency on the one hand to increase the fill factor and on the other hand to decrease the cogging torque. In addition, the air gap and rotational speed have a significant impact on these parameters.

To eliminate the eddy currents in the inlays, the stacking of the inlay can be applied. Since the thickness of the electrotechnical steel sheets could only be produced according to the special standard, the optimal configuration of the stacking could be neglected. According to the standard thickness of the electrotechnical steel, the same electrical steel NO20 as the back iron material is most suitable for the inlay stacking development and w_{no} parameter has a value of 0.2 mm. The second geometric parameter of the slot inlay is the opening width w_{open} and can be determined as follows:

$$w_{open} = w_{sl} - n_{no} \cdot w_{no} \tag{4.10}$$

The number of strips per slot n_{no} should be selected in such a way that the objectives of the inlay application can be achieved to meet any technological requirement. Figure 4.15 illustrates that in case of the slot inlay application, only the height of the inlay h_{inl} remains as a variable geometric parameter for the FEM model. Further variable parameters, as mentioned above, are magnetic permeability of the material of the slot components, resulting cogging torque and back EMF. To describe the behavior of the cogging torque for the developed motor geometry, the following approach is proposed (see e.g. [133] for a detailed explanation).

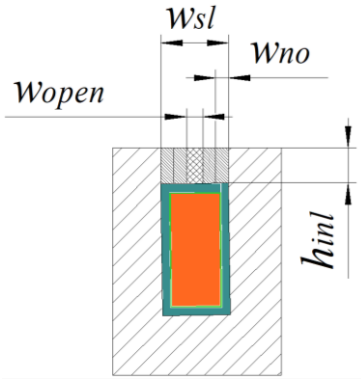

Figure 4.15 – Geometric parameters of the inlay

The geometry presented in Figure 4.15 was modeled and analyzed with Ansys Maxwell. In accordance with the above-mentioned input data, electromagnetic calculations of the variants have been performed for the different ratios of the inlay height and magnetic permeability in order to find the minimum value of the cogging torque. In the simulation, no current is carried through the windings and only the field of permanent magnets is presented. Table 4.2 demonstrates the results of the cogging torque simulation.

μ_r / h_{inl}, mm	1	5	10	20	30	50	100	200	300	500
0.3	120.2	49.7	29.7	12.7	6.8	2.4	4.3	3.9	2.8	2.4
0.6	120.3	45.5	19.1	12.1	4.9	2.0	0.2	0.5	0.3	1.6
0.9	54.6	25.7	20.8	11.5	6.7	2.4	0.8	0.8	0.6	0.3

Table 4.2 – Cogging torque in dependence on the inlay height and the magnetic permeability [133]

The simulation results have shown that at the inlay height of 0.6 mm and at the permeability between the value of 50 and 100, the lowest cogging torque is expected. This value corresponds to approximately 0.03-0.3% of the nominal torque.

The back EMF has been widely investigated by Zhao et al. [185] and can be explained as the reflection of the magnetic field distribution that results in the electromagnetic torque output [179]. The back EMF harmonics present the second characteristic parameter of the motor in the cogging torque calculation that should be taken into account. It can thus be suggested to also calculate the values of the back EMF with the same parameters as by cogging torque simulation.

μ_r / h_{inl}, mm	1	5	10	20	30	50	100	200	300	500
0.3	0.932	0.939	0.939	0.938	0.937	0.936	0.936	0.934	0.934	0.934
0.6	0.932	0.938	0.937	0.935	0.932	0.927	0.916	0.905	0.928	0.867
0.9	0.932	0.936	0.934	0.929	0.925	0.918	0.908	0.897	0.893	0.897

Table 4.3 – Results of back EMF simulation [133]

As illustrated in Table 4.3, the influence on the effective value of back EMF only plays a role for the values of permeability μ_r above 100. Therefore, the dominant meaning in the selection of the height of inlay and permeability μ_r has the lowest value of the cogging torque. In addition, further implementation will have to take into account the technological challenges that arise when the manufacturing accuracy of active motor parts is considered.

The value of the permeability μ_r of 100 and height of the inlay h_{inl} of 0.6 mm can be simulated in detail as a preferable parameter to receive the waveform of the cogging torque. Simulation results of the preferable parameters of the slot inlays are shown in Figure 4.16.

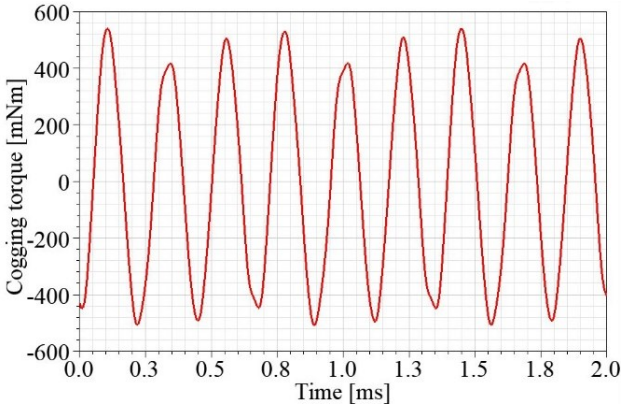

Figure 4.16 – Simulation results of the preferable parameters of the slot inlays

It can be seen how the ripple is substantially reduced when the stator is equipped with slot inlays, because the peak-to-peak value of the cogging torque is 1.04 Nm, which only accounts for 2.7% of the maximum value of the opened slot. This means that the total stored energy of the system does not change so abruptly and quickly, which ultimately leads to a reduction of the cogging torque. In principle, the operation with lower cogging torque fluctuations leads to smoother running, even if noise emission is a less important requirement. Further details of the described approach as well as other aspects related with the detailed electric design can be found in [74] [90].

The further implementation of the conducted investigations offers an inlay design shape that can reduce the cogging torque in electric vehicles and they contribute to the efficiency increase of the developed motor with reduced torque ripple.

4.1.2.4. Simulation Results

Considering the geometric assumptions, parameters and restrictions for both windings, the simulation of the finite element model of the design approach for combined winding was carried out. To validate the developed motor design, the active parts were imported and analyzed into Ansys Maxwell. The methodology of modeling was in accordance with [21] and [90] as follows: The simulation model of the considered magnetic circuit was a rotational model, due to the simplicity of the parametrization of the geometry and the already developed and existing geometric model in CAD. As an assumption and for the sake of simplicity, the mechanical dynamics of the rotor was considered as insignificant and was not taken into account.

The accuracy of the model is limited by the following assumptions that have been made in the modeling process:

- the characteristic of resistance of both windings is independent of the thermal load,
- the saturation effect of the back iron is neglected,
- the possible thermal load of the windings on the permanent magnets was not taken into account,
- the hysteresis, eddy current and other sources of losses are neglected, so only stranded ohmic losses are considered,
- the conductivity of the magnets and eddy current losses in the permanent magnet are neglected, because according to [131] these are very low for the similar motor structure.

The design of motor active parts is primarily modeled using sinusoidal currents as the input signal. This gives an understanding of how the motor will be operated under ideal power supply conditions. Through this overall model, the behavior of the complete motor system could be investigated.

On the first step, a simulation of the induced voltages allows to prove the electromagnetic connection of the motor. Table 4.4 and Figure 4.17 shows a clear trend – a scale-up of the angular velocity results in the changing of the induced voltages with linear relationship by the coefficient of 0.355.

Rotational speed, rpm	100	200	300	400	500	600	700	800	900	1000	1100	1200	1300
Angular velocity, rad/s	10.47	20.94	31.41	41.89	52.36	62.83	73.3	83.77	94.25	104.72	115.19	125.66	136.13
Induced phase voltage, V	35.48	70.94	106.41	141.89	177.36	212.82	248.30	283.78	319.25	354.72	390.19	425.67	461.14

Table 4.4 – Simulation of induced voltages (RMS)

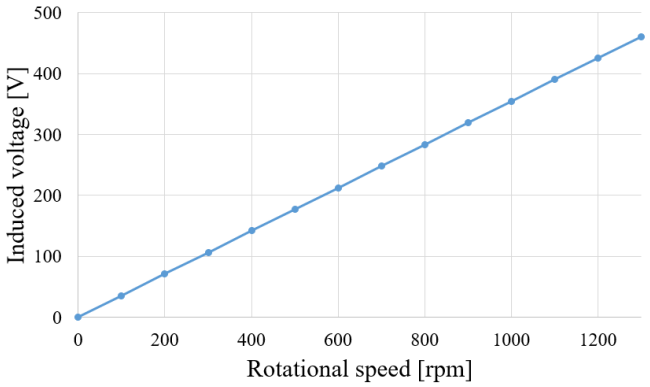

Figure 4.17 – Graph of results of the simulation induced voltages (RMS) vs. rotational speed

The waveforms of induced voltages at 100 rpm are shown as an example of the analysis in Figure 4.18. The non-smoothed curves can be interpreted as that the simulated values are corresponding to the real value progression.

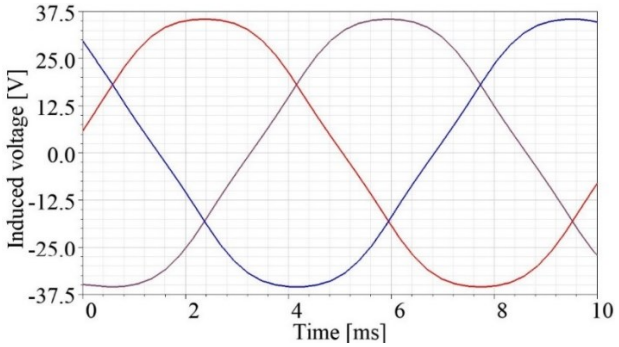

Figure 4.18 – Graph of the waveforms of induced voltages of 3 phases by 100 rpm

The torque characteristics were simulated with the step of 10 A with the maximum current of 220 A. The results of the simulation showed a linear dependency as it is illustrated in Figure 4.19.

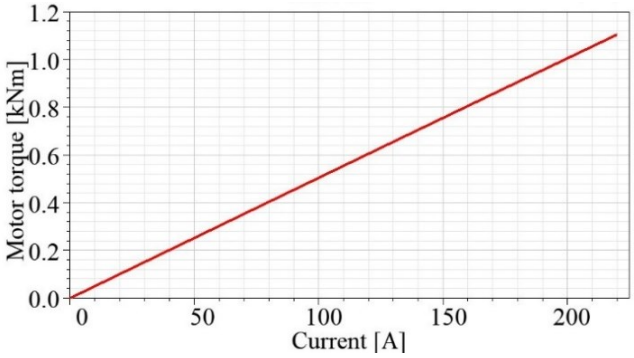

Figure 4.19 – Graph of results of the simulation of motor torque vs. phase current

The current with an effective value of the phase current, which should be available for the development of the nominal torque, is exemplarily shown in Figure 4.20.

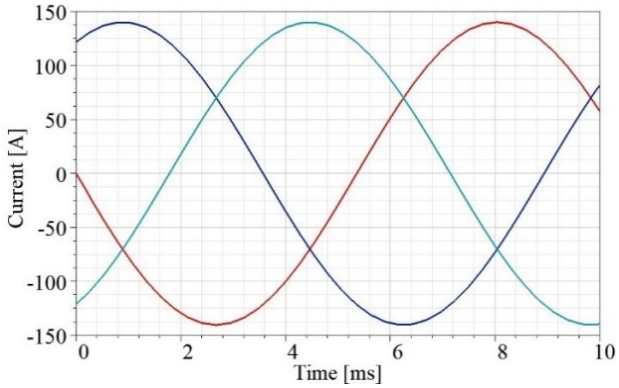

Figure 4.20 – Energization with an effective value of the phase current of 105 A

Figure 4.21 shows the corresponding stranded losses, in which the ohmic losses are dominating.

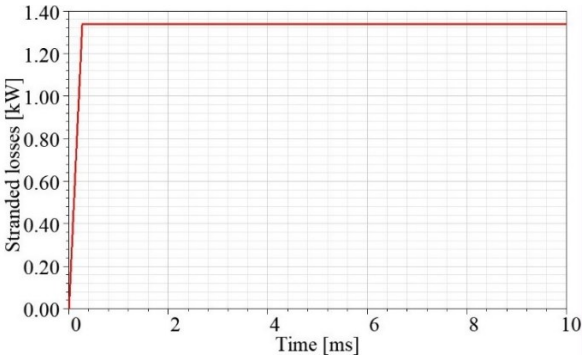

Figure 4.21 – Results of the simulation of stranded losses

Figure 4.22 schematically shows the torque diagram of the developed motor for nominal (565 Nm) and overload (1133.3 Nm) operation. It can thus be reasonably assumed that the overload torque can be reached for a limited period of time because of thermic reasons (see 3.4.3) and the value of the maximum rotational speed of the motor is expected with a smaller torque value. The same graph also presents the achievable power of the motor, whereby its continuous power level lies at the required 69.6 kW and the overload power value amounts to 87.25 kW. It is important to note that the power overload mode of the motor, as well as the maximum torque mode, has a limited amount of time and should therefore have a short time duration or be avoided as far as possible because of thermal stress. Thus, all calculations performed at the FE level showed full compliance with the development requirements.

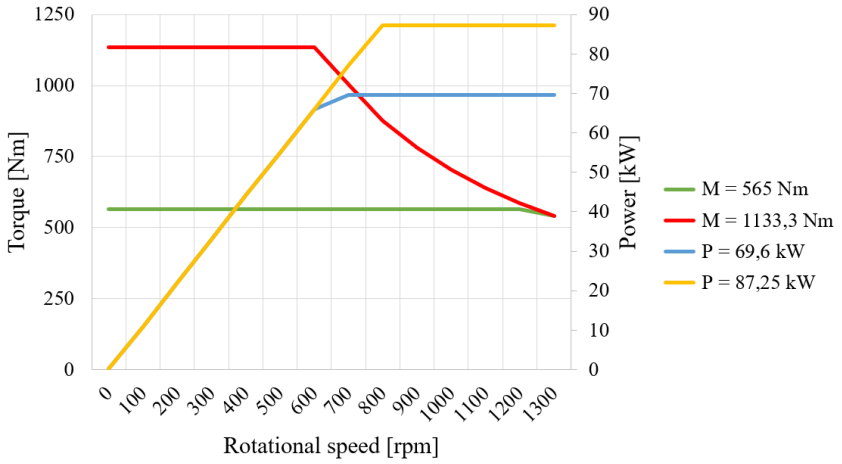

Figure 4.22 – Graph of the results of the simulation of the motor torque vs. rotational speed and motor power vs. rotational speed

4.1.3. Motor Relevant Parts

The integration of an electric in-wheel motor into a wheel is characterized by the difficulty of the integration of a powerful electric drive, wheel bearing, cooling and also power electronics into the wheel. The spectrum of technical solutions to ensure full operation of the electric motor is wide enough. Functionally they are divided into mechanical, electrical and control devices and accessories.

The increasing tendency of the integration of the electronic components also provides a significantly higher power density. The main task of the control system is to control the motor including all safety-relevant and dynamic tasks. The first step of the integration is the elimination of cable connections by the integration of electronics directly in the motor. In this case, some disadvantages can appear due to the intense vibrations of the parts of the power electronics.

The most vital part in terms of motor control is power electronics. In the PMSM motor, the rotor field changes depending on the rotor position and the stator field must be adjusted accordingly. When the motor is operated, a current is carried out through the stator windings, which are switched by keys controlled by the microcontroller. As a result, a smooth torque is possible to be generated. The torque ripple then remains due to fluctuating currents, rotor field or cogging torque. The control task of the PMSM motor can be performed by an electrical commutation consisting of three basic components. These are a bridge circuit of power switches, their control unit or microcontroller and a unit for the detection of the rotor position.

The main task of the microcontroller is to generate the switching signals in such a way that the interaction between the field of the windings and the field of the rotor generates the torque in any of its positions. According to the above presented winding technology by low inductance of the windings and high power of the motor, also a very high switching frequency of the inverter in the range of 150-300 kHz is expected. As a result, high losses and an increase in the temperature of the power electronics are anticipated. A methodology of control for such circumstances is outlined by Golovakha et al. [57] in which a three-phase step-down converter is used for the control and regulation of the motor. Due to the inductances, also small ripples in the current are caused. Therefore, the high switching frequency and sufficient motor inductance avoid high current ripples. It is extremely important to abscond from current ripples because they can cause an arising of unfavorable high-frequency harmonics. Another illustrative example of control by very small inductance of the windings is presented in [90], in which a modified six-step-commutation with additional control of the source current was implemented. Three-phase motors are usually controlled by a three-phase bridge with three half-bridges, each of the half-bridges being provided for a single phase. PMSM motor controllers are typically equipped with MOSFET or IGBT transistors and PWM signals are provided by the microcontroller. MOSFETs allow very high operating frequencies because the switching times of them are in the nanosecond range and IGBTs are designed for currents of up to many hundred amperes and therefore are used in high power applications.

In view of the described control opportunities, an effective use of the installation space is a constraint for the integration of the control system in the wheel. For the developed electric motor under the above described assumptions and restrictions, the cylindrical working space as presented in Figure 4.23 was identified.

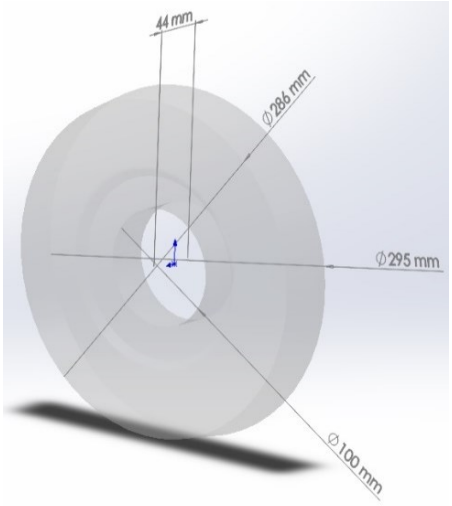

Figure 4.23 – Working space for the electronics of the in-wheel motor

As a further aspect in the area of motor operation, the determination systems of the rotor angular position are an important requirement for the motor operation. Systems of velocity and position measurement are an integral part of any high-quality motor torque control system. The developed motor requires a position sensor in the system. While the general industrial electric motor drive is often bypassed by senseless methods based on the principle of back EMF determination, the developed in-wheel motor requires operation at zero velocities when back EMF is not available.

In the following, detection concepts that are applicable for the developed motor are briefly explained. A detailed description for all kinds of determination of the rotor angular position can be found, for example, in [105]. The most common technical solutions in the field of the precise determination of the rotor angular position for the developed motor are Hall sensors mounted near to the rotor magnets (Figure 4.24, (a)) or an optical encoder system mounted on the rotor cover. On the one hand the optical encoder solution (Figure 4.24, (b)) provides excellent accuracy and integrability in the motor. On the other hand, it also has disadvantages, as it is not space-saving and cost-intensive compared to Hall sensors. The geometrical limitation of the motor in axial direction as well as a possible high temperature in the winding zone limits the use of the Hall sensor in the immediate area of the rotor magnets. A possible solution of this problem is to place an external magnet ring with the equal magnet number as in the rotor on the rotor cover as shown in Figure 4.24, (c). In this case, the signal for phase commutation is provided by the moving of permanent magnets with alternating magnetization relative to the Hall sensors fixed on the stator.

a b c

Figure 4.24 – Variants of the determination of the rotor angular position: a - Hall sensors mounted near to rotor magnets [20], b - Optical encoder system, c - Magnet ring solution

In comparison with the technical side, the listed variants differ both in the technological compatibility of the design solutions and in the cost of their implementation in the mass production of the electric motor. The magnet ring solution is a preferable variant for the experimental test of the developed motor because of its scalability, but the technology of manufacturing of such magnet ring must be simplified.

From the combination of the mechanical and electrical point of view, there are some additional characteristic aspects in the area of electronics that need to be considered such as the following:

- sufficient insulation and dielectric strength of electronics to the stator,
- sufficient thickness and flexibility of the insulation to compensate for any irregularities between electronics and stator,
- the connection of the winding in phases by the terminal clamps, conductor and neutral point rails with a suitable cross-sectional dimension to allow the motor to be used in overload mode,
- connected winding ends require a minimal length to obtain a good heat dissipation and nevertheless insulated contact to the stator surface,
- between all electronic parts a sufficient distance to rotating parts should be maintained, or they should be completely isolated from them,
- the relief of mechanical stress from the cables on the connector through clamps or strain relief of cables.

Another aspect is electromagnetic compatibility, which becomes critical due to the operation of various components in confined spaces. Here, it is necessary to ensure a reliable operation of the control units in close proximity to the switching power supply units and the magnetic components that can emit electromagnetic fields. The question of coverage will be kept open until the tests are carried out. In the next step after the electronics test, a cover made of EMC dampers is optionally available.

4.2. Cooling System

The analysis of thermal properties of the electrical motor is the next important evaluation step in the development process. During the operation of the vehicle, the temperature has to be regulated in order to maintain the required electromechanical output characteristics, as well as to protect the motor and the components installed inside the motor from thermal damage. The temperature and mass flow of the cooling medium at each operating point must ensure that no damaging through overheating anywhere in the motor will occur. Hence, the basic aim of the cooling system configuration is to provide the required cooling capacities with the most compact, lightweight and cost-effective methods within the available space. As mentioned in 3.4.3, the waste heat from the electric motor can be dissipated in different ways. As a preferable solution, the stator has cooling channels and is cooled by the liquid coolant. It is related to the fact that the main losses are caused by the heat from ohmic losses in the motor and they are generated in or near the stator windings, which in this case are surrounded by the external rotor. Therefore, the heat removal in this motor structure, especially in the closed version, is significantly reduced. Also, the motor elements are heated not only because of losses arising in the motor active parts, but also because of the proximity to the heated components: electronics and mechanical parts of the electric motor – bearings and seals.

For the configuration of the cooling system, the requirement to the profile of the vehicle can be used. Thermally critical driving states usually occur at maximum power P_{max} or maximum torque M_{max} of the motor. As it was mentioned above, the main source for the heat is represented by ohmic losses, with the main influence coming from a current carried in the winding. Based on the results of Table 3.3, Figure 4.8, (b), Equation (3.15) and Equation (3.18), a maximum value of the current needed to meet maximum power and maximum torque requirements that can be expected to be 134.2 A for P_{max}. and 216.6 A for M_{max}. The first set of analyses implied that the impact of these values can be carried out, whereby the ohmic losses can be calculated according to [149] as follows:

$$P_{ohmic} = I_{max}^2 \cdot R_{con} \tag{4.11}$$

R_{con} represents the winding resistance, which can be calculated as follows:

$$R_{con} = \frac{\rho_w \cdot L_{con}}{A_{con}} \tag{4.12}$$

The corresponding conductor resistivity ρ_w is a fundamental property of a material that quantifies how strongly it resists or conducts an electric current. The cross-sectional area of the conductors A_{con} is already selected by design related to the winding parameters. In case of a developed motor due to the specific structure of the winding, the total conductor length L_{con} can be calculated as follows:

$$L_{con} = (L_{sw} + L_{agw} + 2 \cdot L_{swh} + 2 \cdot L_{agwh}) \cdot p_p \cdot n_{ph} \tag{4.13}$$

The lengths of the slot winding L_{sw} and air gap winding L_{agw} are equivalent to the length of the magnet l_M. The length of the winding heads of the air gap winding L_{agwh} and slot winding L_{swh} are evaluated by the mean distance between the winding strands under the assumption that the winding heads are shaped like a circle.

Ohmic losses can be calculated as follows:

$$P_{ohmic} = I_{max}^2 \cdot \frac{\rho_w \cdot (L_{sw} + L_{agw} + 2 \cdot L_{swh} + 2 \cdot L_{agwh}) \cdot p_p \cdot n_{ph}}{A_{con}} \tag{4.14}$$

The results of the calculations for the selected parameters shall be presented as a diagram of the current ohmic losses for the developed motor and shall be as specified in Appendix J. It must be pointed out, that the obtained results agree with those simulated by FEM and presented by Sauerhering et al. [145].

In addition to the resistive losses, eddy current losses also occur in the air gap winding and in the stator back iron. Also, hysteresis losses occur which were determined for the motor with a similar principle using a numerical calculation presented in [149] and [94]. From this calculation the relationship between the ohmic losses and other sources of losses by 15% were established. The eddy current losses value in the slot winding becomes negligible, since it is enclosed by the back iron and thus the eddy currents are limited.

Due to the heat transfer into the circulating coolant, it is very important to know which flow regime is involved. Slow flow refers to the laminar properties when the liquid particles, which only move in the direction of flow and different layers of water, slide against each other in the direction of flow. In a turbulent flow, the particles move in all spatial directions, but the average layer is in the direction of flow. An effective reduction of the experimental effort by thermal analysis is achieved by applying the theory of similarity. Here it is assumed that physical relationships can be described by dimensionless indexes or characteristics. Flow regime is determined by the dimensionless Reynolds and Prandtl number. Another key parameter is the Nusselt number. The Nusselt number describes the ratio of the thermal resistance of the heat conduction in the fluid to the heat transfer. Therefore, by determining the capacity of the flow, a minimum coefficient for the heat transfer can be determined on the basis of a specified maximum temperature increase of the cooling water depending on the available transfer surface. An approach to define the characteristic parameters of the cooling system of the developed motor as well as further details on the entire considered system are presented in [145].

One possible path is through the polymer bandage where a part of the heat flows upwards in the form of heat transfer, then by convection through the air gap to the magnets, and then by heat transfer through the magnets, or the adhesive between the magnets. For this reason, the demagnetization resistance of the permanent magnets must also be taken into account in case of overload and heating. Finally, the heat from the rotor flows into the environment by convection and radiation at the surface of the rotor. A large part of the heat flows downwards through the back iron into the stator. The next possible way represents the way from the winding heads either through the polymer bandage into the inner air or into the stator. Most of the heat in the stator is removed from the system by convection into the coolant. However, convection also occurs on the surface of the stator, so that the air inside the motor is heated and the heat is also transported to the cover. In addition, the heat flows by heat transfer from the stator and rolling bearings into the wheel bearing assembly and is transferred by convection and radiation to the environment at the surface.

Another critical point is a number of internals in the cooling structure because they increase pressure losses, so that the higher pumping capacity is required for liquid transport. The geometry of the developed motor should be designed with less elements that could indicate relatively high pressure losses. For this reason, the cross-sectional widening at the inlet and outlet, the sharp-edged bends of the transitions from end face to outer

cylinder surface should be minimized and the cross-sectional changes of the cooling channels should be kept as constant as possible in order to minimize the pressure losses.

In the proposed motor structure, the stator has been designed with an integrated cooling system to manage the losses and to ensure efficient heat removal. An active liquid cooling leads to a complicated design of the stator and to an increase of the stator's design volume.

A serious drawback of the cooling system outlines itself, whereby the subsequence of the cooling of the motor elements has a critical issue. Thus, the subsequence of the cooling is responsible for the driving performance of the developed motor. According to the cooling system sequence of the developed motor, the developed cooling structure in the first step ensures the cooling of the power electronics, which are located inside the stator. For this reason, the front surface of the stator has three cooling channels with maximum possible lengths for the corresponding circles inside the stator. There are four cooling channels inside the stator bar. They are connected with each other, so the cooling liquid flows through the outer and inner part of the stator. Through the geometry of the inlet and outlet it is possible to send the cooler fluid first along the two end faces of the periphery of the stator. This improves cooling directly at the winding heads, where most of the heat must be dissipated. Therefore, the geometry of the stator with the circulating cooling channels on the front face uses almost the full stator volume for cooling. According to the described cooling structure, the CAD model of the stator with cooling channels as shown in Figure 4.25 was derived.

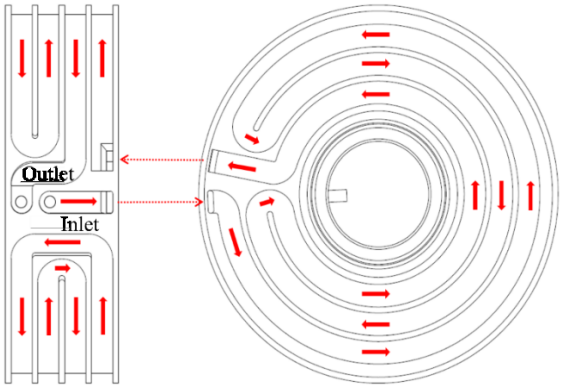

Figure 4.25 – Cooling subsequence of the developed motor [145]

The important path of the cooling medium in the channels is marked with red arrows. Due to the developed stator, the cross-sectional changes over the entire length of the cooling channel were completely avoided. The cooling channels have a rectangular cross-section and have a large cross-sectional area, so that they can reach almost up to the winding heads at the edge of the stator. Cooling channels are integrated into the stator very close to the copper windings to avoid hot spots. It is therefore expected that a significantly larger relation of the surface of the cylinder is covered by the cooling channels. The important parameters of the cooling system are presented in Table 4.5. The lengths of the cooling channels are derived from the CAD files and can therefore differ from real dimensions.

Length, mm	Width, mm	Height, mm	Surface area, m^2	Volume, m^3
5960	8	19	0.307	$0.864 \cdot 10^{-3}$

Table 4.5 – Cooling channel dimensions of the developed stator

Based on the developed cooling structure, EM analysis of the flow velocities (Figure 4.26), pressure losses (Figure 4.27) and heat transport (Figure 4.28) are performed.

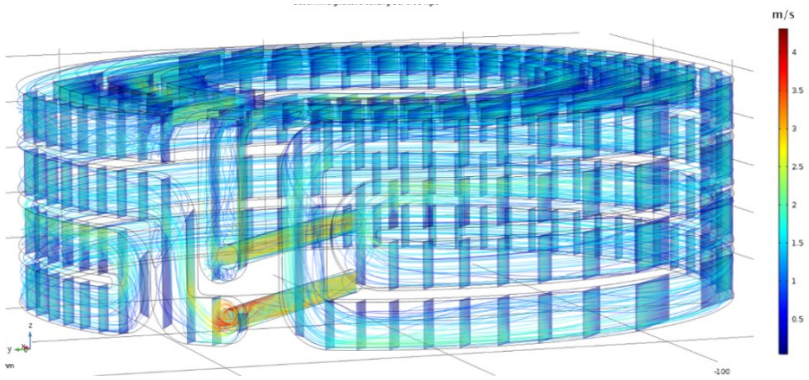

Figure 4.26 – Simulation of flow velocities at the mass flow of 80 g/s for the cooling structure [145]

Figure 4.26 shows the flow-through cooling channel geometry. The stream lines are colored according to the velocity and show rather laminar flow conditions over long distances and an only locally strong turbulence at transitions and deflections.

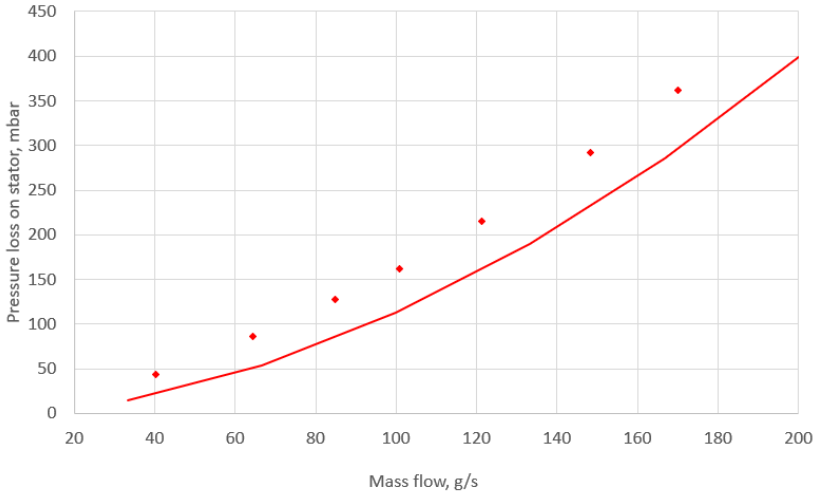

Figure 4.27 – Analytical (pointed) and numerical (full) results of the pressure loss characteristic for the mass flows 40-180 g/s with a parameter variation of 20 g/s gradations [145]

During the calculation and simulation of the pressure loss curve over the mass flow, a slight non-linearity can be noticed. This results from the quadratic function of the pressure loss on the flow velocity.

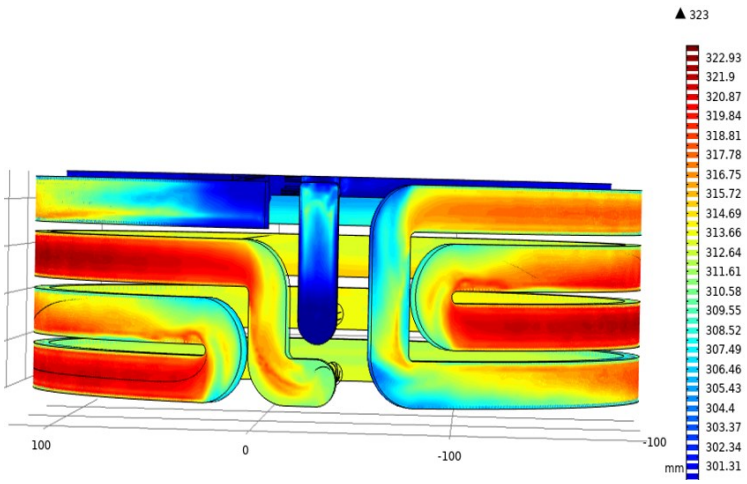

Figure 4.28 – Results of the coupled numerical simulation for a heat load of 8 kW, a cooling water mass flow of 200 g/s and a cooling water inlet temperature of 25°C for the developed cooling [145]

The temperature profiles of the developed cooling system generally show an effective heat removal. The simulation results indicate that a significantly lower temperature of the components can only be detected in the inlet area. For the other areas, a relatively homogeneous temperature distribution can be shown, caused by the design of the cooling channels.

Thus, for the developed motor, power losses of over 8 kW (10% of the maximum required power) exceed the limits of the stationary cooling capacity and should therefore have a short-time duration or be avoided as far as possible [145].

4.3. Mechanical Part

This section provides a more detailed description of the basics - a mechanical analysis of the developed in-wheel motor. The first part of the section gives a more detailed description of the analysis of the bearing system consisting of wheel hub and supplementary bearing. The second part of the section concentrates on the computational analysis of the coupling element. To investigate the consequences that result from mechanical loads on both systems, a finite element model has been derived. The usage of these models offers the opportunity to analyze the influence on the complete motor under maximal static loads. Thus, a changing of the air gap is to be derived. The third part provides information on the analysis of the motor shaft according to its functional area under the motor requirements. The fourth part concentrates on parameters of the sealing system for the developed motor.

4.3.1. Bearing

According to the kinematical structure of the developed in-wheel motor (see Figure 3.10, (b)), it has two separate bearings. The main bearing is defined as the wheel hub bearing and the supplementary bearing is mounted over the wheel hub bearing as it is illustrated in Figure 4.29. Different functions of these two bearings can have certain positive and negative influences on the motor function.

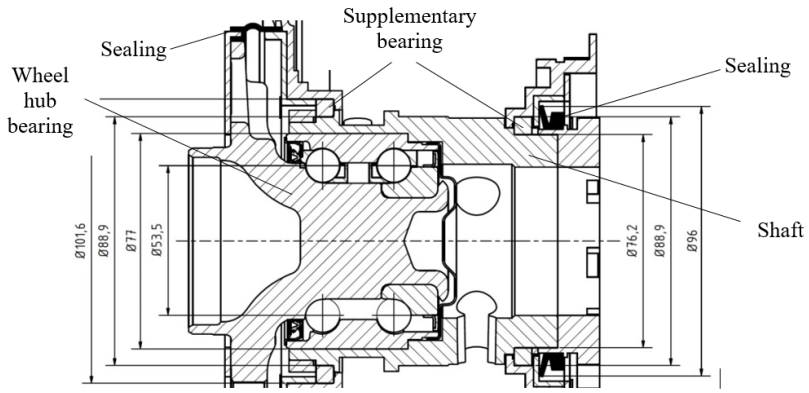

Figure 4.29 – Bearing system of the developed motor [189]

According to consecutions presented in 3.3.3, for further research the following assumption is made regarding the topology of the in-wheel motor: The rigid part in the motor topology is the wheel hub bearing. Wheel hub bearing BAR 2030 as a structural link between the rotating wheel and the static suspension of a vehicle requires a functionality with high speed and heavy-duty loads.

The characteristic property in the use of the wheel hub bearing in the developed motor is that it is not directly connected to the vehicle's suspension. Instead, the main bearing is integrated into the shaft of the motor and is considered to be part of the motor. The shaft then carries the stator. To increase the integration level, to save the installation space inside the motor and to save the weight, the static outer ring flange is turned as it is shown in Figure 4.30. Therefore, the motor shaft and the adapted bearing are connected by the selection of tolerances between them. For the purpose of an axial fixation, three threaded holes are drilled on the cylindrical surface of the outer ring of the wheel hub bearing and the fixation itself is implemented with the help of the bolts. In

this way, the fixed part of the wheel hub bearing is integrated in the shaft of the motor and then into the vehicle's suspension. Described modifications result in the extremely high level of integration of the wheel hub bearing.

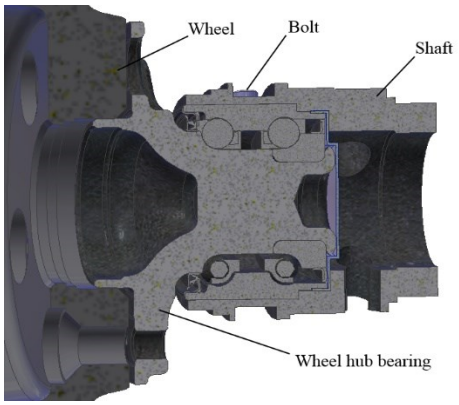

Figure 4.30 – Integrated wheel hub bearing BAR-0230 [174]

According to the manufacturer data, the angular stiffness C_t by radial load on the selected bearing is 5500Nm/° lower, which indicated that the application of BAR-0230 in the in-wheel motor can be interpreted as an additional stiffness in the area of the main bearing. The values of stiffness are valid for the original mounting and the possible impact of the wheel hub bearing integration should be analyzed due to a possible influence of higher wheel mass and axial shifting of the bearing. For this reason, an analysis of the characteristics of the integrated wheel hub bearing by using FEM modeling according to the method described by Vittayaphadung et al. [174] was provided. In the case of the simulation by using FEM, the reduction of the rolling elements of the bearing by geometrical simplification is supposed as it is shown in Figure 4.31, (a). Reduction in the model means, in other words, a substitution of the geometry and modification of material properties, which results in a reduction of the contact problem. As a result, the static analysis with the required loads for the wheel hub bearing can be prepared in a short time and with high accuracy.

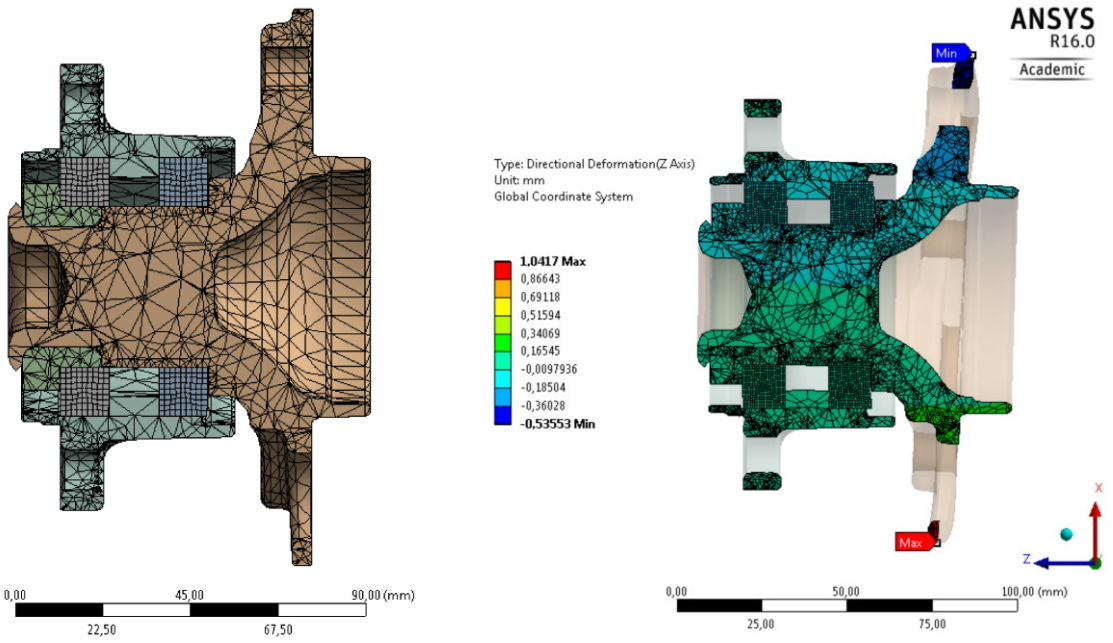

a b

Figure 4.31 – a - Mesh model of the simplified FE model of the wheel hub bearing, b - Results of the FEM analysis of the simplified model of the wheel hub bearing [174]

Provided angular stiffness of the hub bearing results in the deformation of 0.63° by the application of the bending moment of 3500 Nm [158]. With the help of the iteration process, the equivalent elastic modulus of

the bearing ring and deformations in bearing can be calculated. As it is illustrated in Figure 4.31, (b), the maximum axial deformation of 1.04 mm and it occurred at the wheel mounting flange. The results of the analysis show that the absorption of high wheel loads can be achieved by the wheel bearing system and that the weight requirement can be met by an adaptation through a rotation of the suspension side of the wheel hub as well as through extremely rigid ball bearings.

The supplementary bearings in the developed concept are representing the rotor bearings. The study of Frajnkovič [54] reports an analysis of the variable physical air gap, which creates uneven magnetic fields as a result of stator/rotor eccentricity and additionally induces radial forces, resulting in reduced service life of the bearing. Influences of the static eccentricities discussed in [11] show that a reasonable eccentricity equal to 0.1 mm increase the loads by 40% resulting in a 31% life reduction for a standard bearing. Thus, the loads acting on the supplementary bearings are the rotor's own weight and the forces generated by the permanent magnets in the rotor. The supplementary bearing provides a stabilization of the rotor which stands under a magnetic pulling force and absorbs the loads arising from the rotor rotation. The described functions require a high precision of the bearing. In addition to the described loads acting on the supplementary bearing, the rigidity of the bearing is of particular importance for the estimating of the bearing life. The stiffness of the bearing system must be sufficiently high to minimize the displacements in the air gap, since motor torque stability depends crucially on the distance between the magnets and the back iron of stator.

The thin ring bearing from the manufacturer KMF (Figure 4.32) was selected as the supplementary bearing for the motor. The applied bearings are the single row rolling bearings, which have the same square cross-section within one type series, and the thin-walled bearing rings, which are irrelevant for the bore diameter. This bearing can transmit loads in all directions – axial and radial loads as well as tilting moments. The rings of the bearing are simultaneously profiled, hardened by a special manufacturing process. The advantages of the split bearing are easy mounting and the availability of the characteristics of wire-race bearings.

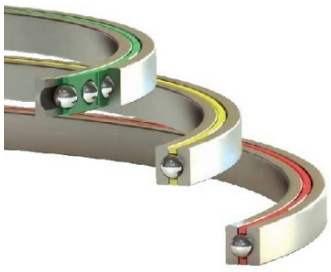

Figure 4.32 – Thin-section bearing PBXA [99]

The design of this bearing allows the integration of the ball cage strip guided by rolling elements. This enables the opportunity to implement the design of the raceway system with a larger number and larger dimensioned balls. As a result, it is possible to achieve higher static and dynamic load carrying capacities compared to similar thin-section bearings of classical design.

Due to installation space reasons, two sizes of bearings have been selected: For the rim side the PBFA035 and for the suspension side the PBXA030. The biggest advantage of the selected bearing is the very low weight compared to the standard bearing of similar size. The weight of a PBXA030 is only 0.06 kg and of a PBXA035 0.07 kg.

According to the loading condition of the supplementary bearings, only the radial loads can be considered, while the axial loads during decoupling are neglected. To determine the forces acting on the supplementary bearing, it is necessary to analyze the maximum bearing load caused by eccentricity in the rotor/stator system. The value of the air gap was assumed as the maximum value of eccentricity, because when this value is reached, contact between the stator windings and the rotor magnets occurs, which leads to motor failure. The calculation was performed in the Ansys Maxwell environment by using parametrical functions for the eccentricity value. This approach aimed at obtaining valid and consistent results while minimizing the time needed to determine the loads acting on the auxiliary bearing.

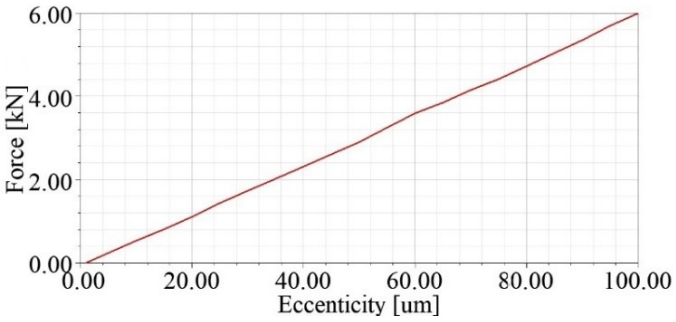

Figure 4.33 – Characteristic curve of the force and eccentricity value in the stator/rotor system

Figure 4.33 shows the force generated by the eccentricity between the stator and rotor. Focusing on the maximum value of the arising force for the maximum loading case of bearing, the characteristic is linear depending on the eccentricity value. Linearity of the arising force is applicable to the calculations of the service life of the supplementary bearing and further influence on the motor performance can be determined.

After the maximum values of the bearing load have been determined, the main factor for rolling bearings, the required service life L_{10}, can be calculated according to [160] as:

$$L_{10} = \left(\frac{C_{dw}}{P_m}\right)^p \tag{4.15}$$

Required service life is measured in millions of revolutions and is significantly influenced by the dynamic load rating C of the bearing and the load rating of the bearing P_m [84]. p in Equation (4.15) represents the life-equation exponent, which is three for ball bearings. The developed concept assumes that the rotor part is decoupled from the forces occurring by driving maneuvers. For this reason, load rating of the bearing P_m corresponds to the maximum force acting at the maximum possible eccentricity P_{r_max}.

However, for the vehicle components, a specification of the service life in hours is not typical. According to approach presented in [161], the value of the required service life can be expressed as mileage L_s by using the dynamic tire radius r_{dyn}, see Equation (4.16).

$$L_s = 2\pi \cdot r_{dyn} \cdot L_{10} \tag{4.16}$$

Palmgren's approach [130] defines a mileage for the wheel hub bearings of passenger vehicles lasts 100000 km. This value can be also assumed for the researched supplementary bearing. Results of the analysis are presented in Figure 4.33 and the value of the L_s are calculated according to Equation (4.16), resulting in 264802.9 km, what meets the typical requirement for automotive parts.

Safety against excessive local deformation in the bearing is described by the static load safety. According to [85], the static load safety factor S_0 is the relation between the basic static load rating C_0 and the highest acting bearing load P_m, see Equation (4.17). The required basic static load capacity C_0 can be found in the manufacturer's catalogue.

$$S_0 = \frac{C_0}{P_m} \tag{4.17}$$

With a static load of the supplementary bearing, the static load safety factor amounts to 2.3. This can be interpreted as the fact that the bearing can withstand the overload, but under the condition that the load is homogeneous. Therefore, a constant value of the air gap is needed.

The methods and calculation procedure for the supplementary bearing described above showed that the bearings can withstand the necessary loads and overloads, so it can serve as the basis for determining the functionality of the motor topology. To validate the calculations, actual tests on prototypes must be performed to verify the conformity to specifications and calculations.

4.3.2. Coupling Element

Braess and Seiffert reported in [25], the deformations in the in-wheel motor system can directly manifest in the deformation of the air gap. Section 3.3 presents the solution for occurring dimensional changes of the air gap consistency, whereby the coupling element is designed to reduce the air gap sensitivity to the loads from driving maneuvers. An elastic coupling element represents a transmission element. The purpose of this element is to transmit torque from the motor to the wheel, whereby the forces acting on the wheel from driving maneuvers are decoupled by the elastic element.

The topology of the concepted in-wheel motor plays a key role for the load distribution. In the solution developed, the loads are not transmitted through the motor parts, but should be transferred from the rim via the outer and inner ring to the wheel center. The loads are carried by wheel bolts and forwarded to the wheel hub bearing. Therefore, the bearing is mounted on the hollow shaft and loads are transmitted to the suspension via the wheel bolts. The described schedule, parts and parameters are shown in Figure 4.34, (a).

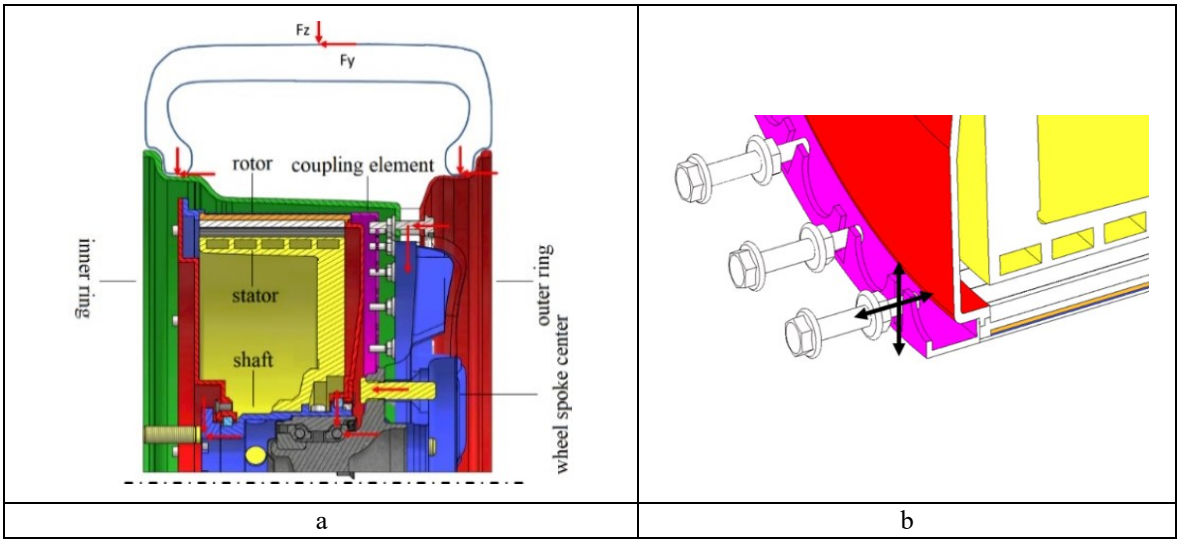

a b

Figure 4.34 – a - Load transfer via the in-wheel motor, b - DOF of the elastic coupling

Because of the loading case, only a bending of the hollow shaft is allowed. Since the stator of the motor is rigidly connected to the hollow shaft, the bending of the hollow shaft affects the inclined position of the stator. Due to this, unrequested reductions of the air gap value can occur. The rotor is rotationally mounted on the shaft and transfers the torque via the elastic coupling element to the rim. The elastic coupling element presents a ring with cut-outs, further called slots. The insertion of a circular hole is not the best form of such a stress-reducing notch. For the first time ever, such stress reduction by extra cut-offs is proposed in popular study of Neuber [119]. The main requirement to the material of the coupling element is high torsional strength caused by the functional use of the motor. The threadless screw ends engage in these slots and have the function to connect outer and inner ring. These screws are movable in radial and axial direction in the slots as it is shown in Figure 4.34, (b). Thus, no deformations from the rim are transmitted to the motor. Additionally, the screws have a connection on the side surface of the slots in the tangential direction and are able to forward the torque to the rim. A more detailed concept description can be found in [92], [138].

The threadless screw ends and slots have a similar principle as gear wheels for the torque transfer, shown in Figure 4.35. Furthermore, for the compensation of displacements in axial, radial, lateral and angular direction, both elements should provide certain elasticity. The geometrical parameters of the coupling element for the developed motor are determined by the interface of the three-piece wheel, so the quantity of the slots is conformed to the quantity of the fixing screws of the wheel. Every load scenario can be a combination of different load cases, for example the maximum torque can be loaded on the motor while the maximum axial force from cornering acts. This is why further analysis comprises individual worst case scenarios with regard to the previous determined load cases in 3.3.2. In order to be able to predict the changing of the air gap under certain forces and moments, the consequences that result from mechanical loads need to be defined.

Further analysis is based upon the assumptions, that the contact between slot and screw is without friction and the contact area between slot and screw builds a line contact. Under these conditions, in case of axial load F_A (see Figure 4.35, (a)), there is only a relative movement between slot and screw, in which the corridor for this movement is limited by the length of both elements. This circumstance allows to conclude, that there is no stress between these parts in the non-friction case.

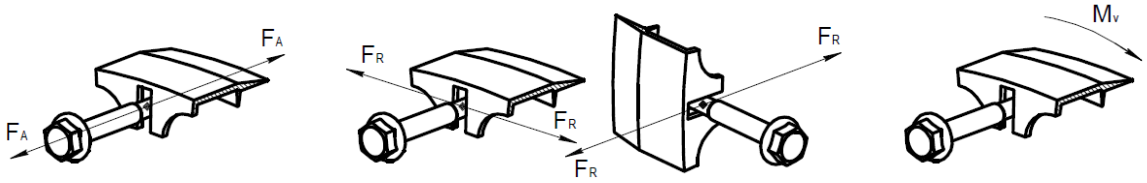

a b c

Figure 4.35 – Load cases by coupling element according to [134]: a - Axial load F_A, b - Radial load F_R, c - Torque load M_L

Thus, in case of radial load (see Figure 4.35, (b)) the maximum load occurs on the one side on the slot and screw surfaces that are lying perpendicular to the force F_R, while the loads on the other slot elements depends on the geometry of the whole coupling element and decreases to zero when the line of force application and the center plane of the contact surfaces coincide. Therefore, the critical load case is a scenario, in which the radial force F_R acts along the slot on one side surface of the slot with a threadless screw end.

The torque analysis is based upon the assumption that torque M_L (see Figure 4.35, (c)) has an equal value for all threadless screw ends and slot elements. The direction of the wheel rotation determines a side of the slot element for this uniform distributed load. The torque force F_T, which acts from one side on the slotted surface and on the threadless cylindrical part of the screw, could be determined from the bolt circle of the wheel.

The geometrical parameters of the coupling element and dimensions of the slot were analyzed through the finite element model of the motor in Ansys Workbench. The input data for the simulations were the above calculated loads acting on the wheel. The 3D-model was imported to the mechanical model component. To reduce the computing time, the model of the motor has been simplified and the finite element model should not contain such irrelevant components as windings, electronics, cooling channels, etc. An adopted model of the wheel hub bearing was implemented into the analysis of the full motor.

In case of the presented load scenarios, the ring with slots is fixed and has a rigid connection to the rotor part and the motor assembly. The loads are transferred to the wheel by using the force and torque function applied to the wheel flanges. This allows to realize an equal load on each screw of the wheel assembly. The calculated model has 135754 elements and 258608 nodes, in which the most usable shape of the mesh element is a second order tetrahedron element. The contact conditions between the elements of the motor and wheel center are bonded, while the contact between screws and ring with slots is shrink sliding due to a frictional contact condition (friction coefficient steel-steel $\mu_f = 0.15$), because a relative movement between threadless ends of the screws and slots of the ring should be provided. This allows to receive results under close-to-real conditions from the FEM-simulation. As expected, equivalent stresses will have areas of contact between slots and ends as it is shown in Figure 4.36.

a

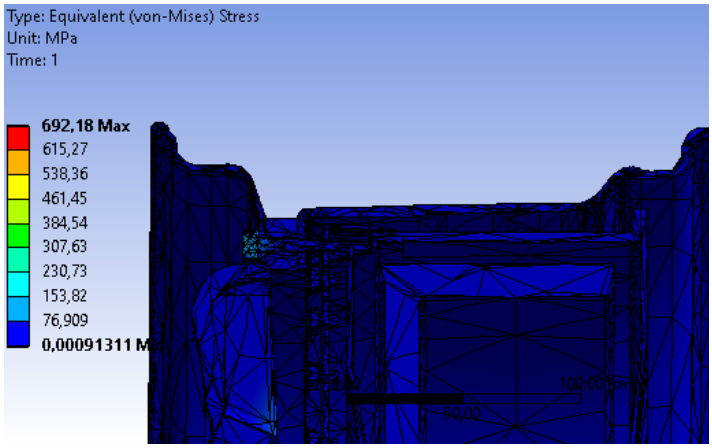

b

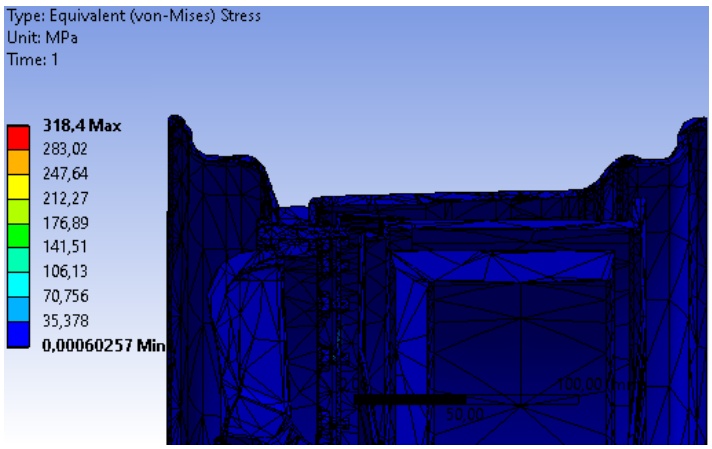

c

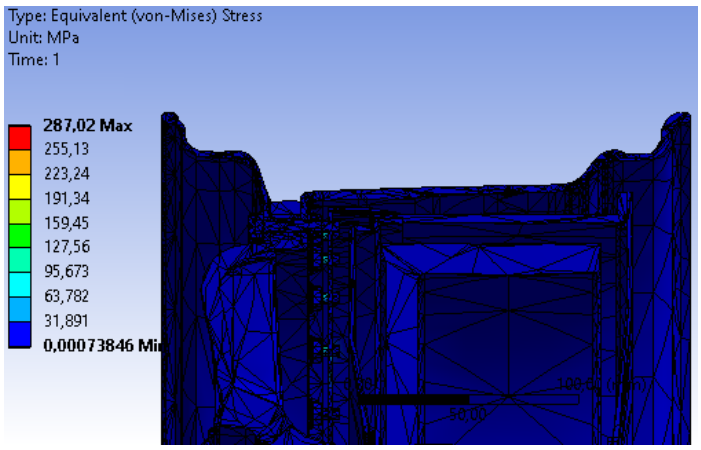

Figure 4.36 – Equivalent stress by load cases: a - Axial load F_A, b - Radial load F_R, c - Torque load M_L

The knowledge about the type of the deformation of the motor parts, especially the rotor and the stator, leads to the possibility of estimating the change in air gap. According to the above described model, the deformations of the motor assembly were FEM-simulated. Results of the deformations by different load scenarios are presented in Figure 4.37.

a

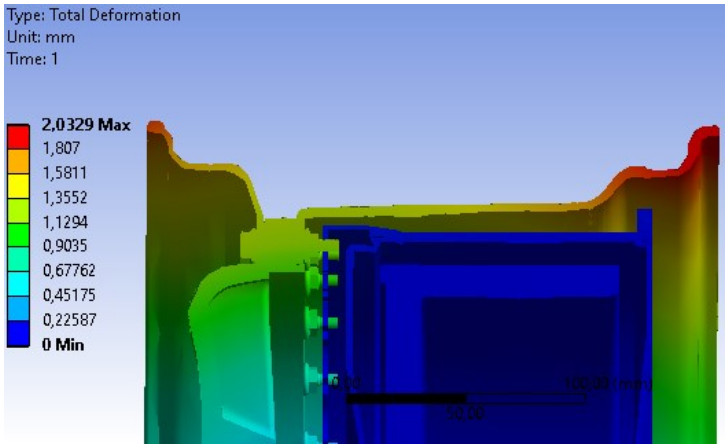

b

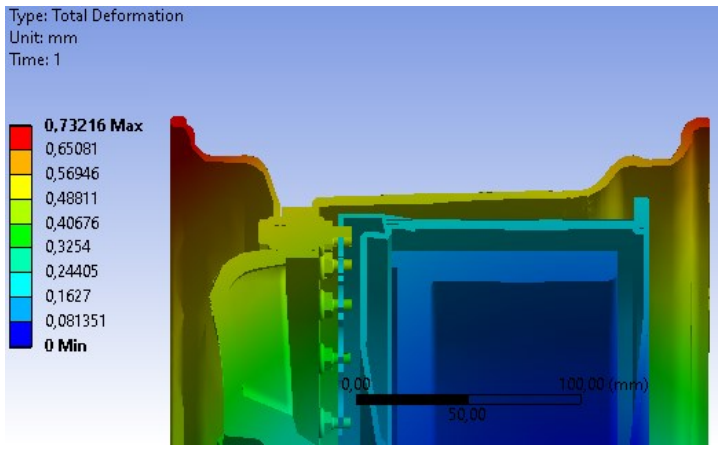

c

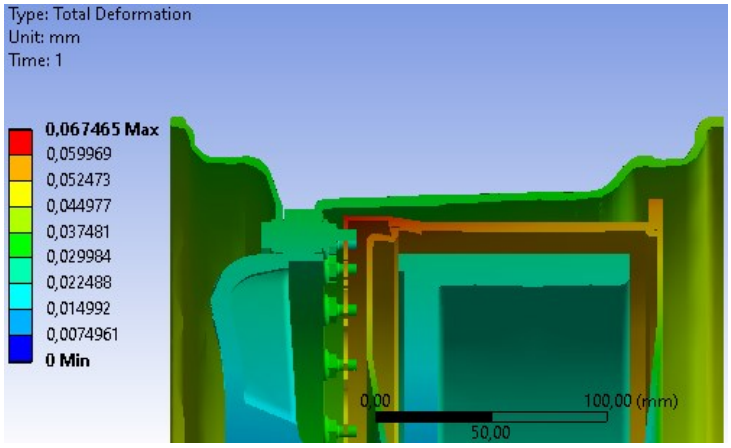

Figure 4.37 – Deformations by different load cases: a - Axial load F_A, b - Radial load F_R, c - Torque load M_L

According to the simulated loads, the total deformations of the developed model are presented in Figure 4.37. For the determination of the main result of the FEM analysis – the air gap deformation, the tool deformation probe is used, which allows to identify the deformations between the stator and the rotor. The results of the simulation have shown that the maximum air gap change due to the application of the developed elastic element can be achieved at 0.083 mm for the worst load scenario – in case of radial load. In reality, the air gap varies due to the action of wheel loads and the electromagnetic forces induced between the windings, back iron and permanent magnets. As it was shown above (4.3.1), the maximum value of the air gap changing is important for the bearing load capacity and also has a huge influence on the electrical motor function. The simulated values can be interpreted as insignificant for the impact on the motor main function.

4.3.3. Motor Shaft

The motor shaft is the central component for carrying other motor parts and loads and the further transfer of loads into the chassis system of the vehicle. The wheel hub bearing and the supplementary bearing are connected to the motor shaft. The stator should have a solid connection to the shaft so that the motor shaft can absorb the motor torque built up by the stator. Due to the connections to other components of the motor and the vehicle, the special connection options have been provided in the design of the motor shaft.

The simulation of maximum loads has shown (see Figure 4.36 and Figure 4.37) that stresses and deformations of a different magnitude are occurring on the motor shaft. The obtained values have less effect on the strength and reliability of the shaft, because the shaft section between the wheel hub bearing and the supplementary bearing is designed to be as stiff as possible in order to minimize the relative displacement of the stator and two covers of the rotor in radial direction. For this reason, by the design of the shaft, the aspect of the high integrability of the motor shaft also needs to be considered. The supply lines for power, signal and cooling must be laid between two motor bearings. Openings for the supply lines are preferably located on the sides, opposite to the points of maximum bending stress. At the same time, another aspect regarding the weight characteristic must be considered, because the shaft preferred should be made of high-strength steel because of the loads occurring in critical load situations. Therefore, the use of steel leads to an undesirable high weight of the motor.

In the area of the connection to the chassis, the equal flange as by automotive connection was implemented to ensure the connection options to standard suspension. The supply lines for the cooling are made of silicone according to the thermal profile of the motor and with the same cross-section of the cooling pipes so that the pressure losses of the motor do not increase. The cable for energy supply is selected according to the requirements of EMC shielding and corresponding to the maximum current carrying capacity in the power supply system of the motor. The size of the CAN cable has been determined according to the requirements derived in section 3.1 (see e.g. Table 3.2).

All supply lines in the shaft were inserted at the points where the minimum stresses are present. A lightweight part was designed for the correct positioning, alignment and sealing of the internal motor components, making further use of the rapid prototyping technique due to the complexity of the part. The isolation of the rotating parts of the wheel hub bearing and supply lines was provided by an aluminum plate integrated in the motor shaft. The final version of the design of the motor shaft is illustrated in Figure 4.38.

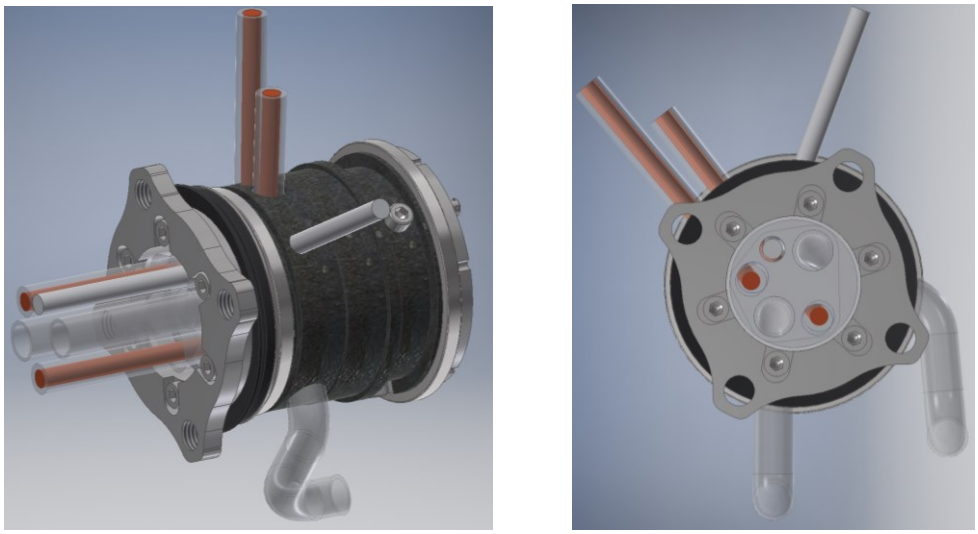

Figure 4.38 – Final design of the motor shaft

The strength values simulated for the maximum loads applied to the motor are only static values. In order to receive an acceptable result of the motor shaft, the strength of the designed components must be tested also on the dynamic loads, as they have an important purpose as a safety component in the vehicle.

4.3.4. Sealing

The functional demands on the sealing systems of the developed motor require absolute leak tightness. It presents a great challenge and loads occur during motor operation with mechanical, thermal or chemical origin and may affect the sealing system [9]. Mechanical loads can arise from deformation and misalignment of the sealing elements to each other. Thermal loads occur in form of high temperatures by frictional contact between parts of the sealing system, which in turn leads to changes in the properties of the seal itself. Low temperatures also have a negative influence on the sealing system and can lead to seal failure. Chemical loads are mainly caused by ultraviolet radiation and by aggressive environmental products. According to [11], the sealing system can have an impact on the motor function and lead to its failure, thus to avoid motor failure, it is necessary to select the seal correctly. Various approaches can be found to solve the issue of sealing in the application of in-wheel motors according to [101].

The starting point for the development of the sealing system is the determination of the boundary conditions of its application. The size of the sealing has a direct impact on losses, which in turn influences a lower efficiency of the developed motor, so that the larger the seal size, the greater the resulting losses. This can generate unintended torques or result in unreliability of the sealing. Also important is the higher costs by bigger sealing. On the other hand, a minimizing of the sealing size is limited by the dimensions that are important for the interface of the suspension and energy/control supply lines of the motor. After a number of iterative steps with regard to design measures and the resulting changes, a seal system layout and design with the required seals were developed. According to the decided motor topology, the sealing system is represented by the sealing of the wheel hub and supplementary bearings. Figure 4.39 illustrates a cross-section of the developed motor and indicates the seal points.

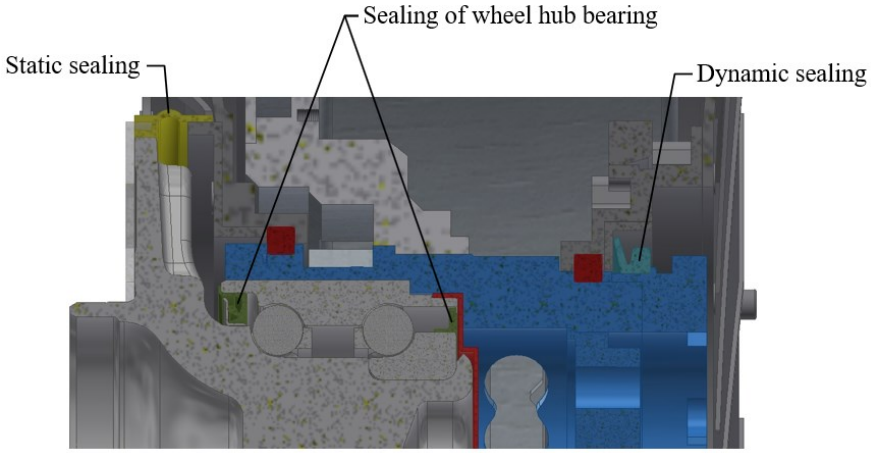

Figure 4.39 – Sealing system of the developed motor

The selected wheel hub bearing BAR-0230 is equipped with automotive cassette seals. This type of seal consists of two components: An insert seal and a counter face seal called flinger as shown in Figure 4.40, (a). The insert seal is constructed like a metal insert with rubberized lips, one or more of which can be arranged in radial and axial direction. The flinger is fitted on the inner ring shoulder and uses the centrifugal effect as it rotates with the inner ring to prevent dust, mud and water from entering the bearing. It is designed to prevent any corrosion that would result in seal failure caused by excessive seal lip wear. According to [160], reliability and performance of the main bearing is provided with high-temperature seal material and life-time grease, which enables it to be used in high-speed rotation with the associated heat generation.

As it can be derived from Figure 4.39, the seal of the wheel hub bearing is fully encapsulated inside the motor. The left side of the sealing is covered by the static sealing of the supplementary bearing and the right side is separated from the environment by aluminum disc. The separation disc also enables non-contact between the inner parts of the shaft and the rotating parts of the wheel hub bearing.

a b c

Figure 4.40 – Sealings of the developed motor: a - Seal of the wheel hub bearing [160], b - Static seal of the supplementary bearing, c - Dynamic seal of the supplementary bearing

The seal of a supplementary bearing is not encapsulated and it can be influenced from the environment. The main function of this sealing is to keep the external environmental influences away from the inside motor parts and at the same time to ensure a reduction in frictional power.

The results of the simulation of the load torque with elastic elements is shown in Figure 4.37, (c), which demonstrates that the twisting of the rotor cover in relation to the flange of the wheel hub bearing amounts to 0.052°. This value is negligible and allows the use of a static seal. The construction of the static seal is shown in Figure 4.39 and Figure 4.40, (b). This seal is fixed on one side by a flange and on the other side by a spacer sleeve.

The dynamic seal of the motor is realized by a V-ring from Trelleborg AB. The V-ring, shown in Figure 4.40, (c), provides a low-friction contact seal. There are three components in the dynamic seal of the developed motor that are responsible for the sealing function: Rotor cover, shaft and V-ring. The shaft carries the actual sealing element. The cover of the rotor transfers the power out of the shaft. The seal represents an interface between the standing shaft and the rotating cover of the rotor. According to the manufacturer data [171] this seal is made of EPDM and offers a wide range of application temperatures from -50°C to +130°C. Due to the influence of the centrifugal force on the contact pressure of the lip, friction losses and heat are reduced to a minimum, resulting in a higher wear resistance and extended seal life. Once the layout of the seal has been selected, the losses of the dynamic seal can be determined. According to the data presented in [53], the power losses of the V-ring seal at the maximum speed of the developed motor (6.3 m/s by seal) are estimated at 22 W. The power loss chart for the V-ring is presented in Appendix K.

To ensure full product life, the motor assembly design allows for seal servicing, ensuring the integrity of the sealing process. This solution satisfied the design specification call for the motor to be sealed to IP6k9k and IP 68 compliance, or in other words allowed high pressure jet wash and the usage of the motor in 1m deep water.

As a highlight of the developed motor concept, considerable progress in the reduction of sealing losses can be achieved through further series application by removing two seals from the wheel hub bearing, since this is encapsulated in the motor, which is expected to increase the efficiency of the developed motor.

4.4. Conclusion to the Chapter

This chapter focused on the determination characteristics of the electric motor for a vehicle with in-wheel motors on the basis of the derived requirements of Chapter 3. Starting from the number of the requirements on the in-wheel motor, an electrical, cooling and mechanical approach has been estimated based on the geometrical restrictions of the motor and requested motor behavior. In the first part of the chapter, the electrical profile of the motor was deduced, whereby the analysis of rotor and stator geometry and material design was simulated by using of finite element models. To fulfil the driving performance requirements, the motor should contain the combined windings and Halbach array magnetic arrangement. The other motor parts, which have an important influence on the motor operation, were presented and analyzed.

In order to guarantee the required electromechanical output characteristics of the developed motor, as well as to protect the motor from thermal damage and the components installed inside the motor, the analysis of the active fluid cooling system was presented. The results contain the developed subsequence for the motor cooling and optimal geometry of the cooling channel, analytical and numerical results of simulation of pressure loss characteristic, flow velocities and heat transport of the developed motor. The conclusion of the analysis results in an effective heat removal and homogenous temperature distribution.

Assuming an electric and a cooling profile, the mechanical profile of the motor was presented. Due to the topological highlights, the substitution model of the wheel hub bearing was presented first. In addition, the calculation of the supplementary bearing showed that the requirement on the maximum service life of the bearing is satisfied. Therefore, the decoupling of the loads in the motor is requested. This challenge is successfully solved by using the developed coupling element. For the evaluation of the function of the coupling element, the critical load case scenarios on the in-wheel motor were analyzed. The use of the finite element method delivered information about the behavior of parts of the coupling element under maximal mechanical loads. Due to the elastic design, a compensation of the forces acting in the in-wheel motor is realized. On the basis of the presented analysis, methods and calculations, the structural integrity of the motor shaft can be examined. Finally, the sealing system of the motor is considered, whereby the amount of losses caused by the sealing is expected to be minimal. Based on the obtained data, a detailed 3D-model of the developed motor was built (see Figure 4.41). In the next steps, the electric motor has to be produced to realize the presented approaches in physical prototypes.

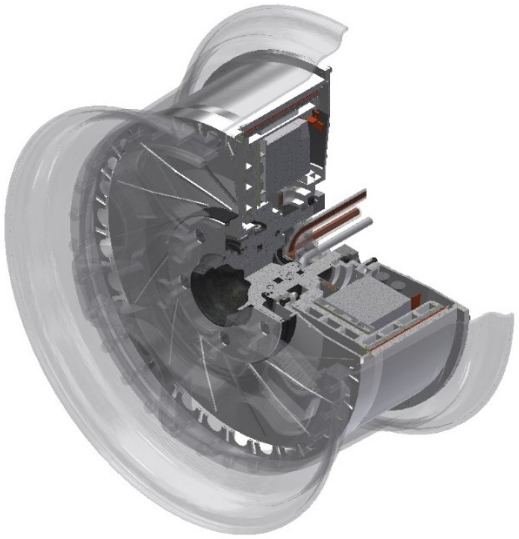

Figure 4.41 – 3D-model of the developed motor

5. Application Specific Design

The production of the electric motor is characterized by the application of a wide variety of manufacturing technologies. Apart from the conventional manufacturing methods for the production of motor components, there are also technologies and processes available that can always provide specific know-how in the field of electric motor production. This chapter focuses on the special factors of manufacturing and determination of the manufacturing of the full-scale motor in order to further validate the findings of this research. Based on the simulation results, topology-optimized design and material data, the technological methods for manufacturing of the developed motor from analyzed materials are defined. In the following, an implementation of the specific design for the developed solutions of the electric motor according to Chapter 4 is carried out. The application refers to the following motor components: rotor including magnets montage, stator main body, stator active parts: back iron, windings for combined winding and its connection.

5.1. Rotor with Magnets

According to the requirements on the lightweight design of the developed motor, the materials of the rotor were standard aluminum alloy, aluminum foam and sandwich consisting of CFRP plates and aluminum foam. Within the first step, the rotors made of full aluminum foam were checked to ensure that the rotor cylinder was concentric (see Figure 5.1). The rotor, which was made completely of aluminum foam plates, proved to be dimensionally inaccurate due to casting distortions and was therefore not suitable for further processing. The measured values have shown that the technology must be further improved in order to maintain the application for the developed in-wheel motor.

a b

Figure 5.1 – Full aluminum foam variant of the rotor (a) and the results of its run-out measurement (b)

The placement of the necessary magnets (Figure 5.2) to form the Halbach array arrangement with prototypical devices in the variant made of non-full aluminum foam led to a geometric distortion in the prototype. As a result, the rotor cylinder of the non-full aluminum foam variant showed deviations in the radial runout.

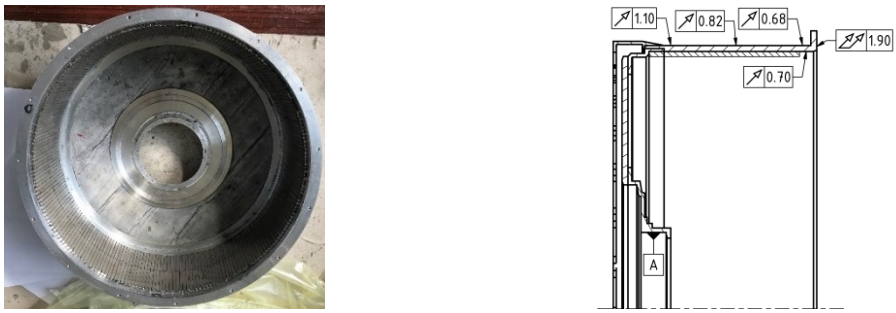

a b

Figure 5.2 – Non-full aluminum foam variant of the rotor (a) and the results of its run-out measurement (b)

In addition, it is necessary to perform an optimization loop in the form of a mechanical redesign of the foaming molds in order to maintain the high tolerances on shape and position while taking into account the production-related distortion. Both metal foam variants offer a high application potential, whereby the full aluminum foam variant enables a weight reduction of approximately 25% compared to the standard aluminum alloy version.

Furthermore, in the sandwich variant, the spongy surface of the aluminum foam of the rotor cylinder did not allow the adhesive to remain on the rotor surface in sufficient quantity. For this reason, the main disadvantage of using aluminum foam in this variant is the reduction of the surface on which the adhesive material must provide a carrier film. Therefore, in order to validate the motor concept, the magnets were glued into the rotor variant made of standard aluminum alloy.

As previously determined, an arrangement according to Halbach was specified for the reduction of the total weight. Apart from the weight reduction of the rotor unit, however, it is relatively more complicated to assemble and install than the traditional dipole arrangement. The manufacturing complexity results from the placement and mounting of the permanent magnets on the rotor cylinder. According to the placement of the magnets, the developed radial-flux motor uses the principle of surface mounted permanent magnets, in which the magnets are fixed to the inner rotor surface. The adhesive technique was chosen for fixing the magnets in the rotor, whereby the different adhesive variants were investigated according to the requirement profile. During the selection of the glue, the main focus was on the adhesive force on the glued surfaces, the strength at maximum temperatures and the shear strength. The influence of aging after long-term thermal and dynamic stress was eliminated. The magnets were glued in a manual way and with the help of special devices. The high forces that arise between differently polarized magnets have caused the development of the gluing device (see Figure 5.3, (a)). For this purpose, a series of experiments were carried out, which led to different concepts for the gluing of the magnets. As a preferable variant, a special device has been developed in which, on the first step, a simultaneous distribution of the radially magnetized magnets of the first row is realized and the gluing of the second row of tangentially magnetized magnets is carried out when the glue of the first row is dried, as shown in Figure 5.3, (b). This device has proven as successful and the further mounting of the magnets was realized with the assistance of it.

a b

Figure 5.3 – Gluing device for the Halbach array (a) and subsequence of the gluing of the magnets (b)

5.2. Stator

This section is dedicated to the most important assembly of the developed motor – the stator unit. The main parts of the stator unit are the back iron, copper windings and additional accessories and parts for the mounting and the connection of the active parts of the stator.

5.2.1. Stator Main Body

The design concept of the stator and stator main body have been fundamentally redesigned in order to achieve the weight reduction targets of the complete motor. The possible manufacturing options and technologies for the realization of the stator main body component is planned and realized in two variants. After the geometry of the stator is detailly specified, the following variants of the material combinations are provided: Standard material variant (aluminum alloy) and hybrid variant (Al-Mg mix).

The challenges in the area of manufacturing of the stators were the connection and closing of the cooling channels by using suitable joining methods. The stator main body with the Al-Mg hybrid according to Figure 4.9 consists of four parts, which are solid connected to each other and must fulfil a number of specific connection effects, such as different behavior of the material pairing (e.g. different thermal expansion coefficients), tightness of connections, corrosion, strength and lightweight design. As Figure 5.4 shows, the Al-Mg hybrid variant offers the advantage that the joining partners for closing the magnesium cooling ring with the magnesium sleeve and the aluminum base with the aluminum cover are made of the same material.

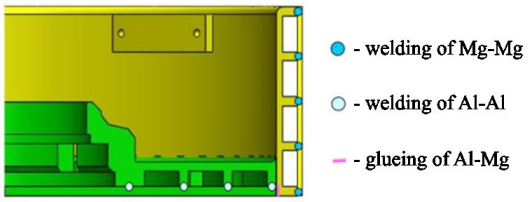

Figure 5.4 – Connection points of the developed Al-Mg stator

For the realization of the welding of Mg-Mg and Al-Al parts, the electron beam welding was selected. Compared to laser beam welding, electron beam welding is characterized by a higher efficiency of the beam generation. If the welding process takes place in a vacuum, there is also no need to use the shielding gas. Due to the higher power of the electron beam, a significantly deeper welding depth can be achieved.

The stator main body presents a material hybrid component. As result, it leads to the development of an Al-Mg compound technology. The solution approaches defined for this purpose made it clear that an essential requirement is to find a surface structure in the contact area between the magnesium insert and the aluminum web base segment that creates a form-fit connection between the two materials, as well as a partial coating of the magnesium insert to prevent contact corrosion between the magnesium insert and the aluminum web base segment. This is due to the fundamentally new concept of the Al-Mg lightweight stator body that is necessary to connect the magnesium insert with an aluminum stator base body segment by using the interlocking method. With regard to the manufacturing of the Al-Mg lightweight web, a concept for the configuration of the interlocking pitching in the sinusoidal shape with an additional adhesive connection between the aluminum web base segment and the magnesium web cooling channel segment was developed. Within the prototyping process, the adhesive bonding for the connection of the magnesium stator segment with the aluminum stator base segment played an important role. On the one hand, the adhesive connection ensured a secure bonding of both segments and, on the other hand, it prevented the contact corrosion between the aluminum and magnesium material. The SikaPower 493 glue was applied for bonding, because it is classified in the group of crash-resistant metal glues for the automotive application.

The manufacturing of the stator variant made of standard materials is more simplified because there are no requirements based on the pairing of different materials and a missing connection between the web base segment and the insert, because these parts are presenting one solid part. A further simplification in the manufacture of the variant from the standard materials is the use of the Y-seal on the end faces of the stator for welding in combination with a press connection of stator and sleeve.

a

b

Figure 5.5 – Variants of the stator: standard material variant (a) and hybrid variant (b)

Design concepts of the developed cooling system were successfully implemented in both stator variants. The system of connecting the stator web (with cooling channels) and the outer sleeve was implemented as a liquid-tight solution. As a result, a two-piece stator made of aluminum and magnesium alloy and one-piece stator made of aluminum alloy were manufactured. The application of the hybrid stator main body allows to reduce the total weight of the stator by 15% in comparison to the standard material design.

5.2.2. Back Iron

In the following, the mounting of the back iron on the stator is explained. For the safe torque transmission, the surface pressure by shrinking the back iron was selected. For the stator assembly, a press fit between the back iron and the stator was selected. It was realized by shrinking during the heating of the back iron and simultaneous cooling of the stator (see Figure 5.6, (a)). To achieve shrinkage, calculations according to [39] were performed in the area of tolerances, which makes the joining process technologically more demanding. Nevertheless, even in these accuracy classes it is considered to be accepted in electrical engineering. The connection of parts by shrinking is necessary because other methods (e.g. gluing) cannot provide optimum heat dissipation of defined areas due to the formation of air cavities and relatively low thermal conductivity of glue.

The back iron is produced by conventional processes for electrical engineering – the bounding process. To increase the active bonding surface for baking the sheets in the back iron, an additional outer ring was attached. The additional ring is shown in Figure 5.6, (b). It prevents the sheets from falling into pieces when the back iron is mounted. The function of the ring is to increase the stability of the back iron and to provide the centering of the sheets by using the holes in the ring during bonding. Therefore, the ring complicates the manufacturing, because it had to be removed after the back iron is placed on the stator. Due to the switch-off, the partial short-circuit of the plates are in the tooth head area and a certain increase of the eddy current losses in the plates can be expected. And the eroding process was used to cut the ring. The cutting by eroding is relatively fine. It results in less eddy currents losses, because it allows to reduce the number of contact points between the sheets.

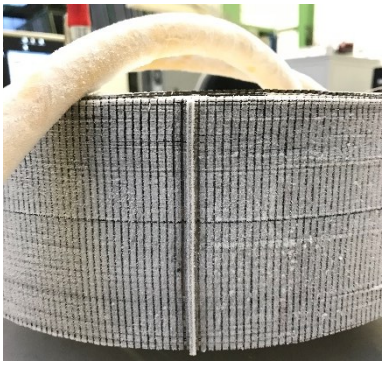

a

b

Figure 5.6 – Cooling of the stator by shrinking (a), mounted stator and back iron with additional ring (b)

For the calculation of the undersize for the shrinking process, a temperature of the back iron of 150°C and temperature of the stator main body of -30°C was assumed. The expansion coefficients of aluminum and NO20 steel are α_{Al} = 23.8·10^{-6} 1/K and α_{NO20} = 11·10^{-6} 1/K. Thus, for the expansion of the back iron of Δ_{bi} = 0.50 mm and constriction of stator main body of Δ_{st} = 0.39 mm. The difference equals 0.45 mm, which enables the assembly of the stator and the back iron using manual devices.

Shrinking as a technology for mounting the back iron has shown that, if the interference fit for torque transmission between back iron and stator is sufficient, it is also suitable for certain thermal load scenarios. The validation of the thermal conditions between the stator main body and back iron can be performed after the mounting of the windings. As a further development, the tolerance which allowed a larger press fit could be chosen. Another approach that simplifies the thermal load on the back iron is to cool the stator with liquid nitrogen instead of heating it. The heat conduction can also be improved by the use of heat conducting greases.

5.2.3. Windings

The winding technology can be classified into the manufacturing process of joining through forming. In this process, a wire is continuously bent to produce a coil. In order to bend the wire into a coil, different winding types and processes are used. A winding type describes the way the winding material is placed in or on the back iron. The type of winding depends on the requirements of the product, such as the fill factor or production costs. Techniques like wild, orthocyclical, helical, cross or toroidal winding are well known for individual and mass production for various types of electric motors. The meander-shaped combined winding consisting of air gap and slot winding differs significantly from classic winding forms and provides a cutting-edge technology for the application in electric motors.

In order to better understand the effects of new winding concepts and the potential of its manufacturing, the following case of implementation was carried out. The following section represents a new winding concept, which is associated with a specific design and novel manufacturing steps. For the implementation of this concept, basic practical work was carried out until the completed laboratory prototypes were provided for analysis and validation of the motor parameters. The investigations were performed on the process of winding the slot winding, following closing of the slots in the back iron, winding of air gap winding on the stator and wiring the windings.

5.2.3.1. Slot Winding

Pyrhonen et al. [140] defines the part of the winding located in a single slot as a coil side, and the part of the winding outside the slot is termed a coil end.

The windings are realized in such a design (see also below following winding process of the air gap winding) that the relatively short connection between the individual coil sides and the coil ends of the winding phases is arranged. The coil ends represent the connection between the coil sides or the phase wires with the shortest possible path of the spatial arrangement, so that alternating current flows in the adjacent phase can be realized. Alternating current flows are defined as the current that changes its orientation between the adjacent phase coil sides, which are connected by coil ends. Thus, all magnets can be used simultaneously for the torque generation. Short coil ends keep the ohmic losses low and therefore increase the efficiency of the motor.

In case of the developed slot winding, the windings are pre-manufactured as finished elements and can be mounted into the back iron of the stator. For the winding of the slot winding, a winding scheme has been developed, which is illustrated in Figure 5.7, (a). According to the developed scheme for a better understanding of the winding process, the CAD model of the slot windings was established (see Figure 5.7, (b)).

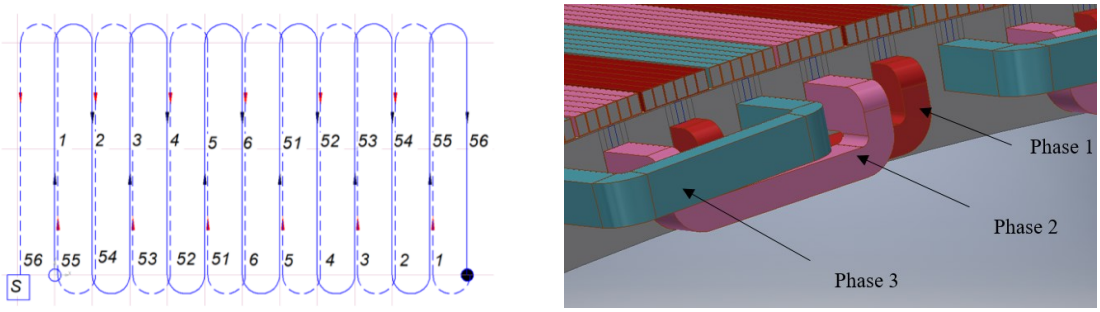

a b

Figure 5.7 – Winding scheme of the slot winding (a) and CAD of the slot winding (b)

The axial length of the coil ends has been analyzed by the variation in the arrangement of the wires in the CAD models and the twisting of the wire outside the slot. The following lengths were obtained for the investigated versions of the coil ends: Strict bended ends of 3.6 mm (Figure 5.8, (a)), twisted ends of 5.2 mm (Figure 5.8, (b)) and rounded ends of 5.6 mm (Figure 5.8, (c)).

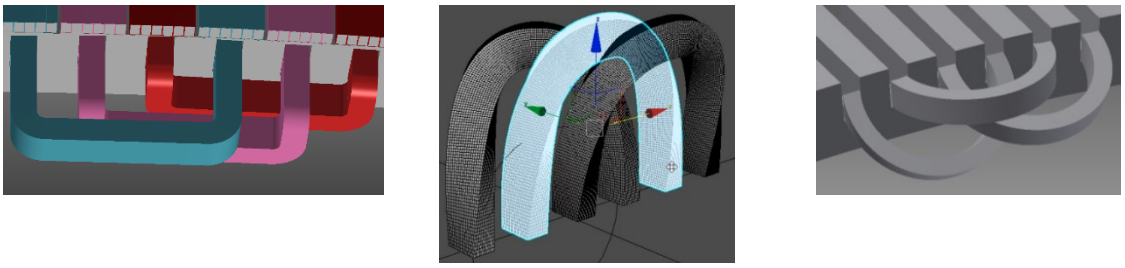

a b c

Figure 5.8 – Variants of the coin ends: a - Strict bended, b - Twisted and c - Rounded

Although rounded coil ends are the longest, they are the most acceptable in terms of prototype production and require the minimum of technological complexity in their manufacturing.

For meander-shaped windings, a special device was developed. The device for coil ends represents a board with 56 slots and 56 pins. The pins provide the shape for the winding end. The free ends of the winding must be sufficiently long (app. 60 mm) to be able to make the phase connections later. The configuration of the developed device and an example of the pre-shaped winding is shown in Figure 5.9.

a b

Figure 5.9 – Device for the pre-shaping of the slot windings (a) and bended windings of the slot winding (b)

In order to provide insulation and prevent the damage of the wires against the sharp edges of the back iron, the endcap for the front sides have been developed. The endcaps (see Figure 5.10) are made from polyamide using the Rapid Prototyping technique (SLS) and glued to the front side of the back iron.

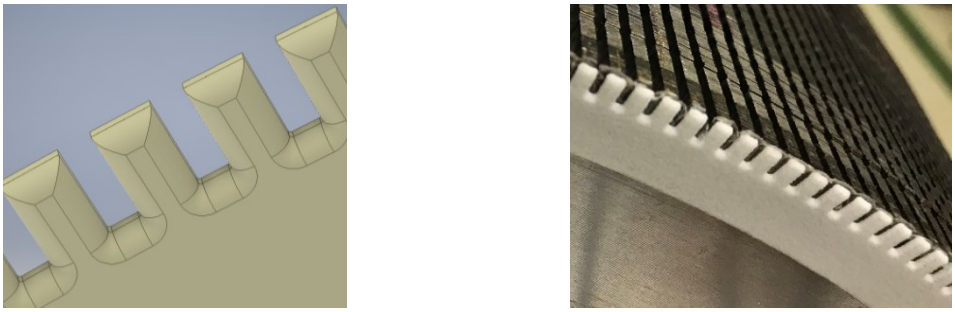

a b

Figure 5.10 – Endcaps of the slot windings: CAD model (a) and realization with SLS technique (b)

The first experiments on the stator have shown that there are technical manufacturing challenges which can lead to the motor malfunction. The test with placing of the pre-shaped windings into the slots have shown that especially in the area of the coil ends, bending over the short side of the wire leads to insulation damage and to further disruptive discharges due to wire compression. This was caused by the massive wire of the slot winding, which is equal to the wire cross-section as in the simulated model. For this reason, a massive wire was substituted by two wires with the reduced cross-section. The new pre-shaped winding was produced with the same principle and adapted device. The cross-section of the winding was reduced by the two insulation thicknesses of the wire. The results of the both winding processes are shown in Figure 5.11.

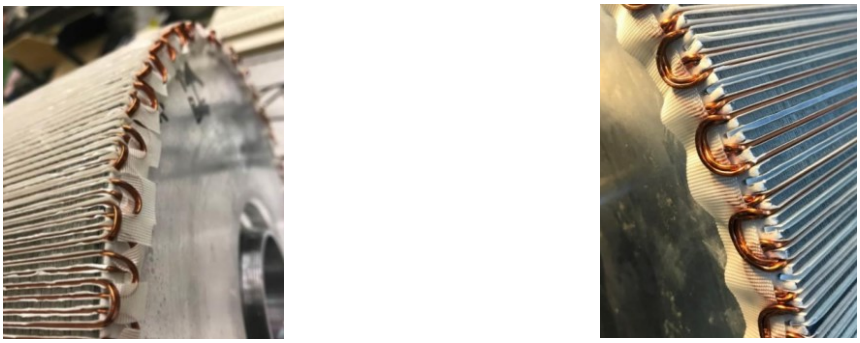

a b

Figure 5.11 – Slot windings with one massive wire (a) and two wires (b)

The advantages of the two-wire version are as follows:

- wire can be bent more readily (coil ends),
- the deformations of the geometry in the area of the 90º bends are relatively low due to the more suitable height/width relation,
- more compact version in axial direction.

Although the winding variant has the disadvantage of double the production time, the slot windings of the prototype can be manufactured with the required electrical safety.

Due to the natural twist of the wire and the existing dimensional tolerances, the wires could not always be secured to the slot bottom, resulting in positioning errors. From another point of view, as already mentioned, the coil ends are thermally particularly problematic because the coil ends overlap at the stator front face and thus cannot be attached directly to the cooled stator body. One possibility to solve both problems is a filling compound. In general, there are different materials available for this purpose. Temperature-resistant epoxy casting resin was used to fix and improve the heat conduction. The epoxy resin SKresin T4 is characterized by a temperature resistance up to 120°C, good UV stability and clear, transparent properties in molding applications. The results on the filling of the front areas of the stator with slot windings can be seen in Figure 5.12.

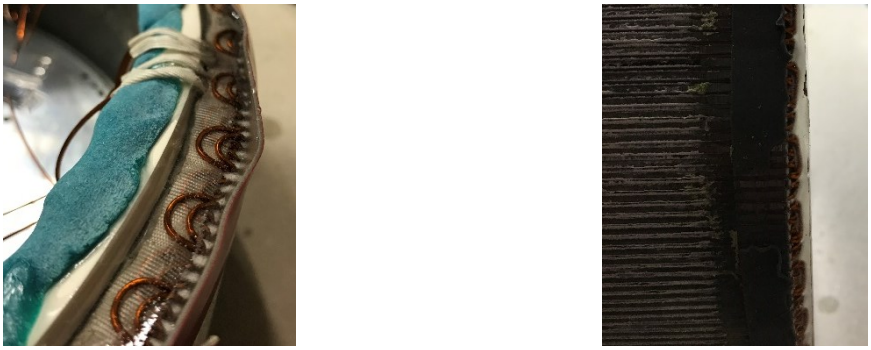

Figure 5.12 – Filling of the front areas of the stator

5.2.3.2. Inlays

In the field of inlays for the slots, different approaches for filling were investigated. In terms of geometry and material, the preferable inlays variant was already defined in 4.1.2.3. The first tests were carried out using the same material (electrical steel NO20) that was used for simulations and to manufacture the back iron. An aluminum sheet, as a non-magnetic material, was chosen as the core of the sandwich of the inlay. This sheet can be easily deformed when the inlay is inserted, thus compensating for shape differences of the back iron is provided. Tests have shown that this is the best solution for the oversized inlay, i.e. the insertion of the wires. The insulation of the down surface of the inlay is achieved by inserting the paper strips made of Nomex® as a cover strip over the wires in the slot.

Subsequent to the manufacturing tests it was determined that the preferred NO20 version could not be manufactured, as it consisted of five separate metal strips, each of which had to be handled and fixed individually. After investigating alternative cutting technologies, it was also discovered that the manufacturing of such fine metal strips is very complicated and the cut inlays have internal stresses and occasionally burrs. These two aspects make the installation of the inlay extremely difficult and directly affect the main function of the motor. However, for the series production it offers high potential, especially if the sheet metal strips are cut off from the sheet or coil.

In the next step, a casting technology was developed as a technologically simpler equivalent for the solid inlay. In this variant, the filling of the slots was investigated, whereby a compound of iron particles and epoxy resin was produced in various proportions. The relative permeability μ_r of the potting in the solid state must be configured in such a way that the cogging torque is minimized, but at the same time the back EMF is not degraded. Furthermore, the compound must have the required dielectric strength values. The stator slots were completely filled with the potting material (see Figure 5.13, (a)). Afterwards, the rests on the stator were removed by grinding. The measurements of the compounds have shown that the values of permeability μ_r are about 11, which modifies the cogging torque of the motor very slightly.

The further experiment of reducing the cogging torque was investigated by filling the slots with a defined flux-suppressor film from Kemet. The advantage of the film is its relatively high flexibility, which facilitates the installation of the inlay. The permeability value μ_r of such a film according to the manufacturer is about 130, which should lead to a significant reduction of the cogging torque. The structure of the inlay of the used sandwich made of the films represents Figure 5.13, (b).

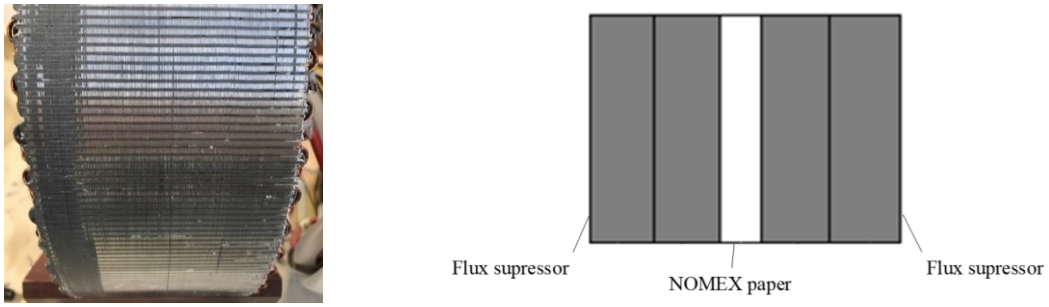

a b

Figure 5.13 – Filling the slots with compound (a) and structure of the inlay with flux-suppressor of Kemet

After completion of the slot filling, the back iron should be grinded in order to achieve a defined roughness. This provides a continuous surface which simplifies the implementation of the winding on the stator.

5.2.3.3. Air Gap Winding

In view of the innovation of the technology, the special feature of the motor with air gap winding is the meandering form of the individual phases of the winding. Therefore, the application of the air gap windings is a major problem for the implementation of the motor concept. In joining technology, force-fit and form-fit joining processes are fundamentally excluded, since one of the motor's priorities is to place only the winding in the air gap.

The wires of the air gap winding have to be applied in one layer around the stator circumference on the outer surface of the cylinder. This means that each wire must be connected to the stator. The manual application of the windings on the stator outer surface is a very time-intensive and fault-sensitive process. A large number of movements around different axes have to be performed to implement this process. For this reason, an automated process is required for economic use. According to [23], for this purpose a winding machine was developed and designed. The machine has 13 axes to provide all positioning movements that are necessary for the winding application process. An application of the machine gives an opportunity of handling a wide range of stator diameters, stator depths, number of wires, number of phases, wire geometries, and winding connections [23].

The structure of the winding machine can basically be divided into six assemblies, see Figure 5.14:

- table consisting of aluminum fixing profiles,
- coil carrier with threaded rods,
- wire feed mechanism,
- portal with actuators,
- the control system (located under the machine table) with a PC for command input.

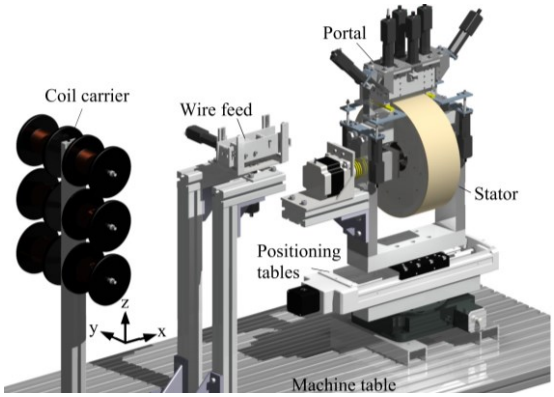

Figure 5.14 – CAD of assembled winding machine [23]

The operation of the winding machine could be described in the following steps:

- the prepared stator is mounted with the help of the flanges and installed in the portal of the winding machine;

- the single wires are fed off the coils and passed through the wire feed to the stator. The tension of the individual wires is adjusted by four bolts on the wire feed, which press the felt mats together;
- at the output of the wire feed, the wires are packaged through the clamps;
- the end of the package is fixed after the portal of the winding machine;
- the wires have to be cleaned before bonding;
- the wire package is pressed onto the surface of the stator with the help of a downholder. Thus, the wire package is bonded and held;
- on the front side of the stator a pin is placed by a linear drive;
- the coil end will be produced, whereby the stator is rotated by 180° around its vertical axis;
- to obtain the correct shape of the coil end, the overbending process should be provided by an additional rotation of +30° and then -30° around the vertical axis;
- the second downholder device is driven so that the second winding package is pressed onto the stator surface;
- the coil end can be bent with maximum angle to the stator front side;
- first and second downholders can be raised and the wire packages are relieved;
- the stator can be rotated around its axis at an angle θ_{pp}. The angle θ_{pp} results from the number of the coil ends of the phase;
- the winding of the one phase contains 112 coil ends (56 left and 56 right). Therefore, the process must be repeated 112 times.

For every wire of the motor, a voltage is induced due to self-induction. According to Lenz's law, this voltage prevents the current from flowing through the wire. In the standard wire arrangement, the magnetic fields of the individual cores are different in magnitude, which means that a compensating current is generated within the conductors, since they are connected together at the beginning and the end. As a result, an internal cross current is produced inside the wire package, which cannot be detected from the outside. Cross currents in the phases are reducing the maximum rated current of the motor. The required maximum of the torque cannot be achieved. To eliminate these disadvantages, it is necessary to compensate for the unequal potential distribution. By a selective wire replacement, the wires should be uncoiled in alternating sequence so that the wires are positioned once at each position in the wire package on the full circumference of the stator. The number of wire changes depends on the number of wires used in the winding package. For eight wires, the wire exchange should be conducted seven times. Wire replacement describes the repositioning of the wire in the wire package from the inside to the outside of the package. The wire replacement must be carried out solely in the area of coil ends, because the phases must be as flat as possible and parallel to the axis of rotation and are not allowed to have a higher dimension in the air gap of the motor.

The bending of the coil ends creates the internal stresses in the bended wires. This leads to wire packets or individual wires being taped off the stator surface. For this reason, the bandaging of air gap winding is necessary. The air gap winding bandaging could be realized on the winding machine, where the tensioned bandage band is fixed by a continuous rotation of the stator. The results of the completed air gap winding before and after bandaging can be seen in Figure 5.15, (a), (b).

a b

Figure 5.15 – Air gap winding before (a) and after bandaging (b)

5.2.3.4. Connection of Phases

The connection of phases is an important factor for the correct motor operation. The wrong connection can be responsible for faulty current flows, which results in a crucial motor fault. To realize the combined winding concept, the ends of the air gap and slot windings should be connected as it is illustrated in Figure 5.16.

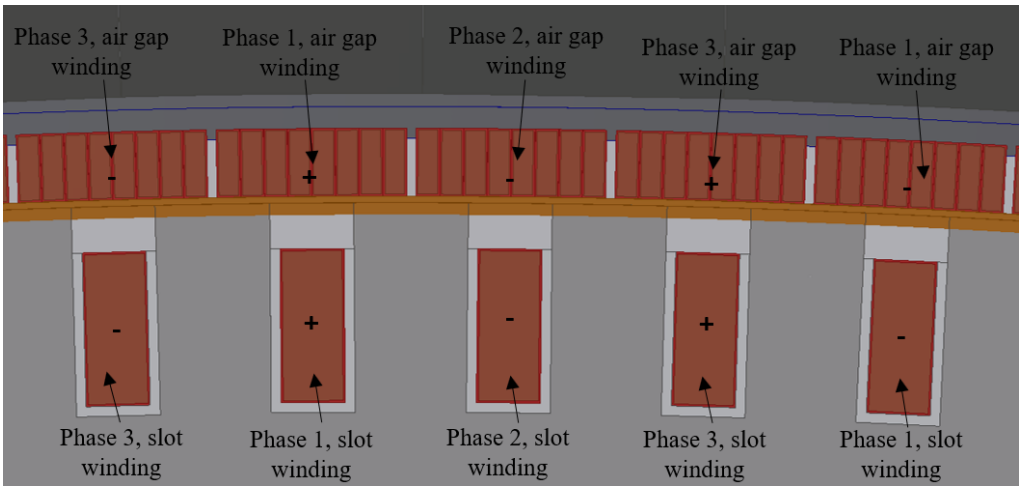

Figure 5.16 – Phase arrangement of the air gap winding and slot winding

The "-" sign in the presented arrangement corresponds to the direction to the stator bottom, and the "+" sign is determined as the direction from the stator bottom.

During the connection, the individual phase windings are connected to each other according to the connection scheme presented in Figure 5.17. The positions for the start and end of the phase windings are selected where the terminal clamps have the shortest distance to the corresponding contact points. The various connection methods can be used to realize this scheme. According to the number of phases of the motor, there is the same number of terminal clamps needed.

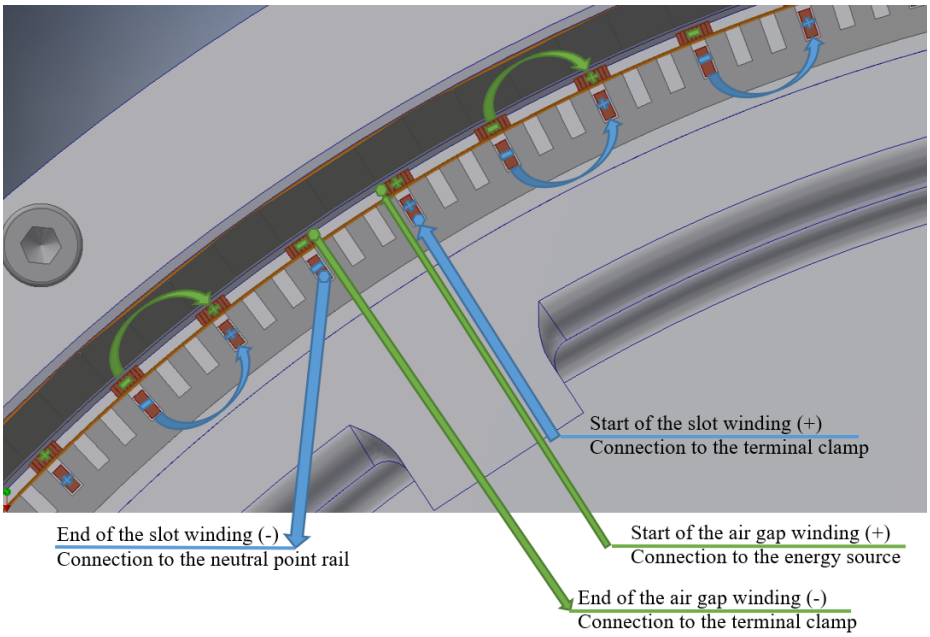

Figure 5.17 – Scheme of the connections for realization of the combined winding

Basically, all connection elements are composed of electrical conductors that are insulated from each other. Copper is typically used as the conductor material while the insulation is provided by an insulation coating. If this method is used, all connections have to be connected directly to the terminal clamps. Due to the relatively large dimensions of the standard terminal clamps, the special sub-assembly was developed (see Figure 5.18).

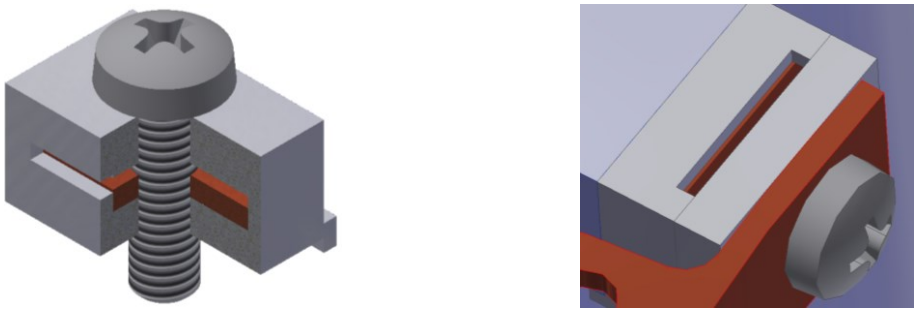

Figure 5.18 – Developed terminal clamps

The main requirements for the development of terminal clamps were:

- the terminal clamps have to realize the series connection,
- the terminal clamps require a good heat dissipating and at the same time insulated contact to the stator surface,
- the clamps also have to keep sufficient distance to rotating parts.

Terminal clamps have a great potential for cost reduction through standardization, but for optimal use of the working space in the stator, special terminal clamps are required which have an additional development requirement.

5.3. Conclusion to the Chapter

Chapter 5 concentrates on the application of the motor specific design of the in-wheel motor. The realized technologies, which have been used as a basis for the manufacturing concepts, have proven to be technologically successful. In some cases, the concepts which have been revised during the manufacturing process also showed to be insufficient (e.g. filling of the slots).

In the area of rotor manufacturing, the full aluminum foam variant and non-full aluminum foam variant of the rotor versions could not be used due to dimensional inaccuracies during production process. The used rotors showed different dimensional faults before and after the assembly phase. Furthermore, the quality of the inside surface is not satisfactory to ensure the fixation of the magnets. The presented light-weight technologies have considerable advantages in weight reduction, but not sufficient for further application in the in-wheel motor under test, because the accuracy of the produced parts is not achieved. The manufacturing of the prototypes was performed with the standard materials. The adhesive bounding was applied for the mounting of the magnets, whereby the special device for the gluing was developed.

In comparison to the rotor assembly in stator manufacturing, the application of the lightweight design variant achieved the required result. The applied combination of materials results in a weight reduction of 15% in comparison to the standard materials.

In the area of the stator manufacturing, the application of the back iron on the stator main body as well as the production of both windings in particular were a technological challenge. The method of winding manufacturing, which was developed using the corresponding devices and tools, proved to be fundamentally applicable, but time-intensive. On the one hand there are partly neither existing technologies nor corresponding experience on the market in the area of winding technologies, on the other hand the assembly technologies were found which do not limit the technical properties of the winded stator in its performance (cooling of the windings). Both requirements were successfully solved by the development of the range of special devices. The derived method of the mounting of the back iron ensures optimum heat dissipation. Furthermore, the problem of the electrical insulation of both windings was solved by the intended use of special manufacturing processes. The solution in the field of connection firstly was presented as the special designed terminal clamps, which can be optimized by the requirements of higher manufacturing needs.

However, it also became apparent that due to the novelty of the development, a number of questions and problems could not be clarified with absolute precision in advance. The unknown factors were so significant

that in some cases, second or third attempts had to be conducted, as by the filling of the slots by different kinds of inlays.

Based on the experience and results of application steps, the respective prototypes were built and assembled (see Figure 5.19). The prototypes can be used for tests as the physical model to validate the theoretical approaches presented within this work.

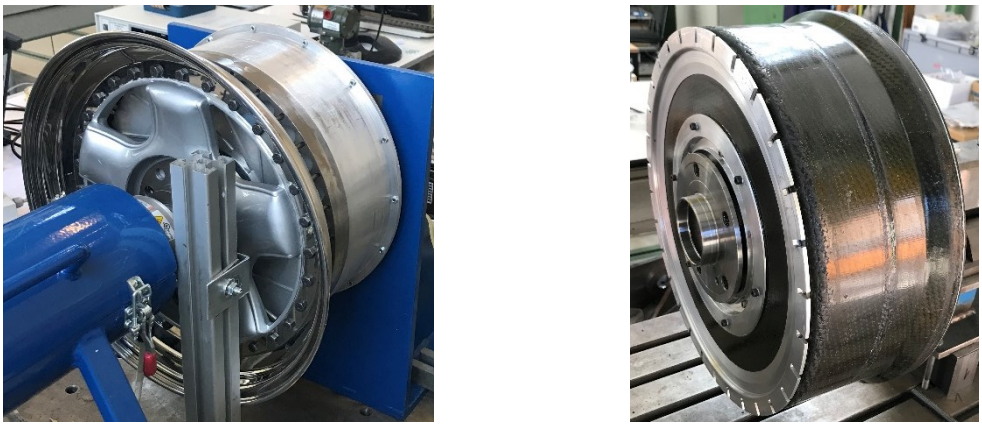

a b

Figure 5.19 – Assembled variants of prototypes: a - Standard materials, b - CFPR

6. Experimental Validation

Despite the diversity of existing approaches and the availability of simulation programs, no universal methodology is being developed that allows a combination of complex processes to be considered by simulating motors. In accordance with requirements for the efficient manufacturing of the motors, it is necessary to use validated analytical methods to estimate the important parameters of the motor.

Chapter 6 concentrates on a validation of the developed in-wheel motor as well as on the impact of boundary conditions and assumptions determined in this study. For this reason, the prototypes were metrologically evaluated and the measured properties were analyzed. The prototypes were measured in special test stands regarding their electrical, magnetic and mechanical properties.

In the first part of the chapter the influence of the forces acting on the wheel on the air gap in the special test stand was presented for validation. Afterwards, the losses due to existing cogging effects are presented and analyzed, whereby the proposed filling principles for the validation of different possibilities of minimizing the cogging effect were tested with the help of a specially developed test stand. The motor parameters represent the essential and important knowledge about its function before the test of the motor on the test stand began. After the preliminary tests of the prototypes were carried out, the measurements on the motor test stand are presented. In the final section, the validation of the required parameters regarding the weight of the in-wheel motor and potentials of the lightweight design are introduced.

6.1. Air gap changing

This section presents the validation and comparison between analytical results and test results using the approach that uses a specially designed test stand.

6.1.1. Approach of validation

To inspect the mechanical structure of the developed motor and the principle of decoupling the forces, a special test stand was developed to assess the static load cases according to the requirements.

As illustrated in Figure 6.1, the test stand consists of the following subassemblies: clamping unit, frame, angle support, hydraulic cylinder and 6-axis force sensor. The wheel alignment on the developed test stand is horizontal. The load is generated hydraulically and is applied to the wheel by the hydraulic cylinder via the clamping unit. The clamping unit holds the wheel flange, it also should be complied with the shape of the wheel and equally distribute the load over the contact surface. The load can be determined approximately by comparing a pressure measurement. The precise measurement of the forces is performed by the 6-axis force sensor, which is installed directly in the clamping unit. The lifting forces can be generated with corresponding hydraulic cylinders up to 100 tons [111]. The oil pressure required for the hydraulics can be applied via a hand pump. The measurement of the oil pressure is carried out via the pressure gauge. The frame construction consists of the profiles connected with each other with screws, which enables quick rebuilding for different modifications of the test objects. With the help of this test stand, it is possible to test the in-wheel motor wheels with different diameters and widths (see Appendix L for details). This can also be done by the stroke of the cylinder or by the sliding of the hydraulic cylinder. In the frame base plate, there are guide rails on which the hydraulic cylinder can be adjusted according to the wheel diameter. In addition, different load cases can be realized by rebuilding the hydraulic cylinder. With radial load, the hydraulic cylinder directly loads the shaft of the clamping unit. Figure 6.1 shows the case of radial load, in which the direction of force is radial to the wheel axis.

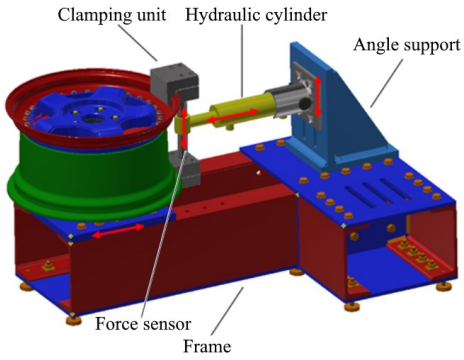

Figure 6.1 – Explanation of the main parts of the test stand and scheme of the radial load

During the torque load, the angle support is displaced from the axes of symmetry of the wheel. This results in a lever arm and a torque can be applied to the wheel via the translational action of the hydraulic cylinder. The torque load is depicted in Figure 6.2, (a).

The axial load presents a simulation of the lateral forces during cornering. The direction of force is parallel to the wheel axes of symmetry. This is achieved by mounting the hydraulic cylinder on the frame base plate, see Figure 6.2, (b).

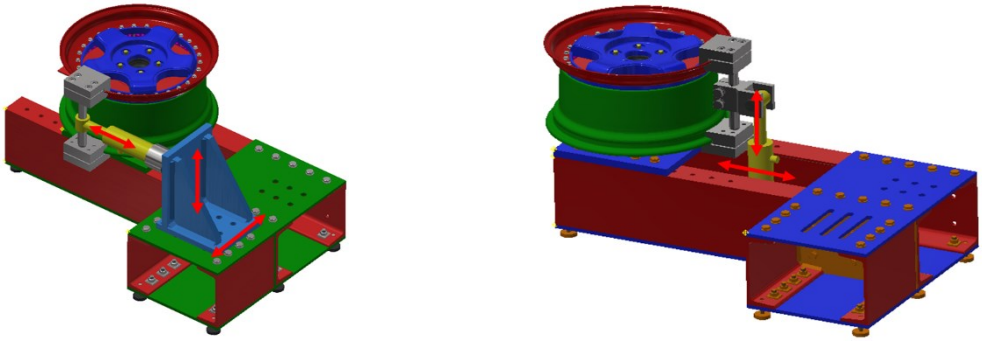

a b

Figure 6.2 – Scheme of the testing of the torque load (a) and axial load (b)

A laser sensor is used to measure the change in the air gap. Due to the limited space, it is not possible to install the sensor directly in the motor. Therefore, for the indirect measurement on the stator, an extension was mounted and the laser sensor was fixed directly on the rotor. The measuring principle described is illustrated in Figure 6.3.

Figure 6.3 – Extension for the measuring of the variation of the air gap

6.1.2. Measurement Results

By the measurement on the prototype of the developed motor on the shaft flange and on the rotor cover, the rotation lock device was attached to provide the symmetrical application of the loads.

The measured courses of force generation were carried out according to the required load characteristic. Since the static load was measured, the load was stopped after reaching the maximum required value. At the same time of loading the change of the air gap was recorded. The results of the measurement for all three required loading cases are shown in Figure 6.4, Figure 6.5 and Figure 6.6.

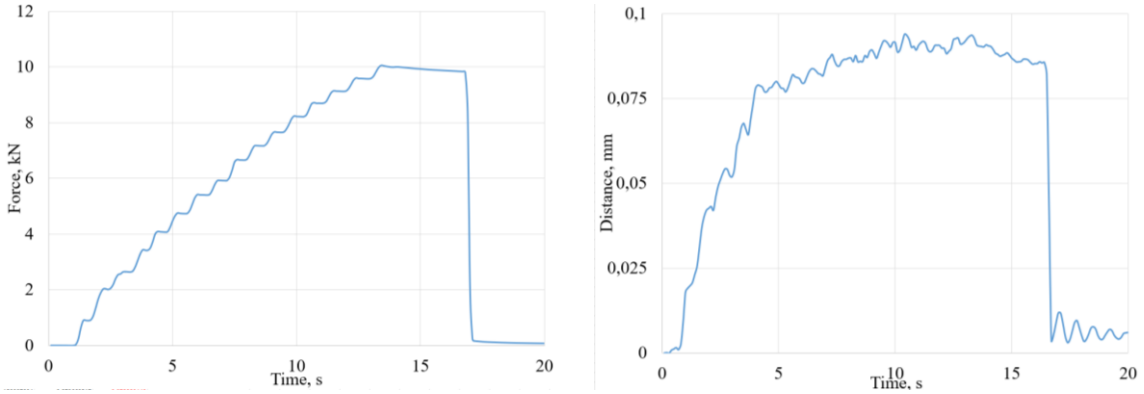

a b

Figure 6.4 – Development of force (a) and corresponding air gap variation under the axial load (b)

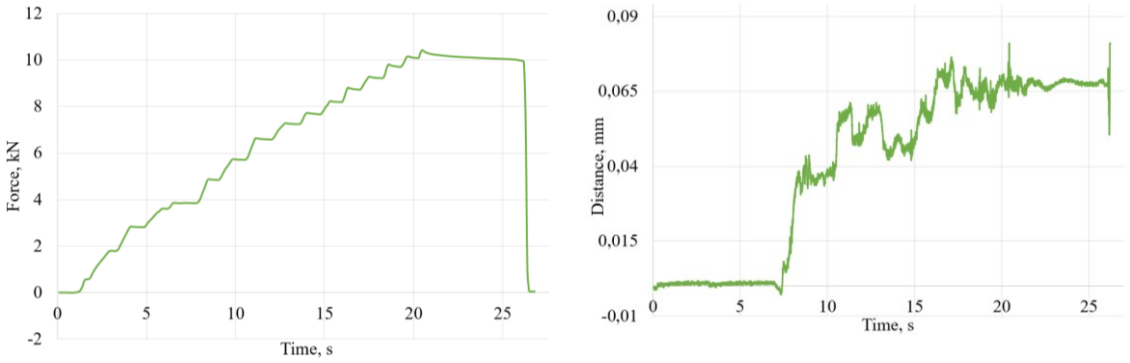

a b

Figure 6.5 – Development of force (a) and corresponding air gap variation under the radial load (b)

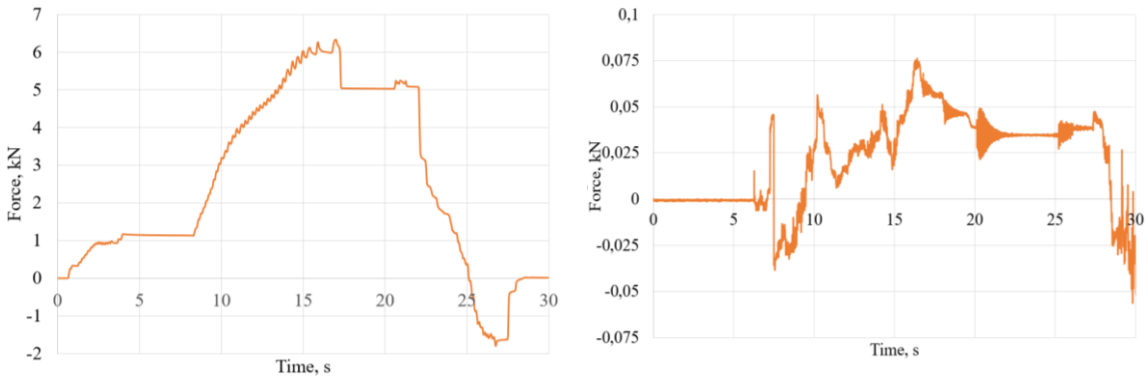

a b

Figure 6.6 – Development of force (a) and corresponding air gap variation under the torque load (b)

The values of the corresponding air gap variations have to be correlated, because the measurement was not directly performed in the air gap. The values shown in Table 6.1 are calculated by eliminating the lever impact of the extension keeping the rule of the proportionality of the triangle.

Type of load	Variation of the air gap, µm	
	Results of the simulation	Results of the measurement
Axial load	70	62
Radial load	83	53
Torque load	58	51

Table 6.1 – Comparison of the simulated and measured values of the air gap variation

The results of the measurement of the air gap variation are 62 µm by axial load, 53 µm by radial load and 51 µm by torque load, which do not strongly align to the simulated results with a maximum error of 36.1% for the radial load case. The reason for this discrepancy can be caused by a higher level of the wheel hub bearing mounted in the prototype.

According to the presented loading cases, it can be seen that the motor is deformed in symmetric relation to the load. Furthermore, it is apparent that the air gap is more sensible in case of axial load. The reason for this is the lower stiffness of the hub bearing in axial direction.

The measured displacements between the stator and rotor under the applied loads are larger than the calculated values. It is caused by the calculation of the motor model with different simplified approaches (e.g. model of the bearing), which lead to the occurrence of this discrepancy.

6.2. Cogging Torque

The validation of the analytical method is carried out using the specially developed test stand, which allows to determine the cogging force. The practical value of validation is that during the development of the test stand, the shortcomings of the motor active parts can be detected in the early stages of the design and it is essential to improve the validation procedure. In addition, this method allows the use of interchangeable parts with standard mounting methods, which allows rapid modification of motor parameters and measurements of various geometric parameters of the motor active parts.

6.2.1. Validation Approach

The test stand has been designed to simultaneously record the values of the detent force depending on the variable air gap between the stator and rotor parts of the motor or an application of different materials to fill the slots. The test stand model was created in the CAD package of Autodesk Inventor and was used to determine the required geometric parameters of the test stand and for implementation in research.

To simplify the design of the test stand, a linear model of the stator and rotor parts was adopted. Thus, the measured value was not the value of cogging torque, but of the cogging force arising and acting along the active parts of the motor. In the following, the part of the rotor refers to the magnets and the part of the stator is a piece of its back iron (see Figure 6.7).

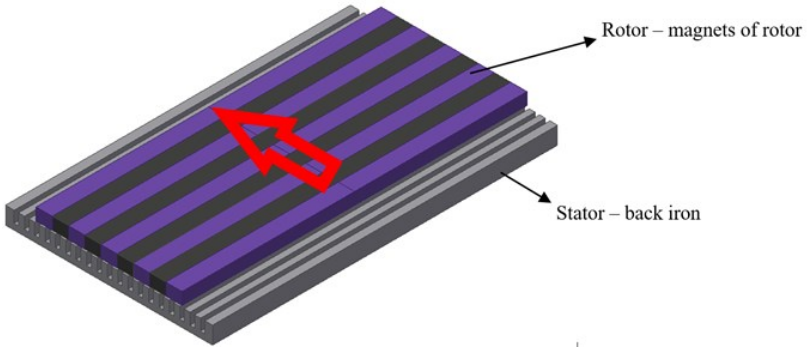

Figure 6.7 – Principle of the test stand with the motor active parts

The test stand has a portal design. In this design, a relative displacement of the rotor relative to the stator takes place by the piece of the back iron. An important condition for an accurate measurement of the cogging force is the deficiency of any effects from the possible slip of the moving parts of the motor and the guided stand parts. The relative motion between motor parts requires a smooth, stable, precise, and linear characteristic. Therefore, the air bearing of the PI-glide RB series linear air bearings was adopted for the test stand implementation, because air bearings are inherently frictionless, they do not exhibit breakaway or running friction, even under their maximum load. A noncontact design between bearing parts means that they do not need maintenance and their accuracy will not degrade over time. For the supply of the compressed air in the air bearing, a standard air preparation module is used.

The relative movement of the parts is realized through an application of stepping motor with threaded spindle from Nanotec company. The stepper motor works by switching the power supply. Furthermore, it was ensured that no ferromagnetic materials were used in the area of the measurement in order to avoid measurement distortions. Due to the limited space of the air bearing for the test stand application, the usage of five poles according to the Halbach arrangement was chosen.

The measurement of cogging force occurs by the loading of the load cell, that is mounted between the spindle of the motor and an extension to the movable platform with the test sample. To evaluate the possible variations of the air gap between active motor parts, the laser sensors are mounted on both sides of the portal.

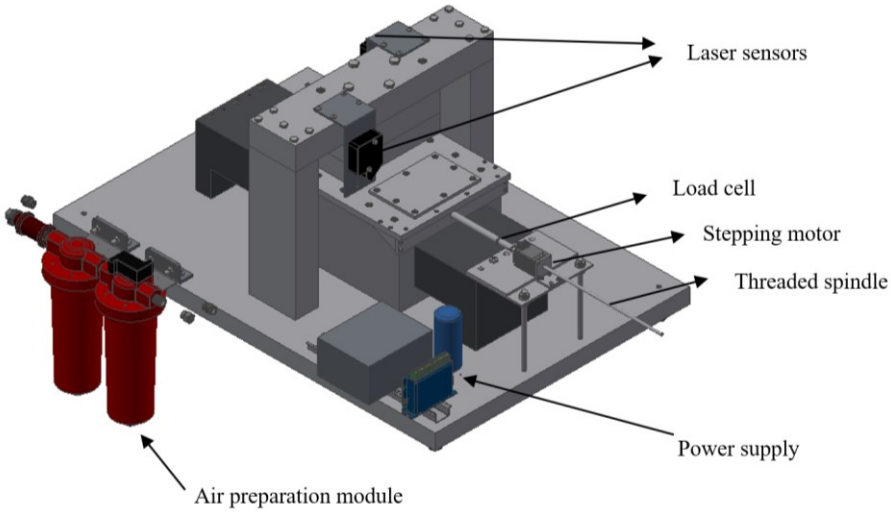

Figure 6.8 – Parts and units of test stand

For the measured value acquisition during an experiment, the software package LabVIEW and the associated NI-DAQmx data acquisition software was used, whereby all installed sensors were evaluated simultaneously. The result of the measurement is the measurement protocol that was generated in LabVIEW.

6.2.2. Measurement Results

Within the first phase of the measurement, the verification of the test stand was realized with an idle condition. During this test, all disturbances caused by the motor were detected. These values are important for further measurements, because the disturbances could be subtracted from measured values of the cogging force.

The measurement investigation was performed sequentially on the same test sample. Thus, the possibility of discrepancies in the results, which may be caused by geometric inaccuracy of the sample itself, was excluded.

The material that was used for the manufacturing of the test sample is NO20 electrical steel, which is equal to the simulated material. The test sample represents a flattened piece of the stator back iron with the same geometry parameters as it was used for the simulation of the cogging effect.

For the manufacturing of the test sample, the sheets were lasered with the same contours as by the back iron, stacked in a special press and pressed together. The test sample was then baked in an oven. The burrs were removed manually before the measurement was performed.

The measurement of the test sample without filling in the slots is shown in Figure 6.9. From the force distribution it can be seen that very high forces of up to 35 N occur at the beginning and at the end of the measurement. The reason for this high force level is obviously clear and can be explained as follows, since the area before and after the magnets is not sufficiently investigated. The simulation model is restricted by the master-slave boundaries, so the magnetic field dispersion is completely missing in the areas before and after the magnets. Therefore, the forces occurring during the entrance and leaving of a test sample in the magnetic field are of high importance. And this is why the simulation results in these areas have a very large difference compared to measured values. Thus, the range of interest by the measurement presents the area which is marked in Figure 6.9 with "A".

For the correct positioning of the filling the copper wires were used, which were planned for the slot winding. For the filling the sandwich (see Figure 5.13, (b) for details) from the in 4.1.2.3 presented material from Kemet was used.

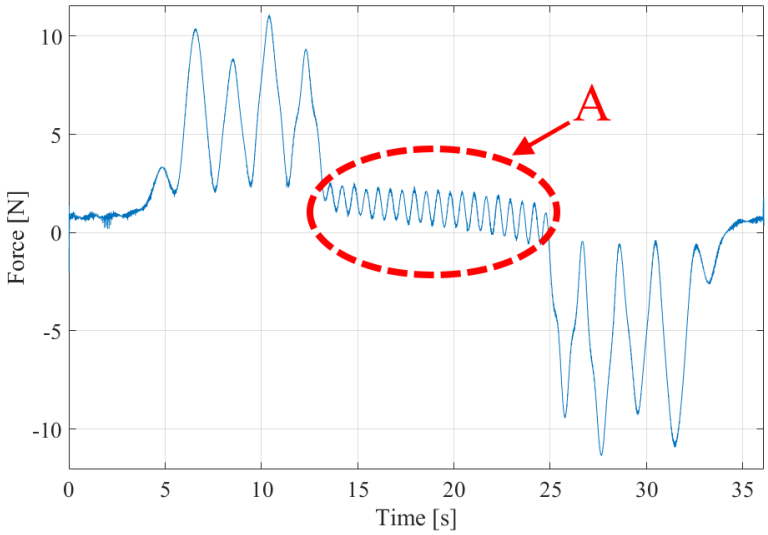

Figure 6.9 – Force distribution during measurement of the test sample without filling

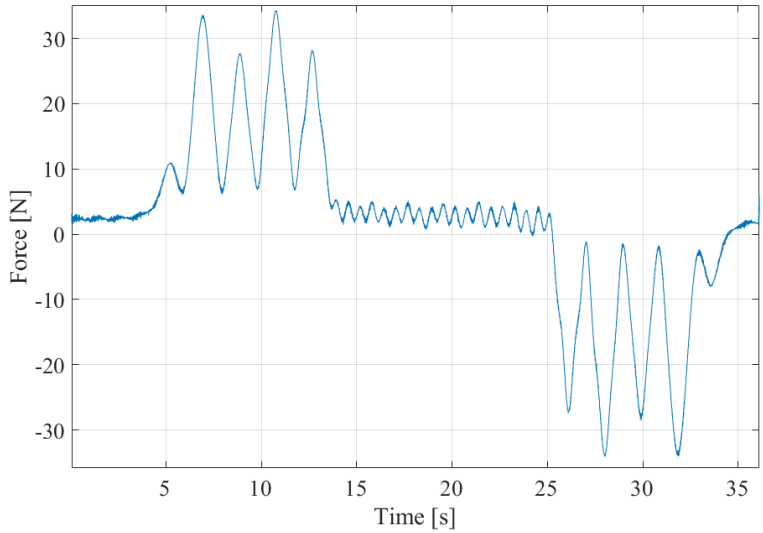

Figure 6.10 – Force distribution during measurement of the test sample with filling

The most intriguing areas of the measurement are presented in Figure 6.11. From the acquisition of the force distribution it is definite that the alternating force variation occurs at the same time as for the test sample with and without a filling of the slot. A further important implication from Figure 6.9, Figure 6.10 and Figure 6.11 is that the filling plays an important role in the reduction of cogging force, as the peak-to-peak values are lower than in a non-filled test sample.

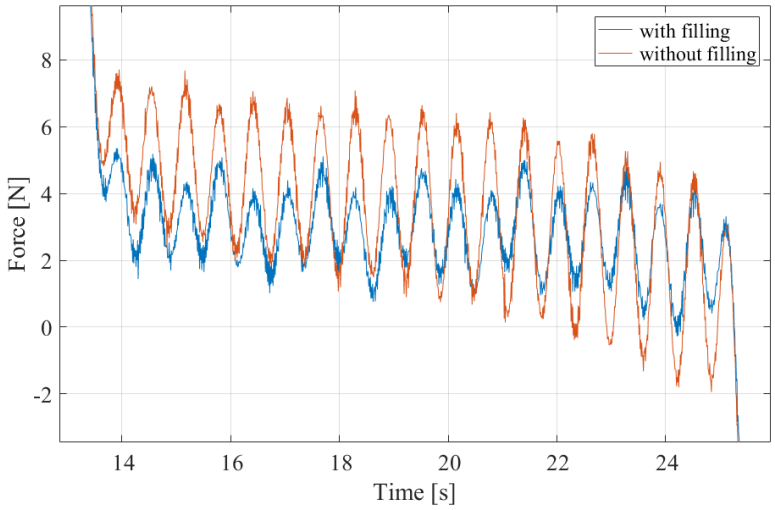

Figure 6.11 – Comparison of the range of measurement of the cogging force associated by the slots

The evaluation of the measurement results was performed by finding the minimum and maximum values over the apparent range of the cogging torque action. The values of interest represent the mean of the peak-to-peak values for both measurement cases – with and without slot filling. The average mean value of the cogging force can be calculated according to the following expression (6.1):

$$F_{cm\_1} = \frac{\sum_{i=0}^{n_{ptp}} F_{cm,i}}{n_{ptp}} \tag{6.1}$$

Where n_{ptp} stands for the number of peak-to-peak amplitudes per measurement and $F_{cm,i}$ is the value of each peak-to-peak amplitude. For both variants of filling it a remarkable effect can be identified, because the mean value of the filled test sample amounts to 3.42 N in comparison with the non-filled test sample of 5.65 N. This demonstrates just how important the filling of the slots is and has a positive effect against cogging force. The mean value of the cogging force can now subsequently be used to calculate the cogging torque.

The cogging torque for the full motor is estimated by the empirical formula given in Equation (6.2):

$$T_{cog} = F_{cm} \cdot r_{st} = F_{cm\_1} \cdot \frac{p_p}{n_{st}} \cdot r_{st} \tag{6.2}$$

The individual cogging torque value of the both test samples eventually resulted in 21.01 Nm for the non-filled test sample and 12.7 Nm for the filled sample. The motor with the filling of the stator has an almost 39.5% lower cogging torque compared to the non-filled variant.

A clear trend in the results of the measurement bears a close resemblance to the simulation proposed in 4.1.2.3. Therefore, the measured values of the cogging torque have certain differences to the simulated model. The reason for this is, firstly, the differences in the geometry and tolerances of the test sample, and secondly, the differences in material properties.

In addition, measurements on the test samples were used to track the position of the moving platform with the signals of the laser sensors. The high stability provided by the air bearing has prevented the keeping of the movable platform and the measured values of the relative displacements are in the range of less than 0.001. These values are comparable or lower than the degree of roughness of the measured surfaces and therefore not considered in the analysis.

6.3. Motor Parameters

In this section an analysis of the motor parameters presented and examined in the previous chapters is carried out. The prototypes and measuring equipment used for the different tests, settings and parameters are presented and discussed. Finally, the results of the validation are shown and the achieved motor characteristics are compared to the simulation results.

6.3.1. Preliminary Motor Measurements

6.3.1.1. Resistance and Inductance

The purpose of measuring the resistance of motor windings is to identify defects such as defective connections, errors in the connection scheme, as well as to clarify the parameters used in the calculation and adjustment of operating modes, regulators and the verification of the calculated motor parameters. Furthermore, the adjustment of the resistance of each phase is necessary for further evaluation of the ohmic losses and induced voltages, for this reason the measurement of resistance was carried out separately for all phases, clamping elements and additional cables. During the measurement of resistance, the temperature of the winding has a particular importance. For this purpose, the measurement of phase resistances is performed with the GOM-805 measuring device, which also provides the temperature compensation function during the measurement. The measured values of the three phase resistances are summarized in Table 6.2.

Phase / Winding	A		B		C	
	Slot	Air gap	Slot	Air gap	Slot	Air gap
Resistance, mΩ	124.4	113.9	123.3	115.1	121.6	115.0
	235.36		240.76		236.81	
% from average	0.95		-1.31		0.34	

Table 6.2 – Phase resistance measurement results

The importance of the inductance measurement is caused by the aspect of control. A very low inductance of the developed motor demands a very high switching frequency for the direct PWM control of the motor. This causes a higher power dissipation and makes it difficult to use standard motor control methods [57]. For this reason, the inductance must be precisely measured for stable development and taken into account in further validation. The inductance measurement was carried out similar to the resistance measurement with the help of the measuring device Sourcetronik ST2827, whereby the phase inductance can be determined by connecting phase and neutral point. The measurement accuracy of the used device is 0.05% with a resolution of 10 MHz and allows to perform very precise measurements. It is therefore conceivable that the measurement was carried out under the hypothesis that the developed motor could be operated at the maximum frequency of 100 kHz, so that the measurement was carried out at this frequency. The results of the inductance measurement are collected in Table 6.3.

Phase / Winding	A		B		C	
	Slot	Air gap	Slot	Air gap	Slot	Air gap
Inductance, µH	21.85	7.79	20.89	7.86	25.96	7.89
	44.42		43.97		44.39	
% from average	-0.36		0.65		-0.29	

Table 6.3 – Phase inductance measurement results

Table 6.2 and Table 6.3 show that the motor has a very balanced winding. The manufacturing of the motor however leads to some notable compromises, which affected the way the windings were wound, the slot openings closed and the phase resistance measured. For example, the design performed in the simulation has one wire with a cross-section of 2.34x1.0 mm and in the prototypes two wires of 1.1x1.0 mm was used. This change was caused by manufacturing difficulties and reduces the cross-section of the wire for slot winding of 6% from the expected value. An additional aspect of the minor variation of the measurement values is that the phase winding was produced in manual and semi-automatic form. However, both measurements demonstrate negligible differences within the range of up to 1.5%, which can be assumed as an insignificant deviation.

6.3.1.2. Disruptive Strength

The reliability and safety of an electrical motor depends on the quality of insulation between its windings and the housing of the electrical motor. Any vehicle is operated under relatively difficult conditions. Vibrations, extreme temperatures, and harsh environmental conditions have a negative impact on the insulation quality and are increasing the risk of insulation damage. Especially high potential hazards present systems in which the in-wheel motor is used. In this case, the phase conductors of the motor are significantly affected by vibrations generated by the suspension. However, failure areas associated with poor insulation quality can occur at any point in any phase.

The well-known detection method for insulation fault location is based on measuring the voltage between the neutral point and the motor body. The potential of the neutral point in case of an insulation fault will change so that an insulation fault can be detected. With this method, insulation faults that may occur in one of the motor phases cannot be localized, but only the presence of an insulation fault can be determined. Therefore, it is a common approach to detect defective winding components using serial search. The windings by this method are disconnected from the DC source and then re-connected one after the other. The appearance of a common insulation fault signal during the connection of the next phase or phase wire indicates a fault.

This approach can only be used in the verification process of a small number of prototypes, as the method has several disadvantages. For example, it cannot be successfully applied if an insulation fault occurs only in a certain stator position relative to the rotor (e.g. radial winding contact of the magnet). Another disadvantage of this approach is that it takes significant time to reassess all phase wires. The test device must be connected every time the wires are connected. If the next phase conductor has proved to be correct, the power is disconnected again and the next phase wire is connected. Hence, it is almost impossible to determine an emergency lead in a reasonable time, especially for air gap windings with a large number of wires.

For the manufactured prototypes, the phases were checked for a short circuit to the stator already during the winding processes. After assembling the motor, the inspection was repeated. The inspection was carried out with a high voltage supply. The stator and phase contact were connected to the DC voltage source. With the requirement according to [41] at a test voltage of 2300 V, no current from the phase may enter the stator. With this method not only the disruptive strength according to the requirement for all phases of the two windings to the stator and against each other was measured, but also all wires under each other were tested. All dielectric strength measurements were completed positively, as shown in Figure 6.12.

Figure 6.12 – Test on disruptive strength

6.3.1.3. Maximum Temperature

Since the ohmic losses make up the largest part of the total power dissipation of the motor and the liquid cooling only runs through the stator, only the stator is examined in the thermal measurements, see Figure 6.13, (a). To heat the winding as evenly as possible, all three phases are connected in parallel and supplied simultaneously. Thus, the winding is used as a heating resistance in order to simulate the power loss for the real operation scenario. This approach assists the validation of the expected values for the developed motor. To determine the power losses and the actual electrical resistance, the input of the current and voltage was measured and

documented. It should be noted that the winding generates much higher ohmic power loss in real operation and that the current is never applied constantly to all phases, but always only for one phase of the air gap and one phase of the slot winding at the same time. During the tests, the coolant constantly passed through the stator at 25°C and at 0.16 kg/s. During the thermal measurements, the current parameter is varied stepwise and changed every 90 s. Because some components of the stator are only thermally resistant to approximately 125°C, this temperature should not be reached.

The temperature measurement was realized with two methods. Firstly, the temperature was measured contact-free with an infrared thermal imaging camera (see Figure 6.13, (b)). This measuring device belongs to the group of color pyrometers. A model of the TI105 from Fluke was used as the thermal imaging camera. The second method of temperature measurement comprises the usage of the PT100 temperature sensors at the winding heads and terminal clamps as feedback for temperature monitoring in the area of the windings and connections. The winding heads are usually warmer than the winding on the stator because the heads overlap each other at some points. In the case of combination winding, there is also an additional factor that the slot winding is already under the air gap winding. This additionally increases the temperature of the winding heads. The test measurements have shown that the warmest spots in comparison to the winding heads are the terminal clamps. For this reason, it makes sense to install temperature sensors at the connections of the various windings to measure the temperature at the stator.

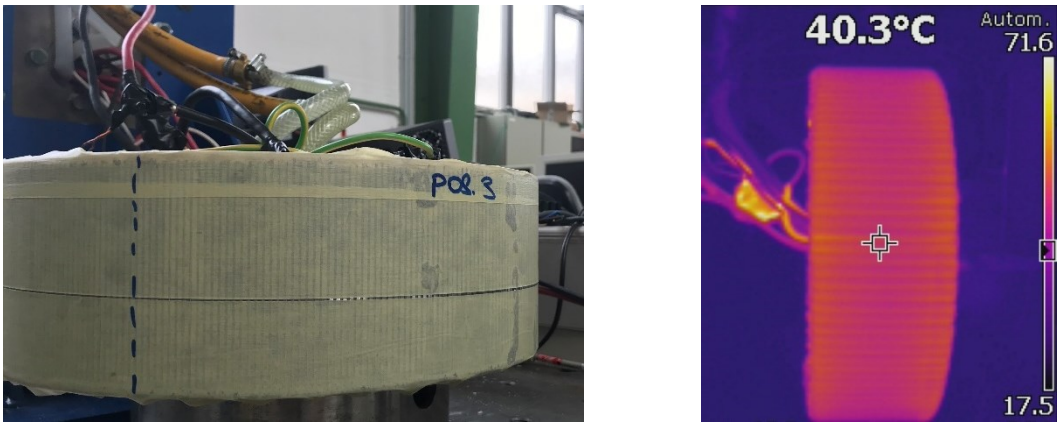

a b

Figure 6.13 – Thermal measurements: a - Test setup for thermal measurement, b - Infrared camera image at a current of 150 A and a cooling water inlet temperature of 25°C

During the thermal measurement of the prototypes some errors were discovered, which led to the incorrect water cooling. The main reason for the incorrect water cooling is assumed to be a manufacturing error during the mounting of the back iron. It is assumed that the geometrical errors of the back iron do not connect the stator and the back iron correctly and can cause air layers up to 0.1 mm thick between the stator sleeve and the back iron. Thus, the contact resistance plays a more important role than the actual thermal resistance of the material, and this parameter depends on the motor layout and manufacturing technology. Due to this problem, measurements are always carried out at the hottest spot. As a result, the maximum current intensity for the three phases must not be exceeded. At a cooling water inlet temperature of 25°C, the maximum current of 240 A was achieved. The increase of the measured temperature at the hotspot in the winding on the stator surface and on the terminal clamp, as well as the varied parameters are shown in Figure 6.14.

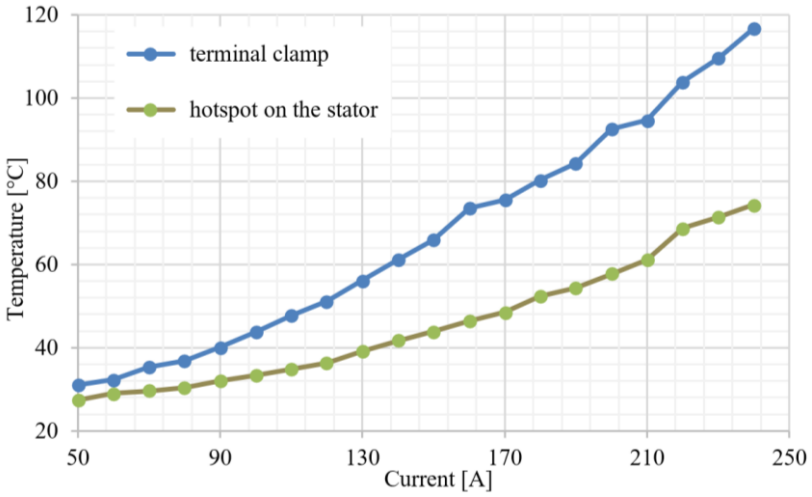

Figure 6.14 – Development of the temperature and corresponding current

The warmest part of the motor was measured with the temperature sensor mounted on the terminal clamp. The higher thermal load on the terminal clamps is mainly caused by the prototype phase ends, which are partly standing around in the air and are not connected to the cooling surfaces of the stator. The temperature characteristics are generally homogeneous over the surface of the stator, but the underside of the stator shows a delayed heating process, which could be attributed to a gap between the aluminum and back iron. However, the cooling surface of the stator leads, with further interpolation, to the conclusion that the cooling system can withstand the most difficult operating conditions of the developed motor in terms of heat generation. However, the measurement has shown that the cooling system is working correctly and the heat dissipation corresponds to the expected simulation results.

6.3.1.4. Mechanical Losses

To separate the losses with mechanical origin, the mechanical losses were measured. Here it was ensured that no iron losses were implemented in the test. In order to determine the losses of the mechanical components, the electrically active components of the prototypes were completely or partially removed.

For the measurement of the mechanical losses, a special measuring set-up was assembled. Figure 6.15 shows the test set-up used to determine the bearing friction. A DC motor is used to drive the in-wheel motor. The DC motor is connected to the in-wheel motor by two torsionally stiff compensating couplings and a torque measurement shaft. The couplings ensure a vibration-free operation of the torque measurement shaft. A light-reflecting strip on the coupling enables the measurement of the rotational speed using a digital speedometer. More detailed description regarding, for example, the measurements on the test set-up are presented in [189].

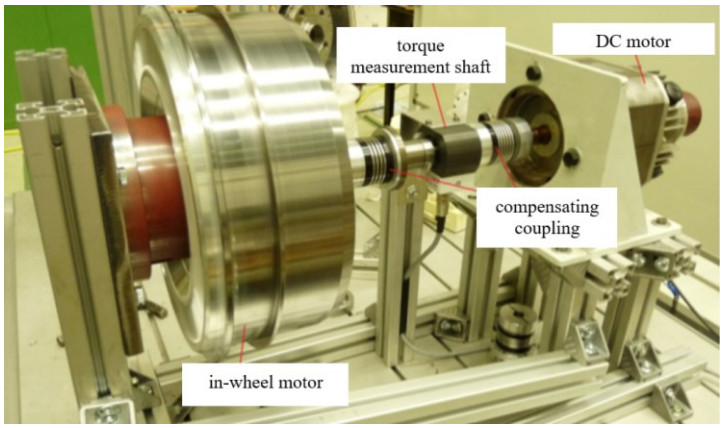

Figure 6.15 – Set-up for the measurement of mechanical losses [189]

According to the measurement setup, the losses of the wheel hub bearing were measured separately in the first step. The run-in and non-run-in curve in Figure 6.16 represents the dependency of the frictional torque from the rotational speed.

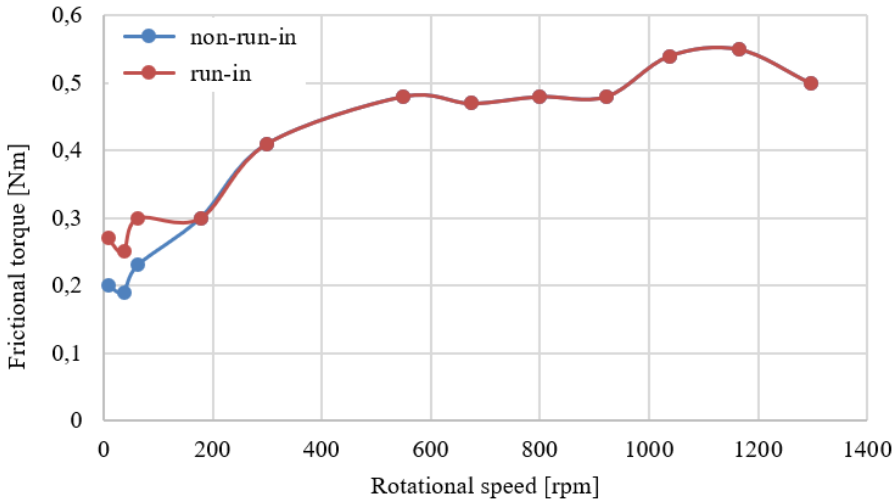

Figure 6.16 – Frictional torque vs. rotational speed for the wheel hub bearing with and without run-in

For design reasons, the measurement cannot be carried out separately for additional bearing and seal. Therefore, in the second step of the measurement, the additional bearing and the seal were measured together. Figure 6.17 summarizes the results of the measurement of mechanical losses for the developed motor.

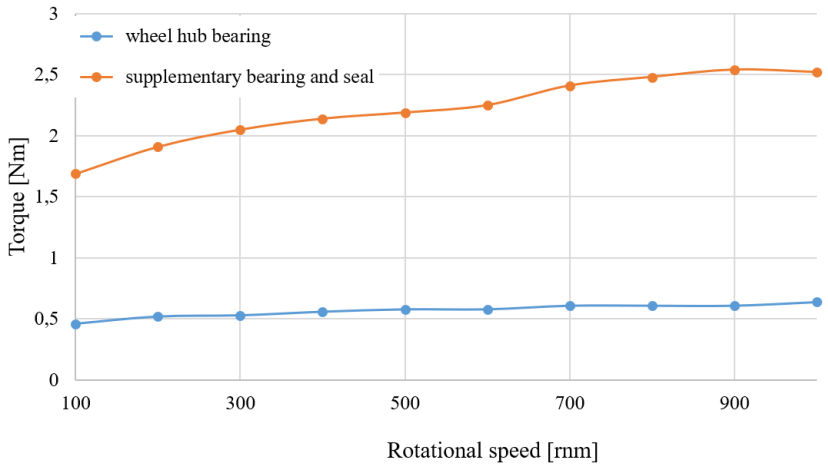

Figure 6.17 – Frictional torque of the individual components

The measurements have shown that the frictional torque of bearings and seal is significantly dependent on the speed. The measured values correspond to the manufacturer's specifications. From the measurement with and without run-in, it has become clear that the other influences not taken into account also have the temperatures of the motor parts. Therefore, the friction of the motor bearings must always be assessed in connection with the operating conditions.

6.3.2. Test Stand and Approach

For the basic investigations of the behavior of the manufactured prototypes, the motor test stand WEKA was used (see Figure 6.18).

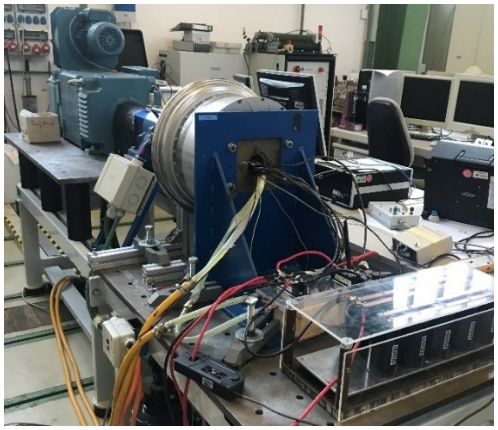

Figure 6.18 – In-wheel motor without the entire wheel (only outer ring) installed on the test stand

The test stand equipment for the motor layout validation includes DC motor, torque sensor, cardan shaft, incremental encoder, prototype and holders. The load machine of the test stand is a DC motor, which keeps the speed of the prototype motor at constant values. The in-wheel motor and the DC motor are coupled by a torque sensor DR 2212 to measure the torque. The measurement principle of the torque sensor is based on strain gauges. If a torque is applied, the shaft is subjected to torsion and thus the strain gauges are deformed. Strain gauges change their electrical resistance even with small deformation. Since in this electrical path the voltage from the supply to the display unit changes only as a function of the strain gauge resistance, a measuring voltage proportional to the torque results at the display unit. The torque sensor has a measuring range of ±500 Nm, whereby the maximum expected measuring error is 0.5 Nm.

A cardan shaft connects the torque sensor to the prototype motor via another shaft. The acquisition of the rotational speed of the motor is measured with an integrated incremental encoder of the type A02H, which can also be used to determine the relative position in addition to the angular velocity. For stabilization there is a bracket mounted to the encoder. The speed can be externally monitored with a PC by using the software LabView.

The motor is attached to a console by a flange connection and fixed with four bolts. The torque is transferred from the wheel to the prototype as it was conceptualized through the decoupling element mounted on the prototype and outer ring of the wheel. Cables for the signals of the sensors are led out of the flange connection and the phase and star point connection cables. The prototype still needs an external cooling water circuit. This requirement was met with an external, temperature-controlled cooling system from Lauda T7000.

The motor is loaded behind the holder through a three-phase bridge VS-130MT of Vishay. An oscilloscope with a differential probe and a current clamp is provided to measure the electrical phase parameters.

Therefore, all the relevant equipment is available for measuring the basic characteristic diagrams of the prototype. The assembled prototypes are first subjected to the basic functional tests of the in-wheel motor. The further reconstruction of the expected power and torque values during the operation were carried out at the test stand. For initial operation and testing, the prototypes were tested without power electronics.

6.3.2.1. B-Field

The magnetic field distribution plays an important role in defining the working conditions in the developed motor, and directly influences the torque performance of the motor. To this end, it is decisive to outline the experimental results to validate the numerical models.

For this experiment, Chen-Yang CYSJ302C linear Hall effect sensors were used to measure the magnetic field strength. The Hall effect sensors were glued on the stator cylinder surface. Since the mechanical gap between the magnets and the winding is only 0.5 mm with applicated air gap winding, measurements were taken on a stator that was not equipped with an air gap winding. The sensors were positioned on the different places of the stator surface: on the teeth, on the slot inlay or somewhere between the teeth and slot inlay. No contact relation between the pins of the sensors and surface of the stator was provided by adhesive foil with Kapton as an insulating layer. After the sensors are connected and checked, the prototype can be assembled. The

measurement procedure assumes that the prototype is mounted on a test stand. After setting a constant rotational speed on the load machine, the measurement can be carried out. The sensor output voltage is measured with an oscilloscope and differential probe. The used Hall effect sensor has a sensitivity of 50 mV per 0.055 T. The experimentational set-up of the measurement is shown in Figure 6.19.

Figure 6.19 – Experimentational set-up for the B-field measurement

Due to the almost identical air gap size and sensor height, two of the sensors were damaged after the prototype was assembled. The remaining four sensors showed a pair of very similar signals, so it is reasonable to use only two signals from the sensors by the evaluation. Figure 6.20 shows evaluated B-field waveforms observed for the manufactured prototype respectively.

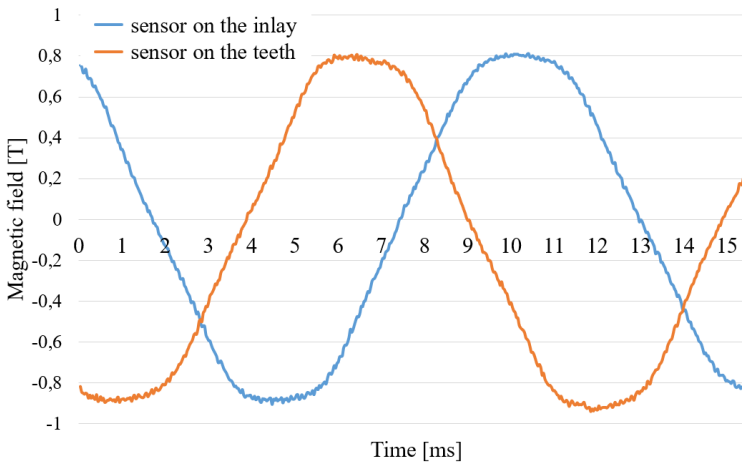

Figure 6.20 – Graphs of the motor B-field waveforms

The results of the experiments are consistent with the results obtained by numerical modeling in the Ansys Maxwell environment. The difference between the results of the numerical modeling and the calculation is about 2-4% depending on the location of the sensor. The possible causes for the differences of the results could be the varying distances between the magnets due to the manufacturing tolerances or non-homogenic material properties.

6.3.2.2. Non-load Test

During the non-load test, the proper interaction between the motor parts can be controlled. The correct operation of the motor will confirm the operation of individual parts, the condition of the friction surfaces, and the right connections of the windings.

In the generator non-load measurements, the induced voltages at the motor clamps were determined using a neutral point in dependence on the rotational speed. In this measurement, both the magnitude and the waveform for the individual phases for each speed presents a useful data. The measurement was made when the load machine was operated in engine mode and the prototype was tested in generator mode. During the measurement, the speed controller of the test stand was activated. Therefore, the control unit of the test stand allows a comfortable starting of the required speed. The setpoint value for the speed was entered over the

potentiometer. The measurement was undertaken for each phase between the terminal and start point for the speed vector of 100 rpm to 1000 rpm in 100 rpm steps.

Results of the measured values are presented in Figure 6.21. According to Figure 6.21, the full motor speed vector and the corresponding induced voltages of the prototype has a linear relationship.

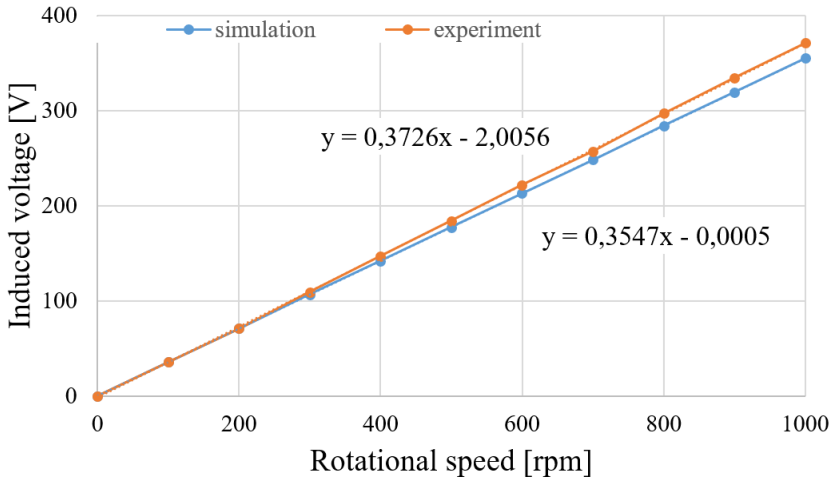

Figure 6.21 – Induced voltages vs. rotational speed

The results show that the amplitudes of the induced voltages in general correspond to the simulated results. After the comparison of the measured values, it was detected that the difference between the measurement on the prototype and the simulation is a maximum of 4.7%. The higher value of the induced voltage means that in the speed range of the motor there is a lower current requirement for the required torque.

As an example, the waveforms of induced back-EMFs at 100 rpm of all three phases were measured with subsequent evaluation in LabVIEW (Figure 6.22). The digital signal of the incremental encoder was used for this purpose. According to the method presented by Schmidt [150], this approach reduces the amount of the data and guarantees an angle-related measurement of the back-EMF for every rotation without any discretization error.

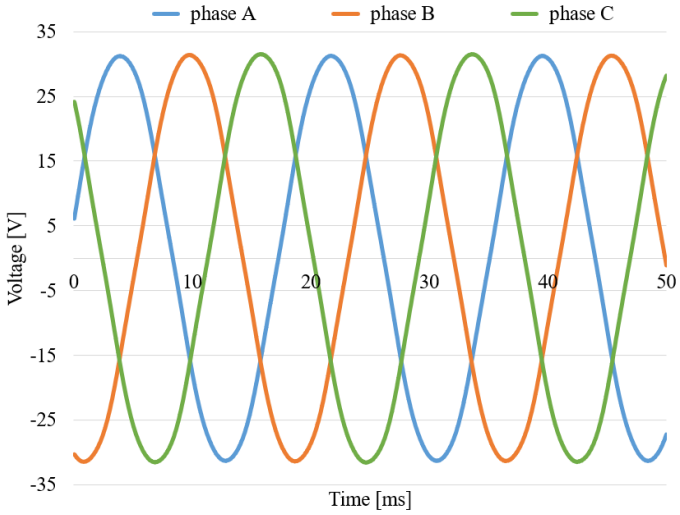

Figure 6.22 – Measured waveforms of induced voltages at 100 rpm

The results of the measured waveforms on the prototype motor appear to be quite close to the sinusoidal.

The reason for the difference between the measurement on the prototype and the simulation can be reasonably assumed with the configuration was carried out using 2D-FEM simulation. Therefore, the influence of 3D-effects on a prototype is not negligible. Another possible reason for the differences in induced voltages can be an asymmetric shape of the rotor or stator. The manufacturing tolerances could be reflected by the asymmetry

in the run-out of the rotor or stator. Due to the concentricity, a different voltage magnitude can be induced in the phases. Manufacturing tolerances of the wires also have a direct influence and should not be excluded.

The last test that can be conducted on the test stand in non-load measurement is the experimental result of the cogging torque value. As it can be seen from the measurement sample in Figure 6.23, the measured value of the cogging effect is non-smoothed and vice versa very jagged. It can be noticed, that every peak-to-peak part of the measured signal corresponds to the area of one filled slot.

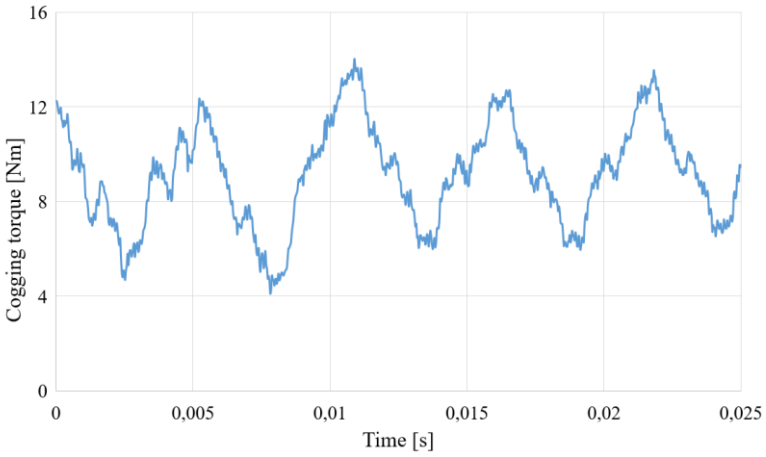

Figure 6.23 – Cogging torque versus relative rotor position (sample from the measurement)

An absolute result of the measurement is a cogging torque value with a maximum of 9.8 Nm. The experimental value for the cogging torque differs from the value previously measured on the test stand by 22.8%. This significant difference between the two measurements can largely be explained by the fact that the measurements on the full prototype are more precise, since the number of simultaneously measured filled slots is the highest possible. However, the measured value of the cogging torque is 53.3% less than the original calculated cogging torque value.

The final conclusion considering the cogging torque is that the cogging torque can be further improved to be under the required value of the motor and the usage of the flux suppressor as a filling of the slots provides a reduction of the cogging torque value as expected. The probable explanation for the difference between the measured results and simulation results is inequality in the geometrical accuracy and in the material configuration.

6.3.2.3. Load Measurements and Efficiency

The most effective test method for an electric motor is the one that is as close as possible to the operation condition. In other words, a full overview of the performance of an electric motor can be provided by testing the motor under load. For this reason, to measure the motor it is required to run the motor under load and measure its power usage.

The measurement was performed with the help of the methodology presented in [150]. The ends of the phases were supplied by the rectifier, which itself was supplied by the power supply unit. The power supply by this method is used in a four-quadrant operation and has the function as a pure current sink. Thus, for one rotational speed, different load points can be inspected using the current sink. The power supply for the motor was provided by two Regatron power supply units. The use of the two power supply units is conditioned by the necessity to cover the voltage and current level with the help of two power supply units. The test stand allows to measure the prototype up to a maximum torque of 300 Nm. The maximum torque was limited because the load machine which was used to measure the prototype was not able to provide the required 600 Nm nominal torque. During the measurement, the values of the average torque, the rotational speed, the phase current, and the voltage at the rectifier are obtained. With the help of these measured variables, it is possible to determine a complete characteristic diagram of the prototype. The selected resolution of rotational speed and current variation enables to determine the values with the requested accuracy.

The test plan included the stationary measurement of the speed-torque characteristic of the motor, which was tested in selected points. To guarantee a high level of accuracy, the current was varied up to 50 A in different steps (5-10 A). The load current reached a maximum value of 50 A, which is related to the thermal instability of the terminal clamp connections. The speed was varied from 100 rpm to 900 rpm in 100 rpm increments. It was not possible to run the power over the full speed/torque range due to the voltage and current limits of the power supply units. The voltage was measured with a differential probe and current using a current clamp. The measured values were monitored using a LeCroy digital storage oscilloscope. Figure 6.24 illustrates a range of measured torque versus phase current for the simulated and experimental variant.

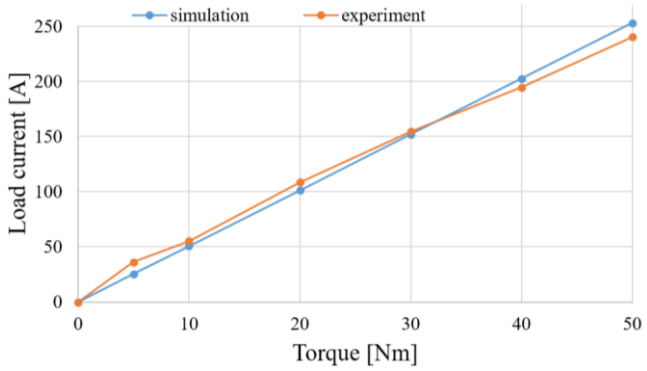

Figure 6.24 – Graph of results of the experiment and simulation of motor torque vs. phase current

The maximum torque produced by the prototype motor was 240 Nm which is 5.1% less compared to the simulated value of the torque. Thus, an expected motor constant value is 5.06 Nm/A will not be achieved and an experimentally defined value is dissimilar with a difference of 7.1% to one simulated earlier. Thus, this value can be extrapolated by the availability of a more powerful power supply and energy source with higher current/voltage value.

The measured values from the experiment allow to determine the efficiency. Here, the input power is measured by measuring the current and voltage at the power supply. Concurrently to this measurement, the resulting mechanical power is captured using a torque measurement shaft and an encoder. The temperatures in the motor are measured by temperature sensors installed in different critical places of the stator. The measured efficiency map for a prototype motor is shown in Figure 6.25.

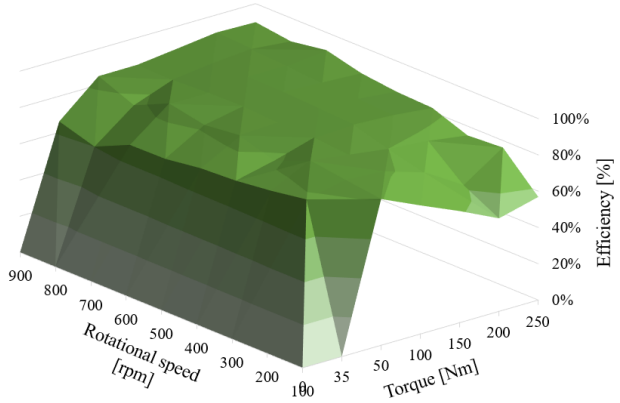

Figure 6.25 – Efficiency map for a prototype motor

In the course of the measurement it was detected that the measured temperatures in the area of the terminal clamp are higher than expected, therefore the value of the maximum phase current was limited. Figure 6.25 shows that the highest efficiency was achieved with 92.8% in the full load range at a high torque of 125 Nm. It can be noticed that the reached efficiency at high speeds (>600 rpm) is 89-90%. The reason for the lower efficiency in this speed range are the load-independent losses that were dominant here due to the lower torque level.

As it can be seen from Figure 6.25 and Figure 6.24, the developed motor can fulfill the required characteristics that were specified in Chapter 3. Unfortunately, the most commonly used speed ranges of vehicles are indicated as high torque and are in the middle range of speed. This means that the developed motor will be operated in lower efficiency regions.

Tests have confirmed the motor's high energy performance. The motor's efficiency of 92.8% was measured in the generator mode under load. However, the measurements also identified a specific heat dissipation problem of the motor. The "paradox" of the situation in this case is that the developed motor has the maximum permissible temperatures of the terminal clamps with a rather high efficiency. The reason for this situation is the concentration of the main part of losses in the stator and a lack of coolant surface development of in a particular technical design of a prototype – especially in the design of terminal clamps. In the future, possible technical solutions to increase the cooling surface and reduce overheating of the motor terminal clamps should be considered more precisely for the developed motor.

6.3.3. Validation of the Weight, Torque and Power

The total weight is a quality feature of the light motor in particular. As it was mentioned above, the weight is also relevant for the mechanical behavior of the motor. The initial scientific objectives of this work focused on the fulfilment of an extremely high torque and power density of the motor with low weight. The power and torque density present a corresponding relation between the nominal value of power or torque to the weight of the motor.

Within the first step, it is necessary to analyze the total weights of the different units and material variants of the developed motor. The other parameters are the generated nominal torque value and the nominal power of the developed motor variant. Using the results of the weighing of the real prototypes and data from the CAD models, Table 6.4 was completed to compare the weights and designs for the developed motor parts using lightweight technologies.

Motor assembly / Variant	Weights, kg				
	Standard materials	Stator: Al-Mg	Rotor: Al foam+CFPR	Rotor: full Al foam	Light weight variant
Wheel hub bearing	2.715	2.715	2.715	2.715	2.715
Rotor	3.858	-	3.262	2.850	2.850
Additional parts of the rotor	3.236	3.236	3.236	3.236	3.236
Stator body	4.100	3.450	-	-	3.450
Additional parts of the stator	6.319	6.319	6.319	6.319	6.919
Total weight, kg	**20.228**				**18.570**

Table 6.4 – Weights and designs for the motor parts using lightweight technologies

According to the results for lightweight motor parts showed in Table 6.4, the weight of a variant made of standard material is 20.228 kg. This is the biggest value of weight caused by using standard materials. The lowest value of weight delivers the variant in which the full aluminium foam rotor with hybrid stator of Al-Mg is combined. The weight of the lightest motor variant is 8% lighter resulting from the use of light weight techniques. Therefore, the torque and power density can be calculated (see Table 6.5).

Ratio / Variant	Standard materials	Lightweight hybrid
Torque / weight	27.93 Nm/kg	30.42 Nm/kg
Power / weight	3.46 kW/kg	3.77 kW/kg

Table 6.5 – Torque and power densities

As it was expected, the presented results of torque and power densities demonstrate more satisfactory values for the variant made with the application of lightweight techniques. The relatively small difference of 8.9% between standard material and lightweight variant is also contingent on the fact, that the in Table 6.4 and Table 6.5 presented weights are referring to the motor inactive parts like housing (rotor) or main body (stator). The weight of the motor active parts like magnets or back iron were also reduced or was completely neglected.

6.4. Conclusion to the Chapter

The chapter started with the mechanical test on the variation of the air gap during the required loads on the in-wheel motor. For this reason, the special test stand was developed that allows to reconstruct the loads acting on the in-wheel motor during its operation in the vehicle. The measurement results show clear advantages when using the developed topology and decoupling element with only 0.062 mm or 12.4% of the air gap change at the maximum load. This provides stability for the essential motor parameters such as the consistency of the torque, which also affects the smoothness of the vehicle. Therefore, an experimentally determined air gap changing correlates well with the theoretical approximations calculated in Chapter 4.

The next important motor operation parameter is the cogging torque, which was measured on the specially developed test stand. An integration of the non-friction air bearing in the test stand enabled precise measurements without any friction influence. As a result of the experimental studies, a data on the values of cogging torque for a test sample were obtained. The results of the measurements correlate very strongly with the simulation, which is presumably due to the differences in the geometry and tolerances of the test sample or caused by the differences in material properties of the test samples.

Preliminary measurements of the phase parameters showed negligible differences in the range of up to 1.5%, which can be noticed as an insignificant deviation. These differences are caused by the technological challenges in the area of the slot winding. Nevertheless, the measured parameters are acceptable considering the manual and semi-automatic methods of the motor windings manufacturing. The next parameter that was examined is the disruptive strength, whose maximum value according to [41] was successfully passed. The continuous power rating of a motor is generally limited by the rate of heat building due to a non-efficient operation and increase of the heat dissipation. For this reason, the thermal test was conducted. Results of the test are also applicable for a further load simulation, because several places of the motor still do not have an optimal cooling. However, the measurement has shown that the cooling system is functioning correctly and the heat dissipation is in accordance with the expected simulation results.

Subsequently, the measurement of the mechanical losses is presented. The measured values correspond to the manufacturer's specifications. The results show that the mechanical components as an undesirable side effect cause the losses, which are much lower than the ohmic losses, though the effect on the motor losses is apparent. The mechanical losses, which vary over time, must therefore be taken into account at the design stage of the motor. Otherwise it can lead to the failure of important motor components such as the seal and bearing system.

The absence of complete electronics with the required parameters made it impossible to carry out a full range of experiments. For this reason, non-load tests were performed in generator mode. In the course of experimental studies, the calculated values of electric motor parameters were fully confirmed, the dependence of induced voltage vs. rotational speed, and the expected value of the magnetic field in the air gap was determined. The induced voltage described in this chapter shows differences of 4.7% compared to the design.

Further measurements of the cogging torque were also carried out, and the results showed a higher reduction in the cogging torque. This phenomenon can be explained by the fact that the prototype has a much larger number of filled slots, which results in a more homogeneous torque distribution and less field dispersion,

compared to the results obtained on a relatively short sample on the test stand for the cogging torque measurement.

With the measurement on the test stand with load, the functional verification of the prototype of the developed motor was performed. In order to determine the torque-speed characteristic curve, motor operating data for different speeds and with different motor loadings on the test stand were obtained. However, despite the differences in motor geometry, the tested motor prototype was found to have very similar speed and torque characteristics. For load measurements, the efficiency was determined directly from the impressed power and the mechanical output power. Based on this data, the efficiency was determined, the maximum of which was 92.8% for the developed prototype. The measurements on the test stand have shown a very good accordance of the results obtained in previous chapters. In some areas, there are some differences between the simulated and measured values. Nevertheless, the deviations are relatively small when the tolerances of the manufacturing process evaluate different components.

The final result of the chapter was firstly the weights of motor prototypes and secondly the values of torque and power densities. The lightweight construction technologies used to realize the designed in-wheel motor make it possible to achieve the goal and reduce the total weight of the in-wheel motor to up to 18.57 kg. This know-how enables to reach the 30.42 Nm/kg torque density and the 3.77 kW/kg power density on the measured prototype.

The functional verification of the developed motor concept was tested exemplarily with the prototypes. Thus, the methodology presented in this thesis was successfully validated. The results presented in this chapter confirm the concept of this research.

7. Summary

To provide a clear structure of carried out research, this dissertation is divided into seven chapters which are summarized as follows.

Chapter 1 considered the reasons and progression of the reactions of climate protection and presents a short history of the development of the electrified vehicle.

In Chapter 2 the general drive techniques of the electric vehicle achieved at the present moment with a special interest on the in-wheel motor is described. A brief overview of the different types of electrical machines and possibilities of their integration of existing electrical power train concepts are described here, with reference to the possible solutions using wheel motors. Additional consideration to principal characteristics of the in-wheel motor and the boundary conditions of the application are discussed and the relevant requirements are derived. To analyze existing in-wheel motor concepts, a comparison with regard to the gravimetric power and torque densities and their presentation date are evaluated. Based on the outlined state of the art, the chapter closes with a problem statement and objective of this work.

In Chapter 3, the requirements on the in-wheel motors are determined. The fundamental requirements for the development include the step-by-step analysis of requirements for the vehicle, requirements of the topology of the in-wheel motor, requirements on the elastic coupling, requirements for the electric motor and requirements on the motor weight. The results of received requirements present a basis for further development.

Chapter 4 is devoted to the development of the in-wheel motor. The development strategy is segmented between an electrical, cooling and mechanical approach based on the geometrical restrictions of the motor and requested motor behavior.

Chapter 5 concentrates on the application of the specific design and focuses on the special factors of manufacturing and determination of the manufacturing of the full-scale motor in order to further validate the findings of this research. The realized technologies, which had been used as a basis for the manufacturing concepts, have proven to be technologically successful.

Chapter 6 includes a validation of the developed in-wheel motor as well as the impact of boundary conditions and assumptions determined in this work. For this reason, the prototypes were metrologically evaluated and the measured properties were analyzed. The prototypes were measured in special test stands regarding their electrical, magnetic and mechanical properties.

Summarizing Chapter 7, the aim of the work was to develop innovative solutions for electrified powertrains in order to further increase the attractiveness and spread of electric vehicles. Technological advances and increased energy efficiency were achieved by optimizing the main component of the drivetrain – the in-wheel motor. Important objectives were defined such as mass reduction, compact designs and reduced material use. Further great potential was found in the structural optimization and the new motor architecture, whereby the requirement for a compact design was successfully implemented. Due to the relatively small iron content in the stator, the motor losses are accordingly reduced, which contributes to a very high degree of efficiency and thus meets the demands for an increased energy efficiency and range. It can be added that in this dissertation a considerable technological progress was worked out in detail and as a whole, which, through a significant increase in competitiveness, provides the basis for the development of new technologies in the field of the electric drive train.

As one of the final statements in reference to the development of the concept of a novel type of winding, the technical advantages of the lightweight motor were significantly improved. In addition to its low weight, a major advantage of the motor in terms of compactness is the reduction in the dimensions of the stator. For example, the motor has a comparatively large interior space and could thus contain various components (e.g. control system). Based on the experience and results of the application steps, the respective prototypes were built and assembled. Thus, the practical results of the dissertation are prototypically manufactured and tested in-wheel motors with reduced weight, a more compact design and performance data that meet the requirements

of the market. The prototypes were used to test the theoretically proposed solutions. According to the requirements on the motor, a series of the test was carried out. The results of the mechanical tests showed clear advantages in the application of the developed topology and decoupling element with only 0.062 mm or 12.4% of the air gap at the maximal load. This provides stability of the essential motor parameter such as the consistency of the torque, which also affects the smoothness of the vehicle. An electro-mechanical parameter for the motor, the cogging torque, was successfully reduced with the help of special material and geometric adjusting. Based on the data from the measurements of the prototypes, the maximum efficiency was determined to be 92.8%. As the final result of the work, the used lightweight technologies for the realization of the concepted in-wheel motor were evaluated. An achievable value of torque/weight ratio reaches 30.42 Nm/kg and the value of power/weight ratio is 3.77 kW/kg. Thus, the methodology presented in this thesis was successfully validated. The overall system of the in-wheel motor works according to the expected results of the calculations and simulations on which the concept was based.

Looking ahead, a benchmark analysis with world-renowned and competing in-wheel motors has shown, that the developed motor technology can replace existing in-wheel solutions and traditional drive systems in the automotive sector in the future.

Appendix A

Parameters of Modern-Line single section and modular wheel

Außenring = Tiefbett outer rim=dish		1,5" = 38mm		2" = 51mm		2,5" = 63,5mm		3" = 76mm		3,5" = 89mm	
7,5J x 16H2	M2	ET 27	IR 5,5"								
8J x 16H2	M2	ET 34	IR 6"	ET 21	IR 5,5"						
8,5J x 16H2	M2	ET 40	IR 6,5"	ET 27	IR 6"	ET 15	IR 5,5"				
9J x 16H2	M2			ET 34	IR 6,5"	ET 21	IR 6"	ET 08	IR 5,5"		
9,5J x 16H2	M2			ET 40	IR 7"	ET 27	IR 6,5"	ET 15	IR 6"	ET 02	IR 5,5"
10J x 16H2	M2					ET 34	IR 7"	ET 21	IR 6,5"	ET 08	IR 6"
10,5J x 16H2	M2									ET 15	IR 6,5"

Appendix B

Parameters of Goodyear Vector 4 Seasons tire

Parameter	Value
Tire width	205 mm
Aspect ratio	60%
Wheel diameter	16”
Load-capacity index	92 (max 630 kg)
Speed index	H (max speed 210 km/h)

Appendix C

Parameters of N45SH material

	Characteristic	Units	min.	nominal	max.
Magnetic Properties	**Br**, Residual Induction	Gauss	13,200	13,500	13,800
		mT	1320	1350	1380
	H_{cB}, Coercivity	Oersteds	12,300	12,750	13,200
		kA/m	979	1015	1050
	H_{cJ}, Intrinsic Coercivity	Oersteds	20,000		
		kA/m	1,592		
	BHmax, Maximum Energy Product	MGOe	43	45	46
		kJ/m^3	342	354	366

	Characteristic	Units	C //	C ⊥
Thermal Properties	Reversible Temperature Coefficients (1)			
	of Induction, α(Br)	%/ºC	-0.120	
	of Coercivity, α(Hcj)	%/ºC	-0.535	
	Coefficient of Thermal Expansion (2)	ΔL/L per ºCx10^{-6}	7.5	-0.1
	Thermal Conductivity	W / (m • K)	7.6	
	Specific Heat (3)	J / (kg • K)	460	
	Curie Temperature, Tc	ºC	310	
Other Properties	Flexural Strength	psi	41,300	
		MPa	285	
	Density	g/cm^3	7.5	
	Hardness, Vickers	Hv	620	
	Electrical Resistivity, ρ	μΩ • cm	180	

Appendix D

Properties of the NO20 electrical steel

Werkstoffdatenblatt Elektroband — **NO20-15** nach EN 10303
Material data sheet Electrical steel strip — *NO20-15 acc. EN 10303*

Magnetische Werte
Magnetic values

	P 1,0$_{50Hz}$ [W/kg]	P 1,5$_{50Hz}$ [W/kg]	P 1,0$_{400Hz}$ [W/kg]	P 1,0$_{700Hz}$ [W/kg]	P 1,0$_{1000Hz}$ [W/kg]
Mittelwert *mean value*	**1,10**	**2,72**	**14,13**	**29,69**	**52,66**
max.	1,16	2,86	15,00	31,17	55,29

	J 2500 [T]	J 5000 [T]	J 10000 [T]	
Mittelwert *mean value*	**1,55**	**1,65**	**1,75**	
Mindestwert/*min.value*	1,48	1,59	1,69	

Mechanische Werte
Mechanical values

	Rm [N/mm²]	Rp0,2 [N/mm²]	A80 [%]	HV	
Mindestwert *min. value*	**440**	**330**	**18**	**160**	

Die hier angegebenen Kennwerte sind als typische Produktionswerte anzusehen und können nicht garantiert werden.
The herein listed properties should be considered only as typical production values, and can not be guaranteed.

Anisotropie max. [%] *Anisotropy max. [%]*	-	**Wärmeleitfähigkeit [W/mK]** *Thermal conductivity max. [W/mK]*	21,56
Stapelfaktor min. *Stacking factor min.*	0,93	**Wärmeausdehnungkoeffizient [10-6 K-1]** *Coefficient of thermal expansion [10(-6)/K]*	12,015
Biegezahl min. *Number of bends min.*	2	**Spez. elektrischer Widerstand [µOhm*m]** *Specific electric resisitivity [µOhm*m]*	0,47
Dichte [kg-dm³] *Density [kg-dm³]*	7,65	**Elektrische Leitfähigkeit [S/m]*(10)^6** *Electric conductivity [S/m]*(10)^6*	2,15
Wärmekapazitität [kJ/(kg*K)] bei 298K *Heat capacity [kJ/kg*K] at 298K*	0,46		

Appendix E

Parameters of the foil 70984

	Adhesive	Carrier film	Adhesive
Type	Transfer adhesive Acrylat	Kapton 100MT	Transfer adhesive Acrylat
Article	CMC 15581	Kapton 100MT	CMC 15811
Adhesive strength	5.5 N/cm		1.0 N/cm
Thickness	0.050 mm	0.025 mm	0.020 mm
Width	140 mm		

Appendix F

Parameters of the copper wire and insulation for air gap winding SFT-AIW 0.31x0.94

Item	Conductor dimension		Thickness of insulation		Overall dimension		Pinhole	Dielectric breakdown voltage	Conductor resistance
	Thickness	Width	Thickness	Width	Thickness	Width			
Unit	mm	mm	mm	mm	mm	mm	Pcs/m	kV	Ω/km
-	0.31	0.94	0.025	0.025	-	-	3	3.0	68.131
max	0.319	1.0	0.04	0.04	0.38	1.045			
min	0.301	0.88	0.02	0.02	-	-			

Parameters of the copper wire and insulation for slot winding SFT-AIW 1.0x1.1

Item	Conductor dimension		Thickness of insulation		Overall dimension		Pinhole	Dielectric breakdown voltage	Conductor resistance
	Thickness	Width	Thickness	Width	Thickness	Width			
Unit	mm	mm	mm	mm	mm	mm	Pcs/m	kV	Ω/km
-	1.0	1.1	0.025	0.025	-	-	3	3.0	20.84
max	1.03	1.16	0.04	0.04	1.08	1.08			
min	0.97	1.04	0.01	0.01	-	-			

Appendix G

Properties of bandaging electrical tape 1339

Properties	Typical value
Thickness	6.5 mils (0,165 mm)
Breaking Strength	275 lb./in (481 N/10 mm)
Elongation	5%
Adhesion to Steel	35 oz/in (3,81 N/10 mm)
Dielectric Strength	5,500V
Temperature Class	130°C
Insulation Resistance	1x105 megohms
Electrolytic Corrosion Factor	1.0

Appendix H

Typical Electrical Properties of DuPont™ Nomex® 410

Property	Nominal Thickness, mm (mil)											Test Method
	0.05 (2)	0.08 (3)	0.10 (4)	0.13 (5)	0.18 (7)	0.25 (10)	0.30 (12)	0.38 (15)	0.51 (20)	0.61 (24)	0.076 (30)	
Dielectric Strength AC Rapid rise, V/mil kV/mm	460 18	565 22	525 21	715 28	865 34	845 33	870 34	850 33	810 32	810 32	680 27	ASTM D149[1]
Full Wave Impulse, V/mil kV/mm	1000 39	1000 39	900 36	1400 55	1400 55	1600 63	N/A N/A	1400 55	1400 55	N/A N/A	1250 49	ASTM D3426
Dielectric Constant at 60 Hz	1.6	1.6	1.8	2.4	2.7	2.7	2.9	3.2	3.4	3.7	3.7	ASTM D150
Dissipation Factor at 60 Hz (x 10^{-3})	4	5	6	6	6	6	7	7	7	7	7	ASTM D150

Appendix I

Properties of the material PA 3200 GF

PA 3200 GF
PA12-GB — EOS GmbH - Electro Optical Systems

Mechanical properties	Value	Unit	Test Standard
Izod notched impact strength (+23°C)	**4.2**	kJ/m²	ISO 180/1A
Izod impact strength (+23°C)	**21**	kJ/m²	ISO 180/1U
Shore D hardness	**80**	-	ISO 7619-1
Ball indentation hardness	**98**	MPa	ISO 2039-1

3D Data	Value	Unit	Test Standard
The properties of parts manufactured using additive manufacturing technology (e.g. laser sintering, stereolithography, Fused Deposition Modelling, 3D printing) are, due to their layer-by-layer production, to some extent direction dependent. This has to be considered when designing the part and defining the build orientation.			
Tensile Modulus			ISO 527
X Direction	**3200**	MPa	
Y Direction	**3200**	MPa	
Z Direction	**2500**	MPa	
Tensile Strength			ISO 527
X Direction	**51**	MPa	
Y Direction	**51**	MPa	
Z Direction	**47**	MPa	
Strain at break			ISO 527
X Direction	**9**	%	
Y Direction	**9**	%	
Z Direction	**5.5**	%	
Charpy impact strength (+23°C, X Direction)	**35**	kJ/m²	ISO 179/1eU
Charpy notched impact strength (+23°C, X Direction)	**5.4**	kJ/m²	ISO 179/1eA
Flexural Modulus (23°C, X Direction)	**2900**	MPa	ISO 178
Flexural Strength (X Direction)	**73**	MPa	ISO 178
Temp. of deflection under load			ISO 75-1/-2
1.80 MPa, X Direction	**96**	°C	
0.45 MPa, X Direction	**157**	°C	

Thermal properties	Value	Unit	Test Standard
Melting temperature (20°C/min)	**176**	°C	ISO 11357-1/-3
Temp. of deflection under load			ISO 75-1/-2
1.80 MPa	**96**	°C	
0.45 MPa	**157**	°C	
Vicat softening temperature			ISO 306
50°C/h 10N	**179**	°C	
50°C/h 50N	**166**	°C	

Other properties	Value	Unit	Test Standard
Density (lasersintered)	**1220**	kg/m³	EOS Method
Powder colour (ac. to safety data sheet)	**White**	-	-

Appendix J

Determination of the copper losses for various currents

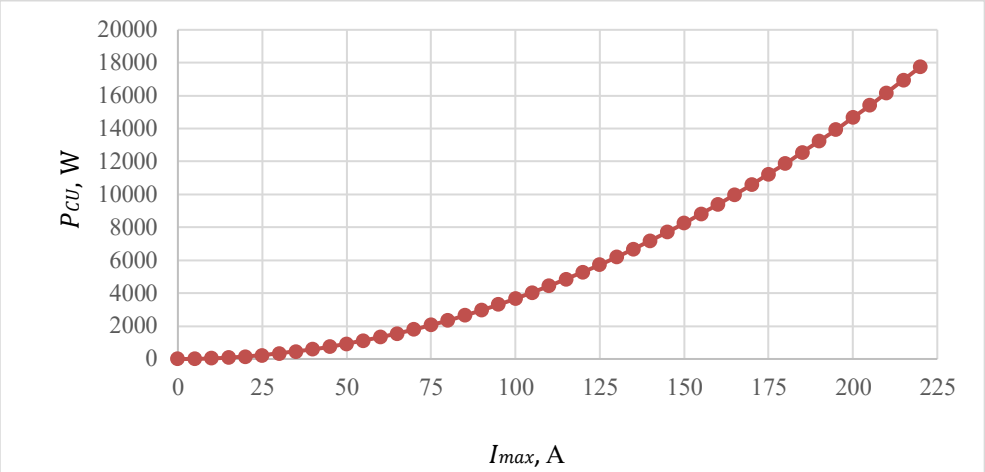

Appendix K

Power loss chart for the V-rings

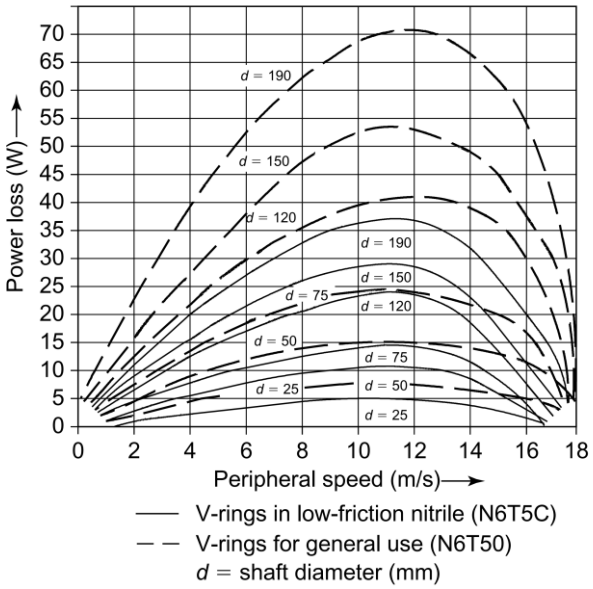

Appendix L

Characteristics of the test stand for the measurement of the air gap variation

Testing	Maximal load	Wheel diameter	Wheel width
Radial load	10 kN	13"-22"	5"-12.5"
Axial load	10 kN	13"-22"	5"-12.5"
Torque load	2000 Nm	13"-22"	5"-12.5"

Bibliography

[1] G. Abhishek, V. Ramsankar, M. Sreesankaran, G. Sabareesh, N. Jalaiah, "Combined effects of vehicle body geometry and drag reduction techniques on drag coefficient," in 8th International Colloquium on Bluff Body Aerodynamics and Applications, Boston, 2016.

[2] ADAC, "Tesla Model S P100D (11/16 - 03/19),"Allgemeiner Deutscher Automobil-Club e.V. (ADAC), 24.02.2019. [Online].
Available: https://www.adac.de/rund-ums-fahrzeug/autokatalog/marken-modelle/tesla/model-s/1generation-facelift/261294/
[Accessed 05.12.2019].

[3] W. Adams, "Electric motor". Patent U.S. Patent 300827, 1884.

[4] S. An, Z. Ma, W. Li, H. Zhang, T. Yin, "Magnetic properties of anisotropic bonded NdFeB/SmCo permanent magnets," AIP Advances, vol. 9, no. 125146, pp. 1-4, 2019.

[5] M. Anderson, D. Harty, "Unsprung Mass with In-Wheel Motors - Myths and Realities," in 10th International Symposium on Advanced Vehicle Control (AVEC), Loughborough, 2010.

[6] E. Andersson, "Optimization and re-design of a wheel hub to reduce unsprung mass of a rallycross car," University of Skövde, Skövde, 2018.

[7] M. Ashby, A. Evans, N. Fleck, L. Gibson, J. Hutchinson, H. Wadley, Metal Foams: A Design Guide, Burlington: Butterworth-Heinemann, 2000.

[8] Automotive Electronics Council, "Failure Mechanism Based Stress Test Qualification for Integrated Analytical Magnetic Circuits". AEC-Q100-Rev.H, 2014.

[9] B. Becker, J. Rusch, U. Rebholz, T. Buerger, B. Bergrath, S. Geisler, "Abschlussbericht des Forschungsprojektes Serienfähige, hocheffiziente Radnabenmotoren mit integrierter Leistungselektronik, SeRiel im Rahmen der Bekanntmachung "Serienflexible Technologien für elektrische Antriebe von Fahrzeugen," Heinzmann GmbH & Co. KG, Schönau, 2016.

[10] M.-A. Beeck, B. Stoffregen, "Measurement of the Projected Frontal Area of Vehicles, A New Contour Tracking Laser Device in Comparison to Other Methods," in International Congress and Exposition, Detroit, 1987.

[11] M. Biček, D. Miljavec, G. Gotovac, S. Zupan, "Mechanical Failure Mode Causes of In-Wheel Motors," Strojniški vestnik - Journal of Mechanical Engineering, vol. 61, no. 1, pp. 74-85, 2015.

[12] M. Biček, G. Gotovac, D. Miljavec, S. Zupan, "Nabenlager Belastungen und Lebensdauer für Radnabenmotor," in DVM 2013 - Zuverlässigkeit und Sicherheit des Elektrofahrzeugs, Berlin, 2013.

[13] M. Biček, T. Pepelnjak, F. Pušavec, "Production aspect of direct drive in-wheel motors," in 52nd CIRP Conference on Manufacturing Systems, Ljubljana, 2019.

[14] D. Boenke, H. Grossmann, A. Piazzolla, "Bordsteinkanten mit einheitlicher Bordhöhe und Bodenindikatoren an Überquerungsstellen," Carl Schünemann Verlag GmbH, Bergisch Gladbach, 2014.

[15] M. Bogner, R. Fischer, "Drehschwingungsdämpfer für einen Elektromotor sowie Radnabenmotor". Schaeffler Technologies AG and Co KG, Patent DE102009038416A1, 2011.

[16] N. Borchardt, R. Kasper, "Analytical magnetic circuit design optimization of electrical machines with air gap winding using a Halbach array," in 2017 IEEE International Electric Machines and Drives Conference (IEMDC), Miami, 2017.

[17] N. Borchardt, W. Heinemann, R. Kasper, "Design of a wheel-hub motor with air gap winding and simultaneous utilization of all magnetic poles," in 13th Mechatronics Forum International Conference, Linz, 2012.

[18] N. Borchardt, B. Penzlin, A. Zörnig, W. Heinemann, R. Kasper, "Entwicklung und Validierung eines BLDC Radnabenmotors mit Luftspaltwicklung," in Effizienz, Präzision, Qualtität. - Magdeburger Maschinenbau-Tage, Magdeburg, 2013.

[19] N. Borchardt, B. Penzlin, R. Kasper, "Mechatronic model of a novel slotless permanent magnet DC-motor with air gap winding design," in IEEE/ASME International Conference on Advanced Intelligent Mechatronics (AIM), Wollongong, 2013.

[20] N. Borchardt, Modellierung, elektromechanische Auslegung und Validierung eines Radnabenmotors mit nutenloser Luftspaltwicklung und hoher gravimetrischer Leistungsdichte. Dissertation, Otto-von-Guericke-Universität Magdeburg, 2014.

[21] N. Borchardt, R. Kasper, "Nonlinear design optimization of electric machines by using parametric Fourier coefficients of air gap flux density," in IEEE International Conference on Advanced Intelligent Mechatronics (AIM), Piscataway, 2016.

[22] N. Borchardt, R. Kasper, "Parametric model of electric machines based on exponential Fourier approximations of magnetic air gap flux density and inductance," Compel: international journal of computation & mathematics in electrical & electronic engineering, vol. 37, no. 1, pp. 520-535, 2018.

[23] N. Borchardt, R. Hinzelmann, D. Pucula, W. Heinemann, R. Kasper, "Winding Machine for Automated Production of an Innovative Air-Gap Winding for Lightweight Electric Machines," IEEE ASME transactions on mechatronics: a joint publication of the IEEE Industrial Electronics Society, the IEEE Robotics and Automation Society and the ASME Dynamic Systems and Control Division, vol. 21, no. 3, pp. 1509-1517, 2016.

[24] H.-H. Braes, U. Seifert, Automobildesign und Technik Formgebung, Funktionalität, Technik, Wiesbaden: Vieweg Verlag, 2007.

[25] H.-H. Braess, U. Seiffert, Vieweg Handbuch Kraftfahrzeugtechnik, 7., aktualisierte Auflage, Wiesbaden: Vieweg & Teubner Verlag, 2013.

[26] R. Busch, Elektrotechnik und Elektronik: Für Maschinenbauer und Verfahrenstechniker. 7., überarbeitete Auflage, Wiesbaden: Springer Vieweg, 2015.

[27] CARS Magazine, "Bridgestone Introduces “Revolutionary” Dynamic-Damping In-Wheel Motor Drive System," CARS Magazine, 01.03.2003. [Online].
Available: https://www.autoserviceworld.com/carsmagazine/bridgestone-introduces-revolutionary-dynamic-dampingin-wheel-motor-drive-system/
[Accessed 31.03.2020].

[28] CERN, "Record-breaking magnet has five-tesla field," CERN Courier, 22.03.2002. [Online].
Available: https://cerncourier.com/a/record-breaking-magnet-has-five-tesla-field/
[Accessed 13.01.2020].

[29] C. Chan, K. Chau, Modern Electric Vehicle Technology, New York: Oxford University Press Inc., 2001.

[30] K. Chau, Electric Vehicle Machines and Drives: Design, Analysis and Application, Singapore: John Wiley & Sons Singapore Pte. Ltd., 2015.

[31] K. Chau, C. Chan, C. Liu, "Overview of Permanent Magnet Brushless Drives for Electric and Hybrid Electric Vehicles," Industrial Electronics, IEEE Transactions, vol. 55, no. 6, pp. 2246- 2257, 2008.

[32] Q. Chen, H. Shu, L. Chen, "Analysis on cogging torque of driving in-wheel motor for electric vehicle," International Journal Electric and Hybrid Vehicles, vol. 4, no. 2, pp. 148-160, 2012.

[33] A. Chernoff, J. Szczerba, J. Montousse, "Driver control input device for drive-by-wire vehicle". Patent US006997281B2, 2006.

[34] J. Coey, T. Mhíocháin, "Permanent Magnet Assemblies," Encyclopedia of Materials: Science and Technology, vol. 2 Edition, pp. 6798-6805, 2011.

[35] J. Davies, Lightweight sandwich construction, Manchester: Blackwell Science Ltd, 2001.

[36] S. Davis, "In-Wheel Motor Systems Will Propel EV Performance," Endeavor Business Media, LLC, 19.07.2018. [Online].
Available:https://www.powerelectronics.com/markets/automotive/article/21864197/inwheelmotor-systems-will-propel-ev-performance
[Accessed 02.04.2020].

[37] N. Depner, R. Graaf, S. Wieglos, M. Arbitmann, K. Mühlbauer, L. Osinski, "MEHREN - A space-efficient vehicle concept with wheel hub drives for urban areas," in 22. Aachener Kolloquium. Fahrzeug- und Motorentechnik, Aachen, 2015.

[38] DER SPIEGEL GmbH & Co. KG, "E-Bikes - die Geschichte der elektrischen Trethilfe," 02.07.2016. [Online].
Available: https://www.spiegel.de/fotostrecke/die-geschichte-des-e-bikes-fotostrecke-135550.html
[Accessed 17.10.2019].

[39] Deutsches Institut für Normung, "DIN 7190 Pressverbände - Teil 1: Berechnungsgrundlagen und Gestaltungsregeln für zylindrische Pressverbände". Standard 2017.

[40] Deutsches Institut für Normung, "DIN EN 60034-6: Drehende elektrische Maschinen - Teil 6: Einteilung der Kühlverfahren". Standard, 1996.

[41] Deutsches Institut für Normung, "DIN EN IEC 60900 VDE 0682-201:2019-04 Arbeiten unter Spannung". Standard, 2019.

[42] A. Donath, "Elektromotoren in Autorädern zum Fahren und Bremsen," Golem Media GmbH, 02.08.2013. [Online].
Available: https://www.golem.de/news/direktantrieb-elektromotoren-in-autoraedern-zum-fahren-und-bremsen-1308-100749.html
[Accessed 19.01.2020].

[43] R. Doolittle, Design and optimization of a direct-drive in-wheel electric motor for automotive applications. Dissertation, Aachen: Shaker Verlag, 2016.

[44] ECOmove GmbH, "ECOmove Powertrain Specifications," 06.2013. [Online].
Available: http://ecomove.dk/wp-content/uploads/2013/06/ECOmove-Powertrain-Specifications.pdf
[Accessed 31.03.2020].

[45] A. Eilenberger, M. Schrödl, F. Demmelmayr, "Elektrofahrzeuge mit Permanentmagnet - Synchronmaschinen," e & i Elektrotechnik und Informationstechnik, vol. 128, no. 1-2, pp. 40-46, 2011.

[46] Elaphe Limited, "Elaphe Announces Production of World's Highest-Performance In-Wheel Hub Motor," 07.05.2019. [Online].

Available: https://in-wheel.com/en/news/elaphe-announces-production-of-worlds-highest-performance-in-wheel-hub-motor/
[Accessed 31.03.2020].

[47] N. Ermolaeva, K. Kaveline, J. Spoormaker, "Materials selection combined with optimal structural design: concept and some results," Materials and Design, vol. 23, no. 5, pp. 459-470, 2002.

[48] Eurostat, "Simplified energy balances," European Statistical Office, 27.02.2020. [Online].
Available: https://appsso.eurostat.ec.europa.eu/nui/show.do?dataset=nrg_bal_s&lang=en
[Accessed 17.10.2019].

[49] J. Fabian, M. Hirz, K. Krischan, "State of the Art and Future Trends of Electric Drives and Power Electronics for Automotive Engineering," SAE International Journal of Passenger Cars - Electronic and Electrical Systems, vol. 7, no. 1, pp. 293-303, 2014.

[50] FG für Straßen- und Verkehrswesen e.V., Handbuch für die Bemessung von Strassenverkehrsanlagen (HBS), Köln: FGSV Verlag GmbH, 2001.

[51] R. Fischer, Elektrische Maschinen. 16. Auflage, 2013: Hanser Verlag, München.

[52] R. Fischer, "Elektrische Radnabenmotren, Konstruktionskiterien und Fahrzeugintegration," ATZ Elektronik, pp. 8-14, 2010.

[53] R. Flitney, Seals and Sealing Handbook, Burlington: Butterworth-Heinemann, 2014.

[54] Forschungsportal Sachsen-Anhalt: ELISA „Radnabenmotor“. [Online].
Available: https://forschung-sachsen-anhalt.de/project/elisa-radnabenmotor-16260
[Accessed 18.06.2020].

[55] M. Frajnkovič, R. Connes, K. Rener, S. Omerović, U. Rožič, J. Kern, M. Biček, "Structural Integrity of In-Wheel Motors," in 52nd CIRP Conference on Manufacturing Systems, Ljubljana, 2018.

[56] Fraunhofer Institute LBF, "Composite fiber wheel with integrated electric motor," 01.10.2018. [Online].
Available: https://www.lbf.fraunhofer.de/en/projects-products/carbon-fiber-reinforced-polymer-wheel.html
[Accessed 10.01.2020].

[57] T. Gebauer, A. Vorderwülbecke, C. Tobisch, "Branchenanalyse Automobilimporteure," Hans-Böckler-Stiftung, Düsseldorf, 2018.

[58] D. Golovakha, H. Amiri, R. Kasper, "Theoretische Modellierung und experimentelle Validierung der Verlustleistung eines dreiphasigen Abwärtswandlers für die Ansteuerung eines Radnabenmotors mit geringer Induktivität," in 13. Magdeburger Maschinenbau-Tage 2017: autonom - vernetzt - nachhaltig, 27.-28. September 2017, Magdeburg, 2017.

[59] M. Griffin, "Discomfort from feeling vehicle vibration," International Journal of Vehicle, vol. 45, no. 7, pp. 679-698, 2007.

[60] D.-I. Gröninger, F. Horch, F. Kock, H. Pleteit, "Elektrischer Radnabenmotor," ATZ Elektronik, pp. 47-51, 2012.

[61] L. Guzzella, A. Sciarretta, Vehicle Propulsion Systems, Berlin, Heidelberg, New York: Springer, 2013.

[62] W. Hackmann, Systemvergleich unterschiedliche Radnabenantriebe für den Schienennahverkehr: Asynchronmaschine, permanenterregte Synchronmaschine, Transversalflussmaschine. Dissertation, Technische Universität Darmstadt, 2003.

[63] K. Halbach, "Design of permanent multipole magnets with oriented rare earth cobalt material," Nuclear Instruments and Methods, vol. 169, no. 1, pp. 1-10, 1980.

[64] Handelsblatt GmbH, "Alternativer Antrieb für das Auto der Zukunft," Handelsblatt Media Group GmbH & Co. KG, 20.04.2010. [Online].
Available: https://www.handelsblatt.com/technik/forschung-innovation/radnabenmotor-alternativer-antrieb-fuer-das-auto-der-zukunft/3415920.html?ticket=ST-6636118-fwmrZgPy0PSPm2UlCr1e-ap4
[Accessed 17.10.2019].

[65] Handelssysteme GD GmbH, "Kleines Felgen-ABC," 02.12.2018. [Online].
Available: https://www.premio.de/tuning/startseite/felgen/kleines-felgen-abc/
[Accessed 27.10.2019].

[66] C. Hanselman, Brushless Permanent Magnet Motor Design, University of Maine Orono: Magna Physics Publishing, 2003.

[67] C. Hanselman, "Effect of skew, pole count and slot count on brushless motor radial force, cogging torque and back EMF," IEE Proceedings - Electric Power Applications, vol. 144, no. 5, pp. 325-330, 1997.

[68] P. L. Hanst, W. E. Wilson, R. Patterson, B. Gay, L. Chaney, C. Burton, "A spectroscopic study of California smog. Environmental Protection Agency Publication," U.S. Environmental Protection Agency, Thousand Oaks, 2015.

[69] R. Heim, I. Krause, S. Weingärtner, "Der Rad-Straßen-Simulator," ATZ - Automobiltechnische Zeitschrift 110, p. 788–794, 2008.

[70] R. Heim, H. Hanselka, C. El-Dsoki, "Technical potential of in-wheel motors," ATZ Automobiltechnische Zeitschrift 114, pp. 4-9, 2012.

[71] B. Heißing, M. Ersoy, Chassis Handbook Fundamentals, Driving Dynamics, Components, Mechatronics, Perspectives, Wiesbaden: Vieweg+Teubner Verlag, 2011.

[72] B. Heißing, M. Ersoy, Fahrwerkhandbuch. Grundlagen Fahrdynamik Komponenten Systeme Mechatronik Perspektiven, Wiesbaden: Springer Vieweg, 2013.

[73] H. Hemdach, Systematischer Vergleich von BLDC-Motorkonzepten mit Anwendung auf nass laufende Wasserpumpen kleiner Leistung. Dissertation, Universität der Bundeswehr München, 2011.

[74] C. Hilton, "A Powertrain in the Wheels – Extreme Integration," in 5th International Conference Advanced EMotor Technology (IQPC), Berlin, 2017.

[75] R. Hinzelmann, N. Kovacs, N. Borchardt, R. Kasper, "Generator mit Kombinationswicklung zur regenerativen Energiegewinnung aus Wasserkraft," in 13. Magdeburger Maschinenbau-Tage 2017: autonom - vernetzt - nachhaltig, 27.-28. September 2017, Magdeburg, 2017.

[76] A. Höfer, H. Friedrich, "Methodical conception and development of innovative + lightweight chassis systems, illustrated by the example of the “LEICHT“ concept," in 5th International Munich Chassis Symposium, München, 2014.

[77] B. Höfner, Integrations- und Systemanalyse elektrischer Radnabenantriebe für zukünftige Pkw-Elektrofahrzeuge. Dissertation, EAA – Forschungsberichte, Band 7, Aachen: Shaker Verlag, 2010.

[78] C. Holzapfel, T. Kochmann, "Elektroblech und seine Eigenschaften," Sonderdruck aus ’STAHL’, vol. 1, pp. 58-62, 1993.

[79] F. Horch, H. Pleteit, M. Busse, "Motor auf Rädern," Internationales Verkehrswesen (4), pp. 28-29, 2011.

[80] C. Hsiao, S. Yeh, J. Hwang, "A Novel Cogging Torque Simulation Method for Permanent-Magnet Synchronous Machines," Energies, vol. 4, pp. 2166-2179, 2011.

[81] I. Husain, Electric and Hybrid Vehicles, Boca Raton London New York Washington: CRC Press LLC, 2003.

[82] M.-H. Hwang, H.-S. Lee, H.-R. Cha, "Analysis of Torque Ripple and Cogging Torque Reduction in Electric Vehicle Traction Platform Applying Rotor Notched Design," Energies, vol. 11, no. 3053, pp. 1-14, 2018.

[83] H. Imine, L. Fridman, H. Shraim, M. Djemai, Sliding Mode Based Analysis and Identification of Vehicle Dynamics, Berlin Heidelberg: Springer-Verlag, 2011.

[84] International Electrotechnical Commission, "IEC 60335-2-85: Household and similar electrical appliances – Safety – Part 2-85: Particular requirements for fabric steamers". International standard, 2002.

[85] International Organization for Standardization, "ISO 281:2007 Rolling bearings - Dynamic load ratings and rating life". Standard 02.2007.

[86] International Organization for Standardization, "ISO 76:2006 Rolling bearings - Static load ratings". Standard 05.2006.

[87] C. Irmscher, S. Koch, C. Daniel, E. Woschke, "Radlastmessung an einem Elektrofahrzeug bei verschiedenen Fahrbahnbelaegen inklusive Sonder- und Missbrauchsereignissen," in 13. Magdeburger Maschinenbau-Tage 2017: autonom - vernetzt - nachhaltig, 27.-28. September 2017, Magdeburg, 2017.

[88] N. Jazar, Vehicle dynamics: Theory and application (3rd Edition), New York: Springer, 2017.

[89] A. Kampker, D. Vallée, A. Schnettler, Elektromobilität Grundlagen einer Zukunftstechnologie, Berlin Heidelberg: Springer-Verlag, 2013.

[90] J. Käsgen, R. Heim, "Product development and testing requirements for electric wheel hub motors," in 10. Internationales CTI-Symposium - Innovative Fahrzeug-Getriebe 2011. Proceedings: Berlin, 5.- 8. Dezember 2011, Berlin, 2011.

[91] R. Kasper, N. Borchardt, "Boosting power density of electric machines by combining two different winding types," in MECHATRONICS 2016: 7th IFAC Symposium on Mechatronic Systems & 15th Mechatronics Forum International Conference, Loughborough University, 5th - 8th September 2016 - IFAC, Loughborough, 2016.

[92] R. Kasper, S. Perekopskiy, "Device for transmitting torque between a wheel and an electric machine integrated into the wheel". Patent WO2019141312A1, 2019.

[93] R. Kasper, N. Borchardt, "Electric motor having an iron-free winding". Patent WO2013029579A2, 2012.

[94] R. Kasper, N. Borchardt, "Electrical machine". Patent WO2017125416A1, 2016.

[95] R. Kasper, A. Zörnig, O. Petzold, R. Hinzelmann, C. Daniel, P. Dyszack, M. Schmidt, N. Borchardt, W. Heinemann, D. Golovakha, H. Amiri, G. Wagenhaus, S. Lüdecke, K. Kuhlmann, T. Stefaniak, „Elektrischer Radnabenmotor für Editha“, Plakat Campus Days, Institut für Mobile Systeme, Fakultät für Maschinenbau, Otto-von-Guericke-Universität Magdeburg, Mai 2015.

[96] R. Kasper, “Lightweight E-Motors for In-Wheel and other Mobile Drives”, in International CTI Symposium: Automotive Transmissions, HEV and EV Drives, Berlin, 5-8 December 2015.

[97] R. Kasper, A. Zörnig, O. Petzold, N. Borchardt, W. Heinemann, R. Hinzelmann, „Radnabenmotor mit Luftspaltwicklung“, Plakat Campus Days, Institut für Mobile Systeme, Fakultät für Maschinenbau, Otto-von-Guericke-Universität Magdeburg, Mai 2015.

[98] R. Kasper, M. Schmidt, R. Hinzelmann, A. Zörnig, N. Borchardt, "New mathematical approach for Eddy Current Loss in Air-Gap-Windings in a PMSM," in 13th IEEE International Conference on Power Electronics and Drive Systems (PEDS 2019), Toulouse, 2019.

[99] R. Kasper, M. Schmidt, R. Hinzelmann, "Skriptbasierte FEM Modellbildung und messtechnische Auswertung eines Wassergenerators mit Kombinationswicklung," in 14. Magdeburger Maschinenbau-Tage 2019 - Magdeburger Ingenieurtage, Magdeburg, 2019.

[100] KBA, "Durchschnittliches Leergewicht von neu zugelassenen Personenkraftwagen in Deutschland im Jahr 2018 nach Segmenten," Statista GmbH, 07.2019. [Online].
Available: https://de.statista.com/statistik/daten/studie/239565/umfrage/leergewicht-von-pkwneuzulassungen-in-deutschland-nach-segmenten/
[Accessed 27.10.2019].

[101] M. Keller, "Lohner-Porsche – Fahrzeuge die ihrer Zeit weit vorraus waren," Markus Keller, Betrieb von Internetseiten und Internetdienstleistungen, 16.02.2020. [Online].
Available: https://www.autowallpaper.de/hersteller/porsche/lohner-porsche.html
[Accessed 02.04.2020].

[102] K.-C. Kim, S.-H. Jeon, "Analysis on Correlation Between Cogging Torque and Torque Ripple by Considering Magnetic Saturation," IEEE TRANSACTIONS ON MAGNETICS, vol. 49, no. 5, pp. 2417-2420, 2013.

[103] KMF Kunststoff-Metall-Formteile GmbH, "SLIM-SPLIT-BEARING," 15.12.2017. [Online].
Available: http://www.kmf-bearings.de/Inhalte/Web-Slim-Split-Bearing-deutsch.pdf
[Accessed 20.10.2018].

[104] S. Kopczynski, W. Lonneman, F. Suttertield, P. Darley, "Photochemistry of atmospheric samples in Los Angeles," Environmental Science and Technology, vol. 6, no. 4, pp. 342-347, 1972.

[105] D. Kostic-Perovic, "Making the Impossible, Possible – Overcoming the Design Challenges of In Wheel Motors," World Electric Vehicle Journal, vol. 5, pp. 0514-0519, 2012.

[106] D.-I. Krebs, "Elektrische Radnabenmotren für leichte Stadtfahrzeuge," ATZ Elektronik, pp. 20-27, 2010.

[107] G. Krebs, R. Weber, S. Leppelsack, U. Hochberg, "Elektrische Radnabenmotoren für leichte Stadtfahrzeuge," ATZelektronik, vol. 5, pp. 20-27, 2010.

[108] A. Kreim, Modellierung und Parameteroptimierung einer permanenterregten Synchronmaschine unter Berücksichtigung von Lastzyklen. Dissertation, Technische Universität Berlin, 2015.

[109] R. Krishnan, Permanent Magnet Synchronous and Brushless DC Motor Drives, Blacksburg: CRC Press, 2009.

[110] T. Krone, A. Mertens, "Optimized design of the electric power train for wheel hub drive systems without friction brakes," in 19th European Conference on Power Electronics and Applications (EPE'17 ECCE Europe), Warsaw, 2017.

[111] A. Kulkarni, A. Kapoor, M. Ektesabi, H. Lovatt, "Electric Vehicle Propulsion System Design," in Subic A., Wellnitz J., Leary M., Koopmans L. (eds) Sustainable Automotive Technologies 2012, Berlin, Heidelberg, Springer, 2012, pp. 199-206.

[112] A. Lmeida, F. Ferreira, J. Fong, P. Fonseca, "EUP Lot 11 Motors," University of Coimbra, 2008.

[113] R. Löffler, "Weltweit produzierte Autos," Robert Löffler Internet-Dienstleistungen, 21.09.2019. [Online].
Available: https://www.live-counter.com/autos/
[Accessed 17.10.2019].

[114] J. Loftus, "Michelin Develops Revolutionary Active Wheel for Electric Cars," 30.11.2008. [Online].
Available: https://gizmodo.com/michelin-develops-revolutionary-active-wheel-for-electr-5100127
[Accessed 10.01.2020].

[115] Magdeburger Hydraulik GmbH, "Magdeburger Hydraulik," 12.03.2016. [Online].
Available: https://mhgmd.pneumatikatlas.com/gruppe/de/einfachwirkende-zylinder-mit-federrueckzug-5-100-tonnenhubkraft/C51C

[Accessed 30.06.2017].

[116] T. Makino, A. Ishikawa, C. Itou, K. Sakai, "Recent Technology Trends of In-Wheel Motor System for Automotive," NTN Corporation, OSAKA, 2013.

[117] P. Mallick, Materials, design and manufacturing for lightweight vehicles, Cornwall: Woodhead Publishing Limited, 2010.

[118] N. Masaki, K. Tashiro, H. Iwano, G. Nagaya, Y. Wakao, Y. Abe, "Entwicklung eines Radnabenantriebssystems mit dynamischem Dämpfungssystem," in Aachener Kolloquium Fahrzeug- und Motorentechnik, Eurogress Aachen, Aachen, 2006.

[119] C. Mayr, "Wellenkupplungen spielfrei und flexibel," 02.10.2018. [Online].
Available: https://www.mayr.com/de/produkte/wellenkupplungen/smartflex
[Accessed 29.11.2019].

[120] F. Meier, Permanent-magnet synchronous machines with non-overlapping concentrated windings for low-speed direct-drive applications. Doctoral Thesis, Royal Institute of Technology Stockholm, 2008.

[121] G. Müller, B. Ponick, Grundlagen elektrischer Maschinen. 9. Auflage, Weinheim: Wiley-VCH Verlag, 2006.

[122] A. Narbut, Avtomobili. Rabochie processy i raschet mehanizmov i sistem, Moscow: Akademija, 2007.

[123] H. Neuber, Kerbspannungslehre, Berlin Heidelberg: Springer, 1937.

[124] H. Neudorfer, Weiterentwicklung von elektrischen Antriebssystemen für Elektro- und Hybridstraßenfahrzeuge. Dissertation, Technische Universität Darmstadt, 2008.

[125] S. Nie, Y. Zhuang, F. Chen, Y. Wang, S. Liu, "A method to eliminate unsprung adverse effect of in-wheel motor-driven vehicles," Journal of Low Frequency Noise, Vibration and Active Control, vol. 37, no. 4, pp. 955-976, 2018.

[126] S. Nishioka, H. Iwano, K. Tashiro, "In-wheel motor system". Bridgestone Corp. Patent EP1961602A1, 2006.

[127] Nissan Motor Co., LTD, "Delivers a car that drives more than ever in the way you truly want," 17.05.2019. [Online].
Available: https://www.nissanglobal.com/TECHNOLOGY/OVERVIEW/in_wheel_motor.html
[Accessed 27.10.2019].

[128] J. Nonneman, S. Schlimpert, I. T'Jollyn, M. Paepe, "Experimental Investigation of Direct Contact Baseplate Cooling for Electric Vehicle Power Electronics," in 18th IEEE Intersociety Conference on Thermal and Thermomechanical Phenomena in Electronic Systems (ITherm), Las Vegas, 2019.

[129] NTN Corporation, NTN Hub Bearings, Catalogue; 4601/E, Osaka: NTN Corporation, 2016.

[130] S. Oh, A. Emadi, "Test and Simulation of Axial Flux Motor Characteristics for Hybrid Electric Vehicles," IEEE Transactions on Vehicular Technology, vol. 53, no. 3, pp. 912-919, 2004.

[131] S. Oh, S.-Y. Cho, J.-H. Han, H. Lee, G.-H. Ryu, D. Kang, J. Lee, IEEE Transactions on Magnetics, vol. 50, no. 2, pp. 841-844, 2014.

[132] OICA, "Anzahl registrierter Kraftfahrzeuge weltweit in den Jahren 2005 bis 2015," Statista GmbH, 07.2017. [Online].
Available: https://de.statista.com/statistik/daten/studie/244999/umfrage/weltweiter-pkw-und-nutzfahrzeugbestand/
[Accessed 16.10.2019].

[133] M. Önal, S. Riaño, K. Binnemans, "Alkali baking and solvometallurgical leaching of NdFeB magnets," Hydrometallurgy, vol. 191, pp. 1-11, 2020.

[134] A. Palmgren, Grundlagen der Wälzlagertechnik, Stuttgart: Francksche Verlagshandlung, 1964.

[135] J. Pander, "Toyota-Konzeptauto Me.We: Innen hui, außen ... Styropor," DER SPIEGEL GmbH & Co. KG, 26.04.2013. [Online].
Available: https://www.spiegel.de/auto/aktuell/toyota-konzeptauto-me-we-mit-kunststoffkarosserie-und-radnabenmotoren-a-896438.html
[Accessed 12.10.2019].

[136] S. Perekopskiy, R. Kasper, O. Heintze, A. Falken, C. Lies, "Potentials of lightweight concepts for ultra-lightweight wheel-hub motor," in 13. Magdeburger Maschinenbau-Tage 2017: autonom - vernetzt - nachhaltig, 27.-28. September 2017, Magdeburg, 2017.

[137] S. Perekopskiy, R. Kasper, "Ultra-Leichtbau-Radnabenmotor (LeiRaMo); Teilvorhaben: Konzeption, Konstruktion, Berechnung und Test des Ultra-Leichtbau-Radnabenmotors: Erfolgskontrollbericht: Laufzeit des Vorhabens: 01.01.16-31.12.2018," Otto-von-Guericke-Universität Magdeburg, 2018.

[138] S. Perekopskiy, R. Kasper, "Development and validation of a new kind of coupling element for wheel-hub motors," AIP conference proceedings, vol. 1959, no. 1, pp. 030018-030027, 2018.

[139] S. Perez, Analysis of a light permanent magnet in-wheel motor for an electric vehicle with autonomous corner modules. Master of Science Thesis, Royal Institute of Technology Stockholm, 2011.

[140] Protean Electric Limited, "Advanced electric-drive corner module designed for next-generation mobility pods," 19.08.2019. [Online].
Available: https://www.proteanelectric.com/f/2019/07/Protean-360-Fact-Sheet-ENG-160719.pdf
[Accessed 31.03.2020].

[141] Protean Electric Limited, "PD18 Data sheet," 07.2019. [Online]
Available: https://www.proteanelectric.com/f/2018/05/Pd18-Datasheet-Master.pdf
[Accessed 31.03.2020].

[142] A. Pruckner, E. Davy, D. Schlichte, S. Kaspar, "Elektrischer Einzelradantrieb: Optimierter Bauraum bei Maximaler Fahrdynamik," ATZ- Automobiltechnische Zeitschrift, pp. 46-50, 03.2014.

[143] H. Pucharapan, K. Maneepan, "10 reasons why SUV owners never go back to regular cars," General Motors Company U.S., 31.05.2018. [Online].
Available:https://media.gm.com/media/th/en/chevrolet/company_info.detail.html/content/Pages/news/th/en/2018/may/0531_10reasons.html
[Accessed 21.12.2019].

[144] J. Pyrhonen, T. Jokinen, V. Hrabovcova, Design of rotating electrical machines, Chippenham: John Wiley & Sons, Ltd, 2008.

[145] A. Rojas Rojas, Passenger Vehicles with In-Wheel Motors: Fundamentals, Potentials and Limitations. PhD thesis, Graz University of Technology, 2012.

[146] L. Roșca, M. Duguleană, "An Online Observer for Minimization of Pulsating Torque in SMPM Motors," PLoS ONE, vol. 11, no. 4, 2016.

[147] C. Ruoff, "A closer look at torque ripple – minimizing its effects on electric machines," Charged. Electric vehicles magazine, pp. 22-32, 07-08.2015.

[148] C. Sadarangani, Electrical Machines. Design and Analysis of Induction and Permanent Magnet Motors. Doctoral Thesis, Royal Institute of Technology Stockholm, 2006.

[149] J. Sauerhering, G. Boye, F. Beyrau, S. Perekopskiy, R. Kasper, O. Stamann, "Einfluss der Kühlkanalgeometrie und der Thermal Interface Materials auf die thermische Belastung eines

Elektromotors mit Luftspaltwicklung", in 13. Magdeburger Maschinenbau-Tage 2017: autonom - vernetzt - nachhaltig, 27.-28. September 2017, Magdeburg, 2017.

[150] Schaeffler AG, "Schaeffler Acquires Drive-by-Wire Technology," Schaeffler AG, Herzogenaurach, 06.08.2019.

[151] Schaeffler Technologies AG & Co. KG, "Mobility for tomorrow. Schaeffler Symposium," Schaeffler Technologies AG & Co. KG, Herzogenaurach, 2018.

[152] B. Schmidt, "Turn on a penny: Hyundai developing electric cars," The Driven Podcasts, 14.06.2019. [Online].
Available: https://thedriven.io/2019/06/14/turn-on-a-penny-hyundai-developing-electric-cars-with-motors-inside-the-wheels/
[Accessed 10.10.2019].

[153] M. Schmidt, A. Zörnig, R. Kasper, "Messung von Verlustanteilen eines elektrischen Motors mit Radialfluss-Luftspaltwicklung und FEM-basierter Validierung der Elektrodynamik," in Elektromagnetismus - Ostfildern: TAE, 2019, Ostfildern, 2019.

[154] M. Schmidt, R. Hinzelmann, R. Kasper, "Standardisierung der Messwertaufnahme für drehende elektrische Maschinen mit Luftspaltwicklung," in 13. Magdeburger Maschinenbau-Tage 2017: autonom - vernetzt - nachhaltig, 27.-28. September 2017, Magdeburg, 2017.

[155] M. Schöttle, "Elektrische Radnabenmotoren, ein Pro und Contra," ATZelektronik, no. 2, pp. 96-99, 2012.

[156] N. Schweizer, A. Giessl, O. Schwarzhaupt, "Entwicklung eines CFK-Leichtbaurads mit integriertem Elektromotor," ATZ-Automobiltechnische Zeitschrift (5), pp. 424-429, 05.2012.

[157] N. Schweizer, A. Büter, "Sicherheitsbauteile CFK-Leichtbaurad mit Motor," Emobility tec, vol. 04, pp. 62-65, 2012.

[158] T. Schwickart, H. Voos, J.-R. Hadji-Minaglou, M. Darouach, "A Fast Model-Predictive Speed Controller for Minimised Charge Consumption of Electric Vehicles," Asian Journal of Control, vol. 18, no. 1, pp. 133-149, 2015.

[159] F. Sedlacek, P. Bernardin, V. Lasova, "Optimal design of a composite bellows coupling using a structural optimization," in 2nd international conference on composite materials and material engineering (ICCMME), Chengdu, 2017.

[160] H. Seinsch, Grundlagen elektrischer Maschinen und Antriebe, Springer Fachmedien Wiesbaden: B.G. Teubner, 1993.

[161] P. Sharma, N. Saluja, D. Saini, P. Saini, "Analysis of Automotive Passive Suspension System with Matlab Program Generation," International Journals of Advancements in Technology, vol. 4, no. 7, pp. 115-119, 2013.

[162] SKF AB, "Internal report "Stiffness & geometry, BAR-0230, BAR-0123"," AB SKF, Gothenburg, 2017.

[163] SKF AB, "SKF bearings with Solid Oil Relubrication-free solutions for wet environments," [Online].
Available: https://www.skf.com/binary/57-251466/0901d196803e61e8-SKF-bearings-with-Solid-Oil---15894-EN.pdf
[Accessed 25.01.2020].

[164] SKF AB, "SKF hub bearing units for automotive and industrial applications," AB SKF, Gothenburg, 2015.

[165] SKF Gruppe, "Wälzlager," 01.2014. [Online].
Available: https://www.skf.com/binary/78-121486/Walzlager---10000_2-DE.pdf
[Accessed 02.02.2020].

[166] O. Stamann, S. Jüttner, A. Zörnig, R. Kasper, "Fügetechnologie für die Kupferdrahtwicklung eines neuartigen Leichtbau-Radnabenmotors," in DVS Congress 2018: Große Schweißtechnische Tagung, DVS-Studentenkongress, Düsseldorf, 2018.

[167] O. Stamann, S. Jüttner, J. Sauerhering, A. Zörnig, R. Kasper, "Untersuchung von doppelseitig klebenden Elektroisolierfolien mit wärmeleitfähigen Klebstoffschichten zum Fügen der Luftspaltwicklung von Leichtbau-Elektroantrieben," in 14. Magdeburger Maschinenbau-Tage 2019 - Magdeburger Ingenieurtage, Magdeburg, 2019.

[168] T. Staudt, T. Akinaga, L. Lopes, F. Maccari, P. Wendhausen, "Impact Analysis of PM magnetization level on motor performance: simulations and experimental results," Journal of Microwaves, Optoelectronics and Electromagnetic Applications, vol. 16, no. 1, pp. 154-164, 2017.

[169] O. Stavrov, Elektromobili, Moscow: Transport, 1968.

[170] Süddeutsche Gelenkscheibenfabrik GmbH & Co. KG, "SGF Wissenswertes," 06.06.2017. [Online].
Available: https://www.sgf.de/de/sgf-sueddeutsche-gelenkscheibenfabrik/service/wissen.html
[Accessed 29.11.2019].

[171] R. Terra, R. Barbosa, "The Influence of Hub Driven Motors on Vehicle Dynamics Behavior," in 25th SAE BRASIL International Congress and Display, São Paulo, 2016.

[172] O. Thomsen, E. Bozhevolnaya, A. Lyckegaard, "Sandwich Structures 7: Advancing with Sandwich Structures and Materials," in 7th International Conference on Sandwich Structures, Aalborg, 2005.

[173] J. Thorton, "In-wheel motors," Electric & Hybrid Vehicle Technology International, pp. 50-56, 07.2013.

[174] Transport Resources International Ltd, "European Industry has Moved to Euro 6," 04.01.2019. [Online].
Available: http://www.dougjack.co.uk/bus-industry-euro-6
[Accessed 17.10.2019].

[175] Trelleborg Group, "Trelleborg sealing solutions," 2018. [Online].
Available: www.tss.trelleborg.com
[Accessed 28.01.2019].

[176] D. Van Schalkwyk, M. Kamper, "Effect of hub motor mass on stability and comfort of electric vehicles," in IEEE - Vehicle power and propulsion conference, Windsor, 2006.

[177] B. Velev, "Comparative analysis of PMAC motors for EV and HEV," in Proceedings // XXII International Scientific-Technical Conference Trans & Motauto, Varna, 2014.

[178] N. Vittayaphadung, A. Zörnig, S. Perekopskiy, R. Kasper, "Simplified wheel hub bearing unit for the Finite Element Static analysis," in 13. Magdeburger Maschinenbau-Tage 2017: autonom - vernetzt - nachhaltig, 27.-28. September 2017, Magdeburg, 2017.

[179] K. Vogt, Berechnung elektrischer Maschinen, Weinheim: VCH Verlagsgesellschaft, 1996.

[180] A. Watts, A. Vallance, A. Fraser, A. Whitehead, "Integrating In-Wheel Motors into Vehicles - Real-World Experiences," SAE International Journal of Alternative Powertrains 1(1):289-307, vol. 1, no. 1, pp. 289-307, 2012.

[181] A. Watts, A. Vallance, A. Whitehead, C. Hilton, A. Fraser, "The Technology and Economics of In-Wheel Motors," SAE International Journal of Passenger Cars - Electronic and Electrical Systems 3(2):37-55, vol. 3, no. 2, pp. 37-57, 2010.

[182] S. Wielgos, N. Depner, R. Graaf, "Research Project MEHREN: Potentials of Highly-Integrated Wheel Hub Drives for New Vehicle Concepts," in 22nd Aachen Colloquium Automobile and Engine Technology, Aachen, 2019.

[183] J. Willberger, AC Motor Design and Evaluation for Automotive Traction Applications. Doctoral Thesis, Graz University of Technology, 2011.

[184] Worldometers.info, "How many cars are there in the world currently," 13.01.2008. [Online]. Available: https://www.worldometers.info/cars/ [Accessed 16.10.2019].

[185] S. Wu, L. Song, S. Cui, "Study on Improving the Performance of Permanent Magnet Wheel Motor for the Electric Vehicle Application," IEEE Transactions on Magnetics, vol. 43, no. 1, pp. 438-442, 2007.

[186] F. Wyczalek, "Heating and Cooling Battery Electric Vehicle - The Final Barrier," IEEE AES Systems Magazine, vol. 19, no. 3, pp. 9-14, 1993.

[187] S. Yasuhiro, T. Katsumi, K. Hisashi, "In-wheel motor system and method of installing in-wheel motor". Patent WO2005101984A2, 2005.

[188] H. Yoshida, H. Shimizu, "Transportation and Safety in Japan: "Ellica" - the 370km/h Maximum Speed Electric Vehicle," IATSS Research, vol. 29, no. 2, pp. 74-77, 2005.

[189] J. Zhao, Z. Gu, B. Li, X. Liu, X. Li, Z. Chen, "Research on the Torque and Back EMF Performance of a High Speed PMSM Used for Flywheel Energy Storage," Energies, vol. 8, pp. 2867-2888, 2015.

[190] S. Zhitkova, M. Felden, D. Franck, K. Hameyer, "Design of an electrical motor with wide speed range for the in-wheel drive in a heavy duty off-road vehicle," in 2014 International Conference on Electrical Machines (ICEM), Berlin, 2014.

[191] L. Zhu, S. Z. Jiang, Z. Q. Zhu, C. Chan, "Analytical Methods for Minimizing Cogging Torque in Permanent-Magnet Machines," IEEE transactions on magnetics, vol. 45, no. 4, pp. 2023-2031, 2009.

[192] A. Zörnig, R. Kasper, "Konstruktion elektrischer Radnabenmotoren mit Luftspaltwicklung für Kraftfahrzeuge," Konstruktion: Zeitschrift für Produktentwicklung und Ingenieur-Werkstoffe (6), pp. 40-43, 06.2015.

[193] A. Zörnig, R. Hinzelmann, S. Perekopskiy, R. Kasper, "Vergleich der Berechnung und Messung der Verluste in Wälzlagern und Dichtungen der Radnabenmotoren der OvGU," in 13. Magdeburger Maschinenbau-Tage 2017: autonom - vernetzt - nachhaltig, 27.-28. September 2017, Magdeburg, 2017.

[194] ZSW, "Zahl der Elektroautos steigt weltweit von 3,4 auf 5,6 Millionen," Zentrum für Sonnenenergie- und Wasserstoff-Forschung Baden-Württemberg (ZSW), 11.02.2019. [Online]. Available: https://www.zsw-bw.de/presse/aktuelles/detailansicht/news/detail/News/zahl-der-elektroautos-steigt-weltweit-von-34-auf-56-millionen.html [Accessed 02.04.2020].